The last 70 kyr of Rano Aroi (Easter island, 27°S) peat record: New insights for the Central Pacific paleoclimatology

Olga Margalef Marrasé
PhD Thesis
Universitat de Barcelona
2014

The last 70 ky of Rano Aroi (Easter Island, 27°S) peat record: New insights for the Central Pacific paleoclimatology

Memòria presentada per Olga Margalef Marrasé per optar al grau de doctora en Geologia. Aquesta memòria ha estat realitzada dins el Programa de Doctorat en Ciències de la Terra sota la direcció del Dr. Santiago Giralt Romeu i el Dr. Sergi Pla Rabes, i la tutela del Dr. Lluís Cabrera Pérez.

Olga Margalef Marrasé
Barcelona, Gener del 2014

Dr. Santiago Giralt Romeu

Dr. Sergi Pla Rabes

Dr. Lluís Cabrera Pérez

"Si no saps on vas, refés les passes
i torna enrere: sabràs d'on véns."
Proverbi guaraní

AGRAÏMENTS/ACKNOWLEDGEMENTS

Per fi, entre tant de nervi i escriptura arriba un moment dolç i fins i tot nostàlgic, el de recordar i agrair a tota aquella gent que m'ha ajudat al llarg d'aquest camí -a voltes incomprès, a voltes complicat- anomenat tesi.

Per començar vull agrair als que han estat els meus directors, Santiago Giralt i Sergi Pla. Per sobre de tots els altibaixos que pot tenir una tesi (estil muntanya russa), han dipositat confiança en mi en tot moment: m'han orientat i esperonat quan semblava que no es veia res clar, mostrant més confiança que jo en els meus propis resultats, m'han empès des del primer moment a desenvolupar estades a l'estranger, a presentar en congressos etc... Els vull agrair de tot cor l'acompanyament tant en el terreny estrictament professional com personal. En Santi i en Sergi són també responsables d'haver-me acollit en un grup de romàntics de la paleoclimatologia, d'apassionats per descobrir i perforar nous llacs (i ara jo afegeixo... i torberes!). Aquesta *troupe* d'individus variadíssims és un ecosistema ideal per aprendre de la visió multidisciplinària que requereix aquesta ciència. D'aquest grup vull destacar per ser còmplices i mentors al Alberto Sáez i al Juan José Pueyo, que han estat sempre disponibles per resoldre qualsevol dubte però també esbossar somriures. Han estat moltes les converses sobre clima, sedimentologia, metodologia i pirateria entre els passadissos de la UB o sobre la plataforma *uwitec*. També vull agrair a l'Armand Hernández, que va acabar la tesi quants uns anys abans que jo, i que, en certa manera, és un pèl culpable de que acabés aquí. Quan em deies que valia la pena treballar en aquest grup perquè més enllà de la qualitat científica eren gent que es preocupava per les persones tenies raó! A partir de cert moment l'Armand es va convertir en amic i còmplice del progrés de la tesi, gràcies! pels savis consells i l'amistat. En aquest grup de personalitats distingides també vull anomenar en Roberto Bao, per l'acompanyament, confiança i moments fantàstics en campanyes i visites a Galicia. També tinc un excel·lent record pel Blas Valero, en campanyes, reunions, congressos i discussions d'articles. Al Lluís Cabrera li haig d'agrair que hagi accedit ser el meu tutor a la UB, agilitzant sempre qualsevol entrebanc burocràtic. Al Valentí Rull voldria agrair-li haver-me obert les portes de l'Institut Botànic de Barcelona, on sempre vaig ser ben rebuda, per aprendre les bases de palinologia que ara tinc. I no, Núria, no m'oblido pas de tu ☺ ! Tu has estat la meva germana acadèmica com qui diu, des del primer dia a la campanya a l'illa de Pasqua, explicant-nos passat i present i especulant sobre el futur. T'haig d'agrair la infinita paciència que has tingut amb mi ajudant-me en el complicat món del comptatge i identificació de pol·len, els mils dubtes que m'has resolt de flora, literatura etc... però per sobre de tot t'haig d'agrair el poder avançar plegades colze a colze en aquesta jungla que és la tesi en els moments més alts i els més baixos. Tot just fa un parell d'anys s'incorporaven al grup dues "víctimes" més... La Guiomar Sánchez i Maria Jesús Rubio, després de conviure en una èpica campanya a les Açores i molts dies de despatx, gràcies també a vosaltres per tot el 'carinyo', ajuda i les bones estones i molta però que molta sort en els vostres projectes, creieu-me que al final s'arriba a bon port!

És obligació per mi agrair al recolzament econòmic sense el qual no hagués estat possible tot aquest treball. Per això vull citar tant els projectes de GEOBILA (CGL2007-60932/BTE) i PALEONAO (CGL2010-15767) com la beca JAE PreDoc (BOE 04/03/2008) que m'han permès desenvolupar totes les activitats i estades a l'estranger necessàries.

I parlant d'estades... I would like to thank for my first short stay abroad to all the hospitable people from LacCore in Minneapolis and Large Lake Observatory in Duluth (University of Minnesota). Especially to Anders Noren, Amy Mirbo and Erik Brown for their help in managing all measurements with Geotek and XRF corescanner. I also feel grateful to Laurie, the hyperactive flat mate and landlady from St. Paul, and Sergei for the nice trip along the Large Lakes between those freezing days. Also to all the people I met there that made this short stay warmer (we were at -20ºC!) and much easier.

I el mateix per l'estada a la Universitat de Bergen. I have to thank Hillary Birks for all her help in learning the methods for treating, sorting and identifying macrofossils from Rano Aroi peat. And also to John Birks for the first approach with statistical analysis on the obtained data set. My very special memories go to Torstein Solhøy, an incredible person, who I had the pleasure to enjoy as a teacher some years before in the 'winter ecology' course. Nobody who worked with him will forget his charming personality and his infinite passion for science, for teaching and spreading his knowledge, and, of course, for the tiny mites. Tusen takk, Torstein. I aquesta estada no hagués estat el mateix sense el retrobament amb el Fede, un apàtrida, petit heroi a Noruega amb múltiples feines precàries per sobreviure entre escandinaus. També vull mencionar l'Antonio (ara amic postal), gràcies a una providencial trobada entre Fløyen i Ulriken vàrem poder re-enllaçar el contacte i la seva companyia va ser indispensable per passar la tardor de Bergen.

Les darreres estades d'aquesta tesi les he desenvolupat a la Universitat de Greifswald, en el grup de Peatland studies and Paleoecology. Aquestes estades han tingut un pes diferent, pel que han suposat a nivell d'aprenentatge del món de les torberes, de rebuda pel lloc d'acollida i les oportunitats laborals que han sorgit en el passat i potser futur. Deswegen möchte ich mich bei einer langen Liste von Leuten bedanken. Angefangen bei unserem "Vater" der Gruppe, dem vielseitige Hans Joosten, ein herausragender Wissenschaftler und Person. Aber natürlich auch an die ganze Familie, ganz besonders an Alex, Martin, Anja, Almut, Annie, René, John, Dierk, Jenny und Suse... Alle zusammen haben mein Aufenthalt in Greifswald zu einem echten Geschenk gemacht. Són molts els llaços que he establert a la ciutat, amb gent tant fantàstica com la Sophie, Juliane, Mira (i Lisa, Stephan, Deborah... llarg etc..) que vaig conèixer en una sortida de camp per l'anàlisi de diferents tipus de torbera a un parc nacional a Bielorússia, entre vodka i extensions kilomètriques de molleres d'*Sphagnum*. No cal dir que una experiència així uneix. També gràcies a la Maite, Glad, Laura, Jan, Luca, Nazareth... Finalment voldria fer especial menció al Ferran, un català rodamón encantador... amb la teva família és més dolç i fàcil passar un hivern a la costa de Bàltic!

Aquesta aventura de la tesi va començar ja fa anys, quan no teníem ni idea en quin terreny ens endinsàvem, ni jo, ni tots els companys de la primera promoció del màster en Cambio Global impartit per la UIMP i el CSIC. Va ser a Palma on un grup de persones d'arreu

vàrem convergir i compaginar classes, escapades i convivència diària per forjar noves amistats. Gràcies al Mateo, Sergio, Iñigo, Alexia, Cristina, Rocío, Mónica, Gleicy per un any màgic. I molt especialment a tres superdones, la Joana, l'Olga i la Patri, amb qui hem pogut conviure taaant més! Sou genials (im-berbe-berbe-rón!), valentes, companyes d'aventura, tan de bo puguem seguir compartint experiències molts i molts anys.

I pel que fa a l'etapa viscuda a Barcelona haig d'agrair a molta gent sense la qual aquesta tesi no s'hagués pogut desenvolupar. Per començar a tota la gent del Jaume Almera com la Marta Rejas, per mostrar-se acollidora des del primer dia, i a la Graciela amb qui he compartit material i estones de laboratori. A tota la gent riallera del centre, Helena, Sara, Bea, Eduard, Ignacio, David, Raquel, Magda, Lola, Lavi, Mar, Alberto, Jan, Alba, Sofia etc... el treball en bona companyia és molt més agraït! I una especial menció pels companys de despatx que han anat canviant amb el pas del temps: Gio, Noe, Fulvio, Ana, Oriol, Giovanni, Dani i en especial per la Flavia (gracias por compartir tanto en este loco mundo de la ciencia que a menudo choca con el loco mundo de la militancia). Agraïments també a tota la gent del Serveis Cientifico-Tècnics de la UB amb qui vaig poder obtenir els resultats d'isotopia: Eva, Rosa, Miquel i Pilar en incomptables hores de microbalança i capsuletes de titani. I gràcies també al Jordi Illa pels llargs dies que vàrem fer ús del laboratori de petrologia sobretot en els primers mesos de la tesi.

De les col·laboracions que han anat sorgint al llarg de la tesi, n'hi ha moltes d'indispensables. Per exemple el treball conjunt i l'ajuda de l'Isabel Cacho. És de veritat inspirador treballar amb persones de gran qualitat científica i tracte tan proper, ple de confiança. Gràcies també per oferir-me la oportunitat de treballar amb el Leo Pena (gracias!), poder viure el congrés de Paleoceanografia (l'ICP) des de dins i conèixer de més a prop el teu grup (va per la Mercè, Patri, Albert, Judith, Itxaso quin fart de riure amb vosaltres ☺). Una altra col·laboració importantíssima pel desenvolupament de la tesi ha estat la establerta amb la Malin Kylander de la Universitat d'Estocolm i l'Antonio Martínez Cortizas, de la Universitat de de Santiago de Compostela. Thank you so much, Malin! Thanks for preparing and measuring with ICP-AES the inorganic content of more than two hundreds of peat samples. This geochemical dataset has become a very important part of this PhD. But beyond the analytical performance… thanks a lot for asking and reading me and for giving very inspiring advices about how to handle this crazy period called PhD. Thanks a lot for the encouraging, specially during the last months and for all those last minute language corrections over the manuscript. A Antonio le quiero agradecer todo lo aprendido sobre geoquímica de suelos y turberas, así como todas las horas dedicadas a la estadística sobre los datos de Rano Aroi. Por contestar dudas con tanta celeridad y buena sintonía. Y por el estupendo recibimiento que tuve en al Universidad de Santiago (A las 11h puntuales café con churros!). També voldria agrair a tota la gent de l'Institut Botànic (IBB) on he compartit múltiples hores de laboratori i dinars de carmanyola: a l'Encarni, Sandra, Juli, Tania, Eli i a la Teresa, per les xerrades dels cinc cèntims i per deixar-me compartir també sopars i dinars de grup. I no m'oblido tampoc del fantàstic team del IPE a Saragossa, cada visita i congrés en què hem coincidit ha estat un plaer! Edu, Josu, Ana, Mario, Graciela, Penélope, Ana... gracias por vuestro cariño siempre!

La primera fase d'escriptura de la tesi la vaig desenvolupar a un indret molt inspirador, la vall de Coma de Burg, entre Alendo i Farrera. Un lloc ideal per desconnectar de la impulsiva vida de Barcelona i poder assentar el cap. Tot i que només va ser un mes, va ser un mes fantàstic i vull agrair a tots els que ho vàreu fer possible, al Lluís, Cesca, Arnau i Oliver del centre d'Art i Natura de Farrera, per deixar-me l'espai per instal·lar-me i treballar, pel vostre 'carinyo' i manera de fer, sou adorables! A tots els habitants de la vall, Anna, Javi, Anna i llarg etc.. Als llogaters de la bordeta, per permetre que pogués dormir-hi i especialment a l'Oriol, per la companyia, converses, sopars i passejades en la meva breu estada al cor del Pallars.

I ara que escric aquestes línies em venen també al cap els millors records dels companys de facultat, apassionats geòlegs i geòlogues molts dels quals heu acabat en la mateixa carrera "tesítica"... algunes de les quals l'heu acabada: Berta, Anna, Manel, d'altres que esteu "en ello" a la UB o altres instituts: Lluís, Ari, Rubén, Marta, Alba, Rake, Laia... moltes forces! ... als que heu emigrat, Cris, Joyo etc .... A molta i molta gent del departament de geodinàmica i estratigrafia de la facultat de geologia amb qui vaig compartir estones els primers anys de tesi (no em vull deixar ningú!). A les futbolistes de geo! Les millors! I molts altres companys i companyes de carrera que segueixen avui en dia igual de genials: Uri, Laura, Marta, Aritz, Ricard, Roger, Raül, Melina, Martí, Xevi, Xavi... estem fets uns xavalins! Ja fa més de 10 anys que trepitjàvem per primer cop la facultat!

Ja m'ho deien al començar (i jo no m'ho creia), la tesi no és una feina qualsevol. Comporta una implicació personal afegida. Per aquest motiu vull agrair també a tots els que heu acompanyat, en general, a la vida durant aquests anys, fent-me sentir sovint una persona molt però que molt afortunada.

Empiezo con la gente de ese gran pequeño pueblo de raíces y flores. Gracias a tod@s l@s josin@s, arriburris y en particularmente a la Peña Pa' Kutio: qué vivan los verdes! Muy especialmente a los maños de Barcelona: Alicia, Silvia y Víctor por esas cenitas! Y claro, muy sinceramente, a Oscar, por todo lo vivido, todo el amor, los años de autobús cada fin de semana, de paseos y abrazos, del calor y las visitas allí donde me mandara la tesi. Y por todo el buen recuerdo de ese tiempo que nos ha hecho crecer. Gracias, alcalde!

Gràcies a tota la gent amb qui he compartit hores i hores d'assemblees, reunions, però també cerveses i festes, tota la gent "del rotllo", que creiem en un món millor, més just per a totes les que estem i les que vindran i que poc a poc construïm alternatives, suport mutu i expectatives de futur. Gràcies a la gent de Revolta, a la gent de la Vila de Gràcia, del Banc okupat i 15M Gràcia, de La Directa, als Cupaires de colors diversos, a la gent de l'Aixada, als de l'assemblea de doctorands diagonal, als que omplen places per denunciar injustícies i obren cooperatives per apuntalar noves realitats.

Gràcies als que han conviscut amb mi al llarg dels anys en habitacions contigües, com l'Olga, la Georgi, Charles, Annaïs, i a la Mariona un agraïment molt especial per tot allò que hem compartit també molt més enllà del pis, el mític "Can Cruelles". A les companyes d'ara: Noe i Iria, és genial arribar a casa i que hi sigueu! Estic molt contenta de tot aquest temps en el pis que mai vàrem inaugurar.

A tots els amics i amigues a seques, que fan de la vida un lloc habitable. Als diables de Les Corts, als salvadorenys que esteu tan lluny i tan a prop, als graciencs i gracienques. A l'Andreu, l'Edu, la May etc... aquesta colla genial de científics inquiets. Al Matthias, per compartir manis, barri i experiències per Alemanya. Al Guillem, company de muntanya i viatges, tant de bo ens poguéssim veure més sovint. Al Dani, per una amistat de fa molts anys, molt i molt sàvia, de tantes coses en comú... Acaba aviat la tesi tu també, que hauríem de muntar algun projecte per treballar plegats! És urgent!

Ai Manuel, et preguntes... i tu? Doncs a tu gràcies per la teva conquesta (pacient, molt pacient), per rescatar-me a estones, per deixar que m'aferri a tu quan fa falta, per l'amor constant, incondicional, de distància prudent, lluny de tòpics. Pel teu humor incombustible, cançons, poemes i per la teva vocació. Ets capaç de tot repte ;). Gràcies per deixar-te veure una miqueta més cada dia, més enllà. I per què tan de bo puguem escriure moltes i moltes pàgines de coses boniques plegats. T'estim.

De la meva família.. ui què dir-ne! Sou columna, aixopluc. Gràcies per inocular-me aquesta curiositat per aprendre i descobrir, per la vostra educació i amor. Gràcies als avis Ramon i Maria, exemple viu de fascinació per la natura. A la iaia Cèlia i tia Pilar, si a algú admiro en aquest planeta és a vosaltres, lluitadores incansables de temps massa turbulents. A absolutament tots els meus oncles i tietes, cosins i cosines, i fills i filles d'aquests, a les arrels que tenim a Barcelona, Mallorca i Teruel. I molt especialment meu pare i la meva mare i al meu germà Jordi que m'han ensenyat tant i de qui he rebut tot el suport, confiança i tendresa. M'han mimat tant els darrers dies de tesi! Moltes i moltes gràcies. Us estimo!

I ja que parlàvem de família, resulta que també en tinc una altra, una colla d'amics que després de créixer tant a prop, de tants viatges, de tantes voltes que dona la vida, esteu sempre allí a peu de canó. En Josep, Jordi, Pau, Àngela, Marc, Laia, Roger, Carles, sou poetes i poetesses de la vida! Inspireu i contagieu amb tot allò que feu, quina sort ser companys de ruta. Us estimo amb bogeria tot i que la vida frenètica no ens permeti veure'ns prou.

Escrivint aquestes pàgines me'n he adonat que és moltíssima la gent que m'ha fet feliç al llarg d'aquests anys de tesi, acompanyant-me en moments tant de fatiga com de màxima il·lusió. Sense vosaltres no hagués estat possible. Moltíssimes gràcies a totes i tots, de tot cor!

RESUM

Introducció (Capítol 1)

Les torberes es donen en ambients humits, pantanosos on la descomposició de la matèria vegetal resulta molt més lenta que la seva producció i per tant es produeix una acumulació neta de la mateixa (Joosten i Clarke, 2002). Aquests ambients solen ser lleugerament àcids, on l'oxigen és ràpidament consumit evitant així una ràpida mineralització de tota la matèria orgànica (Chesworth et al., 2006). Les torberes constitueixen el 3% de la superfície terrestre però contenen alhora aproximadament un terç del carboni total capturat en els sòls (Jackson i Charman, 2010). Això les converteix en elements clau en el cicle global del carboni a tenir en compte en l'estudi de les previsions de canvis climàtics.

Els primers treballs de reconstrucció ambiental mitjançant l'estudi dels diferents nivells de torba acumulada es remunten a fa més d'un segle on el reconeixement de llavors i altres macrofòssils vegetals va permetre la reconstrucció de paisatges i canvis de vegetació passats. De fet, les torberes representen excel·lents registres paleoclimàtics i paleoecològics ja que són ecosistemes sensibles als canvis hídrics i als de temperatura, contenen abundant carboni per datar i es poden estudiar mitjançant múltiples tècniques (Jackson i Charman, 2010). Tant l'anàlisi de la composició química de la matèria orgànica (isotopia i composició elemental) com de la fracció mineral d'origen detrític o eòlic són mètodes àmpliament usats en la recerca per a la reconstrucció ambiental en torberes (Bindler et al., 2006; Kylander et al., 2013). Altres mètodes extensament emprats són l'estudi de indicadors biològics, com el pol·len i palinomorfs no pol·línics, macro-fòssils vegetals o animals, micro-fòssils i pigments entre altres indicadors (Birks i Birks, 2006). Cal destacar que la majoria d'aquests treballs s'han realitzat sobre torberes situades a latituds boreals i temperades. Per contra, a dia d'avui, les torberes tropicals i subtropicals romanen molt menys estudiades, tant des de la perspectiva ecològica i biogeoquímica com paleoambiental i paleoecològica (Page et al., 2010). En aquesta tesi es du a terme l'estudi interdisciplinari d'un registre obtingut de la mollera de Rano Aroi, de l'Illa de Pasqua (o Rapa Nui). Aquest treball contribueix, per tant, a conèixer les característiques dels registres de torba tropicals i subtropicals. A més, la localització de l'illa (27°S, 109° W) representa una oportunitat única per a la reconstrucció de la dinàmica climàtica del Pacífic Sud i Central.

L'Oceà Pacífic és el més extens del planeta Terra i inclou el sistema de surgència marina (*upwelling*) més important del món (vora les illes Galàpagos) (Emery i Meincke, 1986). També conté la major corrent oceànica equatorial i en el seu extrem més austral constitueix una rellevant contribució de la circulació antàrtica (Rose et al., 2010). La dinàmica d'aquest oceà és clau per a la climatologia global, ja que determina l'ocurrència de la variació interanual més destacable: el fenomen de El Niño-Southern Oscillation (ENSO) (McPhaden, 2006). Aquestes característiques fan que el coneixement dels canvis de

circulació atmosfèrica i oceànica de l'Oceà Pacífic al llarg del Pleistocè i Holocè constitueixin contribucions claus per la ciència de la paleoclimatologia. Múltiples registres marins i continentals s'han estudiat per reconstruir l'evolució climàtica del Pacífic i Circum-Pacífic en relació a la variabilitat estadial-interestadial (Rosenthal et al., 2003, Wang et al., 2007; Muller et al., 2008a) i en relació a la influència dels canvis orbitals (Lamy et al., 1998; Pena et al., 2008). Altres autors, en canvi, han aportat contribucions en el coneixement dels principals processos de tele-connexió de fenòmens climàtics entre altes i baixes latituds (Clement i Peterson, 2008).

L'Illa de Pasqua permet aportar importants coneixements en l'estudi de la variabilitat climàtica del Pacífic Central ja que està situada enmig d'una gran àrea en la qual no hi ha oportunitat d'obtenir registres marins per la baixa taxa de sedimentació del fons oceànic abissal. Alhora, la localització de la illa coincideix en una zona d'interacció entre estructures climàtiques importants com la Zona de Convergència Intertropical (ITCZ), la Zona de Convergència del Pacífic Sud (SPCZ), o els vents de l'oest (SW), l'Anticicló del Pacífic Sud (SPA).

Objectius i estructura de la Tesi Doctoral

Els objectius de la Tesi són: 1) la reconstrucció de la història ambiental de la torbera de Rano Aroi a partir d'un estudi multidisciplinari (combinant indicadors biològics i químics) d'aquest registre i 2) aportar dades que permetin entendre la variabilitat climàtica de l'Oceà Pacífic Central i del Sud des de el MIS 4 a l'actualitat, així com les tele-connexions amb les dinàmiques climàtiques regionals i globals.

Aquesta Tesi doctoral està estructurada en 10 capítols. El primer capítol consisteix en una introducció a la ciència de les torberes així com als diferents indicadors normalment usats per a reconstruccions paleoambientals en aquests tipus de registre. També s'inclou un resum de les característiques més importants de circulació atmosfèrica i oceànica de l'Oceà Pacífic en l'actualitat així com els canvis d'aquests al llarg del Pleistocè i Holocè. El Capítol 2 inclou una explicació sobre el context regional, geològic i climàtic del registre estudiat i l'Illa de Pasqua. També es presenten els treballs paleoecològics i paleoclimàtics previs duts a terme a la mateixa illa. La metodologia emprada al llarg del període de recerca s'exposa en el Capítol 3, mentre que en el Capítol 4 es redacten els resultats. La discussió està composta pels capítols 5, 6, 7 i 8. El Capítol 5 suposa la primera aproximació a l'evolució de la torbera de Rano Aroi en què es defineixen tres estadis hidrològics que s'han anat alternant al llarg dels darrers 70.000 anys. També es construeix un model d'edat en base a les datacions de carboni 14. En el Capítol 6 es determinen els processos que determinen la composició química (orgànica i inorgànica) del registre de torba com són els episodis d'elevada precipitació o sequera o bé canvis en la vegetació de la mollera i la conca. Les deduccions dels Capítols 5 i 6 s'integren en el Capítol 7 per reconstruir l'evolució ambiental de forma detallada pels darrers 70.000 anys comparant-la amb altres registres de la illa i del Circum Pacífic. En el Capítol 8 s'empra la variabilitat en la precipitació de l'Estadi Isotòpic Marí 3 (MIS 3) reconstruïda a Rano Aroi per tal de dilucidar les tele-connexions i principals dinàmiques climàtiques que varen regir els canvis en el Pacífic Sud. El Capítol 9 consisteix

una síntesi de tota la discussió. Finalment, el Capítol 10 presenta les conclusions de la Tesi. Com a apèndix es poden trobar les dades obtingudes pels procediments experimentals.

Treballs previs realitzats a l'Illa de Pasqua (Capítol 2)

L'illa de Pasqua es una illa volcànica d'edat miocènica composta per més de 70 cràters i colades magmàtiques. Les roques de l'illa van de composició basàltica (la majoritària) a riolítica (González-Ferran et al., 2004). La topografia no presenta rius o rieres permanents però compta amb la presència de dos llacs (Rano Raraku i Rano Kau) i una torbera (Rano Aroi) situats en antics cràters volcànics. Els treballs paleoambientals previs desenvolupats a l'illa han estat principalment centrats en el llac Rano Raraku (Flenley et al., 1991; Sáez et al., 2009). Aquest llac és un dels indrets més emblemàtic de l'illa ja que en el mateix cràter s'hi troba la cantera dels *moais,* estàtues descomunals esculpides pels antics pobladors polinèsics i icones de la cultura Rapa Nui. Les primeres investigacions paleoambientals es van basar en l'estudi del contingut pol·línic en el registre lacustre de Rano Raraku. A partir d'aquests estudis es varen definir importants canvis de vegetació (com la davallada de la presència de palmeres) en els darrers centenars d'anys atribuïts a la desforestació de l'illa per l'arribada dels humans a l'illa (Flenley i King, 1984). Avui en dia encara existeix una important controvèrsia al voltant de l'edat i naturalesa d'aquesta deforestació (Rull et al., 2010a). Altres treballs centrats en l'estudi de la sedimentologia i/o els macro-fòssils s'han desenvolupat a Rano Raraku (Dumont et al., 1998; Cañellas-Boltà et al., 2012; Sáez et al., 2009) i a Rano Kau (Butler i Flenley, 2004) per tal d'establir les variacions climàtiques dels darrers 34.000 anys. La torbera de Rano Aroi, en canvi, ha estat sensiblement menys estudiada. L'únic treball que s'hi havia realitzat fins el moment es va centrar en l'estudi del contingut pol.línic (Flenley et al., 1991). En la present Tesi es pretén ampliar els indicadors empleats en aquest primer treball mitjançant l'ús de tècniques biològiques, químiques i isotòpiques, i revaluar el model d'edat, ja que aquest es va obtenir mitjançant mètodes actualment obsolets. Per aquest motiu s'estudiaran des de una perspectiva multidisciplinar dos testimonis de 14 i 4 metres de potencia i situats al centre i a un dels marges de la torbera, respectivament.

Metodologia emprada (Capítol 3)

Els dos testimonis estudiats es van obtenir en dues campanyes de camp. La primera es va portar a terme durant març de 2006 en la qual es va recuperar un registre de 14 metres de potencia (ARO 06 01 i dividit en 11 seccions) mitjançant un equip de sondatge de pistó UWITEC i instal·lat sobre una plataforma. La segona campanya es va realitzar al març de 2008 durant la que es va recuperar un registre de 4 metres de potencia (ARO 08 02 i dividit en 4 seccions) del marge de la mollera i amb una sonda russa.

Les seccions dels testimonis ARO 06 01 i ARO 08 02 van ser obertes i descrites a Barcelona i es van definir quatre facies de torba principals en base el tipus de components vegetals, color, i grau de humificació. Aquesta classificació va ser reforçada mitjançant l'observació al microscopi de frotis efectuats en mostres agafades cada 5 cm del testimoni. Es van seleccionar vint-i-set mostres de torba les quals van ser tractades específicament per a extreure el seu contingut pol·línic, el qual va ser datat mitjançant AMS 14C.

Les seccions dels testimonis torba van ser sistemàticament mostrejades cada 5 cm per la determinació dels continguts en carboni total (TC), nitrogen total (TN), sofre total (TS) i isotopia estable ($\delta^{13}C$, $\delta^{15}N$, $\delta^{34}S$). En total es varen obtenir 218 mostres del testimoni ARO 06 01 i 68 del ARO 08 02. Els anàlisis es van dur a terme als serveis Cientifico-Tècnics de la UB (SCT-UB). A continuació es va realitzar l'anàlisi dels testimonis mitjançant un escàner ITRAX de fluorescència de raigs X (FRX) amb tubs de crom i molibdè per tal de determinar la composició química del contingut mineral del registre ARO 06 01. Les mesures van ser preses al laboratori de Large Lakes Observatory (Universitat de Minnesota, Duluth, EEUU). Com a resultat es va obtenir les variacions de calci (Ca), ferro (Fe) i titani (Ti) en comptes per segon (cps) de la seqüència de torba. Per investigar la composició mineral dels nivells que, segons el resultats de FRX mostraven una major concentració de contingut inorgànic, es van seleccionar els grans minerals presents en nivells representatius. Els grans separats van ser fotografiats amb microscopi electrònic de rastreig i la seva composició elemental va ser obtinguda per espectroscopia de raigs X mitjançant el detector EDAX acoblat al microscopi. Aquesta determinació es va efectuar a baix i alt buit al servei de microscòpia del Serveis Científico-Tècnics de la UB (SCT-UB). Finalment, per completar les determinacions de la geoquímica inorgànica del registre i abastir un major nombre d'elements, un conjunt de 207 mostres distribuïdes al llarg del testimoni ARO 06 01 es van seleccionar per ser analitzades mitjançant espectroscopia d'absorció atòmica (ICP-AES). Les mostres de torba es van processar mitjançant una digestió amb àcid nítric i àcid fluorobòric per obtenir-ne el contingut mineral abans de ser mesurades per ICP-AES (Krachler et al., 2002). Mitjançant aquest anàlisis es va obtenir la concentració dels següents elements: Al, Ba, Ca, Cd, Cr, Cu, Fe, Mg, Mn, Sc, Sr, Ti, V, Y i Zr. Aquesta metodologia va ser desenvolupada a la Universitat d'Estocolm per la Dra. Malin Kylander.

Per conèixer estudiar la procedència d'aquesta fracció mineral es varen realitzar anàlisis geoquímics de les roques i sòls de la conca de drenatge. Es va obtenir el contingut elemental mitjançant FRX i mineralògic a partir de difracció de raigs X (DRX) de 9 mostres de roca de la conca de Rano Aroi als SCT-UB. A més, una selecció de 16 mostres que comprenien sòls i roques tant de les rodalies de la torbera de Rano Aroi com d'altres indrets de l'illa van ser analitzades (Ruggieri et al., 2012) per determinar-ne la composició elemental mitjançant espectrometria de massa (ICP-MS) al Institut de Ciències de la Terra Jaume Almera (ICTJA-CSIC).

Pel que fa als indicadors biològics, la seqüència de torba es va estudiar per obtenir-ne el registre de macrofòssils i pol·len. Es van seleccionar quaranta-sis mostres dels testimonis de ARO 06 01 i ARO 08 02 i van ser tamisades 125 i 500 μm. Els residus d'aquestes dues fraccions varen ser observats amb lupa binocular (x12 augments) i els macrofòssils varen ser col·leccionats amb pinces. La identificació d'aquests macrofòssils, principalment llavors, àcars (Oribatida) i escarabats (Curculionoidea) d'entre altres restes, es va efectuar mitjançant la consulta de materials de referència i especialistes taxonòmics (Prof. Torstein Solhøy de la Universitat de Bergen, Dr. Alex Riedel del museu d'Història Natural de Kalsruhe). Tot el procés es va desenvolupar a la Universitat de Bergen sota la supervisió de la Dra. Hilary Birks.

54 mostres van ser atacades per obtenir-ne concentrats pol·línics a l'Institut Botànic de Barcelona (IBB-CSIC) seguint el protocol que inclou digestions amb sosa, àcid clorhídric, àcid fluorhídric i acetòlisis (Montoya, 2011). Com a marcador exòtic es va afegir una pastilla d'espores de Lycopodium per gram de mostra de torba humida per tal de deduir-ne la concentració total de pol·len. Es va efectuar el recompte de pol·len en 25 mostres, comptant fins a 150 grans (sense incloure pol·len d'aquàtiques, semi-aquàtiques i espores, sovint els més abundants) o en el seu defecte, fins a arribar a 40 grans de Lycopodium. Els comptatges es varen realitzar sota la orientació del Dr. Valentí Rull i de Núria Cañellas-Boltà tant a l'Institut Botànic de Barcelona (IBB) com a la Universitat de Greifswald (Alemanya).

Per comparar la senyal climàtica obtinguda a la torbera de Rano Aroi amb els canvis climàtics regionals de l'Oceà Pacífic Sud es va calcular un gradient de temperatura marina superficial (SST) E-W del Pacífic Equatorial usant dos registres marins prèviament publicats (ODP 1240, vora les illes Galàpagos, Pena et al., 2008 i MD 97-2141 al mar de Sulu, Dannenmann et al., 2003). Aquesta tasca es va desenvolupar amb l'ajuda i col·laboració dels investigadors Dra. Isabel Cacho (UB) i Dr. Leo Pena (Lamont-Doherty Earth Observatory of Columbia University).

El conjunt de dades de química orgànica i inorgànica ha estat tractada estadísticament principalment amb anàlisi de components principals (PCA) usant diferents conjunts de dades segons el problema a resoldre. Els tractaments s'ha fet utilitzant els paquets de software R i SPSS (Oksanen et al., 2007; R Development Core Team, 2011). Part del processat estadístic s'ha desenvolupat amb la col·laboració del Dr. Antonio Martínez-Cortizas (Universitat de Santiago de Compostela).

Els resultats de la metodologia (Capítol 4 de la Tesi) estan integrats en aquest resum en la discussió dels capítols següents (Capítols 5, 6, 7 i 8).

Els principals estadis hidrològics de Rano Aroi al llarg dels darrers 70.000 anys (Capítol 5)

En aquest capítol s'empren els resultats del model d'edat (Secció 5.2), la descripció de fàcies (Secció 4.1) i contingut macrofòssil (Secció 4.6.1) juntament amb una part dels obtinguts de geoquímica de la matèria orgànica (TC, TN, C/N, $\delta^{13}C$) dels registres ARO 06 01 i ARO 08 02 (Seccions 4.3.1). També s'usen els perfils obtinguts mitjançant FRX core-scanner (Ca, Fe, Ti en cps) del registre ARO 06 01 (Secció 4.3.2). L'objectiu del capítol és descriure i caracteritzar els diferents estadis ambientals i hidrològics de la torbera pels darrers 70.000 anys.

La caracterització isotòpica de l'aigua descrita en la literatura indica que la mollera de Rano Aroi s'alimenta per aigua subterrània i, per tant, no depèn exclusivament de la pluja, el que en condiciona les seves característiques biogeoquímiques i hídriques (Herrera i Custodio, 2008). Els resultats de les analítiques de la litologia mostren que la conca de Rano Aroi està formada per roques volcàniques àcides de composició hawaitica i toleitica, sovint en forma de pòrfirs amb cristalls de plagiòclasis càlcica i piroxè. La composició mineral és especialment rica en Fe i Ti amb abundants rutils i ilmenites.

Durant l'obertura dels testimonis ARO 06 01 i ARO 08 02 es van definir quatre fàcies de torba diferents. En la part superior d'ambdós testimonis abunda una fàcies de torba fresca (Facies A) amb restes vegetals grollers i amb presència abundant de llavors (principalment de ciperàcies i poligonàcies). La major part de la seqüència està dominada per torba granulada que mostra valors de $\delta^{13}C$ d'entre -14 i +26‰ (Facies B). Aquesta facies es veu intercalada per nivells centimètrics de fang orgànic de color fosc i gra fi, caracteritzat per valors relativament lleugers de $\delta^{13}C$ i nivells alts de Fe, Ti i Ca (Facies C). Per acabar s'observa una facies de torba fosca i de gra fi (Facies D) que mostra evidències de degradació en observacions dels frotis al microscopi (Figures 4.1 i 4.2).

El model d'edat indica que la formació torba es va iniciar com a mínim fa 70.000 anys (Figura 5.2). Entre els 70 i els 40 kyr cal BP, les taxes d'acumulació es varen mantenir més o menys constants (0.3 mm/any). Als 39 kyr cal BP es presenta una discontinuïtat en el registre causada segurament per un període de sequera. Aquesta discontinuïtat sedimentària implicaria que la sedimentació va ser extremadament baixa o inclús es va aturar, perdent-se part del registre sedimentari per degradació de la torba La data exacte de recuperació de la formació de torba és incerta, i hi ha evidències que durant el Darrer Màxim Glacial (LGM en les seves sigles en anglès) la taxa d'acumulació de torba fou baixa i constant (0.03 mm/any). A partir dels 17.5 cal kyr BP l'acumulació va augmentar de nou (0.1-0.3 mm/any). Aquestes condicions es varen mantenir fins a l'entrada de l'Holocè.

La senyal de $\delta^{13}C$ de la matèria orgànica a Rano Aroi és heretada de la signatura isotòpica de la vegetació que va formar la torba (Figures 4.3 i 4.4). Els valors registrats oscil·len de la senyal isotòpica entre -14 i -26‰, que corresponen a valors de plantes de tipus C_4 i C_3 respectivament (Meyers, 1994). Això indica que la senyal isotòpica del carboni constitueix un bon indicador dels canvis de vegetació entre grups amb diferent rutes metabòliques. Alhora, menors oscil·lacions de més alta freqüència poden indicar canvis en la disponibilitat hídrica (Hong et al., 2001) . Així, una mateixa espècie pot mostrar valors més lleugers de $\delta^{13}C$ sota condicions ambientals més humides degut a diferències en el fraccionament dels isòtops de carboni. Per tal d'acotar aquestes oscil·lacions d'isotopia de carboni lligades a la disponibilitat hídrica, es va extreure la tendència a llarg termini (variabilitat C_3-C_4) dels resultats originals per tal d'obtenir la variabilitat d'alta freqüència ($\delta^{13}C_{res}$) lligada a quests events d'humitat.

El titani (Ti), és incorporat a la torbera per entrada de material detrític transportat i es considera un element químic molt estable (no es mobilitza) en torba. Per tant, el titani és un bon indicador de l'entrada de fracció mineral (Weiss et al., 2002). Per altra banda, encara que el ferro (Fe) com el calci (Ca) són també incorporats a la torbera pel mateix procés de transport que el Ti, poden esdevenir mòbils, ja que són sensibles a canvis en les condicions redox (Damman et al., 1992; Shotyk , 1996).

L'anàlisi de components principals (PCA) del conjunt de dades biogeoquímiques (TC, TN, $\delta^{13}C_{res}$, Ca, Fe i Ti) ha donat com a resultat dos components principals significatius (Figura 5.3). El primer component (PC1), que explica un 30.7% de la variància, i està marcat per la contribució de $\delta^{13}C_{res}$ a l'eix positiu i la contribució negativa de Ca, Fe, Ti, TN i TC. Per altra banda el segon component (PC2) captura un 27.8% de la variància explicada i està

definit per la relació positiva amb Fe, Ca, TC i $\delta^{13}C_{res}$ i la negativa amb Ti i TN. El primer component, per tant, sembla estar relacionat amb el contingut de matèria mineral. Valors negatius de PC1 (majors valors de Ca, Fe, Ti) indicarien major entrada d'aquests elements mitjançant l'arribada de material detrític. En canvi, el PC2 separa els elements mòbils (Ca, Fe) dels immòbils (Ti). Les concentracions elevades de Fe i Ca en relació al contingut de Ti es generen en condicions oxidants (Gorham and Janssens, 2005). El segon component per tant, diferencia les mostres que han patit un procés d'oxidació de la matèria orgànica (valors elevats i positius de PC2 i elevats Ca/Ti i Fe/Ti) dels nivells que no han patit oxidació (valors absoluts elevats però negatius de PC2). Les característiques geoquímiques (valors alts de Ti, TN i de $\delta^{13}C_{res}$ lleuger) d'aquest darrer grup de mostres així com el seu contingut macrofòssil (p.e. larves d'*Ephydridae*) indiquen que la torba va ser acumulada sota condicions aquàtiques.

La representació gràfica dels valors de PC1 i PC2 de les mostres (Figura 5.3) evidencia una classificació d'aquestes en tres grups que corresponen a les facies definides. Aquest resultat ens permet reconstruir la història de Rano Aroi considerant tres estadis ambientals. El primer, està caracteritzat per les a Facies A i B (i representaria les condicions de base de la torbera), un altre registrat per les Facies C (que marcaria episodis humits) i un darrer representat per la Facies D (que indicaria condicions de sequera i oxidació). La dominància de les Facies A i B en la major part del registre indica que el sistema ha estat molt estable al llarg del temps, al voltant de les condicions de base, i que hauria virat puntualment cap a un estadi de torbera inundada en períodes humits (d'elevada precipitació). En aquests episodis, la làmina d'aigua hauria estat més elevada i s'hauria registrat l'entrada de material terrigen (marcat per increments de tant de Fe com Ti, molt presents en les roques de la conca) per escorrentia, i la vegetació presentaria valors relativament lleugers de $\delta^{13}C_{res}$ i més elevats de TN. Per altra banda, en el moments en què l'aportació hídrica hauria disminuït, ja sigui per una caiguda de nivell freàtic o per una disminució radical de la precipitació, la torba hauria estat exposada i oxidada (el que registraria la Facies D). Aquest nivell d'exposició (Facies D) es caracteritza per l'enriquiment en Fe i Ca no associat al Ti (relació alta Fe/Ti), causada per la precipitació en forma d'òxids de les formes de ferro prèviament mòbils procedents de nivells reduïts. També és representatiu l'enriquiment en Ca, que és bio-acumulable i estable en condicions oxidades formant compostos orgànics (Zoltai i Johnson, 1985; Shotyk, 1988).

Processos ambientals que controlen la química orgànica i inorgànica de la torba en el registre de Rano Aroi durant els darrers 70.000 anys (Capítol 6)

En aquest capítol s'usen els resultats de la composició química orgànica de la torba (TN, TS, $\delta^{13}C$, $\delta^{15}N$, $\delta^{34}S$) i la determinació química elemental de la fracció mineral obtingut per ICP-AES (Al, Fe, Ti, Ca, Mg, Sr, Y, Zr, Ba, Sc, V, Cr, Mn, Cu, Zn, Cd) del testimoni ARO 06 01 (Secció 4.3.4). També s'ha analitzat la mida i composició dels grans minerals terrígens de nivells representatius mitjançant microscopia electrònica (Secció 3.3.3). Per relacionar els canvis geoquímics amb els canvis de vegetació ocorreguts a la conca s'aporten també els resultats del comptatge de 25 mostres de concentrats pol·línics (Secció 4.6.2).

Un anàlisis de components principals (PCA) ens permet resumir la variància associada al conjunt de dades d'ICP-AES, a 3 components principals significatius (Figura 6.1). El primer component (que explica el 40.8% de la variància) és definit per contribucions elevades d'elements litogènics (V, Al, Sc, Y, Ti, Zr) i alguns metalls (Cr, Cd, Cu). Aquest component es podria relacionar amb la deposició de pols mineral procedent dels sòls circumdants de la conca de drenatge. Elements com Al, Ti, Zr i Cu es troben fortament enriquits en sòls d'origen volcànic. Associacions semblats s'han interpretat, en torberes comparables, com entrades de contingut mineral per erosió dels sòls de la conca de drenatge (Muller et al., 2008b). Els elements mencionats solen estar presents en minerals de neo-formació, compostos organo-metàl·lics, en minerals primaris extremadament resistents i en fases minerals de mida de gra molt fi (10-30 μm). Així, aquest primer component és interpretat com una senyal de llarg termini del nivell base del flux del material terrigen inorgànic que arribaria a la torbera. Aquest procés ha d'estar lligat íntimament a l'evolució edafològica de la conca i ha de ser més intens en moments de major erosivitat dels sòls (per exemple, durant períodes de menor cobertura vegetal).

El segon component (que explica el 23.1% de la variància) està definit per les contribucions de Fe, Mn, Ba, Th, Ti i Zr. El Mn i Fe, són elements sensibles a canvis en les condicions redox, en certs nivells del registre de Rano Aroi, s'han descrit enriquiments en Fe per oxidació (Capítol 5). De totes maneres, no tot el Fe present a Rano Aroi és re-mobilitzat en condicions reductores i per tant, quan s'associa a altres elements immòbils que tenen un sol estat d'oxidació (Ti, Th, Ba, Zr), aquest element segueix essent bon traçador d'entrades de fracció mineral, al igual que el Mn. La majoria d'aquests elements formen part de minerals primaris, minerals de neoformació molt estables i, en el cas del Fe, de secundaris també molt estables en condicions aeròbiques. Els valors del PC2 al llarg del registre (darrers 70.000 anys) mostren un patró de pics que podrien interpretar-se com episodis puntuals de gran erosió degut a fortes precipitacions. Aquests episodis causarien un augment de escorrentia superficial i per tant l'entrada de partícules detrítiques de mida de gra més grollera (entre 30 i 600 μm segons les mesures del microscopi electrònic) que les partícules representades pel PC1 (mides).

El tercer component és caracteritzat per contribucions significatives positives de Ca, Sr i Mg (21.3% de variància explicada). Tots tres elements químics són extremadament mòbils en forma iònica, i poden ser transportats a la torbera en forma dissolta o en forma en grans minerals (Shotyk, 1988). Els valors del PC3 mostren valors més elevats en el període de dominància de vegetació tipus C_4 i en la fàcies D, representativa de fases d'oxidació de la torbera. Per això es pot apuntar que aquests elements indicarien estadis en què la torba hauria estat relativament mineralitzada, tal com ha estat corroborat també en altres registres de torbera (Gorham i Jahnsenss, 2005; Muller et al., 2008) . Tant el Ca, com el Sr o Mg, poden formar compostos orgànics molt estables i ser intensament bio-acumulats per la vegetació.

Tots tres components han estat relacionats amb la composició de la matèria orgànica de la torba. En primer lloc, el PC1 mostra que els valors més elevats estan directament lligats a una signatura isotòpica de $\delta^{13}C$ pesada, indicativa de dominància de vegetació tipus C_4. Els valors de $\delta^{13}C$ disminueixen progressivament amb el pas a la dominància del tipus C_3. El

registre pol·línic mostra que la fase dominada per C_4 és constituïda bàsicament per poàcies i molt poca presència d'arbres o arbustos el que podria indicar un sòl més descobert i susceptible a ser erosionat. D'altra banda, en el tram dominat per vegetació tipus C_3, les asteràcies, ciperàcies i espores de falguera prenen importància en el registre pol·línic. El paisatge que suggereix aquesta combinació de pol·len és més tancat, segurament afavorint major edafogènesis i menor erosió del sòl, el que encaixa amb els valors baixos de PC1 (Figures 6.2 i 6.3). En canvi, els pics de PC2 (entrades de material detrític) afectarien a la torbera independentment de la seva composició florística. Aquests períodes d'erosió intensa, correspondrien a episodis de precipitació concrets que actuarien afavorint la meteorització i el transport de partícules grolleres. El cicle del nitrogen també estaria relacionat amb els canvis de PC1, mostrant valors més elevats de TN i $\delta^{15}N$ en el període de dominància de la vegetació de tipus C_4. Aquests valors més alts tant del contingut total de nitrogen com dels seus valors isotòpics s'han interpretat com a variacions en la productivitat o desnitrificació del sistema.

El cicle del sofre també sembla estar directament relacionat amb el primer component. La signatura isotòpica d'aquest element indicaria que seria principalment d'origen marí, concretament mescla entre aerosols de sulfat procedents de la sal marina i els aerosols de sulfat procedent d'emissions orgàniques com el dimetilsulfur (DMS) (Calhoun i Bates, 1989; Sihna et al., 2009; Figura 6.4). Els resultats de $\delta^{34}S$ i sofre total (TS) indiquen que el cicle del sofre depèn directament del tipus de vegetació de la mollera i mostren que el registre de Rano Aroi estaria afectat periòdicament per processos de sulfatoreducció per l'enriquiment en $\delta^{34}S$ i la pèrdua de sofre (TS).

El conjunt de dades orgàniques i inorgàniques descrites en els Capítols 5 i 6 ha permès deduir una evolució ambiental al llarg dels darrers 70.000 anys, que s'exposa en detall en el capítol 7.

Evolució ambiental de Rano Aroi al durant els darrers 70.000 anys: Interaccions entre la torbera, la conca i el clima (Capítol 7)

En aquest capítol es detalla l'evolució temporal de la mollera, recalcant les interaccions entre la cubeta, la conca i la seva resposta a la configuració climàtica regional. En particular els canvis ambientals a la illa de Pasqua es relacionen amb (1) la posició de la Zona de Convergència Intertropical (ITCZ), ja que aquesta controla directament també la posició de la Zona de Convergència Subtropical (SPCZ), portadora de la precipitació a la illa; (2) la posició dels vents de l'Oest (SW), ja que contribueixen en el transport de tempestes que arriben a l'illa; (3) les temperatures regionals i (4) el nivell del mar, ja que nivells eustàtics baixos podrien haver influït en el nivell freàtic de l'illa i en la generació de tempestes d'origen convectiu (Figura 7.1).

Durant l'Estadi Isotòpic Marí 4 (MIS 4, 70-59.4 kyr BP) les dades biogeoquímiques indiquen que la torbera es va mantenir estable, dominada per vegetació de tipus C_4 amb un percentatge molt elevat de poàcies. Ambdós factors i les característiques climàtiques descrites a la regió (temperatures fredes i nivell del mar baixos) suggereixen que es tracta d'un episodi fred i no especialment humit a l'illa (Kaiser et al., 2005; Grant et al. 2012).

Aquest escenari climàtic regional va comportar un constant i elevat flux d'elements litogènics i metalls de la conca cap a dins de la producte de l'elevada erosivitat dels sòls circumdants.

El MIS 3 (60-27.8 cal kyr BP) pot dividir-se en dos estadis diferenciats. La primera fase (entre 60 i 42 kyr BP) és caracteritzada per episodis humits abruptes amb major entrada de terrigen associat a les Facies C, com a conseqüència de una major precipitació a l'illa. L'inici del MIS 3 va comportar un ascens de les temperatures regionals i del nivell del mar, sobretot a partir dels 62-61 kyr BP. Registres climàtics sensibles a la posició de la ITCZ mostren que, cap els 59 kyr BP la ITCZ es trobava en la seva localització més austral (Peterson et al., 2000). Tot i que la ITCZ no és directament la responsable de les tempestes que arriben a l'illa, sí que és determinant de la posició de la SPCZ. Aquesta darrera estructura és el cinturó de baixes pressions que genera els ciclons que arriben al Pacífic Central empesos pels vents de l'Oest meridionals (SW). Al llarg de la transició entre MIS 3 i MIS 4 aquesta configuració climàtica regional (SPCZ al sud, SW al nord) detonaria l'inici d'episodis humits a l'illa. Aquests períodes amb major precipitació estan representats en la geoquímica del registre del Rano Aroi per valors elevats de Th, Fe, Mn, Ba, Ti i Zr, tal com resumeix els canvis en el segon component principal del Capítol 6 (PC2). Les característiques tèrmiques d'aquest període (temperatura més elevada; Kaiser et al., 2005) i hídriques (mes precipitació) van forçar probablement el canvi de vegetació que mostra la senyal de $\delta^{13}C$ i el diagrama pol·línic obtingut. Les herbàcies i palmeres que semblen dominar el paisatge al voltant de Rano Aroi es veurien progressivament desplaçades per l'expansió de plantes compostes, segurament arbustives, falgueres i ciperàcies, com mostra un percentatge més elevat de pol·len d'aquestes famílies (Figura 6.2). Aquest viratge fou probablement degut al canvi climàtic que suposà l'arribada del MIS 3, encara que també es pot especular que fos degut a l'arribada d'alguna espècie nova (de tipus C_3), capaç de colonitzar les zones humides de l'illa. El canvi de paisatge també comportà amb un canvi en la evolució de sòls més evolucionats. La vegetació dominant en aquest període sembla haver contribuït a la formació d'un sòl més evolucionat, menor erosió i un menor transport de partícules de material terrigen fines cap a dins de la torbera. A aquest canvis també pot haver contribuït l'establiment d'un cinturo de vegetació emergent en el litoral.

A finals del MIS 3, la mollera del Rano Aroi pateix una dessecació que resulta en l'exposició aèria de la superfície de torba de 39 kyr BP d'edat. La torba que queda per sota mostra evidències d'oxidació, com les relacions elevades de Fe/Ti i s'enriqueix en elements com el Ca, Sr o Mg (Facies D). L'episodi de sequera va succeir a l'illa durant un període posterior als 40 kyr BP i no ha estat possible determinar exactament llur duració ja que, segurament, hauria arribat a causar l'erosió de part de la torba acumulada anteriorment. Les condicions àrides entre els 39 i els 31 cal kyr BP i que varen comportar probablement una baixa precipitació a l'illa també s'han descrit en altres zones del continent Sud Amèrica i a latituds semblants (Lamy et al., 1998; Stuut i Lamy, 2004). Aquesta sequera es podria atribuir a una posició centrada al sud dels vents de l'Oest meridionals (SW) i a un progressiu descens del nivell del mar. L'edat de recuperació de l'acumulació a la torbera és incerta ja que, després d'una pausa temporal, els primers nivells que es van acumular possiblement van incorporar carboni antic.

El MIS2 (27.8-14.7 kyr cal BP) i l'Últim Màxim Glacial (LGM en les seves sigles en anglès) es va caracteritzar per una reducció de la temperatura i una caiguda del nivell del mar a nivell global (Grant et al., 2012). Al registre de Rano Aroi presenta evidències de l'ocurrència d'episodis humits als 20.9-19.5 i 16.4 cal kyr BP a la Illa. Aquesta elevada precipitació segurament va ser la causa pel qual la torbera va romandre activa durant aquest període (tot i que amb taxes d'acumulació molt reduïdes). Aquestes pluges serien el resultat de la intensificació i posició dels vents de l'Oest meridionals (SW), que es trobarien en la seva posició més boreal al llarg del darrer cicle glacial (Lamy et al., 1998). El registre de Rano Aroi mostra taxes d'acumulació molt elevades durant el període glacial tardà (17.5-11.7 cal kyr BP, Figura 7.1) alhora que el clima es va anar tornant progressivament més càlid. El nivell del mar va ascendir després del LGM presentant un augment molt ràpid cap als 14 cal kyr BP. Aquesta és l'edat en què les taxes d'acumulació a Rano Aroi van ser més elevades. La pujada eustàtica juntament amb la de les temperatures van contribuir a unes tasses d'acumulació més elevades a la torbera de Rano Aroi, potser també condicionades per una major ocurrència de tempestes d'origen convectiu.

L'inici de l' Holocè (11.7 kyr BP fins al present) va ser humit, però va acabar esdevenint un període relativament sec a la illa, com ha estat descrit a través del registre sedimentari de Rano Raraku (Sáez et al., 2009). A Rano Aroi també es registra aquesta tendència, bruscament interrompuda per un episodi de major precipitació, als 5.8 cal kyr BP. A partir dels 2.5 kyr BP es varen registrar de nou condicions humides. A l'edat de 1.3 cal kyr. BP (655 AD), es registren elevats valors de $\delta^{13}C$ i una caiguda del C/N el que suggerira una major mineralització de la matèria orgànica i presència de plantes de tipus C_4. Aquest episodi ha estat relacionat temptativament amb una possible pertorbació ambiental causada per l'arribada de l'home a l'illa. De totes maneres també pot estar registrant els efectes de l'anomalia climàtica medieval (1205-705 yr cal BP) que va suposar condicions àrides i menys pluviositat a les illes de la Polinèsia del Pacífic oriental (Nunn, 2007).

Variabilitat en la precipitació a escala mil·lennial a l'Illa de Pasqua (Pacífic Sud) durant el MIS 3: Tele-connexions inter-hemisfèriques amb els episodis freds de l'Atlàntic Nord (Capítol 8)

En aquest capítol es pretén estudiar amb detall les oscil·lacions de precipitació registrades a Rano Aroi durant el MIS 3. Això permetrà contribuir en el coneixement de la variabilitat climàtica d'aquest període, caracteritzat per l'alternació d'estadials i interestadials. Per tal d'aconseguir aquests objectius el registre de Rano Aroi s'ha comparat amb registres del Circum-Pacífic, de l'Atlàntic tropical i també amb seqüències d'altes latituds, com les de gel de Groenlàndia i Antàrtida. A més, els episodis amb canvis en el règim de pluja s'han relacionat amb canvis en el gradient de Temperatura Marina Superficial (SST) equatorial calculat entre dos registres marins prèviament publicats.

Degut a la discontinuïtat descrita anteriorment (Capítol 5 i 6) durant la segona meitat del MIS 3, i per tal d'estudiar la naturalesa dels episodis humits dels qual es té un bon control temporal, el període de temps d'estudi d'aquest capítol ha estat limitat entre els 65 i els 38.5 kyr BP. El PCA amb el subconjunt de les dades de TC, TN, $\delta^{13}C_{res}$, Ca, Fe i Ti per aquest període de temps mostra que els dos primers components són significatius i interpretables

de la mateixa manera que s'ha fet en el Capítol 5. El segon component resulta íntegrament dominat per la contribució positiva de Ti, TN i negativa de $\delta^{13}C_{res}$. Aquestes variables indiquen una major làmina d'aigua (majors valors de Ti per entrada de material detrític i de TN per major contribució de matèria orgànica d'origen aqüàtic, menor $\delta^{13}C_{res}$ per fraccionament en condicions humides o canvis en la relació C_3/C_4). Per aquest motiu l'eix PC2 pot ser usat com a índex de disponibilitat hídrica de manera que valors més elevats representaran major precipitació.

En base a les oscil·lacions del PC2 es van poder definir set períodes d'elevada precipitació entre els 65 i els 38.5 kyr BP i que han estat anomenats Ar1-Ar7. Tres d'ells (Ar3, Ar5, Ar7) són els més prominents, amb un inici abrupte i un final progressiu, i presenten duració mitja aproximada de 2000 anys. Els altres quatre episodis (Ar1, Ar2, Ar4, Ar6) també presenten un inici abrupte però una durada i intensitat menors. La comparació del PC2 de Rano Aroi amb registres de gel de Groenlàndia (Svensson et al., 2008) indica que els episodis majors van succeir de forma sincrònica als Heinrich estadials 6, 5a i 5 ocorreguts a l'hemisferi nord (aproximadament als 60, 54, 45 kyr cal BP respectivament). A més, els episodis menors coincidirien amb estadials de Dansgaard-Oeschger (DO), d'intensitat menor. Aquests períodes estadials varen correspondre a episodis de més pluja a l'Illa de Pasqua però a episodis secs en les latituds tropicals i subtropicals de l'Hemisferi Nord (Figura 8.3). Aquest patró ha estat definit en diversos registres com bé són els obtinguts en la Cova de Hulu (Xina, 32°N, Wang et al., 2007), a la conca de Cariaco (Veneçuela, 10°N, Peterson et al., 2000) o el mar de Sulu (Filipines, 8°N; Rosenthal et al., 2008). En canvi, els períodes estadials coincideixen amb episodis humits als tròpics de l'Hemisferi Sud com ha estat descrit a formacions de travertins del Nord de Brasil (Wang et al., 2007), en un registre de torbera a Austràlia (17°S, Muller, 2008a) o a la costa Atlàntica de Sud Amèrica (3°S, Arz et al. 1998). Aquest patró asimètric entre hemisferis en la distribució de la precipitació ha estat explicat per la migració de la ITCZ. Durant els stadials del Atlàntic Nord, la ITCZ va migrar en direcció sud mentre que en interestadials quedava centrada al nord de l'equador (Clement and Peterson, 2008).

Diversos mecanismes han estat proposats per explicar aquestes tele-connexions. Alguns models suggereixen un major flux de calor de sud a nord durant expansions de gel al Atlàntic Nord que culminen amb una redistribució de la cèl·lula de Hadley (Chiang i Bitz, 2005). Altres propostes que ressalten mecanismes atmosfèrics per la transmissió d'aquests canvis climàtics donen especial importància al transport d'humitat i temperatura entre els oceans Atlàntic i Pacífic mitjançant l'istme de Panamà via ones de Rossby (Dong i Sutton, 2002; Zhang i Delworth, 2005). Els models climàtics que reforcen aquests processos proposen una configuració del Pacífic Sud durant els períodes estadials anàloga a les condicions El Niño actuals (Niño-like, Dong i Sutton, 2002). Per altres models, el mecanisme transmissor més important és l'oceànic mitjançant l'ajustament baroclínic. Segons aquesta proposta, la reducció de la circulació termohalina durant els estadials va derivar en canvis en la termoclina del Pacífic sense invocar una relació directa amb canvis anàlegs als diferents estadis del fenomen de l'ENSO (Huang et al., 2000; Timmermann et al., 2005).

A Rano Aroi, la pluja no pot ser atribuïda a una influència directa de la ITCZ, ja que la precipitació deriva de les tempestes generades per la SPCZ que es desplaça cap a l'est amb

l'ajut dels SW (Junk i Claussen, 2011). Si a l'Illa de Pasqua es registren majors precipitacions quan la ITCZ es troba en la posició més austral significa que la migració cap al sud comporta a l'hora una intensificació o un desplaçament cap a l'est de la SPCZ, fent d'aquesta manera que arribin un major percentatge de tempestes. Aquest fet és d'especial rellevància ja que, tot i que múltiples treballs versen sobre els canvis en la ITCZ, no existeixen registres sedimentaris per aquest interval de temps capaços de descriure la dinàmica de la SPCZ. Per entendre el patró oceànic del Pacífic equatorial durant aquests estadials, el registre de Rano Aroi s'ha comparat també amb el gradient de SST equatorial (Figura 8.2). El resultat de la comparació mostra que durant períodes de major precipitació a l'illa, el gradient és marcadament menor, el que significa una circulació menys intensa, un encongiment de l'Anticicló del Pacífic Sud (SPA) i per tant una configuració del Pacífic análogues a les condicions d'un event El Niño.

A més , la relació entre els episodis plujosos i els processos climàtics a altes latituds també és remarcable. Segons varis autors, el desplaçament cap al sud de la ITCZ i el conseqüent augment de pressió sobre l'Hemisferi Sud provocaria una intensificació dels vents de l'Oest meridionals, fet que també contribuiria a una major precipitació sobre l'illa pel transport de les tempestes generades a la ITCZ (Toggweiler et al., 2006; Anderson i Carr, 2010).

Els períodes estadials que suposen reduccions dràstiques de temperatura a l'Atlàntic Nord corresponen a episodis d'escalfament tèrmic i fusió de gel a l'Antàrtida, tal com ha estat explicat mitjançant els mecanisme del "balancí" (seesaw). El retrocés de gel antàrtic juntament amb la intensificació dels vents de l'Oest meridionals contribueixen a una formació més intensa de aigües intermèdies antàrtiques (AAIW). Registres recuperats a la costa de Nova Zelanda mostren que els períodes de major formació d'aquesta massa d'aigua també es correspondrien amb els episodis de major precipitació a Rano Aroi (Pahnke i Zahn, 2005; Skinner et al., 2010).

Capítol 9 i Conclusions

En aquesta tesi s'han obtingut resultats de tres tipus:

1. S'ha caracteritzat la mollera de Rano Aroi i s'han aportat contribucions rellevants en el coneixement de la dinàmica de les torberes subtropicals o tropicals particularment pel que fa a la biogeoquímica.

- S'han descrit 4 facies en funció de la composició dels restes vegetals, humificació, color i geoquímica i l'observació de frotis al microscopi òptic

- S'ha obtingut un model cronològic robust.

- S'han reconstruït importants canvis en la vegetació de la torbera de Rano Aroi i la seva conca s'han reconstruït a partir de la senyal de $\delta^{13}C$ i del contingut pol·línic. Durant el període en què la signatura isotòpica de la torba indica que està composta per plantes de tipus C_4 el registre pol·línic mostra una completa dominància de

poàcies i la presència de palmeres. En canvi, les asteràcies, ciperàcies i falgueres esdevenen més abundants en el període en què la senyal de $\delta^{13}C$ indica dominància de plantes de tipus C_3.

- Les condicions de redox en el moment d'acumulació de la torba i diagènesis inicial s'han pogut reconstruir mitjançant la senyal de $\delta^{15}N$, que és capaç de registrar canvis en productivitat i processos de desnitrificació. La ocurrència de processos bacterians com la sulfato-reducció s'han pogut evidenciar amb la combinació de les mesures de sofre total (TS) i $\delta^{34}S$. Aquests darrer paràmetre indica un origen marí del sofre present a la mollera, i juntament amb el TS donen informació sobre el cicle d'aquest element.

- A partir de canvis en la composició geoquímica de la fracció inorgànica (mitjançant la combinació dels nivells de V, Al, Sc, Y, Cr, Cd, Ti, Zr i Cu) s'han reconstruit les variacions en el flux de material terrigen que s'incorporaria a la torbera, probablement per transport eòlic i degut al grau d'erosivitat del sòl.

- Els episodis de major precipitació han pogut ser reconstruïts per l'associació de Fe, Mn, Th, Ba, Zr, Ti així com per elevats valors de TN i lleugers de $\delta^{13}C$.

- Una paleo-superfície definida de 39 cal kyr BP d'edat és indicativa d'un període de sequera recurrent hauria succeït a la illa. Aquesta perllongada sequera va permetre l'exposició, oxidació i probablement erosió de part del registre. La mineralització és pot traçar per l'enriquiment en Ca, Sr, Mg (i Fe, Cu, Mn en menor mesura).

- En base a la caracterització biogeoquímica de la torbera s'ha definit que l'evolució ambiental de l'illa, la qual comportaria l'alternança entre tres estadis diferents: (1) un nivell de condicions de base, (2) un de torbera inundada, (3) i un de sequera i oxidació.

2. S'ha aportat una nova aproximació a l'evolució paleoambiental de la illa i en particular de la mollera de Rano Aroi

- Durant el MIS 4 les condicions hídriques i ambientals varen ser estables. La vegetació de la conca consistia en amplis prats de Poaceae. La formació de la torba es produïa per acumulació de restes de plantes de tipus C_4. Aquest escenari s'emmarcava en un Pacífic Sud de temperatures fredes i nivell del mar baix.

- L'inici del MIS 3 va estar caracteritzat per l'ocurrència d'episodis de forta precipitació, els principals dels quals van succeir al voltant dels 60, 52 i 42 kyr BP. Durant aquest període, les creixents temperatures i l'elevada precipitació varen afavorir l'establiment d'Asteraceae (presumiblement petits arbres i arbustos) formant possiblement petites clapes de bosc. Alhora, la torbera va concentrar una major presència de falgueres i ciperàcies als voltants. La vegetació de tipus C_3 va colonitzar la torbera, tot produint un canvi en la isotopia de carboni present fins a dia

d'avui. El final del MIS 3, es va ser caracteritzat per un llarg període sec situat en algun moment entre els 39 i els 31 kyr cal BP.

- A l'inici del MIS 2, la làmina d'aigua de la torbera es va recuperar i la acumulació de torba es va reactivar, però amb taxes d'acumulació molt baixes, presumiblement degut les baixes temperatures. Les evidències de desglaciació són concordants amb el registre de Rano Raraku, als 17. 5 cal kyr BP.

- L'Holocè és caracteritzat regionalment com a període àrid, de precipitació reduïda, el que seria concordant amb el registre de Rano Aroi. El període àrid es veu interromput puntualment per un episodi humit també registrat a Rano Raraku als 5.8 kyr BP.

3. L'estudi dels processos ambientals ha permès realitzar contribucions significatives en la paleoclimatologia del Pacífic Central pels darrers 70.000 anys.

- Al llarg del MIS 3, set episodis humits van succeir com a resultat de l'expansió cap a l'est de la SPCZ, la migració cap el sud de la ITCZ i un encongiment del Anticicló del Pacífic del Sud. Aquests episodis coincidirien temporalment amb els stadials definits a l'Atlàntic Nord, el que revelaria una estreta tele-connexió entre altes i baixes latituds en la variabilitat climàtica del MIS 3.

- Els episodis humits de Rano Aroi han estat correlacionats amb períodes de gradient E-W de SST reduït en el Pacífic Equatorial, suggerint una configuració anàloga a la de El Niño a dia d'avui.

- Els canvis en el règim de precipitació també serien consistents amb els canvis de circulació d'altes latituds succeïts a l'Hemisferi Sud. Durant els estadials produiria una formació d'aigua intermèdia antàrtica (AAIW) més intensa directament relacionada amb la intensificació dels vents de l'Oest meridionals.

-

CONTENTS

CHAPTER 1

INTRODUCTION

The Pacific Ocean hosts the Earth larger water masses, covering a surface of 165 million km^2 over both hemispheres and operating as a main actor modulating global climate (Emery and Meincke, 1986). Moreover, it contains, among other features, the first planetary upwelling system and the largest equatorial current; and acts as a predominant contribution to Antarctic circulation (Rose et al, 2010, Sigman et al., 2010). The most prominent interannual climate variation on Earth, the El Niño-Southern Oscillation (ENSO) climate phenomena, consists in fluctuations on oceanic and atmospheric circulation from the Southern Pacific circulation (McPhaden, 2006). Because main climatic processes underwent cyclic oscillations on millennial and orbital timescales, the Late Pleistocene and Holocene paleoclimatic studies over the Southern Pacific become key contributions to understand oceanic and atmospheric long-term feedbacks and interhemispheric teleconnections (Blunier et al., 2001; Oppo et al., 2003; Pahnke et al., 2003; Clement and Cane, 2008; Pena et al., 2008; Leduc et al., 2009). Due to the isolated location of Easter Island, its recent palustrine sedimentary sequences are the only inland records capable to reflect the timing and nature of the major oceanographic and atmospheric changes affecting the southeast Pacific. This is because Easter Island is situated thousand of kilometers away from continental and marine potential paleoclimatic records (Lamy et al., 1998; Baker et al., 2001; Moy et al., 2002; Rosenthal et al., 2003; Wang et al., 2007; Kaiser et al., 2008; Muller et al., 2008a). Climate of Easter Island is controlled by large-scale atmospheric and oceanic patterns, and it is not biased by the continental effects on local convection as circum Pacific sites. Several works have been done on lacustrine sedimentary cores using pollen and diatoms as indicators to determine timing of human arrival and deforestation (Flenley and King, 1984; Flenley et al, 1991; Dumont et al., 1998, Cañellas-Boltà et al., 2013). Other approaches describe the late Quaternary paleoclimatic changes using sedimentological, mineralogical, geochemical and biological proxies together (Flenley et al., 1991; Azizi and Flenley, 2008, Sáez et al., 2009; Cañellas-Boltà, 2012). Despite most of the paleoenvironmental works have been centered on the Rano Raraku and the Rano Kao lakes, the Rano Aroi mire constitutes an extraordinary archive storing Late Pleistocene and Holocene information (Flenley et al., 1991). The later site combines hydroclimatic sensitivity, a strong signal of vegetation changes and a large peat sequence (14 meters of peat recovered but without reaching its base). The Rano Aroi environmental evolution has been driven by the interaction of the responses to climate, ecological autogenic processes and, in very recent times, the effects of human footprint. As the tropical and subtropical mires have received traditionally much less attention (Page et al., 2004 and 2006; Dommain et al., 2010) than the boreal to temperate ones, the multi-proxy study of Rano Aroi mire constitutes a novel contribution on Southern Hemisphere low latitude quaternary peat science.

This PhD Thesis presents the oldest, to date, long-term peat record from the Southern Hemisphere, tracking environmental changes for the last 70 kyr BP. The Rano Aroi dataset sensibly contributes to develop the use of a wide type of biogeochemical proxies to determine environmental changes on tropical peatlands. Inorganic geochemistry (trace and major elemental concentrations) is combined together with the use of bulk peat stable isotopes and biological proxies to interprete the dominant biogeochemical processes occurred. Peat biogeochemistry allowed us to assess the timing and nature of the processes that drive changes in peat composition as vegetation type, detritic input or water table oscillations. Finally, the Rano Aroi climate record and events of the last 70 kyrs BP have been also correlated with marine and continental records located in the tropical and subtropical Pacific and Atlantic to build an integrative regional picture of late Quaternary climate.

MIRES AND PEATLANDS

1. 1. Peat and peatlands: a general overview

1. 1. 1 What is peat?

Peat is an extremely carbon rich soil that consists of at least of 30% (dry mass) dead organic material formed by a limited decay of plant remains (Joosten and Clarke, 2002). The formation of peat occur when plant production is higher than decomposition rates and results in a positive carbon balance. Peat accumulation takes places in ecosystems known as peatlands or mires and is mainly controlled by water level, temperature and plant composition (Joosten and Clarke, 2002). While a peatland is an area with a peat layer on its surface, a mire is a type of peatland where currently new formed peat is accumulating.

Water is a very relevant factor on peat formation processes, thus on flooded areas or saturated soils, water leads to (1) decrease temperature and (2) diminish oxygen, two mechanisms that inhibit decomposition and decline the rate of organic matter decay (Charman, 2002, Joosten and Clarke, 2002). For this reason, hydrological characterization of peatlands has been traditionally used to classify them. The peat botanical assemblage is also an important factor determining its formation, as some plant species are more inclined than others to contribute to peat formation because of different propensity to decay (Joosten and Clarke, 2002).

Two parts can be distinguished on most of peat forming ecosystems. The upper layer or **acrotelm**, consists in a 10 to 50 cm thick layer which has lower porosity and higher hydraulic conductivity. Usually it presents aerobic conditions and therefore the rate of decomposition is relatively high. The deep part or **catotelm** is usually anaerobic, with low hydraulic conductivity and low rates of organic matter decay.

It is estimated that 3% of land area on Earth (approximately 4 million km^2) is occupied by peatlands (Figure 1.1). Despite covering a relative reduced surface, the role they play in the biogeochemical cycles of major and trace elements is important on a global scale. Moreover, mires are crucial for the global carbon cycle because they act as a long-term carbon reservoir

and sink, storing about one third of the global soil carbon (Joosten and Clarke, 2002), up to some 550 Gt C (Jackson and Charman, 2010), but being at the same time an active source of greenhouse gases such as methane. Mires arise as an essential key to understand global climate because of the importance of their expected and unexpected feedbacks over carbon cycle under global change.

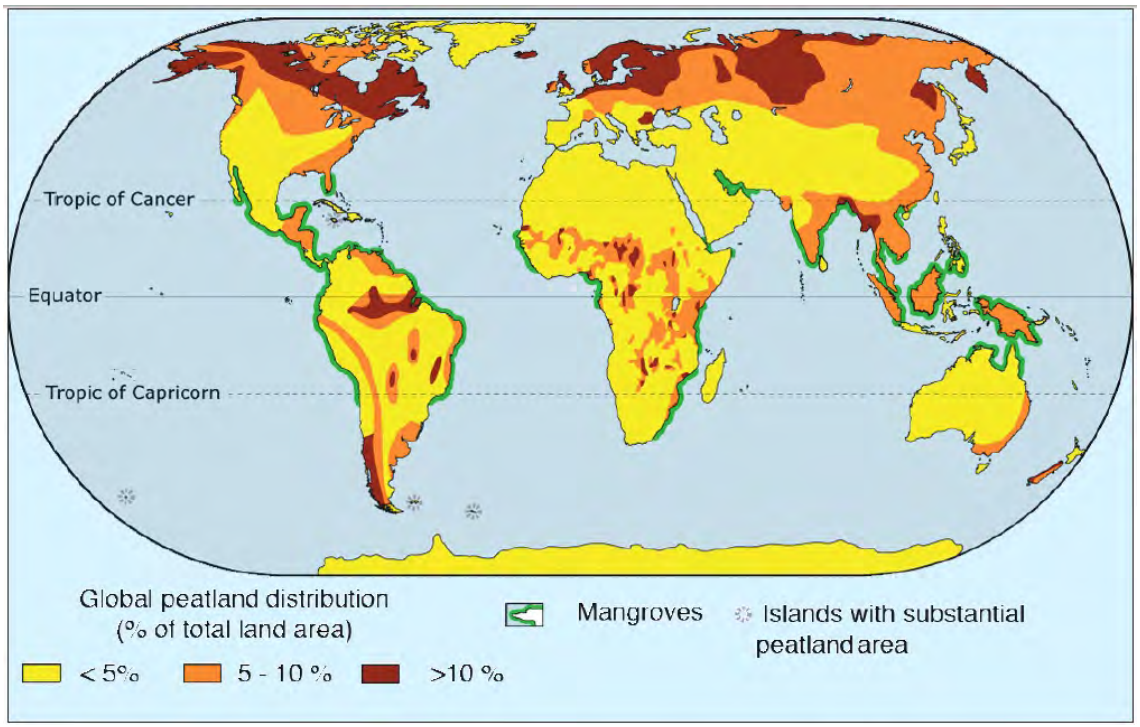

Figure 1.1. Global peatland distribution (Jackson and Charman, 2010).

1. 1. 2 Mire and peatland types

There are many different ways of classifying peatlands and mires, depending on the aims of classification and the large heterogeneity of landscapes that are capable to accumulate peat. A widely used traditional approach has distinguished between fens and bogs: (1) **Fen** is used to define peatland normally situated in depressions, and fed by groundwater (geogenous). (2) **Bog** is used to describe a peatland that is fed exclusively by rainwater (ombrogenous) and is commonly formed as a raised surface above the landscape. A different classification, but also directly related to water origin, separates peatlands following its trophic state, pH, nutrient availability and characteristic plant species as ecological mire types (Joosten and Clarke, 2002).

When considering the role of hydrological processes a hydrogenetic classification can be performed. Among the mires that develop in horizontal surfaces in the landscape a distinction can be made between **terrestrialisation**-mires when peat develops in open water (for example from a lake) and **paludification**-mires when peat develops over a wetting mineral soil (Joosten and Clarke, 2002; Rydin and Jeglum; 2006). This first classification can be expanded considering different hydrogenetic types depending on water level and water-flow (Table 1.1). For example, terrestrialisation mires can be divided into **schwingmoor** mires

(peat accumulated as floating mats) or **immersion** mires (peat accumulated underwater). Paludification mire can be classified in: (1) **Water rise** mires or (2) **Flood** mire types. Water rise mires consist in peatlands where water level rises over a drier surface very slowly avoiding open water formation. The rising water level can be supplied by a gradual increase of water flow, by sea level rise, or by the formation of stagnating layers in the soil (from autogenic or allogenic origin). On the other hand, **Flood** mires are other paludification mires, located in areas that are periodically inundated by fresh, brackish or marine water (Table 1.1).

	Level water level mires			
Peat formation strategy	**Schwingmoor**	**Immersion**	**Water rise**	**Flood**
Water supply	Continuous	Mostly continuous	Small	Periodic
Mire slope	None	None	None	None/small
Internal water storage	Large	Mostly large	None	Small/large

Table 1.1. Hydrogenetic classification of mires that develop in horizontal landscapes (Joosten and Clarke, 2002). Main characteristics (water supply, mire slope, internal water storage) are detailed. All these mire types can be ombrogenous (fed by rain water) or geogenous (fed by sea water or groundwater).

When the mires cover a slope surface and the water is lost by lateral flow (retarded by peat itself) they can be classified as (Table 1.2): **Surface flow** mires (where water loss and oxygenation and enhanced decay occurs periodically), **acrotelm** mires (that accumulate plant remains with reduced ability to decompose and peat with a big water storage coefficient that guaranties deep peat layers permanently saturated even during oscillating water supply), or **percolation** mires (with large water supply and constant water level) (Joosten and Clarke, 2002).

	Inclining water level mires		
Peat formation strategy	**Surface flow**	**Acrotelm**	**Percolation**
Water supply	Frequent	Frequent	Continuous
Mire slope	Small/large	Small	Small
Internal water storage	Very small	Rather large	Large

Table 1.2. Hydrogenetic classification of mires that develop in sloping surfaces (Joosten and Clarke, 2002). Main characteristics (water supply, mire slope, internal water storage) are detailed. All these mire types can be ombrogenous (fed by rain water) or geogenous (fed by sea water or groundwater).

1. 1. 3 Tropical and subtropical peatlands

Because larger peatland areas are found in boreal latitudes of the Northern Hemisphere such as Canada and Alaska and Northern Russia they have been traditionally more studied than temperate to tropical ones (Jackson and Charman, 2010; Page et al., 2010). Nevertheless, tropical peatlands cover around 11% of global peatland area (Weiss et al., 2002; Page et al., 2010), but represent 17 to 19% of global peat C pool (Rydin and Jeglum, 2006). The most important tropical mires are found in Central Africa, South-East Asia and Amazonia basin among other sites of Caribbean, Central and South America. The South-East Asia peatlands are by far the largest ones, consisting the 57% of total tropical peatland surface. All of them are on areas with high precipitation rates and a topography that facilitates a poor drainage,

permanent flooding and the soil acidification (Figure 1.1). Due to the biased knowledge between high and low latitude mires, sometimes the "conventional" classification is difficult to strictly apply over the tropical ones. Floating meadows and different types of fen on floodplains or lake edges occupy large areas of central Africa, SE Asia and Amazonia (Figure 1.2), but the most relevant mire type in terms of thickness and stored carbon are the swamp forests (Figure 1.3).

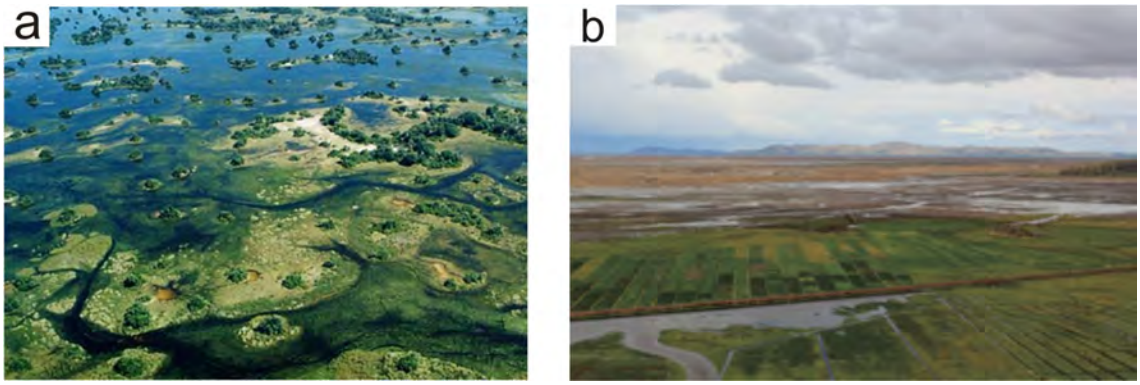

Figure 1.2. a) Tropical flood plain peat at Okavango delta (Botswana) (Photo by Russell Weston) b) Wetlands around lake Titicaca (Bolivia) (Photo by Darren Alff).

Forested mires cover, for example, very extensive lowland areas in Malaysia and Indonesia (Page et al, 2010, Dommain et al., 2011) and are a hotspot area under severe risk of rapid degrading due to increasing population and land use changes (Figure 1.3) (Page et al., 2002).

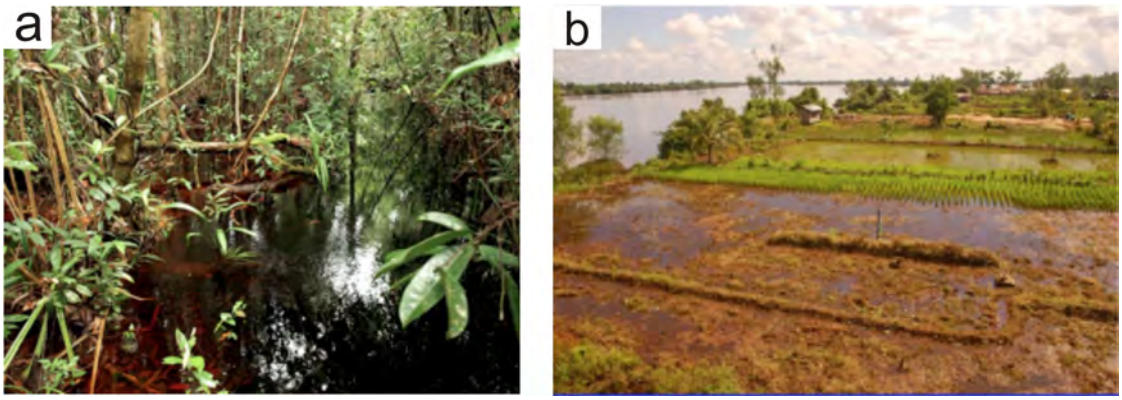

Figure 1.3. a) Tropical peat swamp forest (Kalimantan, Indonesia) (http://vrconservation.org) b) Drained and degraded peatlands for agricultural use (Kalimantan, Indonesia) (photo by Rene Dommain).

On the high altitude lands of the tropics, however, mountain peatlands are also present as moss or sedge blankets, showing a wide range of hydrological and trophic status depending on altitude, water supply and location.

1.2. Chemical processes within peat.

1. 2. 1. pH and Redox conditions

Redox and pH state are main relevant factors in conditioning peat or soil chemical reactions. In turn, these parameters are depending on peat producers (vegetation type) and water origin and hydrochemistry.

On peatlands, pH level is commonly low, acid or slightly acid, due to release of organic acids through organic matter decay (Charman, 2002; Joosten and Clarke, 2002). Under humid climates -where mires normally develop- peat acts as a sink for protons, therefore major base cations (Na, K, Ca, Mg) are removed from solid phases by leaching. Ombrotrophic mires show lower pH values than mires fed by groundwater (Figure 1.4). Several internal physicochemical processes contribute to define peat pH including cation exchange in the water, because peat and some peatland plants have a high cation exchange capacity (CEC) (Clymo, 1983). For example, *Sphagnum* itself provides the main source of hydrogen ions in a lot of peatland systems through cation exchange. Carboxyl groups (COO^-) act as exchange sites and can constitute between 10 and 30% of *Sphagnum* dry mass. In ombrotrophic bogs the rate of terrigenous minerals is low and not enough to consume the protons generated by organic acids. On minerotrophic mires, the hydrolysis of added minerals will raise pH, especially if calcite or dolomite minerals is provided (Figure 1.4). The acidity gradient has been shown to characterize plant abundances and also plant community occurrence in peatlands (Dierssen, 1982; Glaser, 1987; Rydin and Jeglum, 2006).

In water saturated peat, oxygen diffusion is low and it is rapidly depleted, which leads to anaerobic conditions in depth (Charman, 2002). Moreover, organic matter becomes an important source of electrons in soil when organic matter decay takes place (Chesworth et al., 2006). In ombrotrophic mires, Eh varies independently of the very constant low pH, sometimes reaching the boundary for CH_4 generation (Figure 1.4) (Cheswroth et al., 2006). On the other hand, in minerotrophic mires, Eh changes result more complex. The main reason is that the relevant addition of Fe-containing minerals tends to produce a redox profile close to the Eh-pH stability boundary of the ferric-hydroxide (Figure 1.4) (Chesworth et al., 2006). Fe is the most abundant element with more than one valence, and therefore undertakes changes that can set the overall redox state of the organic soil (Chesworth et al., 2006). Although it has been shown than several elements can be immobile in peat, changes in redox potential -specially driven by watertable oscillations- can be the most important mechanisms in determining the distribution of heavy metals (Damman, 1978; Clymo and Hayward, 1982; Damman et al., 1992).

Different anaerobic conditions together with pH changes determine the chemical transformations that take place as a result of bacterial activity. In moderate anaerobic conditions and after oxygen consumption, nitrate (which implies a loss of N, releasing N_2O to the atmosphere), manganese and iron reduction take place (Reddy and D'Angelo, 1994; Rydin and Jeglum; 2006). When redox potential decreases, sulfate reduction is carried out, with resulting products as hydrogen sulfide (H_2S), pyrite (FeS) or S bounded to organic compounds. Lastly, under extreme anaerobia, carbon dioxide reduction can occur and methane (CH_4) is

produced (Reddy and D'Angelo, 1994). Plants present morphological adaptations to overtake conditions of anoxia. Some plants grow roots consisting in 60% pore space to allow oxygen diffusion; other species develop very shallow root systems, while other plants only occupy the drier microsites (Wheeler, 1999; Rydin and Jeglum; 2006).

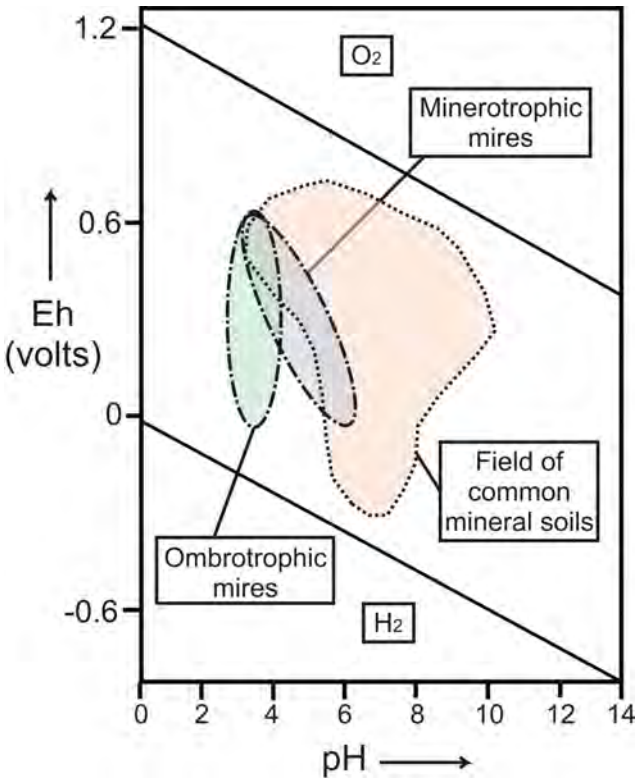

Figure 1.4. Eh-pH diagram indicating the geochemical environments of ombrotrophic, minerotrophic mires and common mineral soils. Mires develop in acidic soils specially the ombrotrophic ones (modified from Chesworth et al., 2006). Thick black lines indicate the stability limits of water in the system.

1. 2. 2 Peat carbon and nitrogen: organic matter decay and isotopic signature

Cellulose rich organic matter has usually high carbon to nitrogen (C/N) molecular ratio values (>20) what can be used to distinguish the terrestrial organic matter from the aquatic one. Organic matter from lake algae has C/N ratios values much lower, usually between 4 and 12 (Meyers, 2003). In accordance with observations on worldwide peatlands carbon loss occurs relatively quickly after deposition (Clymo, 1984, Kuhry and Vitt 1996, Borren et al. 2004). Nevertheless, fundamental differences and signatures of organic matter can be recognized after peat accumulation (Meyers, 2003). Aerobic decay of organic material results in a carbon loss of dry mass in the peat before it is incorporated in the deeper catotelm provoking a lowering of C/N ratios (Clymo, 1984). In catotelm, slow anaerobic decomposition results in additional carbon loss through methanogenesis or sulfate reduction (Kuhry and Vitt, 1996). C/N ratio has been traditionally related to peat humification degree, but it is known that several considerations have to be previously taken, because C/N can change depending on the peat-forming plants type (Kuhry and Vitt, 1996; Biester et al., 2004). The nitrogen input in peatland ecosystems is mainly in both the form of atmospheric deposition from precipitation and dry fall, and the nitrogen fixation by cianobacterias. Nitrogen is lost from the

acrotelm through denitrification, grazing, burning, superficial runoff, and erosion. In peatlands, however, the greatest amount of nitrogen becomes immobilized in the catotelm (Kuhry and Vitt, 1996).

Carbon stable isotope ratios are useful to distinguish between plant remains with different metabolic pathway for photosynthesis (Meyers, 1994, Talbot and Johannessen, 1992, Huang et al., 1999, Giresse et al., 2009, Aucour et al., 1999) (Figure 1.5). C_3 Calvin pathway produces a shift of -20‰ from the carbon source ($\delta^{13}C$ = –7 ‰ PDB), while C_4 Hatchslack pathway creates a shift of -7‰. Consequently, average $\delta^{13}C$ values are -27‰ V-PDB for C_3 pathway plants and -14‰ V-PDB or C_4 plants (O'Leary, 1988, Meyers, 2003) (Figure 5). For the plants that use Crassulacean Acid Metabolism (CAM) pathway, like some ferns, desert plants and succulents, discrimination can vary from -4 to -20 ‰ V-PDB from atmospheric carbon source (Meyers and Lallier-Vergès, 1999).

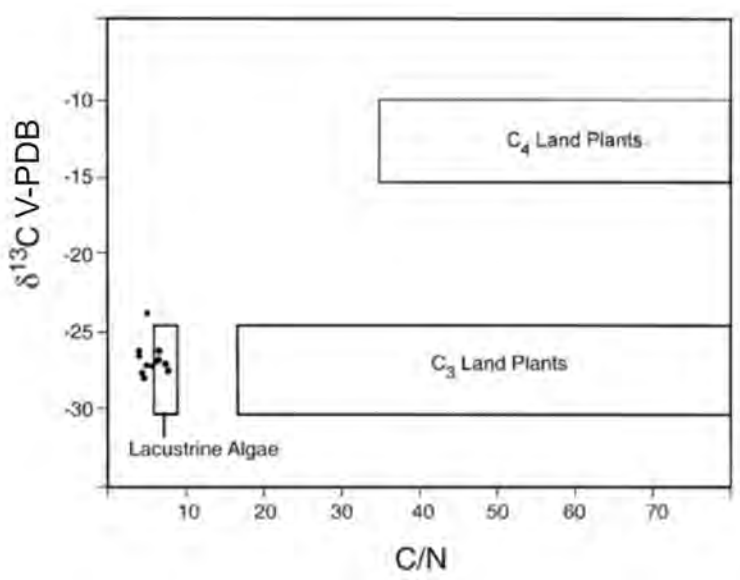

Figure 1.5. Generalized $\delta^{13}C$ V-PDB and C/N values of major sources of plant organic matter to lake sediments (Meyers, 2003)

Despite some organic substances are more reactive than others providing the opportunity for selective diagenesis, carbon isotopic composition in peat seems to be little sensitive to significant fractionation (Meyers, 1994, Talbot and Johannessen, 1992). According to literature, carbon can become lighter ($\Delta\delta^{13}C$ = - 4‰) when cellulose (heavier than lignin) is preferentially degraded (Tyson, 1995). When organic matter decay is driven by fungi, resulting carbon can be enriched ($\Delta\delta^{13}C$ = +2-6‰) as its metabolism fractionates immobilizing heavy carbon (Henn and Chapela, 2000). Recent studies over moss tissues show that decomposition as derived from C/N ratios does not affect significantly carbon isotope values on a-cellullose (Tillman et al., 2010). The single cause of significant changes in carbon isotopy during early diagenesis is methanogenesis which can enrich $\delta^{13}C$ up to $\Delta\delta^{13}C$ =25-65‰ (Miyajima et al., 1997).

The nitrogen isotopic signature that is found in organic matter can be the result of several processes that lead to fractionation (Talbot & Johannessen, 1992). Atmospheric

nitrogen can be directly incorporated to organic matter by cyanobacteria fixation (resulting in $\delta^{15}N$ values between 0 and +2‰) but also incorporated by ammonia and nitrate assimilation (Talbot, 2001). Other important processes are denitrification as a bacterial reduction of NO_3^- to N_2. Denitrification requires anoxic conditions and leads to heavy $\delta^{15}N$ residuals on organic matter because the nitrogen is fractionated and the light isotope is preferred as the gaseous form. Another inorganic process important in nitrogen cycling is N_2 dissolution and ammonia volatilization. While terrestrial plants have average $\delta^{15}N$ values between +2 and +10‰, aquatic macrophytes depict lighter signatures between -10 and 0 ‰. However measurements on soil samples show than the organic matter $\delta^{15}N$ oscillates around +5. Finally, common values for peat or organic matter of lacustrine sediments varies between -2 and +20‰ depending on the nitrogen source but also the diagenetic processes (Talbot, 2001).

1. 2. 3 Peat ash: the role of peat in element cycling

The inorganic or mineral content is also an important component on the biogeochemical cycles of mire systems. Peat components that are not originated from organic matter remains are known as '*peat ash*'. This can be incorporated into the mire either (1) transported by ground- or surface-waters (as dissolved or solid compounds) or (2) as dust blown by wind and introduced into the mire by dry or wet deposition. If the element is hosted in a stable mineral, the concentration in peat can be assumed to reflect the original dust. However, under acid/oxidized conditions many primary minerals can become unstable and break down releasing ions to solution (Chesworth et al., 2006). For this reason, once incorporated into the mire, the element cycling will strongly depend on pH and redox conditions within the peat. Four processes will determine the final peat composition and elemental cycling: the mineralogical composition of the inorganic fraction, the geochemical composition of the mire, the rate of peat accretion and the interference of human activities (Chesworth et al., 2006). Main insights concerning chemical cycling in peat are described hereafter for main major and minor elements.

Water origin

Chemical characterization of peatland waters is strongly dependent of water origin. For example, on ombrotrophic bogs, predominant cations present in the water are Mg and Na (specially if there are located near the coastline), while in minerogenous fens, Ca turns to be a very important cation (Shotyk, 1988). Calcium will be especially abundant in calcareous terrains but also in mires developed over mafic lithology. A mafic bedrock also acts as a good supply of Fe and Mg solutes originated by weathering of minerals as olivine, pyroxenes or feldspars. On the other hand, mire waters from granitic terrains will be preferentially enriched in uranium (U), silica (Si) and potassium (K). Water circulating in peat is predominantly acid and with low oxygen content (see section 1.2.1). These conditions entail that several metals not soluble in "common freshwaters" -as Al, Fe, Mn or Si- can be dissolved in peat environments (Shotyk, 1988).

Element cycling

Sodium (Na) and potassium (K) are monovalent cations very soluble in aqueous solutions and both are relatively depleted in peat when their concentrations are compared to what is found in peat forming plants. However both elements display different patterns on peatland systems. As K is essential for plants it is bioaccumulated in surface, while Na is directly lost by solution (Damman, 1978, Shotyk, 1988).

Calcium (Ca) and magnesium (Mg) are also very soluble cations, but differently to K and Na decaying organic matter exhibits affinity for these divalent cations and they can become bounded as part of organic complexes (as Dopplerite) (Bates and Jackson, 1980). As described above, Ca is more abundant in minerotrophic environments because it is transported as a product of bedrock weathering. Actually, the Ca/Mg ratio has been used to distinguish between ombrotrophic (low ratios) and minerotrophic (high ratios) areas or levels on peat profiles (Shotyk, 1988).

Elevate silica (Si) or aluminum (Al) concentration in peat is normally associated to levels with high mineral content. This fact indicates that its distribution is related to dust or runoff input events. They depict lower post-depositional movement than Na, K, Ca or Mg cations presented before (Chapman, 1964). Nevertheless, Al becomes extremely soluble at very low pH (<4), easily reached in peat waters, and therefore can migrate and precipitate in more alkaline environments (Shotyk, 1988). Titanium (Ti) has been broadly associated to Al in peat records (Norton, 1983) and is known to be strongly immobile in peat even under acidic conditions (Weiss et al., 2002).

The main geochemical feature of iron (Fe) and manganese (Mn) is that they are soluble in acidic (pH <3) and anaerobic environments and can be remobilized and accumulated as oxide or hydroxides under aerated conditions. Among the inorganic substrate components, Fe plays a very important role because is the most abundant element with more than one valence. Although peat is enriched in Fe when it is compared to peat forming plants, it is relatively depleted when compared to crustal abundance. Peat profiles show how Fe and Mn concentrations usually decrease in depth and depict maximum levels near water level, where reduced dissolved iron forms get in contact with an oxidized environment and precipitate (Clymo, 1983, Damman et al., 1992).

Nickel (Ni), vanadium (V) and chromium (Cr) have a very conservative behavior in peat profiles. They are abundant as a result of weathering on mafic and ultramafic terrains. Chromium minerals are highly insoluble but under intensive oxidation can be mobilized and precipitate in the reduced zone (Shotyk, 1986). Nickel is not an essential element for plant growing and form very insoluble compounds. As Ni and Cr, V is more common in peat formed over volcanic mafic terrains and it also forms highly insoluble compounds. Vanadium can form hydroxides that are stable even under low pH values (Goldschmidt, 1954).

Copper (Cu) has a strong calcophile character; a remarkable affinity for organic matter and it is insoluble under anaerobic conditions. Moreover, Cu is essential for plant growing as oligonutrient and enrichments of this element close to the surface have been attributed to

bioaccumulation (Sillampää, 1972). Uranium (U) shows a similar behavior than Cu. The oxidized U specie is soluble but not the reduced one. This fact confers to U cycle an intimate relation to oxidation. Due to its stability under anaerobic conditions and its organic matter affinity, U is commonly enriched in peat and organic-rich soils (Shotyk, 1988).

Zinc (Zn) has only one oxidation state and therefore is not sensitive to redox changes (Damman, 1978) but, as Cu or U, it has a strong affinity to organic matter. Both oxidized and reduced forms of lead (Pb) seem to be stable in neutral aqueous solutions. However, it can be dissolved under low pH and can be also complexed as an organic acid (Livett, 1979).

Complexation with organic matter is the most important mechanism for fixing heavy metals to peat. It has been calculated that 99% of Cu, Pb or Zn are bound to organic molecules in peat either in solid or in dissolved phase (Shotyk, 1995, Chesworth et al., 2006).

Sulfur (S) has a complex cycling and can be introduced into mires by air-blown dust (specially in mires close to the sea) or water dissolved sulphate if there are S-rich minerals in the catchment lithology. When S is deposited on to peat, sulfate can undergo reduction by the dissimilatory sulfate reduction (DSR) carried out by bacteria (Mandernack et al., 2000). Once reduced under anaerobic conditions sulfur is mainly incorporated as carbon-bounded molecules to organic matter. Up to 75-85% of total sulfur is considered to be in this form in peat profiles. The remaining portion is usually forming iron sulfides (Mandernack et al., 2000; Spratt and Morgan, 1990). Pyrite and other iron sulfides are unstable under very low pH. For this reason they require anaerobic but neutral alkaline conditions in order to be preserved in the sediments. Because mires are heterogeneous environments, it is though that reduction and oxidation of sulfur may coexist but it turns out that in very few peatland systems sulfur oxidation has been estimated (Marnette et al., 1992).

The cycling of several of these elements, specially the ones widely used in industry, is seriously modified by anthropogenic emissions. Atmospheric anthropogenic contribution of Zn, Cu or Pb is especially high, followed by elements as Cr, Fe, or Mn. For this reason, high concentrations horizons found on surface peat layers have been attributed to human activity (Shotyk, 1988; Chesworth et al., 2006, Martínez Cortizas et al., 2007).

1. 3. Peatlands as environmental archives

Peatlands are important paleoenvironmental archives because of their hydroclimatic sensitivity allows to register atmospheric, hydrological and ecologic changes. They also show rapid accumulation rates, contain large amounts of carbon for dating, and can be studied from many different approaches or proxies. While first peat records had been studied to understand peat accumulation and decay dynamics (Clymo, 1984) and the contribution of these organic soils to the global carbon cycle (Gorham, 1991), recently a wide range of studies concerning climatic and environment reconstructions have been performed.

1. 3. 1 Dating peat records

Radiocarbon

^{14}C radiocarbon dating is by far the more used method for determining peat age because of the large amounts of available carbon. Depending on the site characteristics, the radiocarbon dating can be performed over bulk peat samples, pollen concentrates or macrofossils. Macrofossils (that are above-ground plant parts such as terrestrial moss remains, seeds and leaves) or pollen concentrates are preferentially used over bulk material because they reveal the age of peat surface at the time it was deposited, with no apparent contamination of newer or older carbon, as expected from roots and rootlets (Blaauw et al., 2010). Percolation of particulate or dissolved organic carbon from above by root exudations or dying rhizomes and roots can be an important process in fen peats that contain a large percentage of roots penetrating down from more recent vegetation (Sjörs, 1991; Rydin and Jeglum; 2006). Despite is known that palynological fraction can undergo certain vertical movement under determinate flow regimes (Clymo and Mackay 1987, Joosten and de Klerk, 2007, Blaauw et al., 2010), recent studies in tropical peat records point pollen concentrates as the most reliable dating fraction on peat, in particular in tropical mires, where deeply rooting communities are commonly present (Wüst et al., 2008).

A traditional age-depth construction consisting in linear interpolation between obtained radiocarbon ages is widely performed. This assumes a quite unrealistic presumption, considering that changes in accumulation rates do not occur between samples. Other age models including convex and concave curves or Bayesian statistics -as BACON, developed exclusively for peat (Blaauw and Christen, 2011)- can produce more realistic profiles (Blaauw, 2010). However, they require the support of detailed facies description and stratigraphy, what should be included as prior conditions in the Bayesian age model if a robust and reliable age model shall be obtained (Blaauw and Christen, 2011).

Alternative dating methods have better precision for recent times, which are broadly used to date peat levels accumulated during the last century. These methods are: determination of type and quantities of Spheroidal Carbonaceous Particles (SPC) and ^{210}Pb as a cosmogenic isotope, among other radionuclides (Swindles, 2010).

Spheroidal Carbonaceous Particles (SPCs)

The products of fossil-fuel combustions are fused organic spheres formed from the mineral component of the original fuel (Rose, 2001). In fact, three types of fly ash can be distinguished: the non-combustible material, known as inorganic ash spheres (IASs), the combustible that was not burned (SPCs) and new matter that was formed during combustion.

The non-combustible material form hollow ash spheres (IASs) named *cenospheres* (Raask, 1984), *solid spheres* and *plerospheres* (Figure 1.6). These particles are spherical, can display several colors and consist in the 95-98% of coal fly-ash and less than 20% of oil fly-ash. On the other hand, SPCs are formed by hydrocarbons. They are not formed from wood, biomass or charcoal and therefore they do not have a natural source. They are usually black,

and depict a complex internal structure, with porosity and are never completely spherical (Figure 6).

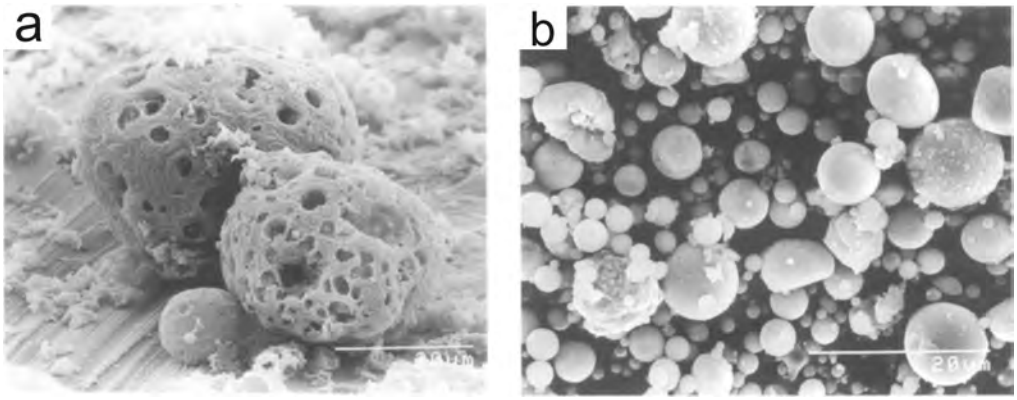

Figure 1.6. a) Spheroidal carbonaceous particles (SPCs) from oil combustion photographed by SEM. b) SEM photograph of inorganic ash spheres (From Rose, 1996).

SPCs particles are well preserved in sediments and have been especially useful to reconstruct recent chronologies (spanning the last 150 years) thanks to well-known concentration patterns (with some geographical variations) between 1850s and present day (Rose and Appleby, 2005). There are three main features employed: a start of the record in 1850s, a rapid increase in the 1950s and the higher point at 1979 with a gradual decrease thereafter (Swindles and Roe, 2006). Because regional variability can occur, the curve has to be compared with independent dating methods. A cumulative matching of SCP percentiles between different cores (dated and undated) of the same area can be used to allocate SCP dates to undated records (Rose, 2001). Because in very remote areas of the northern hemisphere similar SCP distribution have been found a hemispherical SPCs background has been proposed over which the regional signal is superimposed (Rose, 2001).

Cosmogenic isotopes (^{210}Pb)

Lead-210 is another common dating method for determining recent peat chronology (Krishnaswami et al., 1971, Robbins, 1978; Carroll and Lerche, 2003). This method is supported on the basis that radionuclide atoms undergo a radioactive decay through a known exponential rate, and therefore the age of the sample can be determined measuring the number of remaining parent nuclide. ^{210}Pb dating results very useful to date the last 150 years (Le Roux and Marshall, 2011).

Lead-210 is produced by the decay of ^{238}U through intermediate daughters as ^{222}Rn or ^{226}Ra. For this reason ^{210}Pb activity is directly related to granites that can be uranium-rich. When ^{210}Pb concentration is measured it is important to consider that there is a lead fraction produced in situ (by the decay of ^{226}Ra and ^{222}Rn) and another fraction introduced by the decay of atmospheric ^{222}Rn. The deposition of the atmospheric radionuclide can be favored by precipitation (Appleby et al., 1997). Moreover, nuclear accidents and activities also release radionuclides that have to be taken into account (Smith and Beresford, 2005).

There are three ways to determine ^{210}Pb activity: by measurement of gamma emission, by measurement of its alpha-emitting ^{210}Po (a product of ^{210}Pb decay) or measuring beta-emission of ^{210}Bi (not used so far in peat records). Different age models with variable degrees of sophistication have been developed to convert ^{210}Pb in robust dates. The first ^{210}Pb model was the Constant Flux, Constant Sedimentation (CF-CS) by Krishnaswami et al. (1971) and Robbins (1978). Thereafter several new models have been proposed. The most used nowadays are the Constant Rate Supply (CRS) (Appleby and Oldfiled, 1978; Appleby et al., 1979) or the Constant Initial Concentration (CIC) models (Appleby, 2001). Nevertheless, it is always recommended to validate ^{210}Pb chronology with independent methods as SCPs.

Dating beyond radiocarbon limit (~50 kyr BP)

Most of paleoenvironmental works carried out on peat records are not older than the radiocarbon limit detection. Nevertheless, pretty old peat records have been successfully studied using alternative dating techniques as the uranium disequilibrium series (^{230}Th/U) (Rowe et al., 1997, Schirrmeister et al., 2002; Geyh and Müller, 2005). During the 1980s two geochronological laboratories established the ^{230}Th/U dating for peat (Heijnes and van der Plicht, 1992). The dating is based in the principle that peat is suitable medium because humic acids absorb dissolved uranium in groundwater. If clastic sediment is deposited covering the peat levels it acts preventing further uranium input and converting the peat in a closed system what is adequate for dating (Schirrmeister et al., 2002).

Another robust dating tool on peat sequences is tephrochronology based in dating using tephra layers (Plunkett et al., 2004) and comparing its geochemical characterization with previously geochemically studied and dated ash layers (Swindles et al., 2010).

Although Optical Stimulation Luminiscence (OSL) dating has been used as a chronological method in archeological sites and lake sediments, it not easily applicable in peat. Minerals as quartz or plagioclase have to found as sand grains in the record, but moreover, the matrix effect of very high organic matter and water content negatively interfere in the radiation signal that has to be measured (Duller, 2008).

1. 3. 2 Biological proxies on peat records

Past ecological and environmental changes can be reconstructed on peat records using quantitative techniques based on pollen or macrofossil analysis (Bindler, 2006; Barber et al., 2003; Birks and Birks, 2006). The quantitative analysis of pollen, spores and non-pollen palynomorphs (NPP) in peat is a common tool and very efficient proxy for determining changes in the vegetation and its responses to environmental changes such as abrupt climate changes and/or human landscape modifications (van Geel, 2001; Ortu et al., 2006; Twiddle, 2012). Pollen data combine local and regional pollen and spores, which can provide information from autogenic changes, ecological successions or climatic and environmental changes, especially when combined with other proxies (Booth and Jackson 2003; Chambers and Charman 2004; Charman and Chambers 2004; Birks and Birks, 2006). An additional fruitful tool for paleoecology is the charcoal analysis, which complements pollen data, by

reconstructing long-term variations in fire occurrences or regimes (Whitlock and Larsen, 2001).

Macrofossils analysis consists in the identification, counting and ecological interpretation of plant and animal remains that are visible to the naked eye (median range between 0.5 and 2 mm). The technique also result an excellent proxy for peatlands environmental reconstructions (Birks and Birks, 2006). Contrary to pollen, most of these plant and animal macrorests can be identified up to species level, what allows accurate reconstructions. The main difference between the plant macrofossil and the pollen approach is that macrofossils are not commonly transported far from the parent organism, therefore giving a stronger local signal rather than regional (Mauquoy et al., 2010). Macrofossil data has been used to reconstruct among others: bog surface wetness (van Geel et al., 1996), mire development pathways (Hughes and Barber, 2003) and nature of carbon sequestration in peat deposits as well as to puzzle out archeological questions (Mauquoy et al., 2010). Moreover, animal macrofossils as parts or remains of insects, chironomides, mites among others can provide key ecological information to complete the environmental reconstruction of the site (Birks and Birks, 2006).

An additional important contribution to reconstruct moisture changes on peat records is the study of amoebae, single-celled organisms that rapidly respond to environmental oscillations. They are generally well preserved and therefore good moisture indicators in oligotrophic peatbogs, were transfer function have shown to infer past water table depths (Charman 2001, Mitchell et al. 2008).

1.3.3 Geochemistry on peat records

Organic geochemistry

Many geochemical approaches to reconstruct past environments considered the characterization of bulk peat samples or specific organic compounds like some biomarkers or cellulose. In both cases, this geochemical characterization can be carried out at elemental (TC, TN) or isotopic level. Within the isotopes, the most analyzed ones are $\delta^{13}C$, δD, $\delta^{18}O$ and $\delta^{15}N$.

Quantification of organic carbon in peatlands (by Lost on Ignition (LOI) or alternative methods) can be useful to estimate past C-accumulation rates and calculation of cumulative C over different time periods (Chambers et al., 2011). The total amount of C in peat can be obtained by the combination of bulk density (g/cm^3) and total C content (%). For quantifying C content, several works assume that the 50% of organic matter mass is carbon (Chambers et al., 2011). However, this can vary depending on the plant type remains. Peat density changes have traditionally been used to roughly describe different decomposition states because well-preserved peats tend to be lighter and with lower density and viceversa (Yu et al., 2003). Peat humification determines the degree of decomposition and can be measured following a wide range of procedures including field and laboratory analyses (Chambers et al., 2011). In fact, humification data on peat cores provide insights on local surface wetness changes (Kylander et al., 2013). However, this technique has to be used among others to provide reliable information (Chambers et al., 2011).

$\delta^{13}C$ over bulk peat or specific organic sediments gives insights on carbon pathways present in the organic matter (Meyers, 1994, Talbot and Johannessen, 1992; Aucour et al., 1999; Huang, 1999; Novák et al., 1999; Giresse, 2009) and can be used to determine and can be used to determine major vegetational shift between C_3 and C_4 plants (see Section 1.2.2). When measured over specific compounds, biomarkers (e.g. C_{29} *n*-alkane, biomarker for terrestrial higher plants) or over identified plant macro remains, $\delta^{13}C$ can provide information about past changes in productivity and environmental conditions like insolation or effective humidity (McKenzie and Hollander 1993; Leng 2005; Castañeda et al., 2011). Plants respond to variations in water availability and relative humidity by regulating the aperture of leaf stomata what leads to changes in the stable carbon isotopic composition (Hong et al., 2001). For this reason, $\delta^{13}C$ together with δD and $\delta^{18}O$, can track the hydrologic changes occurred in the mire as wet to dry transitions or changes in the balance between precipitation and evaporation (Hong et al., 2001). Lighter (heavier) $\delta^{13}C$ have been interpreted as changes in the isotopic composition of terrestrial plants when the isotopic composition of precipitation is higher (lower) (Aucour et al., 1999; Hong et al., 2001; Muller, 2006).

Because nitrogen is a fundamental nutrient for primary producers, its cycling is relevant to understand and characterize present and past peatland environment. Traditionally, the $\delta^{15}N$ record has not been used as much as $\delta^{13}C$ in peatlands, maybe due to its cycling complexity and pathway. This is because nitrogen can be present in different forms and several oxidation states and isotopic fractionation can occur between the various N-compounds and in many biochemical processes.

When $\delta^{15}N$ is close to atmospheric values (0-2‰) it can be reflecting nitrogen fixation by cyanobacteria activity. Studies performed on organic-rich soils or sediments detected lower $\delta^{15}N$ in some levels as a result of enhanced eutrophication (Brenner et al., 1999; Talbot, 2001). On other records, heavy $\delta^{15}N$ signatures ($\delta^{15}N \geq 8$ ‰) have been explained as reflecting denitrification due to more persistent anoxic conditions (Hecky et al., 1996). An alternative cause of very high $\delta^{15}N$ values is ammonia formation and volatilization, for what alkaline conditions (not common in mires) would be required (Talbot and Johannessen, 1992). On the other hand, in minerotrophic mires with inputs of organic matter from the catchment, $\delta^{15}N$ can be use to track changes in soil organic matter decomposition of surroundings (Wolfe, 1999). However, a slight enrichment of $\delta^{15}N$ at greater depths is common in peat records to the loss of gaseous nitrogen by the different processes explained above: denitrification or ammonia volatilization (Novák et al., 2003).

In summary, in paleoenvironmental records, $\delta^{15}N$ has mainly been used to determine organic matter sources, nutrient loading or catchment changes. However, it requires to be used as a part of a multiproxy study, specially when isotopic results are ambiguous (Handley et al., 1999, Talbot and Johannessen, 1992, Meyers and Ishiwatari, 1993).

Inorganic geochemistry

Recently, inorganic geochemistry characterization of peat records has arisen as an important proxy to perform high-resolution environmental reconstructions (Bindler, 2006; Muller et al., 2008b; Kylander et al., 2013). Several works have demonstrated that peatlands are reliable repositories of major and trace elements that can be measured by X-Ray Fluorescence (XRF), inductively coupled plasma Mass Spectrometry (ICP-MS) or inductively Coupled Plasma Atomic Emission spectroscopy (ICP-AES). Characterization of the inorganic fraction of peat records has been used as a tool to estimate environmental changes through times or among sites (Shotyk, 1996; Shotyk et al., 2001, Weiss et al., 2002). Several authors have worked with mire mineral content as atmospheric dust indicator (Martínez Cortizas et al., 2002; Kylander et al., 2005), showing that peat records can become useful to identify changes on wind regimes (Kohfeld and Harrison, 2001), vegetation coverage, wet to dry transitions (Muller et al., 2008b) or the anthropogenic signal over metal cycling, frequently caused by pollution (Shotyk, 1996; Martínez Cortizas et al., 2002,). However, changes in the inorganic content can also be driven by detritic input and therefore indicating changes in precipitation, water table or hydric regimes, or changes on the redox state (Muller et al, 2008b; Margalef et al., 2013).

Another promising approach concerning the mineral content of the peatlands is the chemical characterization of Rare Earth Elements (REE). This group of elements can be used to trace source regions of aerosols or sand grains because the original REE signature is very particular from the rock source and inherited and not lost during the transport. Two REE elements present particular anomalies: These are Europium (Eu), that can be reduced during high temperature processes (>250ºC) and Cerium (Ce), that can be reduced at low temperature and oxidizing conditions. On peat records, Eu anomalies are interpreted as inherited from source area while Ce anomalies are considered to be acquired during or after deposition (Taylor and McLennan, 1985; McLennan, 1989). REE determination on peat profiles has been therefore used to reconstruct changes in dust origin as well as postdepositional processes occurring within the peat (Aubert et al., 2006; Kylander et al., 2007).

1.4 Paleoenvironmental reconstructions from tropical peats

Most of the works performing climate or environmental reconstructions from peat cores are based on ombrotrophic boreal to temperate mires on the Northern Hemisphere (Shotyk, 1996, Charman; 2002). Although receiving increasing attention, the Southern Hemisphere peatlands remain substantially less explored, specially the tropical ones (Page et al., 2010). South East Asia (Malaysia, Sumatra, Borneo and New Guinea) is the tropical area where more efforts have been made to reconstruct the environmental history using peat records. In particular, from records retrieved from (1) the freshwater swamps distributed along lowland rivers and coastal plains or from (2) the ombrotrophic convex-shaped swamps of inner lands (Weiss et al., 2002; Dommain et al., 2010). These studies include the reconstruction of carbon accumulation rates and its relation to global climatic changes (Page et al., 2004; Page et al., 2010), palynological records (van der Kaars et al., 2001; Anshari et al., 2001), stratigraphy and lithofacies description (van der Kaars et al., 2001; Wüst et al., 2004)

or the major, minor and trace elements determination from mineral content, to elucidate changes in dust deposition (Weiss et al., 2002; Wüst et al., 2004). Additionally, some holistic synthesis, compiling the regional paleoenvironmental data, timing and patterns of peatland formation in response to external drivers as temperature changes or sea-level have been recently performed (Dommain et al., 2010). The oldest SE Asian peat sequences recorded environmental information up to the last 26 to 30 kyr BP bringing insights of peatland evolution and climate interactions during LGM, deglatiation and Holocene (Anshari et al., 2001; Page et al., 2004).

Paleoenvironmental reconstructions have also been successfully obtained by studying the geochemical signatures of organic rich sediments of African lakes (Talbot and Johannessen, 1992, Street-Perrott et al., 2004). Most of these studies used $\delta^{13}C$ and TOC records to reconstruct the vegetational history, an approach that has also been used over ombrotrophic peat records (Aucour et al., 1999; Hillarie-Marcel, 1989).

Many studies carried out in Latin-American peatlands or wetlands reconstruct past vegetational changes using pollen and NPP analyses. Examples of these works include records from Brazilian plateau swamps, rainforests or coastal peatlands (Barberi et al., 2000; Garcia et al., 2004; Medeanic and Silva, 2010) or the Venezuelan Gran Sabana (Montoya et al., 2011) but also high altitude mires as on the Northern Andes (Servant and Servant-Vildary, 2003; Rull, 2005; Skrzypek et al., 2011).

Another outstanding peatland archive has been found on Oceania where an extensive multi-proxy research has been performed on Lynch crater peat record (Queensland, Autralia) to reconstruct the environmental evolution for the last 45 kyr BP. Lynch crater record has been studied using pollen (Turney et al., 2001), carbon isotope and major, minor and trace elements determination from ash layers (Muller et al., 2008b) or REE (Kylander et al., 2007).

In this framework, the peat record of Rano Aroi (Easter Island, 27°S) constitutes a new subtropical peat record situated in easternmost Polynesia. This must be seen as an opportunity to provide insights about the climate evolution of the Central Pacific because the Rano Aroi mire is situated thousand kilometers away from the continent and from other paleoclimate marine records and in a key region for understanding long-term climate variability on the Pacific Ocean. This is because it lies in the interplay of main oceanic and atmospheric structures of the Central Southern Pacific. Exhaustive description of Pacific Ocean features, climate dynamics through time and its relevant role in contributing to global climate regulation are indicated and described in the following section.

PAST AND PRESENT OF SOUTHERN PACIFIC OCEAN CLIMATE

1.5 Regional climate

1.5.1 Oceanic circulation

The Pacific Ocean is the largest Earth's Ocean, covering the 46% of the planetary water surface. The termohaline circulation (THC) in the South Pacific Ocean consists in a very large-scale gyre centered on eastern Pacific (Emery and Meincke, 1986; Mmayev, 1975). Cold and low salinity waters derived from the Antarctic Circumpolar Current (ACC) flow from Southern Chile to Northern Peru following the South American shore, forming the Peru or Humboldt Current (Mamayev, 1975) (Figure 1.7). This marine current constitutes one of the major upwelling systems, being highly productive (>300 g C $m^{-2}yr^{-1}$). The upwelling is active year round near the Equator and during spring at higher latitudes due to the displacement of the South Pacific Anticyclone (Tsuchiya et al., 1989). The upwelled waters contribute on the formation of the South Equatorial Current, a significant mass of water that flows westwards driven at surface by trade winds until the South East Asia and the Oceania coast (Kessler, 2006). The gyre is completed by the East Australian Current (EAC) that displaces the warm water from Sulu Sea south and eastward, to the coast of Australia (Figure 1.7). Finally, part of this water mass is incorporated to the Antarctic Circumpolar Current which completely circles Antarctica, flowing clockwise and connecting Atlantic, Indic and Pacific Basins (Emery and Meincke, 1986, Tomezak and Godfrey, 2001).

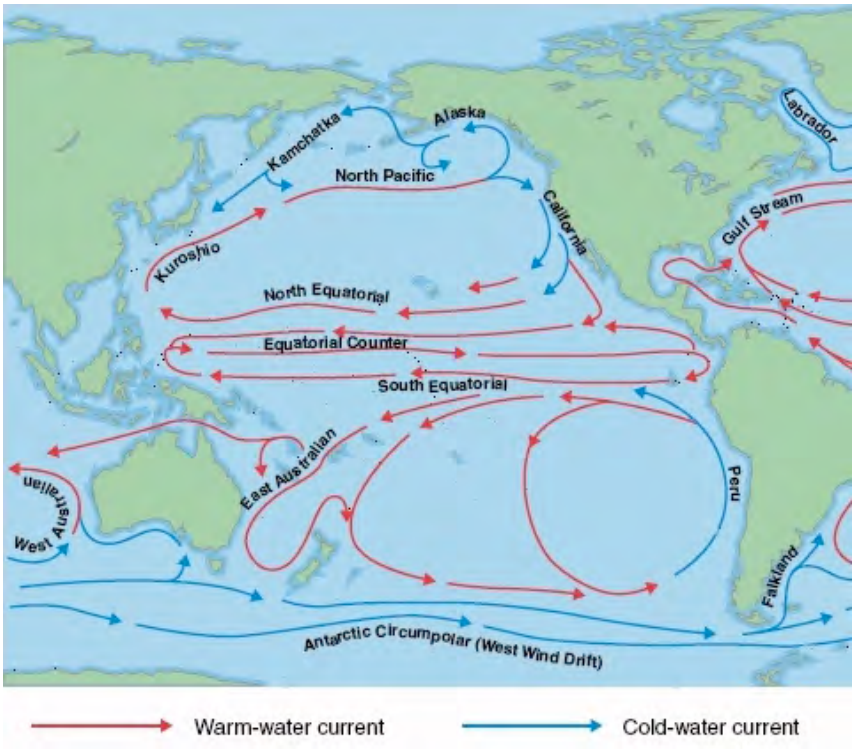

Figure 1.7. Simplified Pacific Basin oceanic circulation (http://donsnotes.com/science/earth/images/ocean.current.map.jpg)

An important oceanic feature of the Southern Pacific is the formation of deep and intermediate water masses. On one side there is the formation of the Antarctic Bottom Water (AABW) from surface water-cooling in polynyas areas (open water surrounded by sea ice) in the Polar Antarctic Zone (PAZ) (Rose et al, 2010, Sigman et al., 2010) (Figure 1.8). The Antarctic surface water is cooled and enriched in salt due to ice formation, what provokes an increase of density and the sink across the Antarctic margin down to 4000 m depth (Figure 1.8). The Antarctic Intermediate Water formation (AAIW) is the water mass of low temperature and relatively low salinity formed under the Antarctic Polar Front influence, between 50º and 60ºS. Because of its relative low salinity it sinks to depths between the 700 to 1200 m. The AAIW flows northward as far as 20°N with trace amounts even at higher latitudes. Further north, above the Sub-Antarctic Front (SAF) and on the Sub-Antarctic Zone (SAZ), between 40° and 50° S, the Sub Antarctic Mode Water (SAMW) sinks over the AAIW, around 500 m depth and becomes entrained in the South Pacific subtropical gyre (Rose et al, 2010, Sigman et al., 2010) (Figures 1.8, 1.9).

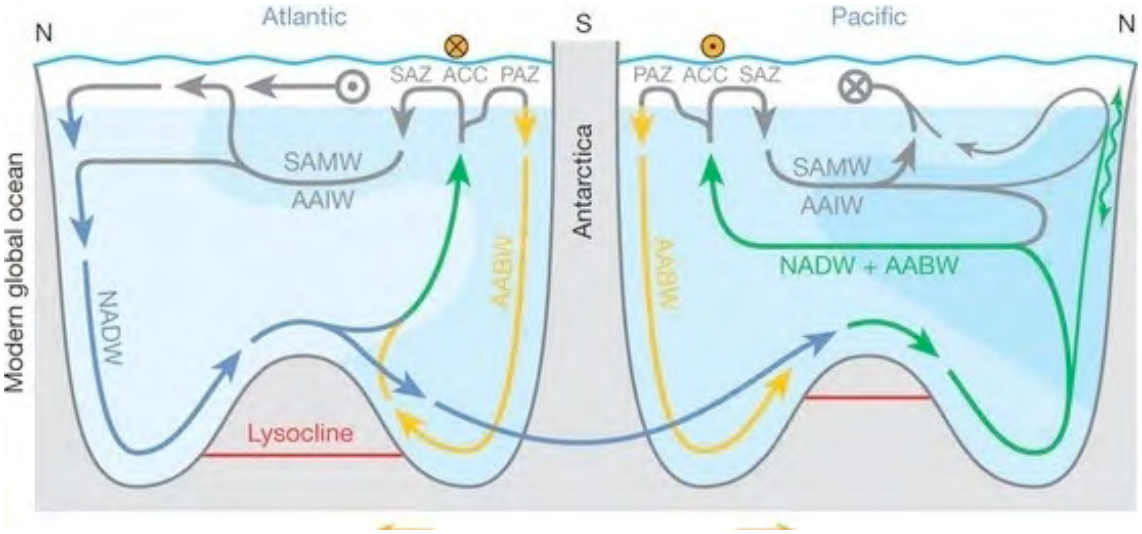

Figure 1.8. Summary cartoon of present global circulation of the Atlantic and Pacific Basins including the flow of the main water masses: North Atlantic Deep Water (NADW), Antarctic Bottom Water (AABW), Antarctic intermediate water (AAIW), Sub Antarctic Mode Water (SAMW). PAZ (Polar Antarctic Zone), Sub Antarctic Zone (SAZ) and Antarctic Circumpolar Current (ACC). Modified from Sigman et al., (2010).

A significant water volume for the formation of AABW, AAIW and AAIW is supplied by the Circumpolar Deep Water (CPDW) (Georgi, 1981; Thoma et al., 2008) (Figure 1.9). This water mass upwells under the ACC influence, and carries a strong contribution of North Atlantic Deep Water (NADW).

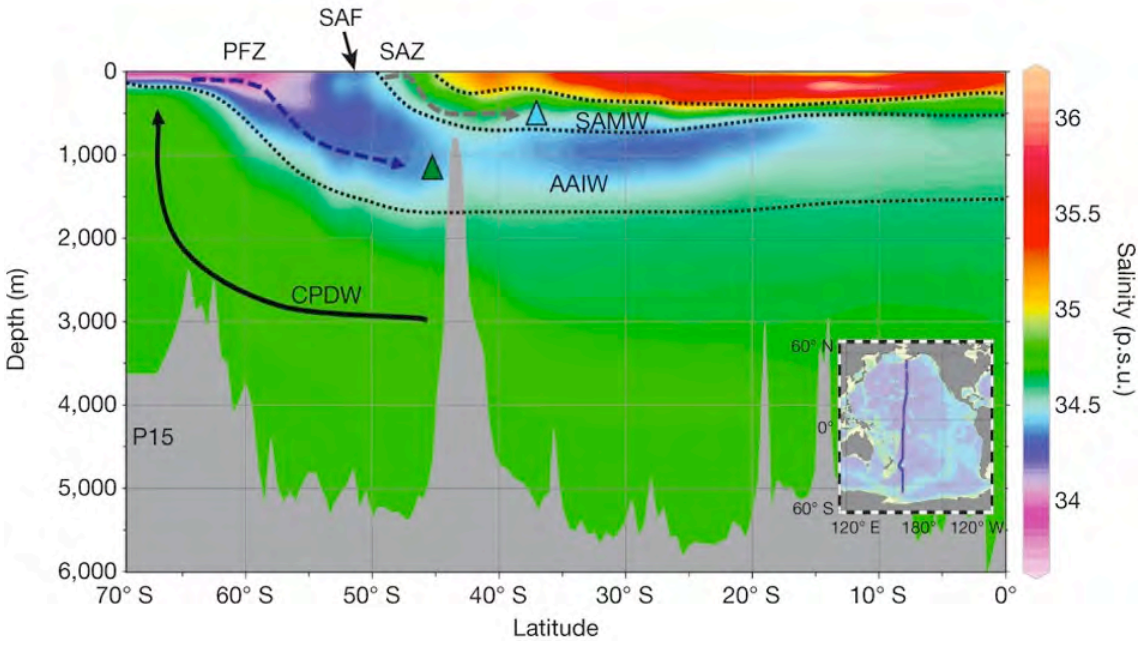

Figure 1.9. N-S Ocean circulation in the South Pacific Ocean and the formation of different water masses according to their by salinity values (p.s.u., practical salinity units). Antarctic intermediate water (AAIW), Sub Antarctic Mode Water (SAMW). SAF (Polar Antarctic Front), Sub Antarctic Zone (SAZ) and Circumpolar Deep Water (CPDW), Polar Frontal Zone (PFZ) are represented (Rose et al., 2010).

1.5.2 Atmospheric circulation

South Pacific atmospheric circulation is strongly dependent on Walker and Hadley cells configuration. The Intertropical Convergence Zone (ITCZ) is located over the equator where the northeast and southeast trade winds converge (Figure 1.10), forming the ascending branch of the Hadley cell. Because is formed by vertical motion air masses, the ITCZ is associated to a band of clouds and the occurrence of convective thunderstorms (Vincent et al., 2009). The South Pacific Convergence zone (SPCZ) is a northwest to southeast oriented structure, spur of the ITCZ. It is considered an important low-pressure belt, associated to storm formation, which position is strongly influenced by the ENSO state and monsoons (Russell and Johnson, 2007). Another important feature is the South Pacific Anticyclone (SPA), a subtropical anticyclone located on the South Eastern Pacific, which center is located around 30ºS - 110º W (Figure 1.10). The Southern Westerlies (SW) are strong prevailing winds that blow southeastward south from the subtropical highs. The SW are the main drivers of extra tropical cyclones and therefore considered as an important stormtrack (Heirman, 2011).

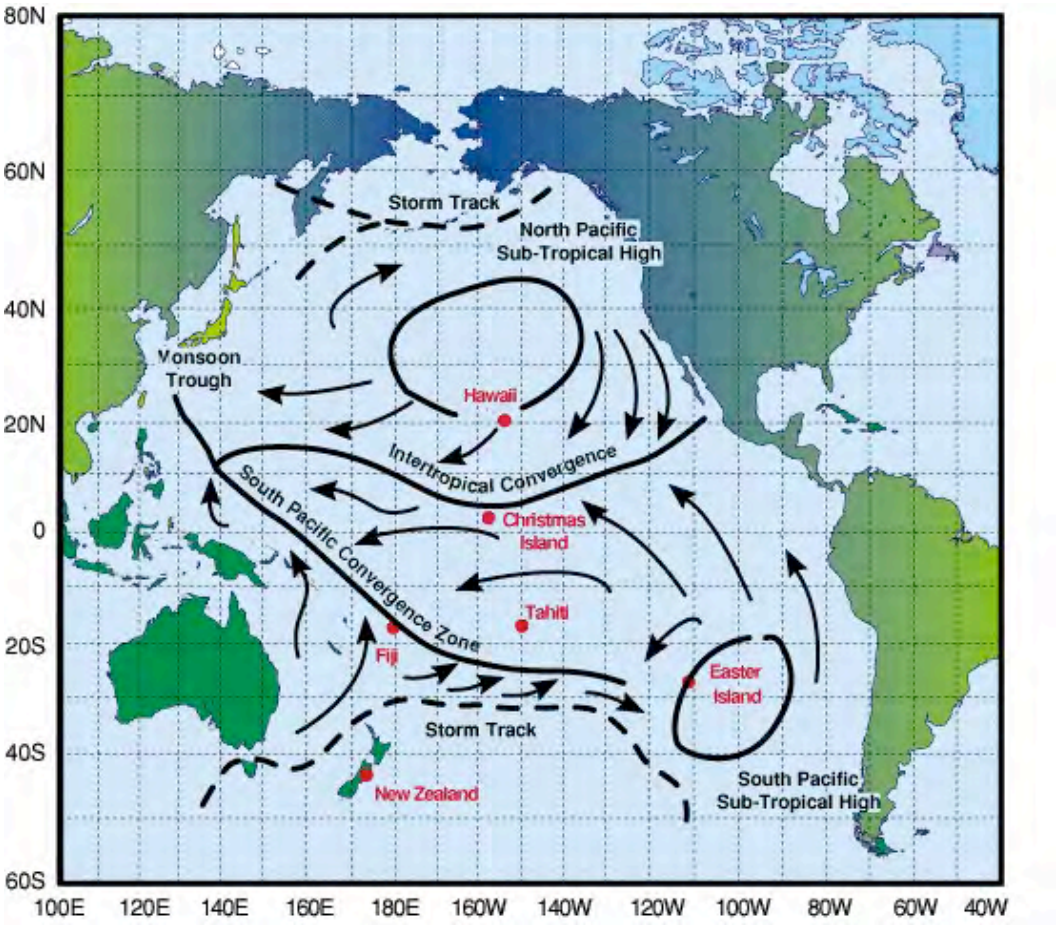

Figure 1.10. Main atmospheric patterns over Pacific Ocean (http://joannenova.com.au).

These oceanic and atmospheric structures determine the precipitation distribution over the entire Southern Pacific Ocean, which depicts a strong seasonal variability (Waliser and Somerviller, 1994). Figure 1.11 clearly indicates that higher precipitation rates are located over the SPCZ, the Sulu Sea and entire Brazil during the austral summer (December, January, February, DJF). Rainfall rates increase at the northern edge of the ITCZ during March-April-May (MAM), while the SPCZ moves slightly northwards provoking enhanced precipitation over SE Asia (Figure 1.11). During the austral winter (June-July-August, JJA), the Asian Monsoon occurs at its maximum and the ITCZ guaranties strong rain at its yearly northernmost position, while the SPCZ loses strength. Therefore, during JJA, precipitation decreases over Brazil and concentrates over Central America and Venezuela. During September-October-November (SON), the SPCZ starts to be more active again and very high rain is expected over SE Asia and Oceania (Figure 1.11) (Vincent et al., 2009).

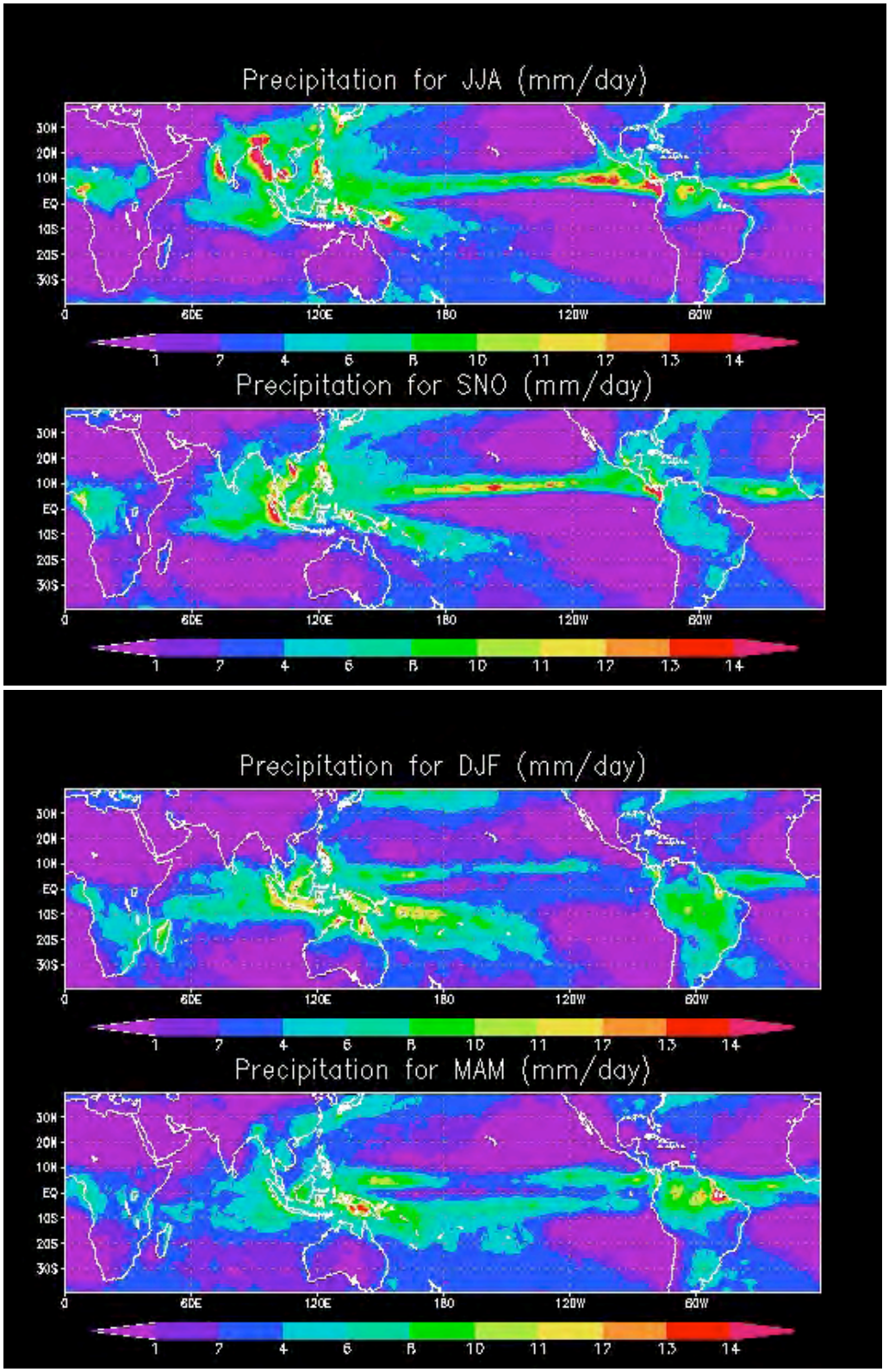

Figure 1.11. Seasonal distribution of precipitation over the Pacific Ocean (mm/day) using basic statistics of Tropical Rainfall Measuring Mission (TRMM) Precipitation Data (Huffman et al., 2007). From http://disc.sci.gsfc.nasa.gov/precipitation/additional/science-focus/TDST_SCI/statis_Basic.shtml

1.5.3 Climatic modes

El Niño-Southern Oscillation

The El Niño-Southern Oscillation (ENSO) is the year-to-year climate signal responsible of the largest climate variability on Earth (McPhaden, 2006). It consists in the modification of the Pacific gyre oceanic circulation due to anomalous water temperatures occurring on East Equatorial Pacific (Figure 1.12). This circulation perturbation is coupled to a tropical western Pacific air pressure anomaly (McPhaden, 2006). The fluctuation between two states constitutes the Southern Oscillation: On one hand, during the warm ENSO episodes (El Niño) the Eastern Pacific seawater temperatures are anomalouly warm (of at least 0.5ºC averaged over the annual mean), slowing the Humboldt current and leading to weaker upwelling and the deepening of the thermocline (Cane, 2005, McPhaden, 2006). This oceanic phase is coupled to high air surface pressure in the western Pacific. On the other hand, during the cold ENSO (La Niña), an enhanced upwelling, shallower thermocline as well as stronger Walker circulation lead to colder temperatures on Easter Pacific (Figure 1.12).

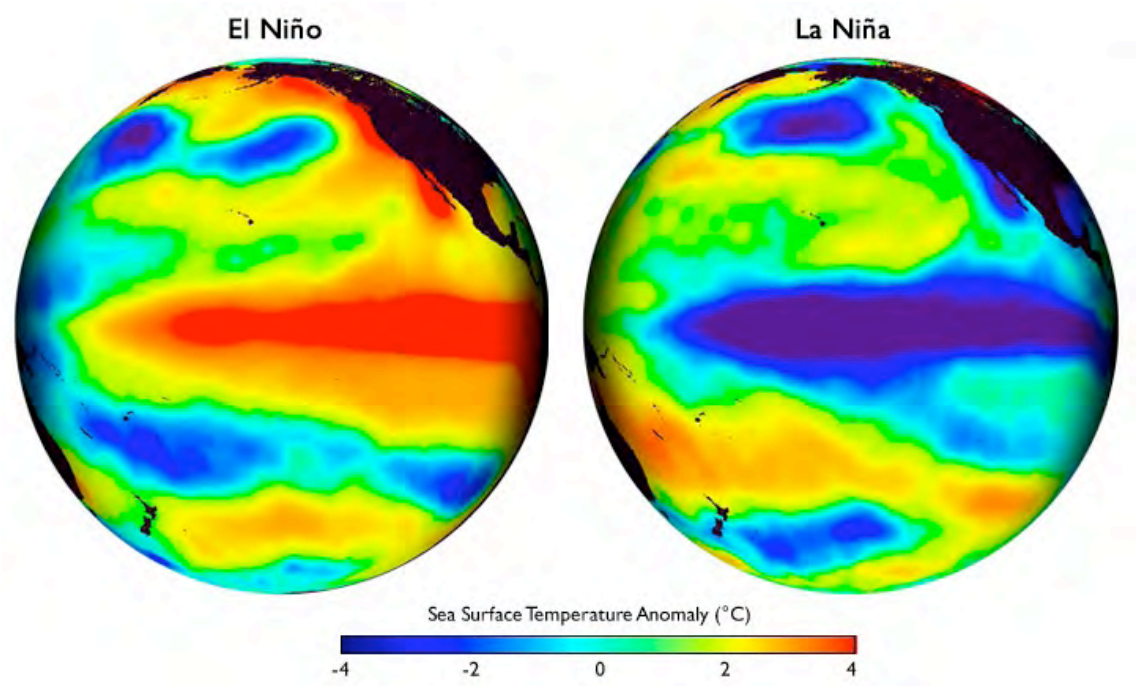

Figure 1.12. Warm ENSO event (El Niño) and cold ENSO event (La Niña) anomalies in Sea Surface Temperature (SST).

The occurrence of the ENSO is the natural climatic phenomenon that entails higher worldwide socioeconomic consequences (McPhaden, 2006). During El Niño episodes the warm waters of Eastern Pacific block the upwelling of the nutrient-rich deep waters provoking the decrease on fisheries. Other consequences are the increase of precipitation on Central America and Central Pacific because of the weakening on the Walker circulation (Dai and Wigley, 2000). At the same time warm episodes over South East Asia and extreme droughts over Australia are expected (Figure 1.11). Conversely, during the cold episodes, deep nutrient-rich waters are upwelled having a strong impact on the entire marine food-web and largely increasing fish abundance. As a consequence of the enhancement of the Equatorial and

Humboldt Current flowing, lower temperature than usual are expected on Central and South America and increased rainfall over South East Asia and Australia (Figure 1.13).

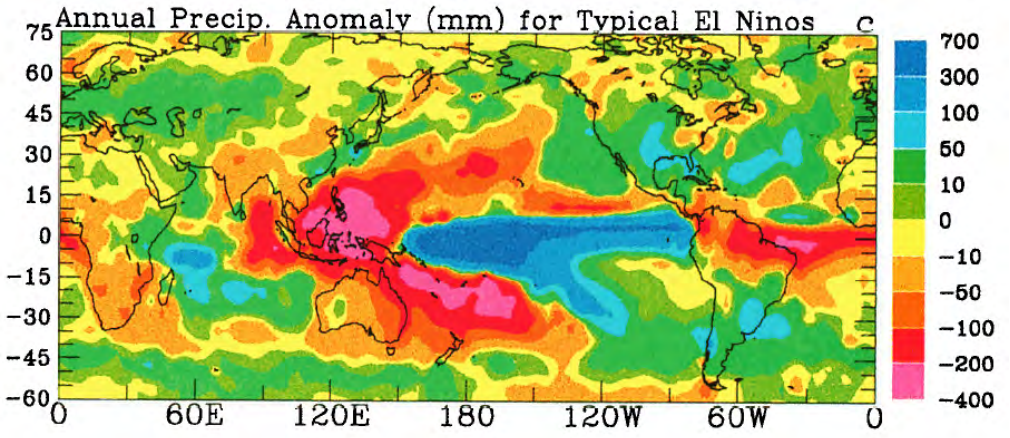

Figure 1.13. Annual precipitation anomalies during warm ENSO events (Dai and Wigley, 2000).

The mechanisms controlling how the system shifts from warm to cold ENSO events and why is occurring for this periodicity (from 2 to 7 years) are still a matter of study. The main hypothesis proposed at present day can be summarized in two main groups (Cane, 2005). The first group suggests that ENSO is the result of an oscillation of a self-sustained ocean-atmospheric coupled system, while the other group states that it has a stochastic origin (Wang and Fiedler, 2006).

Several indexes are currently used to measure ENSO intensity. For example, the South Oscillation Index (SOI) compares the air pressure between Darwin (Australia) and Tahiti using 5 months average series. The SOI index is negative during El Niño episodes and positive during La Niña events. At the same time there are sea-based indexes, as NIÑO 1, NIÑO 2, NIÑO 1.2, NIÑO3, NIÑO 4 and NIÑO3.4, indicated by SST anomalies on specific Equatorial Pacific areas that are very sensitive to ENSO events (Figure 1.14). For example, NIÑO3.4 index is defined as the average SST anomaly in the area bounded between 5°S-5ºN and 170°W-120°W (Figure 1.14). A warm event is indicated if in the 5-month average of NINO3. 4 index exceeds 0.4°C during half a year. A cold event is described if the average anomaly is below -0.4°C for the same period of time.

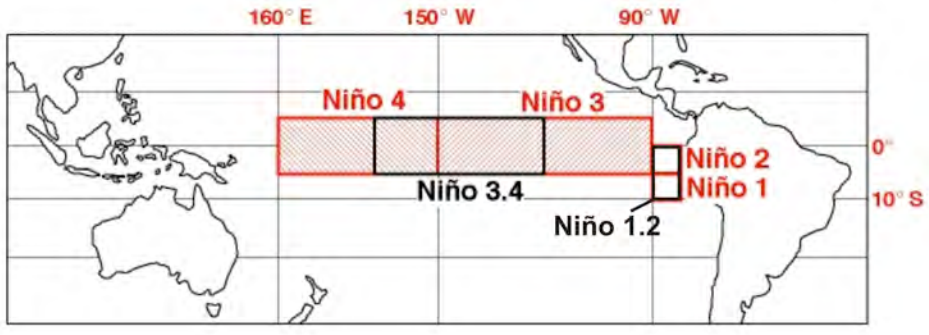

Figure 1.14. Location of El Niño 1 (5°-10°S, 80°-90°W), El Niño 2 (0°-5°S, 80°-90°W), El Niño 1.2 (0-10ºS) El Niño 3 (5°N-5°S, 150-90°W), El Niño 4 (5°N-5°S, 160°E-150°W) and El Niño 3.4 (5°N-5°S, 120-170°W) areas over Pacific Ocean.

Several efforts have been applied to describe the teleconnections responsible of the link between ENSO signal and Southern Hemisphere high latitude dynamics. Instrumental data indicate a relation between the sea ice extension, the ENSO state and the jet stream intensity (Yuan, 2004). When a warm ENSO state occurs, sea ice in the Pacific sector of the Southern Ocean is reduced while the Atlantic sector presents larger sea ice extension. The action of stationary Rossby Waves create a persistent anomalous high-pressure over the Pacific coast of Antarctica trough the Antarctic Dipole (ADP), that generates a jet stream dynamics redistribution (Yuan et al. 2004). This pattern results in enhanced subtropical jet (centered near 25°S) bringing positive rainfall anomalies over the Central Pacific in front of the polar front jet activity.

Southern Annular mode

The Southern Annular Mode (SAM) otherwise called the Antarctic Oscillation (AAO), is a low-frequency climate mode of atmospheric variability characterized by changes on the latitudinal position and strength of Southern Westerlies (Gillet et al., 2006). SAM state has a very relevant role related to the polar position and the transport of storm systems. For this reason it controls rainfall in mid to high latitudes of the Southern Hemisphere but also influences the tropical Pacific SST (Ding et al., 2012). Positive SAM episodes happen when weaker westerlies contract towards Antarctica. On the other hand, negative SAM events take places during the expansion of Southern Westerlies. This leads to the intensification of the activity of the storm track and enhanced precipitation at mid latitudes. It is important to remark that SAM rules about 20-30% of the extra tropical total climate variance (http://www.atmos.colostate.edu/ao/introduction.html).

Pacific Oscillations

The Pacific Decadal Oscillation (PDO) is a climatic mode of variability centered on northern Pacific and it is defined by anomalies in the Sea Surface Temperature (SST). A positive or warm (negative or cold) phase of the mode occurs when the western Pacific becomes cold (warm) while there is a warming (cooling) of the eastern part. The oscillation takes places north of 20ºN at an inter-decadal time scale, around 20 to 30 years (Pena, 2008). The prevailing hypothesis is that the PDO is caused by the forcing of the ENSO oscillations through the atmospheric bridge: During El Niño events deep convection and enhanced heat transfer to the troposphere generates Rossby waves that propagate and are refracted back from the pole to the tropics. In this way ENSO driven patterns modify SST, wind and clouds distribution over the North Pacific (Alexander et al., 2002). A reemergence of North Pacific SST anomalies in subsequent winters combined with stochastic (white noise) atmospheric forcing have been proposed as sparking off mechanisms (Newman et al., 2003, Deser et al., 2004). The Interdecadal Pacific Oscillation (IPO) is characterized by similar SST patterns, but it affects both Hemispheres and at higher frequency, every 15 to 20 years (Schneider and Cornuelle, 2005).

1.6. The Southern Pacific Late Pleistocene and Holocene climate

Because the South Pacific region is considered a key area for understanding global climate, multiple efforts have focused on reconstructing Late Pleistocene climate evolution and atmospheric and oceanic responses.

South Pacific Ocean dynamics have been studied from a wide range of approaches. Speleothems, which provide well-dated series, have contributed to this knowledge with hydrological reconstructions (Cruz et al, 2005; Wang et al., 2004; 2007). Peatland and lake records have supplied with a large variety of climate and environmental reconstructions at different time-scales. For example, several high altitude lacustrine records located on the Altiplano have been used to reconstruct environmental and climatic history (Baker et al., 2001, Valero-Garcés et al., 2005), tropical and subtropical lake records have been used to reconstruct El Niño signal (Moy et al., 2002, Conroy et al., 2003) and peat and lake records from Australia and Oceania have been used to reconstruct precipitation and temperature (Azizi and Flenley, 2008, Sáez et al., 2009).

The marine paleoclimate records are concentrated on coastal or on high productivity areas where elevate accumulation rates are found. On the Southern Pacific several studies centered on Chilean offshore have been performed to explain changes on the Southern Westerlies position and its influence over the continent and oceanic circulation slope (Lamy et al., 1998, Stuut and Lamy, 2004; Kaiser et al., 2007). Another traditionally studied zone is the East equatorial Pacific, close to Galápagos islands. This is because it is a very sensitive zone to changes in the Walker circulation, upwelling rates and ENSO states (Koutavas et al., 2006; Pena et al., 2008, Pena et al., 2013). The Western Equatorial Pacific has also been extensively studied to reconstruct SST and hydrological changes, providing relevant information about Asian monsoon evolution through time (Dannenmann et al., 2003; Oppo et al., 2003). Finally, records located at higher latitudes, like New Zealand coast or closer to Antarctica are clue to determine changes in ACC dynamics and the AABW and AAIW formation (Toggweiler et al., 2006, Anderson and Carr, 2010, Skinner et al., 2010).

Coral reefs mainly found on tropical and subtropical Pacific islands, constitute another important set of records to reconstruct Ocean Pacific history. These records, together with raised beaches, give independent (not affected by isostasy) time series of sea-level changes on the Pacific basin (Tudhope et al., 2001).

1.6.1. Factors controlling the Last Glacial cycle climate variability

Stadial-interstadial variability

The last glacial cycle presents millennial scale climate variations, otherwise called stadial-interstadial oscillations (Figure 1.15). The occurrence of this variability has been defined over North Atlantic as Dansgaard-Oeschger (DO) and Heinrich events (Dansgaard et al., 1983, Heinrich, 1988). Stadial times depict conditions analogous to a glacial ages, but in shorter timescale and intensity. In particular, stadials are identified on North Atlantic Ocean by large armadas of icebergs owing to the collapse of the Northern Hemisphere larger ice-

sheets, forming the so-called Heinrich events, which induced a rapid weakening or even shut down of the Atlantic Meridional Overturning Circulation (AMOC) (Heinrich, 1988; Broecker, 1994; Ganopolski and Rahmstorf, 2001; Hemming, 2004). On shorter timescales and during the Holocene, the Bond events have been described as climate fluctuations occurring every 1470±500 years. These events have been defined based on ice-rafted material on North Atlantic (Bond et al., 1997).

The bipolar seesaw hypothesis states that there is a direct connection between North and Southern Hemispheres through THC during Late Pleistocene in which DO cold episodes on Northern Atlantic correspond to Antarctic warmings and vice versa (Figure 1.15) (Stocker et al., 1998). This idea has been revised from climate modeling and paleo-works to elucidate (1) if this process involved a strict antiphase or a lead-lag relation and (2) to clarify what mechanisms could allow THC to propagate such temperature signal (Bender et al., 1994, Steig and Alley, 2002; Schmittner et al., 2003, Blunier and Brook, 2001).

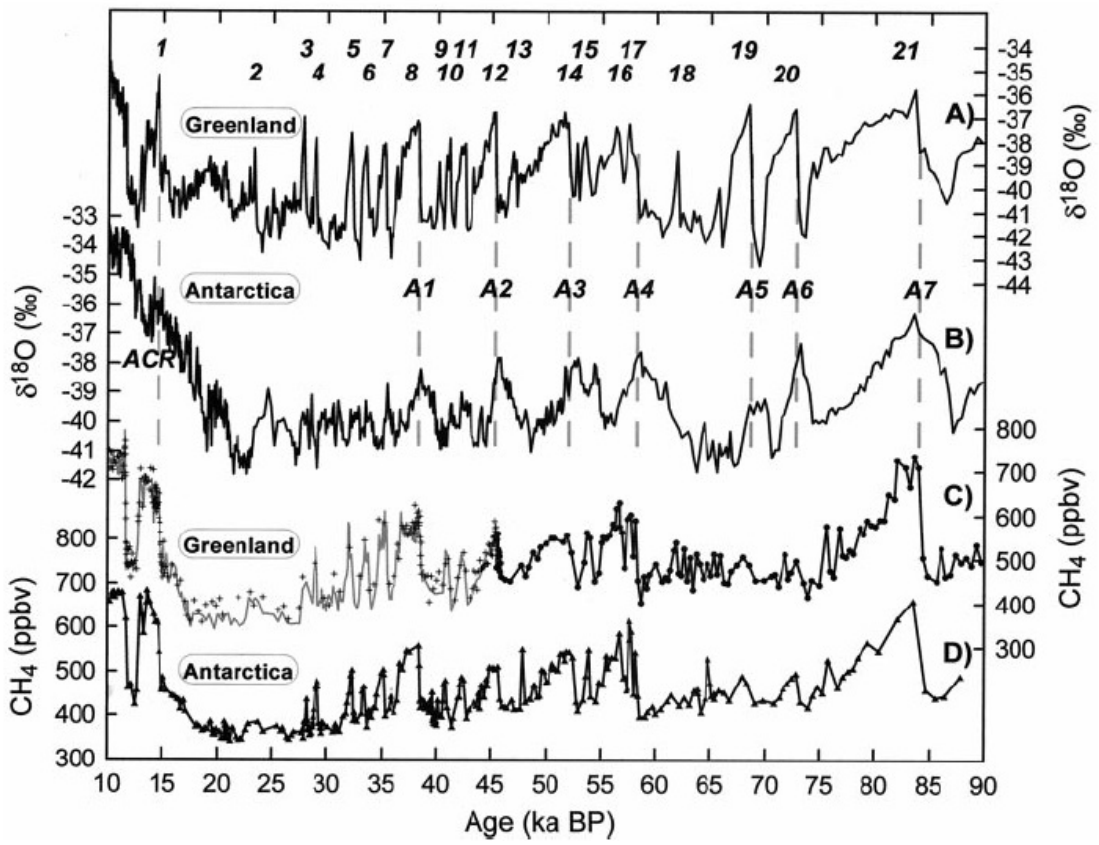

Figure 1.15. Isotopic and CH_4 data from Greenland and Antarctica on the GISP2 (Greenland) ice cores showing how cold periods on North Atlantic correspond to Antarctic warmings. A) $d^{18}O_{ice}$, from GISP2, Greenland. The numbers indicate DO events B) $d^{18}O_{ice}$ from Byrd station, West Antarctica. Letters indicate the Antarctic warmings C) CH_4 data from GISP2 (crosses and dots) and GRIP (solid line) ice cores. D) CH_4 from Byrd station (from Blunier and Brook, 2001).

The simplest explanation states that a slow down of the THC can trigger a warming in the Southern Hemisphere due to reduced heat export to the north (Broecker, 1998; Stocker and Johnsen, 1998). Some studies have proposed that the fast signal transfer can be explained by Kelvin waves propagation along the coastal boundaries of oceanic basins, mechanism could explain relatively rapid responses (Stocker and Johnsen, 2003). However, and because the

Southern Ocean does not have land lateral boundaries to propagate rapid responses as Kelvin waves, the thermal response is expected to be slower. According to this idea, Stocker and Johnsen (2003) proposed a combined thermodynamic mechanism. The classical seesaw has been complemented with the coupling of a Southern Ocean heat reservoir that damps in time thermal changes of North Atlantic. These studies conclude that maximum correlation is achieved when 1000 to 1500 years are considered for adjustment in front of 300 to 500 years proposed by ocean circulation models run under modern conditions (Stocker and Johnsen, 2003). This explains why the temperature records between both hemispheres are not strictly anti-correlated (lead-lag relation) and include relevant differences on both events onset pattern and duration: the response of Antarctic climate is slow and it consists in longer lasting events compared to North Atlantic abrupt temperature changes (Knutti et al.,2004; Siddall et al., 2006; Stocker and Johnsen, 2003).

Orbital forcing over Southern Pacific

The Milankovich theory postulates that changes on Earth orbital parameters as eccentricity (100 kyrs cycles), obliquity (41 kyr cycles), and combination of apsidal and axis precessions (21 to 23 kyr cycles) have a direct influence on insolation, leading to different climatic patterns. Despite it has been traditionally considered that high latitude are the most sensitive regions to changes in insolation and seasonality, important responses to orbital forcing have been also described over low latitudes and tropical areas. This has been explained by atmosphere-ocean coupled models that evidence that orbital changes lead to radiation fluctuation, which, in turn, provoked large tropical oceanic and atmospheric restructuration (Clement and Cane, 1999, Clement et al., 1999).

Precession changes work as the most important radiative control on low latitudes, what it has been confirmed by studies on marine and terrestrial records. In particular, periods of high precession values are characterized by enhanced insolation and lower seasonality and viceversa. Pena et al. (2008) suggested that the asymmetric seasonal insolation brought by low precession periods has direct consequences on enhancing SST Equatorial gradient during the last 275 kyr BP, which leads to a La Niña-like South Pacific configuration. Marine records have stated that ENSO-like variability driven by precession changes ruled primary productivity oscillations through time on Equatorial Indo Pacific Ocean (Beaufort et al., 2001; Molfino and McIntyre, 1990) and environmental shifts on Northern Australia (Turney et al., 2006). Late Pleistocene long-term wet periods over the Bolivian altiplano have been attributed to periods with maximum insolation, what drives the intensity of the South American Summer Monsoon (Baker et al., 2001). Other studies have shown how precession had a strong influence in controlling the Southern Westerlies latitude for the last 120 kyr BP (Lamy et al., 1998). Cyclic variations of grain-size and mineralogy measured in sediment records located offshore Chile have been identified as a good proxy to reconstruct the occurrence of wet and dry periods (Figure 1.16). High precession, as happened during the Last Glacial Maximum (LGM), contributed to an equatorward shift of SW, and therefore lead to higher seasonal precipitation over central Chile (Lamy et al., 1998).

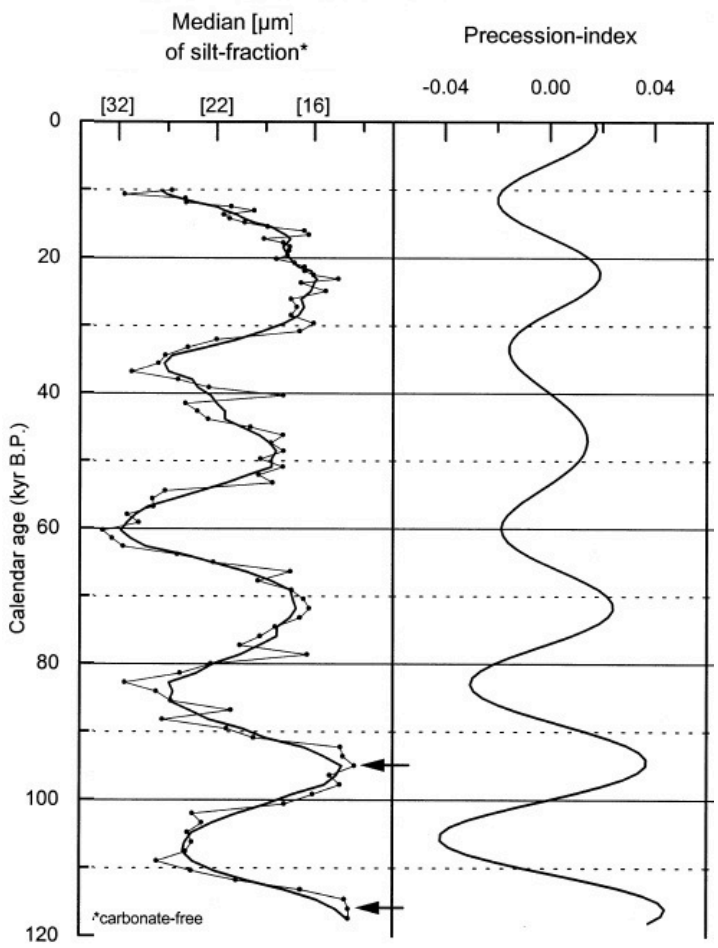

Figure 1.16. Median (mm) silt-fraction grain size data of GeoB 3375-1 core, located offshore Chile, 27ºS (Lamy et al., 1998) and precession index (Berger and Loutre, 1991). Higher precession lead to wetter climate and enhanced seasonal precipitation. Increased chemical weathering and fluvial sediment caused the deposition of finner grain-size detritic material. Modified from Lamy et al. (1998).

On the other hand, obliquity is known to have a stronger influence at higher latitudes with an important control on seasonality. For example, high obliquity values have been related to reduced Antarctic sea-ice, intensification of ACC and stronger CPDW upwelling because of higher summer insolation (Pena et al., 2008). As obliquity forcing over low latitude insolation is relatively small compared to the radiation received along the year (<3 W/m^2), it is likely that while precession is the main orbital pacemaker for tropical and subtropical climate, obliquity can act as modulating the signal amplitude (Lee and Poulsen, 2005; Pena et al., 2008). Two possibilities stand out to explain how 41 kyr periodicity cycles have been also observed in SST records from equatorial Pacific (Clemens et al., 1991; de Garidel-Thoron, 2005). It has been proposed that the high latitude obliquity signal propagates northward via atmospheric (Chiang and Lintner, 2005) or oceanic teleconnections (Bostock et al., 2004; Fedorov et al., 2006). Some authors have suggested that obliquity indirectly influenced other factors, as atmospheric CO_2 concentration (Ruddiman, 2003). Following these ideas, Lee and Poulsen (2005) used a coupled ocean-atmosphere model to run two glacial simulations with high and low axial tilt. The results showed how extratropical water heating was enhanced by the reduction of sea-ice. The anomalous warming generated dynamical responses as a weakening of midlatitude westerlies, contributing to a 20% reduction in the flowing of Pacific gyre. This situation together with advection and reduction of tropical heat export resulted in warming of subsurface waters of equatorial Pacific and a deepening of the thermocline (Lee and Poulsen, 2005).

1.6.2 Main atmospheric and oceanic processes during the last glacial cycle over Southern Pacific

Intertropical Convergence Zone migration

As stated from models and several records, during cold periods on Northern Hemisphere such as glacial, stadial and Heinrich events, North Atlantic Deep Water formation slows down and the polar front advances to lower latitudes. The tropical response to this configuration is a southward movement of both the Equatorial current and the Intertropical Convergence Zone (Clement and Peterson, 2008). Most tropical reconstructions of precipitation agree with the southward latitudinal migration of the ascendant branch of the Hadley cell. Records located in the Northern Hemisphere and $\delta^{18}O$ reported from Hulu Cave speleothems on eastern China (32°30'N) (Wang et al., 2004, 2007), reflectance measurements from sediment cores of Cariaco basin (10°43'N) (Peterson et al., 2000; Haug et al., 2001) as well as $\delta^{18}O_{sw}$ records changes in Sulu Sea from MD 97-2141 marine core (8.8°N) (Oppo et al., 2003; Dannenmann et al., 2003; Rosenthal et al., 2000) show a dominance of dry conditions during global stadials. In contrast, Southern Hemisphere records are consistent indicating humid climate conditions. These wetter humid conditions have been described offshore of the South American Atlantic coast in base to the Ti/Ca ratio of GeoB 3912 and GeoB 3104 cores (3°40'S, Arz et al., 1998). The same climatic pattern has been described by Muller (2006) from Lynch crater (17°S) peat record in Australia and also in Boutuverá Cave (27°S, Brazil) or in Northern Brazil travertine formations (10°S, Wang et al., 2007). This opposite hydrologic trend suggests an antiphase precipitation pattern for tropical Northern and Southern Hemisphere (Peterson et al., 2000; Tierney et al., 2008; Leduc et al., 2009).

Southern Westerlies and high latitude configuration

An additional consequence of the ITCZ southward migration is a higher equator-to-pole pressure gradient over Southern Hemisphere which contributes to the South Westerlies (SW) intensification (Anderson and Carr, 2010; Heirman, 2011) and northward migration (Lamy et al., 1998). This configuration has been a proposed as climate scenario for the LGM (Lamy et al., 1998, Stuut et al., 2004, Toggweiler, 2006). Furthermore it has been described that SW position has been strongly depending on precession cycles (Section 1.6.1).

A process intimately linked with the SW is the formation of intermediate water masses in the Southern Ocean. During DO stadials changes in the formation rate of the Antarctic Intermediate Water (AAIW) have been described in the marine record MD97-2120 from Chatman Rise, east New Zealand, in base to the $\delta^{13}C$ from benthic foraminifera (Pahnke and Zahn, 2005). Periods of increased AIWW production are in phase with Southern Hemisphere warmings and southward shifts of the ITCZ (Pahnke and Zahn, 2005). During DO stadials, due to the bipolar seesaw, the Antarctic continent and the Southern Ocean warmed, and consequently the Antarctic sea ice retreated (Anderson and Carr, 2010; Skinner et al., 2010). The reduced sea ice extension would further lead to a southward shift of the ITCZ and a strengthening of the SW which would contribute to enhanced upwelling of circumpolar deep water and to a more efficient downwell for AIWW (Anderson and Carr, 2010; Skinner et al.,

2010). This oceanic situation also induced the release of oceanic CO_2 stored in poorly ventilated deep water masses (Anderson and Carr, 2010; Skinner et al., 2010).

Paleo-ENSO

Because its undeniable importance for understanding present day ENSO dynamics, many modeling efforts intended to figure out the evolution of this climatic phenomenon during Late Pleistocene and Holocene.

Some modeling works have suggested that radiative forcing acts as the main driver controlling ENSO variability (Zebiak and Cane, 1987). A coupled ocean-atmosphere model proposed by Zebiak and Cane (1987) (ZC model) predicted a differential answer to radiative anomalies from East and West margins of the Pacific Ocean. When there is a homogenous radiative anomaly across the Equator, the oriental Pacific has a reduced response compared to the occidental one, following what is called the "oceanic thermostate" (Clement et al., 1999). The shallower position of the thermocline in the eastern margin of the Pacific Ocean keeps the oriental equatorial Pacific cooler than the occidental part (Bjerkness positive feedback). The asymmetric responses over East and West Pacific lead to El Niño or La Niña-like scenarios. The ZC model has been used to test if there has been an influence of Milankovich cycles over ENSO dynamics on orbital timescales (Figure 1.17). Results from coupled modeling show changes on the number and amplitude of El Niño and La Niña-like events as a response to insolation changes caused by prescession for the last 150 kyrs (Clement et al., 1999).

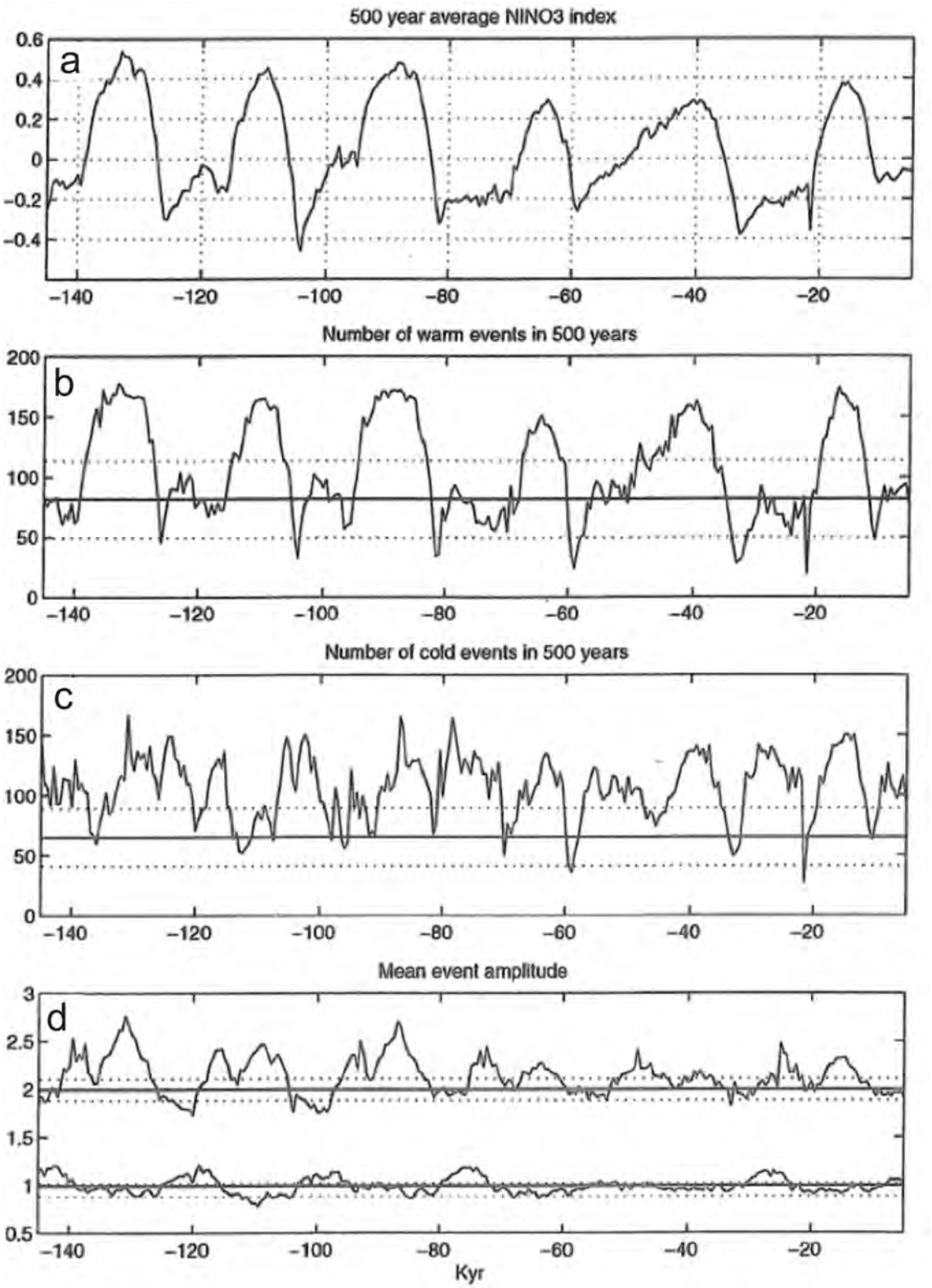

Figure 1.17. From the top to the bottom: (a) 500 year average NINO3 (in ºC degrees) index from Zebiak-Cane model forced with Milankovitch solar forcing, (b) Number of El Niño-like events for 500 year non-overlapping periods (c) Number of La Niña-like events for 500 year non-overlapping periods, (d) Mean amplitude of warm (top curve) and cold (bottom curve) events. The thick line indicates the mean values for each statistic for the control run with 95% confidence limits (dotted lines) (Clement and Cane, 1999). The results show that strong precessional forcing can be defined from model.

Other coupled general circulation models (CGCMs) were developed with the purpose of determining the influence of Atlantic Meridional Overtuning Circulation (AMOC) changes on tropical Pacific, and specifically over ENSO dynamics. Timmermann et al. (2007) obtained that a substantial weakening of the AMOC reorganizes the tropical atmospheric circulation favoring the strengthening of the northeasterly trade winds and the southern migration of the ITCZ. According to these authors, the southward shift of the ITCZ leads to a weakening of the annual cycle in the eastern equatorial Pacific and a subsequent intensification of the ENSO recurrence (Timmernann et al., 2007).

Evidence for a late-Pleistocene active ENSO dynamics have been obtained not only from modeling but also from paleoenvironmental reconstructions. Tudhope et al. (2001) used $\delta^{18}O$ from Porites corals from different time intervals to reconstruct changes in the Pacific circulation. These authors suggested that ENSO has been active during the last 130 kyr, also during glacial times. Mg/Ca ratios in foraminifera from marine sediments near the Galápagos Islands were used by Koutavas et al. (2002) to reconstruct SST and equatorial Pacific temperature gradient. For these authors, a lower SST gradient during LGM weakened Hadley and Walker circulation cells suggesting an El Niño-like scenario during glacial times. This pattern is coherent with the proposed southward displacement of the ITCZ and the results of some CGCMs (Timmermann et al. 2007). However, conflicting evidence have been published and other authors inferred a "La Niña-like"conditions for the same period (Beaufort et al., 2001; Andreasen et al., 2001).

Due to the scarcity of long-scale time records with the appropriate resolution to accurately characterize the ENSO signal, most of paleo-ENSO reconstructions span the Holocene period. There is a general agreement that ENSO variability was weak (or even not active) during early Holocene (10 to 6 kyr BP), that increased along the Holocene and achieved its maximum intensity between 1 and 2 kyr BP. Since then its intensity has been decreasing up to nowadays (Sandweiss et al., 1997, Moy et al, 2002; Conroy et al., 2008) (Figure 18). The recent low ENSO activity has been attributed to increased radiation during the boreal summer, what activates the "oceanic thermostate" mechanism, leading to a high SST gradient along the equator and La Niña-like configuration for Southern Pacific.

Geoarcheological works carried out at northern Perú investigating marine faunal inventories and human settlements suggest a main climatic change at 5 kyr cal BP and the onset of ENSO activity thereafter (Sandweiss et al., 1997). However, other records show how ENSO was active during the entire Holocene, even in a weak form. The Pallcacocha Lake (Southern Ecuador) receives enhanced precipitation during El Niño events due to a more vigorous convection over the warmer waters of Equatorial coast (Figure 18). Moy et al., (2002) studied the reflectance of the sediment cores from Pallcacocha Lake reconstructing precipitation intensity and showing how ENSO events became progressively more frequent along the Holocene period (Figure 14), depicting an amplitude peak between 2 and 1 kyr cal. BP, which decreased thereafter (Moy et al., 2002; Conroy et al., 2008).

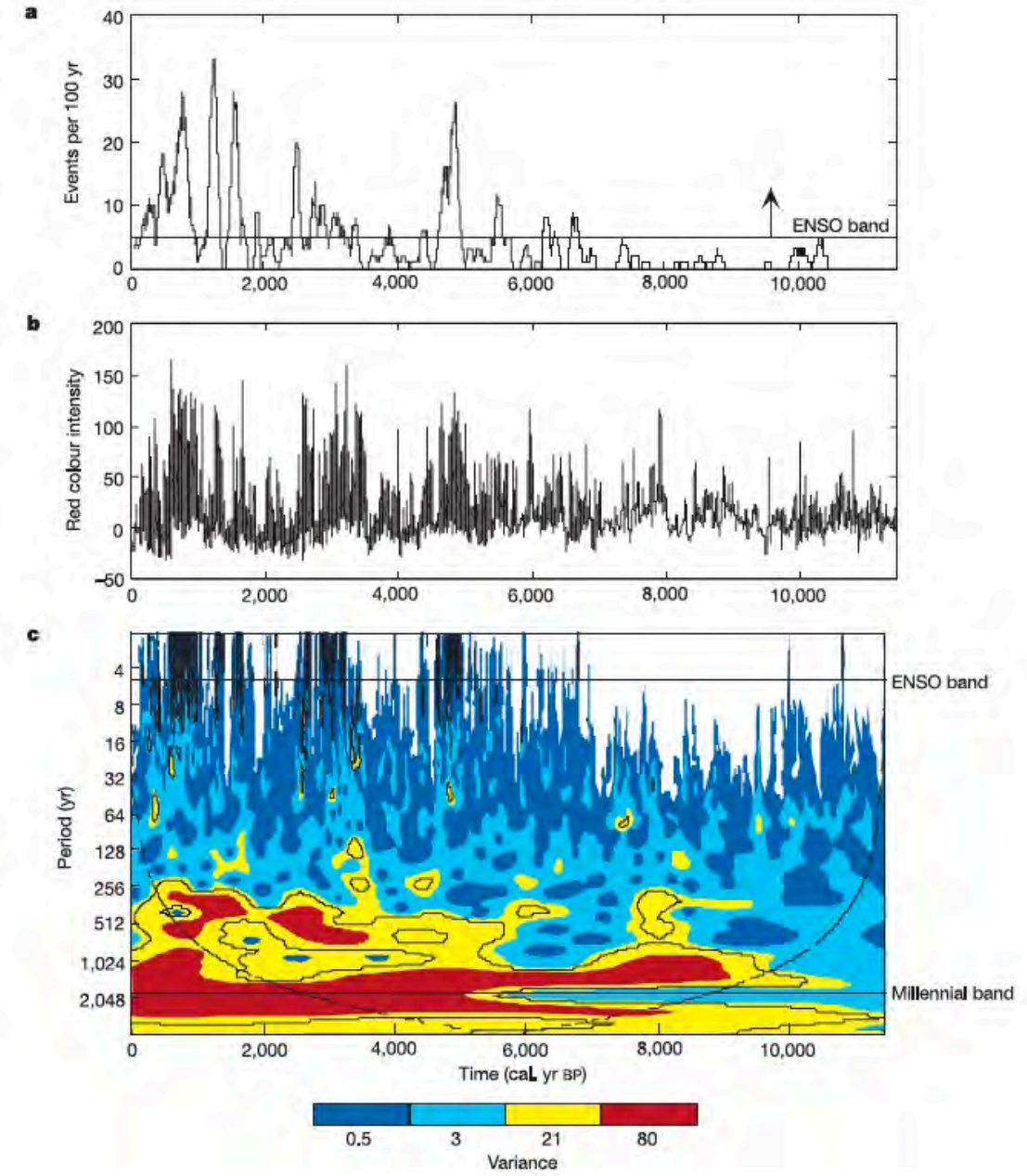

Figure 1.18. Time series and wavelet spectrum of the Pallcacocha Lake sediment reflectance showing ENSO variability during the Holocene. a) Time series illustrating the number of events in 100 yr overlapping windows. The solid line indicates the minimum number of events in a 100 yr window needed to produce an ENSO band variance. b) Last 11.5 kyr BP measurements of red colour intensity of sediment core as a proxy of ENSO activity. The absolute intensity and the width of the laminae do not correspond to the intensity of ENSO events. C) Wavelet power spectrum on the series of red color intensity (Morlet wavelet) (Moy et al., 2002).

The Pallcacocha record also shows a 2 kyr cycling millennial variability that has been associated to Bond events (Section 1.6.1, Bond et al., 1997). Another record from the Cariaco basin (Venezuelan offshore) track changes in precipitation caused by shifts in the ITCZ position (Haug et al., 2001). A main change between 3.8 and 2.5 kyr cal BP depicting a strong oscillation of the ITCZ position has been related to increased ENSO variability by comparing the Cariaco basin record with other ENSO sensitive records (Peterson et al., 2001). The direct relation between ENSO and the ITCZ position plays a relevant role in ENSO variability reconstructions.

AIMS

The aims of this PhD Thesis are: a) to reconstruct the environmental history of Rano Aroi mire using an interdisciplinary approach, combining chemical and biological proxies and b) to understand the climatic variability occurred on Southern Central Pacific from MIS 4 and its mechanistic teleconnections with regional to global climate dynamics.

THESIS STRUCTURE

This thesis is composed of 10 Chapters. Chapter 1 provides a state of the art introduction to peatland types and characteristics as well as the most common techniques used to study them as palaeoenvironmental archives. Introduction also includes a presentation on main Southern Pacific oceanic and atmospheric circulation and past and present climatic features. The regional setting of Rano Aroi mire, including explanations on geology, hydrology, climate, flora and former studies carried out in Easter Island are found in Chapter 2. All methodological procedures employed are described in Chapter 3 while Chapter 4 includes the results of the chemical, biological and statistical analyses performed.

Discussion is composed of Chapters 5, 6, 7 and 8. Chapter 5 represents the first approach to Rano Aroi record. The age model is constructed and peat facies are interpreted. This information combined with the macrofossil record and the results of TC, TN, $\delta^{13}C$ and Ti, Fe, Ca measurements permited us to define the main hydrologic states of Rano Aroi. Chapter 6 the peat mineral fraction composition is used to determine the three main environmental processes that controlled peat organic and inorganic chemistry. Mineral matter composition changes through time are compared to the stable isotope composition of organic matter (TC, TN, TS, $\delta^{13}C$, $\delta^{15}N$, $\delta^{34}S$) and to the results of the pollen analyses. Chapter 5 and 6 main outcomes are integrated in Chapter 7 to draw a complete environmental reconstruction of Rano Aroi stages and processes from 70 kyr BP to late Holocene. In this chapter, the mire history is compared to other Easter Island and regional records. Chapter 8 focuses in the rapid MIS 3 climate variability in the Southern Pacific. The main climatic changes recorded in Rano Aroi are compared to several sequences representative of tropical to high latitude climate dynamics. This procedure permits to assess the mechanistic processes affecting hydrologic changes in Central Pacific during this period of time. On chapter 9 a synthesis of entire discussion is performed. Finally, chapter 10 provides the concluding remarks of the thesis and future works proposed to decipher some of the remaining open questions. The raw data obtained during the experimental procedures are listed in the appendices.

CHAPTER2

THE STUDY SITE

The island of Rapa Nui was named as Easter Island by the explorer Jacob Roggeven after the first European arrival on 1722 (Sharp, 1970) and is considered the easternmost Polynesian spot. Other local names given by native people in their own language (Rapa Nui) to this land are Te Pito o Te Henua ("navel of the world") or Mata kit e Rangui ("eyes that look to the sky"). This tiny (24 km length) and volcanic island is situated on Central Pacific (27° 07'S, 109° 22'W) at 3526 km from South America, the closest continent (Figure 1).

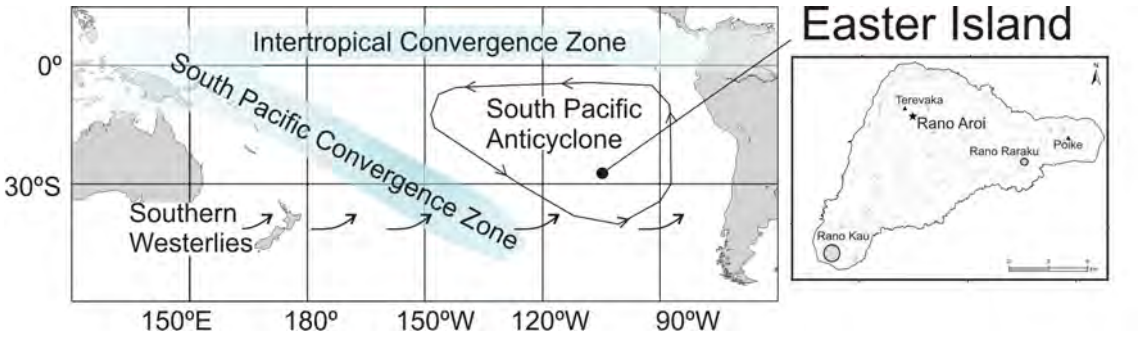

Figure 2. 1. Left: Easter Island location in Central Southern Pacific Ocean. Main atmospheric patterns affecting the climate of the island are shown: (1) Intertropical Convergence Zone and (2) South Pacific Convergence Zone are low pressure belts associated to the descending branch of Walker circulation therefore storm formation areas. (2) South Pacific Anticyclone is a mid latitude high pressure center located at 30ºS and (3) Southern Westerlies are strong prevailing winds main drivers of extra-tropical cyclones. Right: Main geographic features are shown of Easter Island. Terevaka (highest summit, 511 m asl) and Poike are two important volcanic centers. The three permanent water bodies are Rano Kau, Rano Raraku (lakes) and Rano Aroi (mire).

2. 1. Climate in Easter Island

Easter Island climate is subtropical, with average temperatures between 18°C and 24°C (Junk and Claussen, 2011) and highly variable annual rainfall (mean of 1130 mm) oscillating between 500 and 1800 mm/y (Figure 2.2) (CONAF, 1997). Three interacting climate modes rule precipitation in the eastern Pacific: the South Pacific Anticyclone (SPA), cyclonic storms carried in by the Southern Westerlies (SW) and the South Pacific Convergence Zone (SPCZ) (Figure 2.1). The island itself is located under the influence of the SPA, what commonly leads to high-pressure values being 1016 mb the annual average (CONAF, 1997).

The weakening of the SPA during the winter, the northward migration of the SPCZ and SW lead to the island the highest precipitation from April to July (Figure 2.2). In winter, rainfall occurs due to depression fronts, while summer rain is mainly driven by the land–sea breeze and convection induced by the warmer Sea Surface Temperatures (SST) and Easter Island orography (Mucciarone and Dunbar, 2003; Junk and Claussen, 2011). No correlation has been found so far between rainfall of the island and the biggest year-to-year climate

variation on Earth, the El Niño-Southern Oscillation (ENSO) (MacIntyre, 2001a, 2001b; Genz and Hunt, 2003), although ENSO variability and dynamics are responsable for changes in the SST and the predominant wind direction in the region (Mucciarone and Dunbar, 2003; Anderson et al., 2006). Stable isotope studies carried out in coral reefs of Easter Island show how during warm ENSO events the winter SST are higher and the summer temperatures lower, leading to weaker seasonality (Mucciarone and Dunbar, 2003).

Westerlies winds blow the 68% days of the year with average velocities between 5 and 7 knots reaching sporadically the 15 knots. During summer the prevalent winds blow from E and SE while during austral winter (specially July) there can be strong winds blowing from NW, W and SW. Ascendant air masses are common over the island as it is effectively warmed by sunlight in contrast with the relatively cold ocean water. This process triggers the formation of frequent convective storms. Relative humidity oscillates between 75 and 81% reflecting a strong oceanic signal (CONAF, 1997).

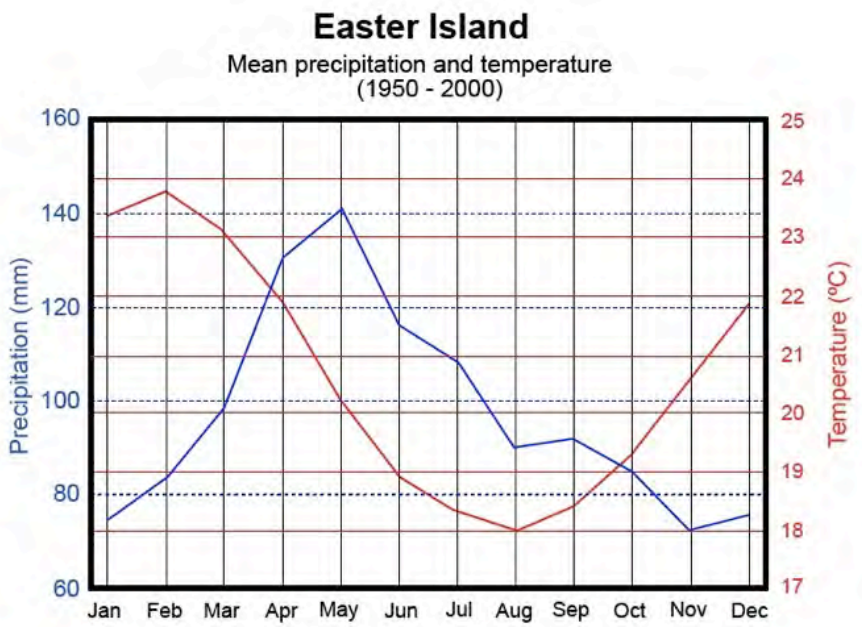

Figure 2.2. Easter Island climograph including average monthly precipitation and temperature for the interval between 1950 and 2000.

2.2 Geological and hydrogeological setting

Easter Island is the highest point and the single area above sea level of a seamount range situated on the Nazca plate (Figure 2.3). This seamount range lies close to limit of the plate. Easter Island microplate has been originated by the interaction of a hot spot and the oceanic ridge (González-Ferran et al., 2004). The range is around 400 km long and volcanic activity started 5 million years ago. Geological and lithological surveys have dated Easter Island oldest rocks by 3.0-2.64 ± 0.28 million years, age that is given to the onset of the aerial phase of the island (Figure 2.3).

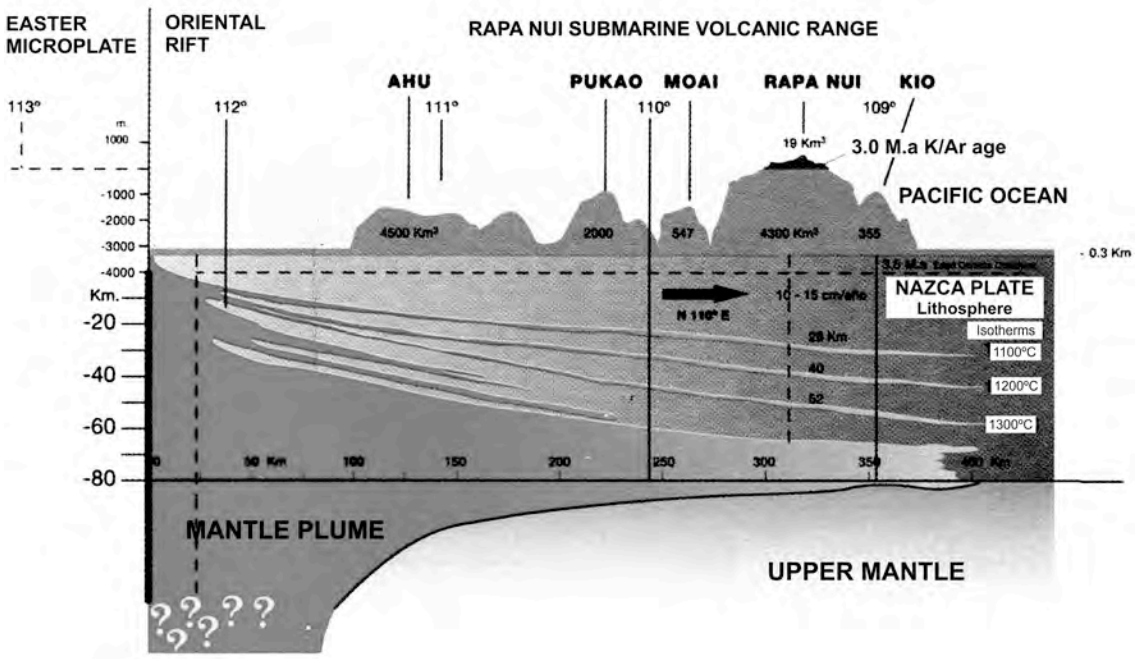

Figure 2.3. Easter Hot Spot schematic cartoon. Isotherms are deeper on the oriental sector due to the cooling of the younger area of the Nazca Plate (modified from González –Ferran et al., 2004 and Haase and Devey, 1996).

The island is the result of the volcanic activity of three main structures: the Terevaka fissure complex, the Poike strato-volcano and the Kau caldera, each of them constituting one vertex of its triangular shape (Figure 2.1). The topography of the island is characterized by more than 70 volcano craters, and rolling surfaces of lava flows (Baker et al., 1974; González-Ferran et al., 2004). Lavas of Easter Island show a very diverse compositional ranging from tholeiites, hawaiites (the most abundant lithology), mugeraites, benmoreites, trachytes and rhyolites (Figure 2.4). Main volcanic formations are basic and mafic while the intermediate and acid rocks are concentrated on the southwestern part of the island. In general, the Easter Island basaltic rocks have high contents of Fe, Ti and Zr and are low in K and Mg whereas the old Poike lava flows are lower in Zr, Y and Zn than younger formations. Olivine is abundant in basalts, in particular in the younger flows of Rohio area were microphenocrysts are very common depicting high contents of Mg, Ni and K (Baker et al., 1974).

Except for a few coastal creeks, a surface drainage network does not exist in Easter Island, because precipitation infiltrates immediately in the very pervious lava flows (Herrera and Custodio, 2008). Studies from Alamos and Peralta (1992) indicate permeabilities greater than 1000 m/day for most of the young volcanic formations with scoria layers and obtained transmissivity values between 20.000 and 40.000 m^2/day from pumping tests carried out in several boreholes. From hydrological surveys a low-permeability volcanic core is expected but its exact altitude is uncertain. Average recharge is estimated to be around 300-400 mm/yr and the total freshwater outflow as 50-60 Mm^3/yr (Herrera and Custodio, 2008).

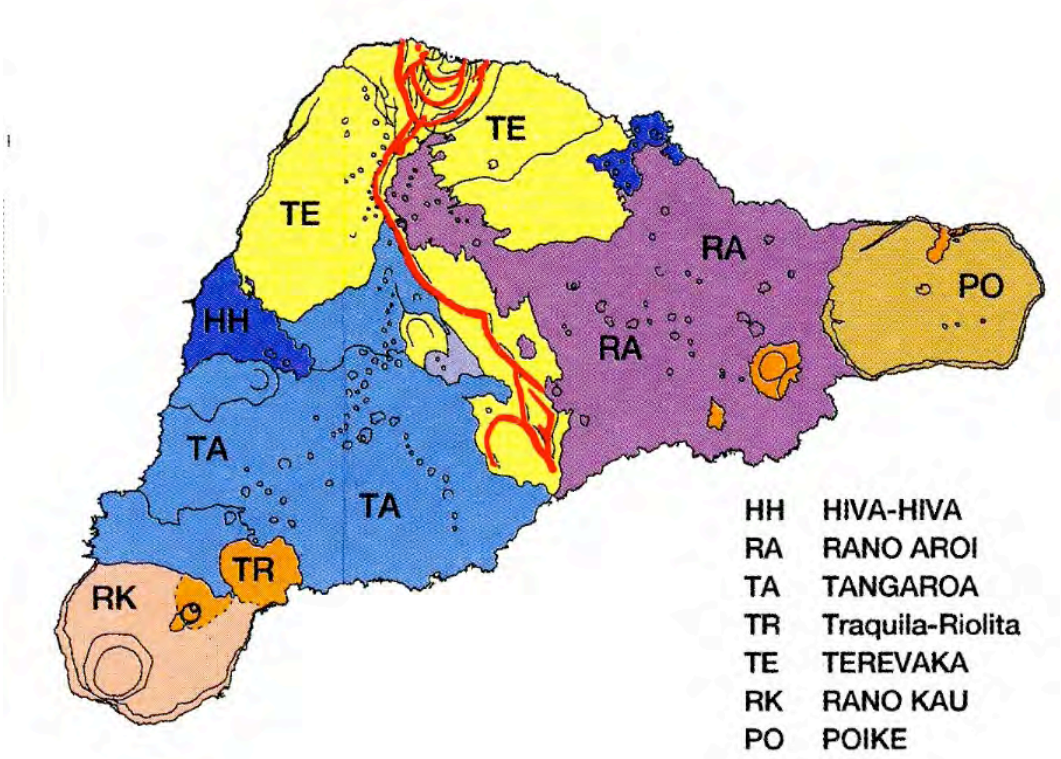

Figure 2.4. Summarized geologic map of Easter Island showing the main volcanic groups. Hiva-hiva group: Younger area (Rohio), olivinic basalts with pyroclastic cones. Rano Aroi group: Lavas resulting from Rift activity. Dominant lithology is strongly porphyritic hawaites, tholeites and mugearites. Tangaroa group: Terevaka volcano is responsible of the central volcanic activity of the island; the area is characterized by olivinic tholeites and hawaites. Trachyte-rhyolite group: Lava dome of trachytic or rhyolitic composition. Rano Kau group: Alcaline basalts, olivinic tholeites among others forming a shield volcano caldera. Poike group: Volcanic shield composed of olivinic basalts, hawaites and mugearites. Thick lines indicate volcanic subsidence and associated landslides (From González-Ferran et al., 2004).

There are three permanent water bodies in Easter Island: Rano Raraku (Figure 2.5), Rano Kau (Figure 2.6) and Rano Aroi (Figure 2.7). Water isotope analyses ($\delta^{18}O$, δD) show that Rano Raraku and Rano Kau are hydraulically perched above water table probably sustained by lacustrine low permeability formations (Figures 2.5 and 2.6). This is because they present a water isotopic signature evidencing evaporation of accumulated rainfall. By contrast, Rano Aroi mire (Figure 2.8) water signature shows that it may correspond to a perched aquifer or water table outcrop as indicates renovated underground origin (Herrera and Custodio, 2008).

Other water chemistry investigations on a set of 52 rainfall, lagoon, lava tubes and groundwater samples indicate that the sodium-chloride water type dominates especially on the coastal sites because of the direct marine influence (Figure 2.8; Herrera and Custodio, 2008).

Figure 2.5. Rano Raraku crater (Picture by O. Margalef).

Figure 2.6. Rano Kau crater (Picture by O. Margalef).

Figure 2.7. Rano Aroi mire (Picture by O. Margalef).

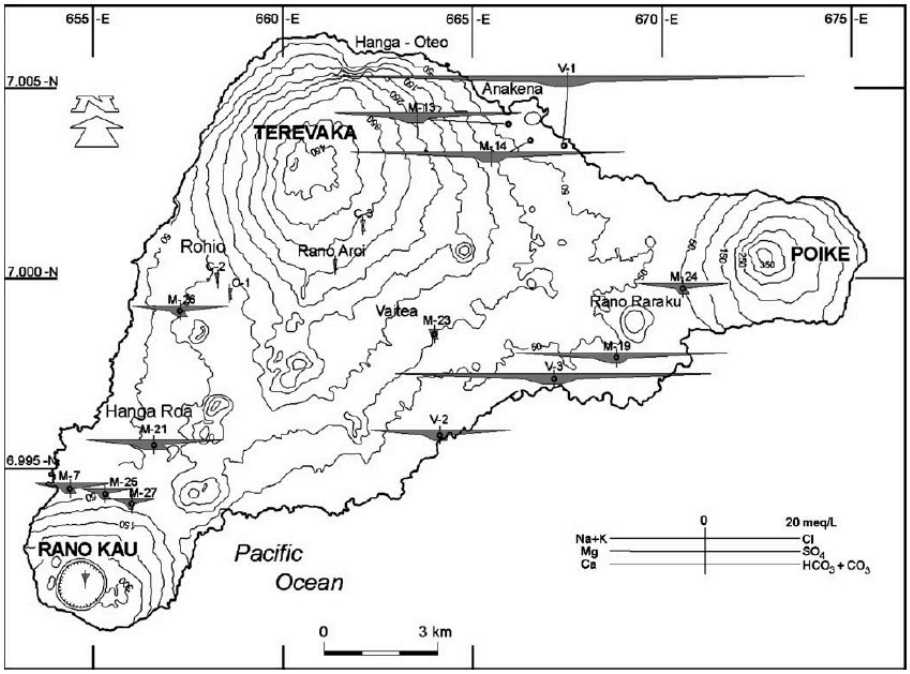

Figure 2.8. Modified Stiff diagrams of Easter Island groundwaters showing ionic composition of Na+K, Cl, Mg, SO_4, Ca, HCO_3+CO_3 (Herrera and Custodio, 2008).

2.3 Easter Island flora

2. 3. 1 Present day flora

The Easter Island flora exhibits low diversity because it has been almost completely altered by humans. The reduced size of the island and its obvious isolation from main continent and other islands have also been considered as important factors to explain the low diversity. Anthropic pressure is still threating vegetation composition with activities as grazing by horses and sheeps or by the introduction of invader species (Zizka, 1991; Rull et al., 2010a). The island is covered nowadays by meadows (90%), forests (5%), shrublands (4%), and pioneer and urban vegetation (1%) (Etienne et al., 1982; Rull et al., 2010a). An exhaustive flora review from Zizka (1991) propose that there are up to 179 angiosperm species, being 30 native from the island (Figure 2.9), 141 introduced and 8 of uncertain origin. Many of the native species still present in the island have been preserved on the steep slopes of Rano Kau crater and on Motu Noi, a small islet situated in front of the Southwest coast of Easter Island. These areas are hard to access what has prevented human activities to strongly modify the vegetation as in other parts of the island. Interestingly, the native plants seem to have been established in the island by bird transport, as most of the angiosperm found do not present wind dispersal mechanisms for such distances.

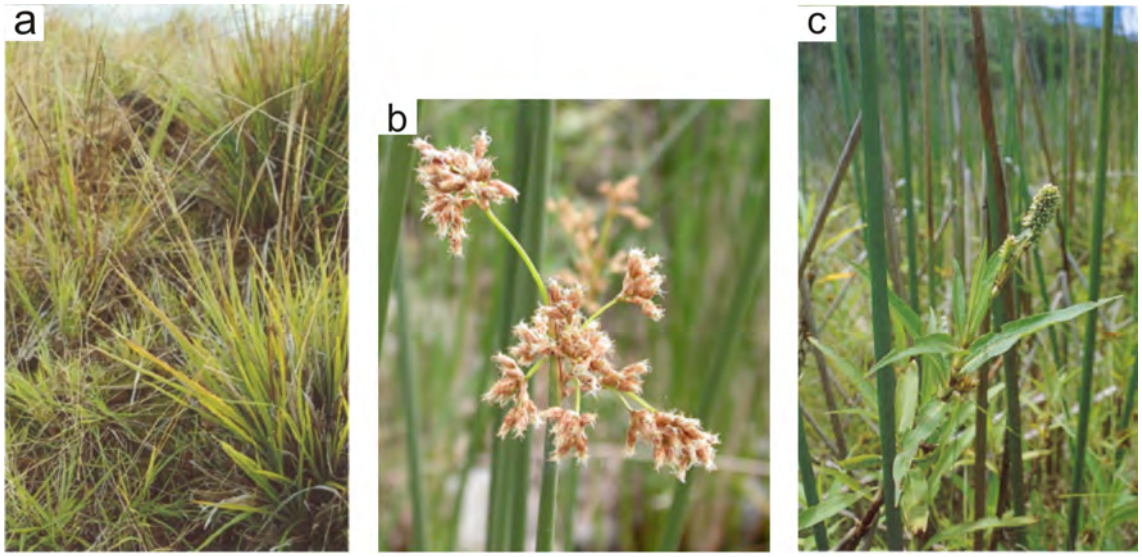

Figure 2.9. Three native plants of Easter Island. From left to right (a) The endemic Poaceae *Axonopus paschalis* (local name Herike Hare) (b) The flower of *Scirpus californicus* (Cyperaceae) (local name Ngaatu) and (c) *Polygonum acuminatum* a common Polygonaceae on Easter Island lakes and mires (local name Tavari) from Zizka (1991).

The families with more species are Asteraceae (19), Fabaceae (18) while Poaceae (9) and Cyperaceae (5) are the families that include more native plants (Zizka, 1991). *Sporobolus indicus* and *Paspalum scrobiculatum* are the grasses that dominate the Easter Island meadows, together with *Axonopus paschalis*, common on the Terevaka area. The introduced *Psidium guajava* (Myrtaceae), is the most abundant bush forming large shrublands. On the Island there are several plantations of introduced *Eucalyptus* spp. (Myrtaceae) and *Dodonaea viscosa*

(Sapindaceae). These two introduced trees and the *Thespesia populnea* from Malvaceae family (it is unknown if it was native or introduced by Polynesian settlers) constitute the scarce forested areas (Zizka, 1991). Macrophytes are common around the lakes and on Rano Aroi mire. Permanent fresh water guarantees the habitat for *Scirpus californicus* (Cyperaceae) and *Polygonum acuminatum* (Polygonaceae), commonly found on the edges of the water body (Figure 2.9).

2. 3. 2 Ancient native flora

As the native Easter Island flora has been intensely perturbed, pollen analysis becomes an invaluable tool to decipher former vegetation. Palynological results and its comparison with the vegetation of other polynesic islands have been used to reconstruct past flora composition. Hereby the pollen types found on Rano Aroi mire peat cores (obtained in section 4.6.2) are listed and compared to the appearance of the taxa in relatively nearby islands (Flenley et al., 1991, Azizi and Flenley, 2008).

Trees and herbs pollen types

- **Asteraceae.** Species belonging to this family **and** consisting in arbustive types are present in Hawaii (as *Campylotheca* spp. Schultz-Bip and *Chrysogonum* spp. L.) Rapa or Juan Fernandez Islands. They form scarce-forested landscapes near lava flows or in between true forest. Nowadays Asteraceae native species are not found on Easter Island (Brown, 1935; Flenley et al., 1991, Zizka, 1991) (pollen picture on Figure 4.10).
- **Poaceae:** Native and endemic **Poaceae** are nowadays found in meadows and open landscapes. Some of the species are: *Bromus catharticus* Vahl present in Rano Kau crater and Motu Nui. *Agrostis avenacea* J. F. Gmel and *Paspalum forsterianum* Flüggé is very common in Motu Nui. *Dichelachne crinite* (L. f.) Hook. f. and *Dichelachne micrantha* (Cav.) Domin are found in Rano Kau, Rano Raraku and Terevaka forming grasslands. *Sporobolus indicus* (L.) R. Br. Axonopus paschalis *(Steud.)* Chase ex P. Beauv. 1911 is found in mid altitude meadows, near Terevaka summit while *Danthonia paschalis* is very common near seaside (Dubois et al., 2013).
- **Arecaceae:** The presence of native palm trees have been corroborated by the found of this pollen type in lake sediments (Figure 4.10), but also by the presence of ancient root traces and small coconuts in archeological sites. This extinct Palm tree has been defined as *Paschalococos disperta* based on the description of the endocarp of fossil seeds (Dransfield et al., 1984, Zizka, 1991). Its main features indicate that this specie was very similar to *Jubaea chilensis* (Molina) Baill, a very tall Palm tree present in Chile (Dransfield et al., 1984, Flenley et al., 1991) (Figure 4.10).
- ***Plantago*:** Two Plantago species (from Plantaginaceae family) have been described to be present in the island nowadays (*P. major, P.lanceolata*). These two herbaceous species have been classified as introduced by humans and *Plantago cf.* pollen has been identified by palynologic studies in Rano Raraku and Rano Aroi (Flenley, 1991).
- ***Triumfetta semilotroba:*** (local name: Hau Hau) is a plant from the Malvaceae family found on Central America and Caribbean. It can be a small shrub or a tree and it is nowadays found on the open areas of Rano Kau crater, above 110 m high (Zizka, 1991; Dubois et al., 2013).

- ***Sophora toromiro:*** is an endemic Fabaceae (local name: Toromiro). It can be a shrub or a small tree, currently extinct in nature but cultivated in several botanical gardens. Trials of growing and reintroducing this tree on the inner slopes of Rano Kau have been performed since 2010 (Zizka, 1991; Dubois et al., 2013).
- ***Coprosma:*** This is a common pollen type in Rano Aroi peat and it represents a genus of Rubiaceae family present on many Pacific sites of similar latitude as New Zealand, Hawaii, Borneo, Rapa, Juan Fernández (Brown, 1935) but completely extinct nowadays from Easter Island (Flenley, 1991; Figure 4.10).
- **Macaranga:** Although this family is neither found nowadays in the island, the presence its pollen type in ancient lake sediments has been reported by Flenley et al. (1991) and Horrocks et al. (2013). Moreover it has been also identified from wood fossil remains from archaeological deposits (Orliac, 2000). This family is present in other relatively nearby Polynesian islands like Raivavae Island (Dr. Matthew Prebble, personal communication).
- Other pollen types found and previously described on Rano Aroi peat but less abundant are: *Acalypha*, *Pinus*, *Sapinus*, Ulmaceae (Flenley et al., 1991).

Aquatic and semiaquatic plants and ferns

- **Cyperaceae:** This is an abundant pollen type predominantly representing taxa found in moist and waterlogged parts of grassland meadows or peatlands (Table 4. 4). Zizka (1991) presented four Cyperaceae species can be considered native: *Cyperus eragrostis*, *Scirpus californicus* (sin. *Schoenoplectus californicus*, local name N'gaatu), *Cyperus cyperoides* and *Cyperus polystachyos* (Dubois et al., 2013).
- ***Polygonum acuminatum*** (sin. *Persicaria acuminata*, local name: Tavari): This is a very common aquatic Polygonaceae present in Central America and Caribbean. It is found in ancient sediments and nowadays occupies the edges of lakes or mires of the island and it is associated to *Cyperaceae* species.
- **Fern spores** constitute an important part of the palynologic record of Rano Aroi, in contrast to what is found in Rano Raraku lake sediment cores (Flenley et al., 1991, Cañellas-Boltà et al., 2013). Although some species present different requirements (substrate, altitude), in general, we can assume that ferns are present in moist, shady areas of meadows and rocky outcrops or caves, but not in completely waterlogged soils or peaty environments. The list of the native ferns found nowadays in the island include: *Thelypteris espinosae* Lam., *Pneumatopteris costata* Brack*., Christella dentate (*Forsskal), *Cyclosorus interruptus* (Willd.) H.Itô, *Psilotum nudum* (L.) P. Beauv. 1805, *Microsorum parksii Link* Hort. Berol. 1833, *Ophioglossum lusitanicum* L., *Doodia paschalis* R. Br., *Asplenium obtusatum* G. Forst, *Elaphoglossum skottsbergii* Krajina, *Diplazium fuenzalidae* Espinosa, *Polystichum fuentesii* Espinosa

2. 4. Human arrival and late environmental history

The explorers that first occupied almost all Pacific Islands came from the western Pacific Rim (Papua New Guinea). The Lapita matrilineal culture moved out from Bismark Archipelago around 3280 cal yr BP (Nunn, 2007) to travel east, towards an ocean punctuated by small islands. They were excellent sailors and colonized most important islands of

Melanesia including Vanuatu, New Caledonia, Fiji and arriving to Samoa and Tonga. After 2500 cal yr BP Lapita culture disintegrated and evolved in newer polynesic traditions along their movements from island to island (Burley and Clark, 2003). Gradually, polynesic expeditions colonized oceanic islands from west to east.

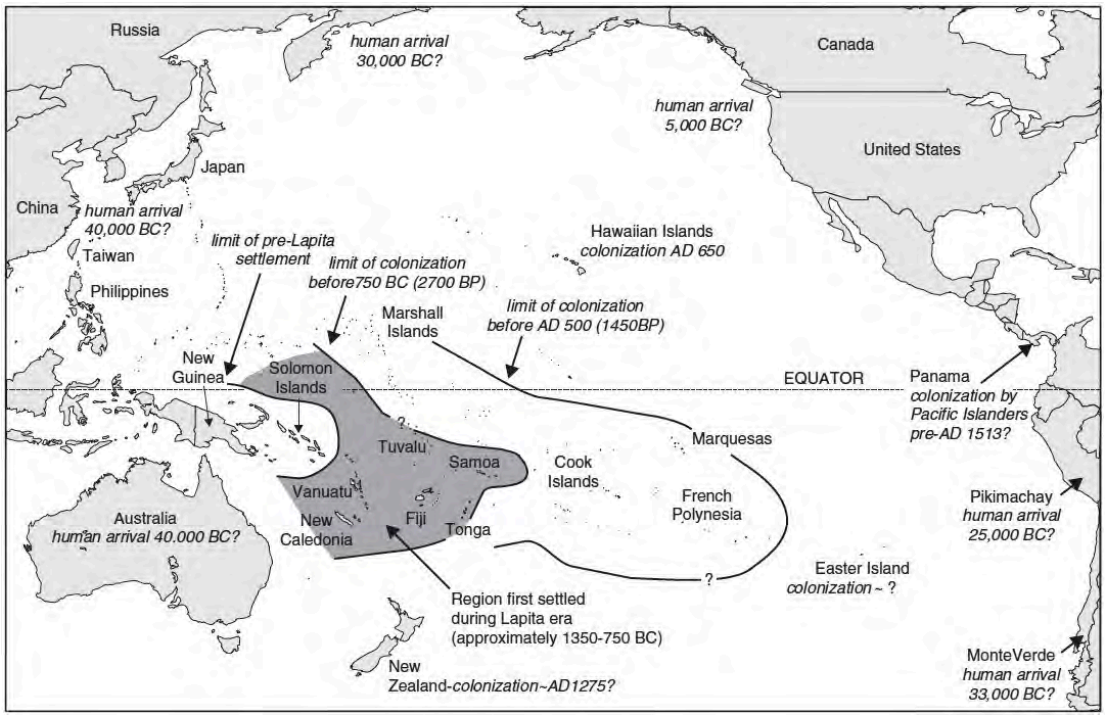

Figure 2.10. Map of the Pacific Ocean showing human settlements and proposed age of islands colonization (modified from Nunn, 2007).

The Polynesian canoes reached the French Polynesia around AD 600, the island of Hawaii at about AD 650 and the arrival to New Zealand was probably later, about AD 1250-1300. However, the precise timings of colonization are still a matter of debate, especially in the case of Easter Island. It seems that climatic factors as prevailing winds controlled by ENSO dynamics could have had an important role in providing better climatic conditions for migration (Anderson et al., 2006). A radiocarbon dates compilation and meta-analysis realized by Wilmshurt et al. (2010) suggested two short episodes of population radiation to eastern Pacific: at AD 1025-1120 (in the Society Islands) and at AD 1190-1290 (remaining areas as New Zealand, Hawaii, Rapa Nui). Nevertheless, the most accepted view from archeological evidence is that the initial colonization of central Polynesia (including Marquesas and Society Islands) occurred c. AD 300-900 (Kirch and Kahn, 2007).

Former archeological and paleoenvironmental studies in Easter Island situated the age of first Easter Island settlements around AD 800 (Martinsson-Wallin and Crockford, 2002; Vargas et al., 2006) while others propose a later arrival (Hunt and Lipo, 2006). However, new paleoenvironmental reconstructions carried out in Rano Raraku show vegetation change associated to human disturbance far earlier, around 450 BC and therefore some 1500 yr. before than previously proposed dates (Figure 2.11) (Cañellas-Boltà et al., 2013). This study remarks both the need of future investigations to puzzle several evidence that are commonly used to date past anthropic disturbances (with a very wide range of ages) and also it points

out that the connection with American settlers has to be reconsidered. Despite the modern islanders descend from Polynesia (Hagelberg et al., 1994; van Tilburg, 1994; Flenley and Bahn, 2003) there are evidence of contact with early American settlers such as the prehistoric introduction of South American sweet potato (*Ipomoea batatas* (L.) Lamarck) and the bottle gourd (*Lagenaria siceraria* (Molina) Standley) to Polynesia (Clarke et al., 2006) or the pre-Columbian introduction of Polynesian chickens in South America (Storey et al., 2007). If this contact consisted in an early American settlement or a Polynesian arrival to South America and backwards (if existing) it still remains as an unsolved question (Heyerdahl and Ferdon, 1961).

Enormous sculptures called *moais* and carved between AD 1100-1680 have became an iconic image of the Rapa Nui culture and history. Because the first European written report from Jakob Roggeveen Dutch expedition (1722) described a deforested landscape and impoverished society that no longer carved sculptures, the island has been presented as a dramatic example of environmental degradation brought by humans, directly related to a cultural collapse (Flenley and Bahn, 2003; Diamond, 2005). The most important evidence used to state this historic reconstruction is the pollen analyses of lake sediments, that showed a clear change of vegetal assemblages dominated by palm trees to grass dominated ones. This apparent abrupt environmental change has been interpreted as an anthropic deforestation event (Flenley and King, 1984; Flenley et al., 1991, Flenley, 1993, Mann et al., 2008; Mieth and Bork, 2010). Although a strong human impact over environment was described in other tiny islands of Pacific Ocean (Kirch, 1997) a big debate is still centered on the timing and nature (abrupt or not) of the forest clearance because most of the sequences studied in Easter Island presented an extended sedimentary hiatus between the forested and deforested phases preventing to properly date and characterize the change (Flenley and King, 1984; Flenley et al., 1991; Dumont et al., 1998; Mann et al., 2008; Sáez et al., 2009; Rull et al., 2010a). Controversy also concerns the causes of this drastic shift because not only anthropic activity has been considered as the cause of the landscape change. Several authors have proposed alternative or complementary causes as climatic (McCall, 1993; Hunter-Anderson, 1998; Nunn, 2000) or the action of introduced fruit-eating rats preventing palm regeneration (Hunt, 2007; Hunt and Lipo, 2009). According to Rull et al. (2010a) even the scenario of a completely forested island remains to be demonstrated because a former landscape constituted of scattered forest patches around main water bodies cannot be rejected.

The history of Rapa Nui people after European contact consisted in a dramatic succession of events, including violent abductions to sell the natives as slaves for the nitrate extraction in the Chilean mines and devastating epidemics (Routledge, 1919). The population diminished to few dozens of inhabitants and much cultural knowledge was lost by European pressure. During the XX century the small Rapa Nui population recovered and was mixed with Chilean people arrived from the continent (Routledge, 1919).

2.5 Previous works on Easter Island environmental reconstructions

Despite a large amount of environmental and climatic research have been conducted in Easter Island, the environmental history of the island is still poorly understood (Rull et al., 2010a).

Paleo-environmental reconstructions from Easter Island have traditionally been based on pollen studies (Flenley and King, 1984; Flenley et al., 1991; Dumont et al., 1998; Butler et al., 2004; Gossen, 2007; Azizi and Flenley, 2008; Mann et al., 2008, Cañellas-Boltà et al., 2013) and macrofossil remains (Dumont et al., 1998; Orliac and Orliac, 1998; Orliac, 2000; Peteet et al., 2003; Horrocks and Wozniak, 2008; Mann et al., 2008; Cañellas-Boltá et al., 2012). Several studies have described local responses to Last Glacial and Holocene climate changes far before any human presence (Flenley et al., 1991; Azizi and Flenley, 2008).

The oldest pollen records interpreted in terms of a formerly forested island extend back to ~35–37 ^{14}C kyr BP and they were obtained in Rano Raraku and Rano Aroi sites. From 35 to 28 ^{14}C kyr BP Arecaceae pollen dominated Rano Raraku record with scattered occurrences of other elements. This was interpreted in terms of a forest dominated by palms with a shrubby understory of *Sophora*, Asteraceae (Tubuliflorae), *Triumfetta*, Urticaceae/Moraceae and Macaranga (Flenley et al., 1991). The same forest, but in a more open conditions, was assumed to exist between ~28 and 12 ^{14}C kyr BP. Openness was suggested by a decline in palm pollen, and an increase of shrubs and Poaceae (Flenley et al., 1991). With the beginning of the Holocene period, up to ca. 5 ^{14}C kyr BP, palm forests recovered again. In Flenley et al. (1991) a sedimentary gap spans along the period between ca. 5 to ca. 0.8 kyr BP. The uppermost part of this sequence presented a marked reduction of Palm pollen. The important pollen assemblage shift before and after the gap has been interpreted as the consequence of human influence on the later phase (Flenley et al., 1991). However, the precise age of this clearance is still a matter of debate. A recent study from Cañellas-Boltà et al. (2013) presents a very reduced hiatus and therefore provides the most complete record spanning the last 2000 yr. This work links the decline of palm trees abundance to the presence of *Verbena litoralis*, a common weed, which is associated with human activities and an increase of charcoal concentration (Figure 2.11). The authors suggest that from 1790 to 450 BC Rano Raraku developed as a mire with a very low watertable (presenting an accumulation gap between c. AD 500- c. AD 1126) and was flooded again after c. AD 1200. The age of rewetting could match the AD 1300 pan-Pacific event characterized by wet conditions on Easter Pacific (Nunn, 2007). From c. AD 1475 to c. AD 1875 the pollen record is dominated by herb species. A short gap between c. AD 1570 and c. AD 1720 indicate a second late drought phase coinciding with Little Ice Age (Figure 2.11).

Studies carried out in Rano Kau basin mainly show a similar history for the Holocene to what has been interpreted from Rano Raraku, but presenting complicate dating uncertainties (Butler and Flenley, 2004). Age reversals in cores retrieved from Rano Kau floating mat patches have been attributed to top down peat growing and floating mats flip over.

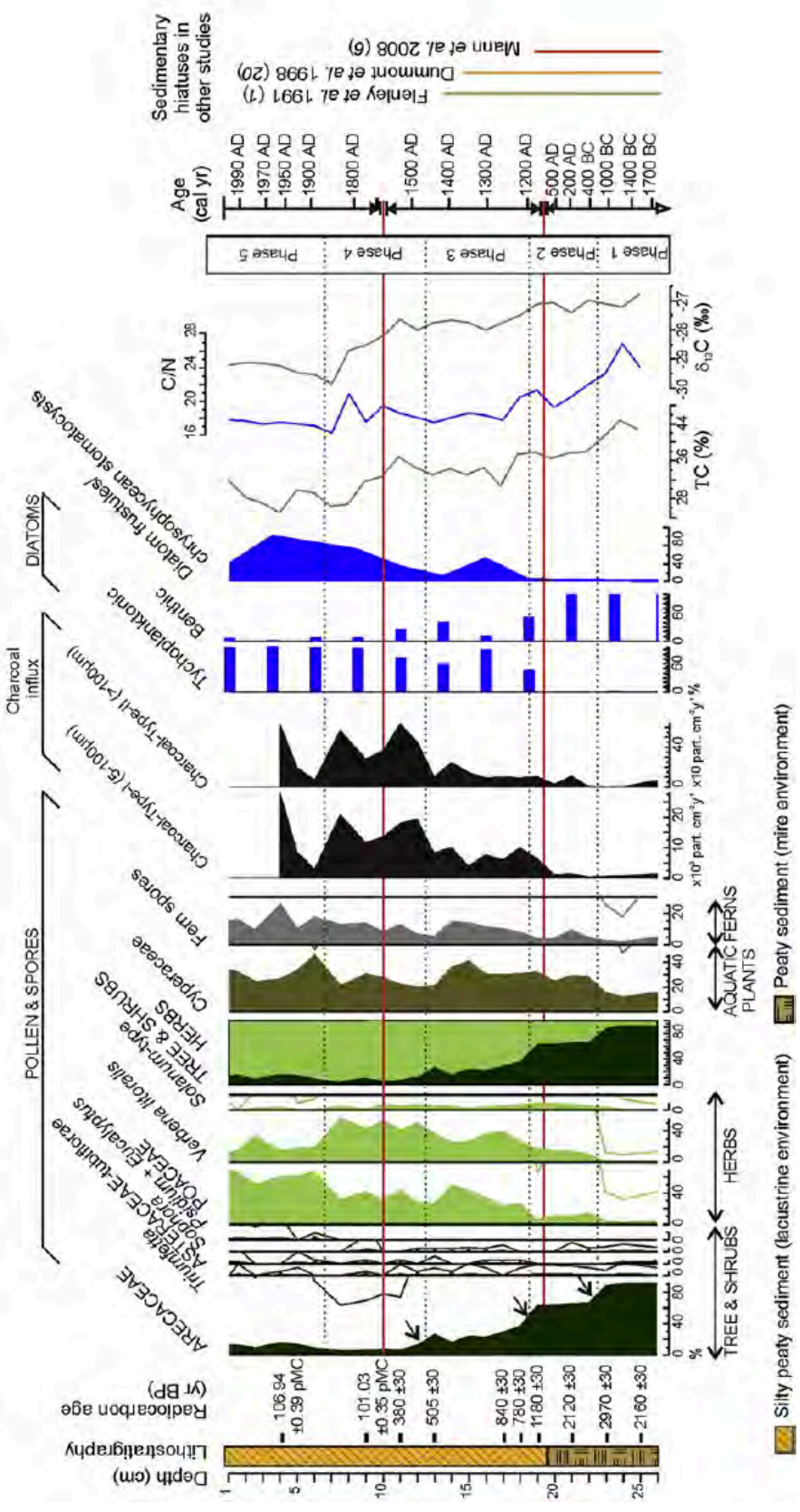

Figure 2.11. Summary multiproxy diagram of the uppermost 26 cm of the sedimentary sequence from Lake Raraku. AMS ^{14}C radiocarbon dates are indicated on the left of the diagram, and calibrated dates according to the age model used on the right. The arrows in the Arecaceae curve indicate palm decline events. Two sedimentary hiatuses present in the sequence are depicted by horizontal red lines. The sedimentary hiatuses observed in other studies are indicated on the right of the diagram. Note that early human settlement (450 BC) and the gradual nature of ecological change fall within the hiatuses of earlier studies (from Cañellas-Boltà et al., 2013).

An additional evidence used to reconstruct extinct forest has been soils and dwelling areas with root remains and grass charcoal layers (Arnold et al., 1990; Orliac and Orliac, 1998; Orliac, 2000; Mieth and Bork, 2003, 2005). Several authors have found palm root casts on ancient soil levels along the island, specially on Poike area were advanced gullying provide natural outcrops of soil sections. Soil levels that present root casts are covered by charcoal layers, and sometimes by later associated archeological pieces as *ahus* (traditional stones platforms) that evidence human activity after Palm forest loss. These authors describe more than one deforestation event dated between c. AD 1250 and c. AD 1500 (Mieth and Bork, 2005, 2010).

The identity of the Palm species has also been a matter of remarkable interest (Section 2.3.2). The most accepted hypothesis is that the Easter Island native palm, nowadays extinct, belonged to the Cocosoideae tribe. Dransfield et al. (1984) proposed that the Palm was a closer relative of *Jubaea Chilensis*. His study was based on the nut endocarp morphology and root casts remains (Figure 2.12). A new genus was defined; Paschalococos, and the small fossil coconuts found in Easter Island were assigned to the new species: *Paschalococos disperta* (Dransfield et al., 1984; Hunter-Anderson, 1998, Rull et al., 2010a).

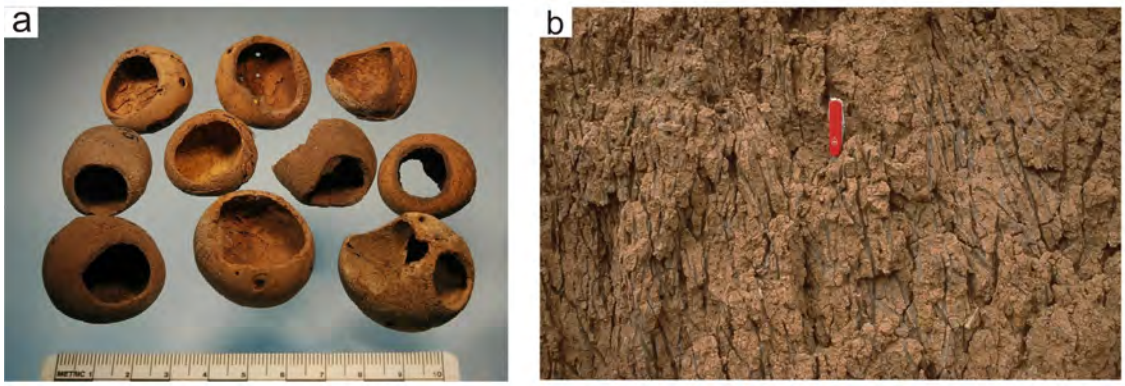

Figure 2.12. (a) Ancient rat-gnawed coconuts from Rapa Nui from collections at the P. Sebastian Englert Anthropological Museum, Rapa Nui (from Hunt, 2007). (b) Casts of palm roots in a Holocene soil of Maunga Orito at Easter Island (from Mieth and Bork, 2010).

Phytoliths and macrofossils have also been used to reconstruct the environmental evolution of Rano Kau and Rano Raraku (Horrocks et al., 2012a, 2012b, 2013). Around Rano Raraku ancient shorelines have been defined 10 m above present lake level indicating that in former time water level was much higher (Horrocks et al., 2012a). These authors found evidence of horticulture activity in Rano Raraku, but also on the steep slopes of Rano Kau (Horrocks et al., 2012b). Other works including pollen and diatoms determination detected American phytoplankton species on Rano Raraku cores when main environmental changes and the end of *moai* carrying took place (Dumont et al., 1998). These authors attempt to relate the hypothetical arrival of American travelers with a cultural and environmental collapse (Dumont et al., 1998).

Multiproxy studies of the sediments of Raraku Lake, which combined sedimentological, mineralogical, geochemical and macrofossil data, allowed a detailed reconstruction of the

large hydrological changes that have taken place on Easter Island since ca. 34 cal kyr BP (Figure 2.13) (Sáez et al., 2009; Cañellas-Boltà et al., 2012). Geological and biological proxies have characterized the glacial period as cold and relatively humid (Azizi and Flenley, 2008; Sáez et al., 2009), ending in a two-step Termination 1 (with warming evidence at 17.3 and 12.5 cal kyr BP). Sáez et al. (2009) and Cañellas-Boltá et al. (2012) show how from 11.2 cal kyr BP onwards, the Raraku Lake records a decreasing water availability trend, whereas intense drought periods during the Middle and Late Holocene were responsible for a long sedimentary gap (Sáez et al., 2009).

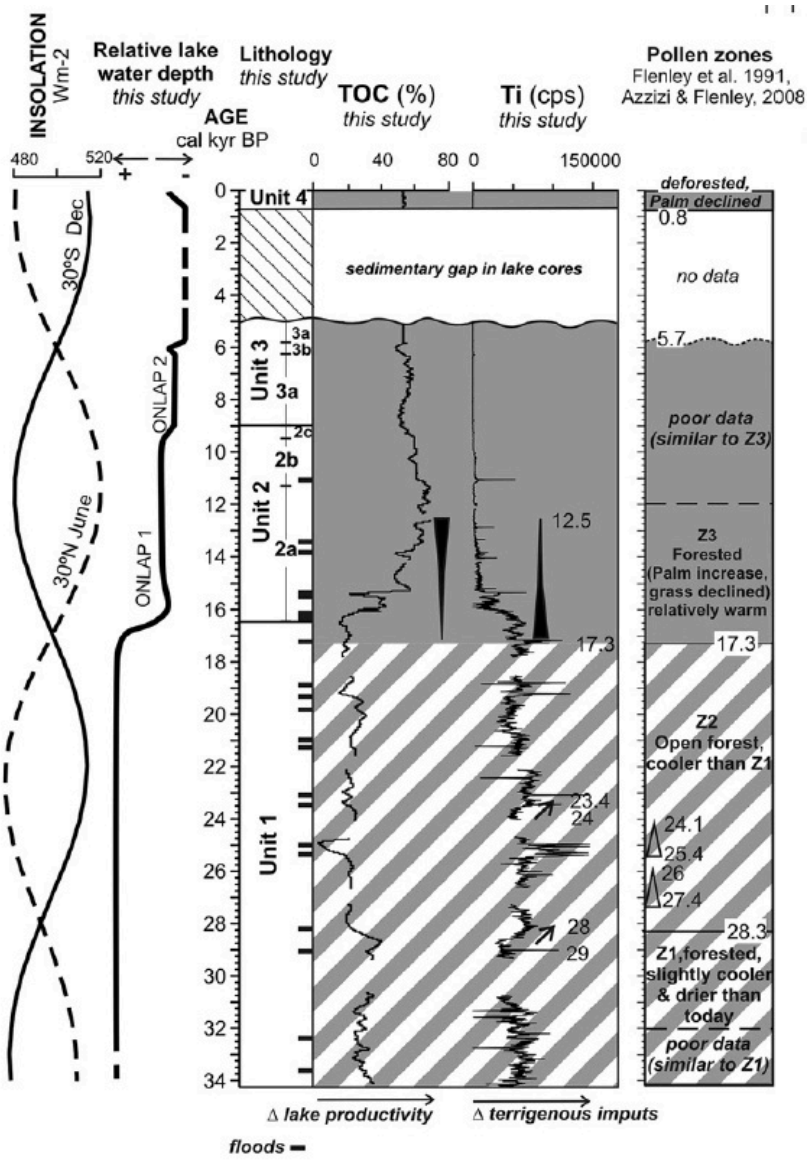

Figure 2.13. Easter Island environmental history and climatic patterns during the last 34 cal kyr BP from Rano Raraku lacustrine record. (from Sáez et al., 2009). From the left to the right: the insolation curve for 30°S and 30°N (Berger and Loutre, 1991); the relative Raraku Lake level changes established by (i) the frequency of flood events and thickness of flood deposits into the lake, (ii) the occurrence of onlap surfaces in Raraku Lake and (iii) the diatom presence in some intervals; the evolution of lake productivity is shown by the percentage of TOC and the terrigenous input is indicated by XFR Ti (counts per seconds) and the pollen record zones from Flenley et al. (1991) and Azizi and Flenley (2008).

2. 6 The Rano Aroi site

The Rano Aroi mire (27°S, 108°W, 430 m a.s.l.) is located in an ancient Pleistocene volcano crater near the highest summit of the island, Mauna Terevaka (Figures 2.1 and 2.14). The gentle crater slopes form a small catchment (15.82 ha) of very porphyritic olivinic tholeite, basalt and hawaiite lava flows (González-Ferran et al., 2004) that are covered by grassland and planted eucalyptus. The mire (0.13 km^2) almost fills the main depression volume and is covered by vegetation that is dominated by *Scirpus californicus, Polygonum acuminatum, Asplenium polyodon var. squamulosum, Vittaria elongata and Cyclosorus interruptus* (Zizka, 1991).

The natural outflow follows a small ravine and infiltrates before reaching the coast. The construction of an artificial outlet in the 1960s partially drained the basin, and the water levels have been controlled since that time (Figure 2.14). The chemical composition of the flowing Rano Aroi outlet (slightly acidic, pH = 5.5–6.5) is similar to that of the groundwater, indicating that it represents the discharge of the main aquifer or a perched spring of a highly saturated zone (Herrera and Custodio, 2008). Water isotopic data ($\delta^{18}O$, δD) show that the residence time of Rano Aroi water is short and the water is renewed through discharge from an aquifer very sensitive to seasonal variations in precipitation (Herrera and Custodio, 2008). Therefore, Rano Aroi can be characterized as a geogenous fen, a peatland or mire fed by groundwater or water that has been in close contact with the mineral soil or bedrock (Joosten and Clarke, 2002; Grootjans et al., 2006).

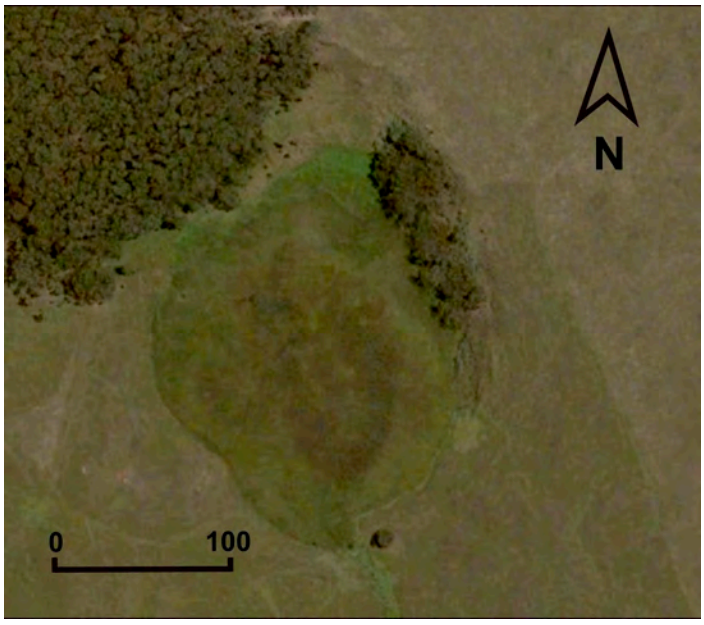

Figure 2.14. Rano Aroi aerial view from Google Earth satellite images. A forest of Eucalyptus grows on the NW vicinities of the mire. Water outflow is transported southward through a small ravine.

Two previous works include references to Rano Aroi environmental history. Flenley et al. (1991) studied the pollen recorded in ARO1, a 11.45 m depth core that did not reach the bedrock. The core was described as made up entirely of peat, alternating changes between the presence of fine and coarse detritus. Eleven radiocarbon dates were performed on ARO1 core

providing a basal age of 37680+1200-1040 yr. BP. Radiocarbon measurements were performed during the 80s over large sample size of bulk peat. Ages had not been calibrated.

The pollen diagram obtained by Flenley et al., (1991) showed a dominance of Poaceae on the basal levels. Asteraceae pollen started to be abundant from 8 meters depth while the presence of fern spores increased around 7 m. depth. The fact that Poacea pollen was the most common pollen type of the entire record depicts a quite different scenario than the one described from Rano Raraku and Rano Kau. In these other sites Arecaceae pollen was the most abundant. This fact was used by Flenley et al. (1991) to argue that Rano Aroi lies above the elevation limit for Palm trees development. Locally, the mire also supported the presence of Cyperaceae and semiaquatic plants. A second work carried out on Rano Aroi focused on a short core section (between 2 and 2.9 meters depth) and was studied by Peteet et al., (2003). Although the pollen data was in agreement with the former work of Flenley et al. (1991) strong age uncertainties were found owing to the presence of age reversals.

CHAPTER 3

METHODOLOGY

3.1 Core retrieving and peat facies description

Two peat cores (ARO 06 01 and the backup one ARO 06 02, 27°05' 37.53'' S - 109° 22' 26.27'' W) reaching 13.9 and 16.3 m depth, respectively, were recovered with a UWITEC® corer from the central part of Rano Aroi during the coring expedition that took place in March 2006 (Figures 3.1, 3.2).

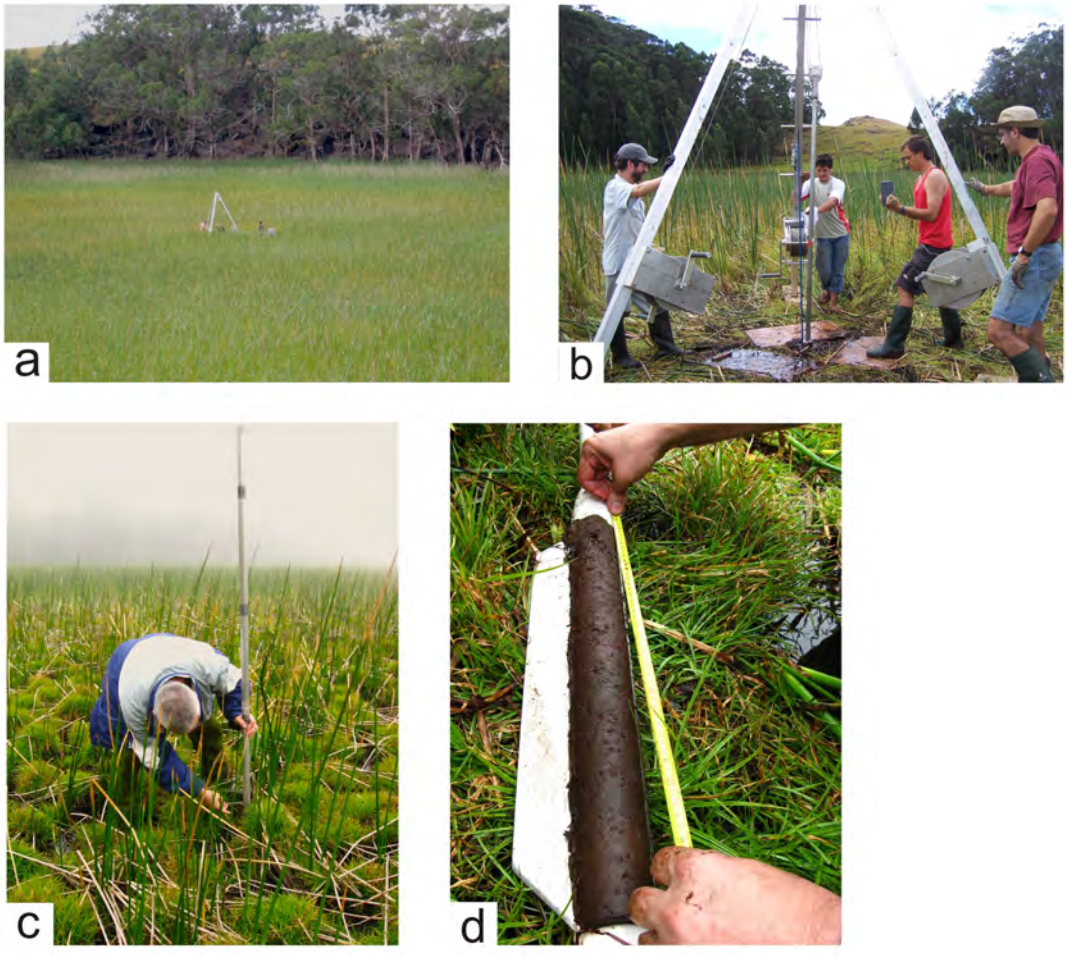

Figure 3.1. Images from the field campaigns in March 2006 and September 2008. a, b) Coring with UWITEC platform over the central part of Rano Aroi (Pictures by A. Sáez) c) Coring with a Russian Corer from the northern edge of the mire (Picture by O. Margalef) d) The cores retrieved with the Russian corer were described on the field (Picture by O. Margalef).

ARO 06 01 required 6 drives using PVC tubes of two meters length. ARO 06 02 was obtained after eight drives using two meters PVC. The uppermost two meters of the sequence

were rejected to avoid potential anthropic remobilization, as described in previous studies (Flenley and King, 1984; Flenley et al., 1991). The recovered 2 m long tubes were cut to obtain one-meter sections. ARO 06 01 was divided in 11 sections, while ARO 06 02 was split in 12 sections. Afterwards, all sections were sealed, transported to the laboratory in Barcelona and stored at +4 °C until sampling.

In October 2008, three additional peat sequences were retrieved with a Russian corer from the north and eastern margins of the mire (ARO 08 01, ARO 08 02, ARO 08 03), an area that was potentially not affected by recent human activities (Figures 3.1 and 3.2). All recovered sections had 50 cm length. ARO 08 01 (27° 5' 35.99" S - 109° 22' 27.6" W) consisted in three overlapping drives until reaching 1.5 m depth. ARO 08 02 (27° 5' 36.0306" S - 109° 22' 25.94" W) was recovered using 8 drives and reaching 4 m depth. A backup core (ARO 08 03) of ARO 08 02 was obtained at the same location after 5 drives until 3.83 m depth. The recovered cores were measured, described and photographed on the field (Figure 3.1). Later, the cores were sealed transported to the laboratory in Barcelona and stored at +4 °C until sampling. None of the cores retrieved in either campaign reached the bedrock.

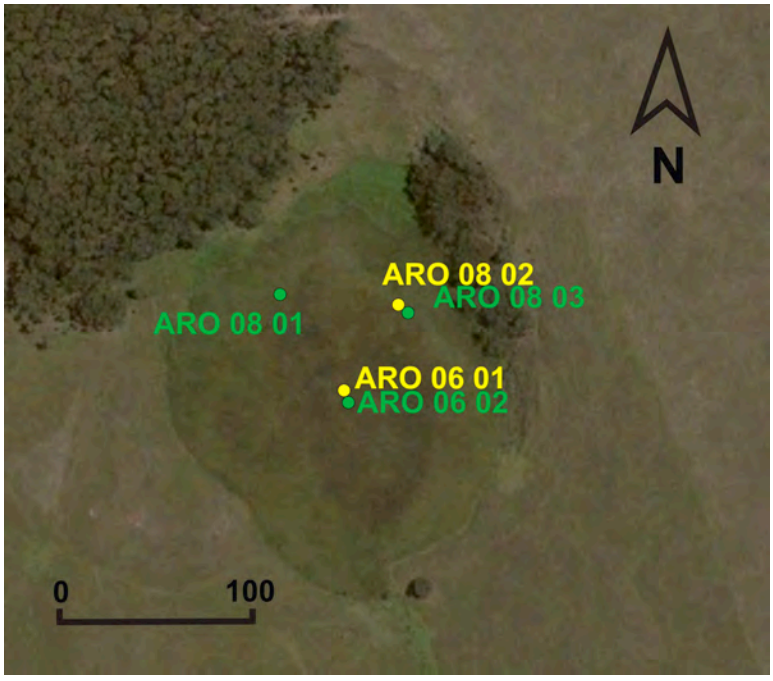

Figure 3.2 Situation of the peat sequences obtained from Rano Aroi. ARO 06 01 and ARO 06 02 were obtained with an UWITEC corer on May 2006 (27°05' 37.53'' S - 109° 22' 26.27'' W). ARO 08 01 (27° 5' 35.99" S - 109° 22' 27.6" W), ARO 08 02 and ARO 08 03 (27° 5' 36.0306" S - 109° 22' 25.94" W) were retrieved using a russian corer on October 2008. In yellow the records used for this study.

This study is focused on the 13.9 m deep core from the center of the mire (ARO 06 01) and a 4 m deep core from the edge of the mire (ARO 08 02). Both cores together compose a sequence that spans from 0.75 until 13.9 m depth.

The main lithofacies were defined in both cores according to color, size and proportion of plant remains and decomposition degree. Useful guidance for describing peat facies can be found in Meier-Uhlherr et al. (2011). Visual description was completed by smear slides observations (performed every 5 cm) under optical microscope ZEISS® Axioplan 2 imaging (x400 magnification). On smear slides, the origin of some plant remains could be identified, as well as vegetal structures indicating variable organic matter decomposition degree.

3.2 Radiocarbon dating

Age models for both cores were constructed from 27 radiocarbon AMS dates of pollen concentrates that were prepared by acid digestion (Rull et al., 2010b, Montoya; 2011) and measured at the Poznan Radiocarbon Laboratory (Poland). The pollen concentration protocol was followed as detailed:

- Weight 3-4 mg of sample
- Transfer the samples into 50 ml test glass tubes
- Add 15 ml of potassium hydroxide solution (10%), stir and heat in a water bath for 20 min
- Add distilled water up to 50 ml, stir, centrifuge and decant
- Rinse minimum two times with water until the pH of distilled water is attained
- Sieve trough a 200 μm mesh
- Add 15 ml of hydrochloric acid (37%), stir and heat in a water bath for 10 min
- Add distilled water up to 50 ml, stir, centrifuge and decant
- Rinse minimum two times with water until the pH of distilled water is attained
- Transfer the suspension to Teflon test tubes, centrifuge and decant
- Add 15 ml of hydrofluoric acid (70%), stir and heat in a water bath for 20 min, centrifuge and decant
- Add 15 ml of HF, stir and left overnight (~12 hours)
- Add distilled water up to 50 ml, stir, centrifuge and decant
- Transfer the suspension to small glass vials with screw cap

The obtained radiocarbon ages were calibrated using CALIB 6.02 software and the INTCAL 09 curve for the Southern Hemisphere (Reimer et al., 2004) for samples younger than 20 kyr BP and CalPal online calibrated to a Hulu curve for older samples (Danzeglocke et al., 2008, Weninger et al., 2008). No reservoir effect correction was applied to the radiocarbon dates since the dated pollen predominantly derived from sedges, herbs and other emergent and surrounding vegetation using atmospheric CO_2, and the pollen enriched concentrates did not contain significant amounts of amorphous organic matter that could have been of aquatic origin. Unfortunately it was not possible to apply a Bayesian fit to the ages because this approach considers the complete record and the lowermost section of Rano Aroi was beyond the radiocarbon limit. Furthermore, works with the IntCal calibration curves, which only allow to calibrate radiocarbon dates younger than ca. 50,000 radiocarbon ages. CLAM software was not able to construct the chronological model for the lowermost part of the record (Blaauw, 2010). Therefore, considering that the sedimentological and geochemical features of the record beyond the radiocarbon limit were similar to those within the radiocarbon chronology we decided to apply the simplest approach (linear extrapolation). According to the linear extrapolation model, the recovered Rano Aroi sequence covers the last 70 kyr BP (Sections 4.2 and 5.2)

3.3 Image acquisition and physical parameters from core sections

ARO 06 01 core sections were imaged at the Limnological Research Center Core Facility (LacCore) of University of Minnesota (Minneapolis, EEUU). Photographies were acquired using *DMT CoreScan Colour* line-scan camera that provides high resolution digital photography (Figure 3.3).

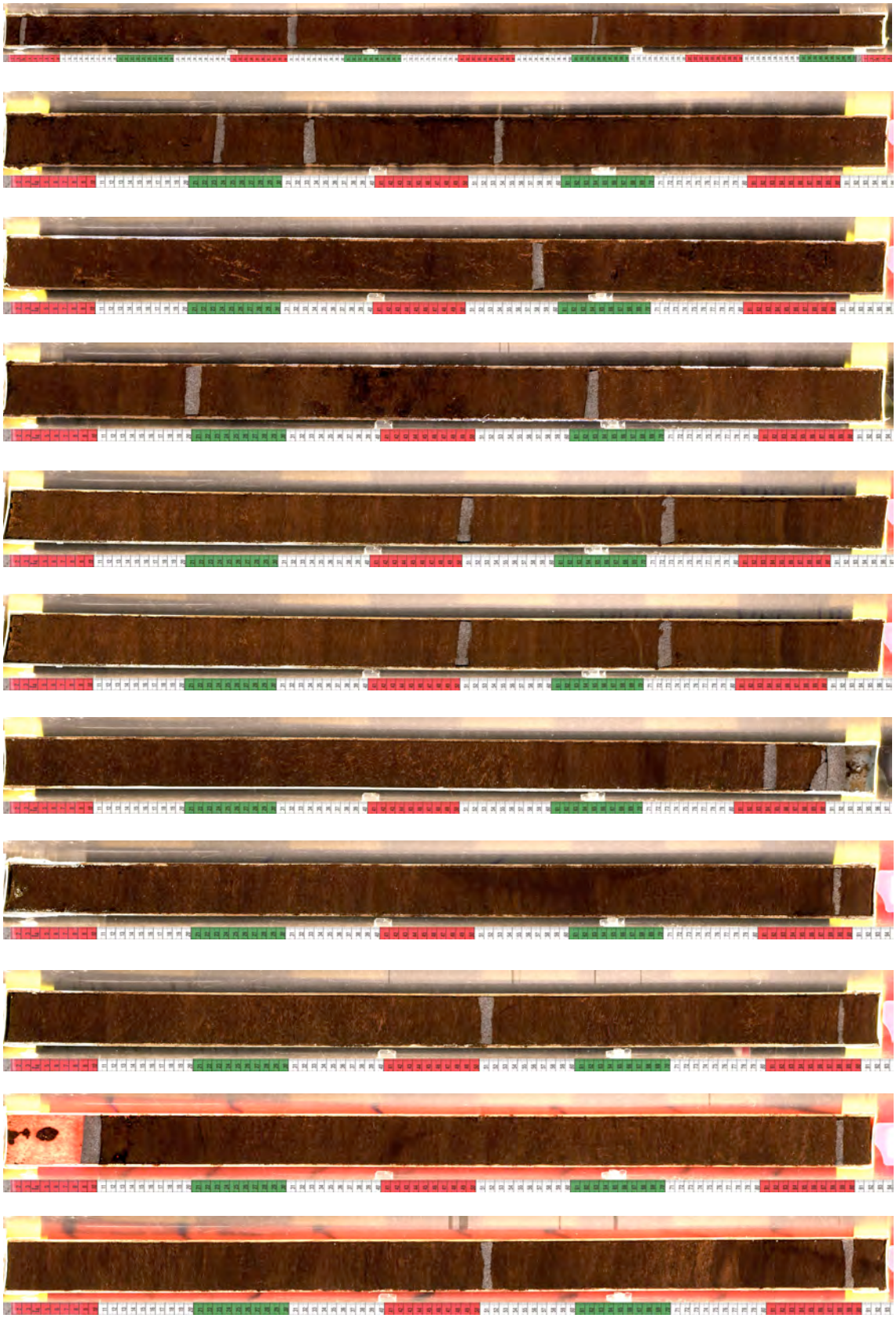

Figure 3. 3. Images acquired from (up to down) ARO 06 01 section 01, 02, 03, 04, 05, 06, 07, 08, 09, 10, 11 with a line-scan camera. Foam was used to cover missing material sampled for radiocarbon dating.

The measurement of magnetic susceptibility is a non-destructive method that can be used in lake sediments or peat cores to estimate the amount of ferromagnetic or paramagnetic minerals (Dearing, 1999) Magnetite, hematite, Fe sulfides, Fe-Ti oxides, Fe-Mn carbonates or iron-bearing silicates depict high (the ferromagnetics minerals) or weak positive (the paramagnetics minerals) susceptibility (Nowaczyk, 2001; Thomson and Oldfield, 1986). In lake sediments these iron mineral assemblages are commonly characterized by a detrital or endogenic origin.

Magnetic susceptibility of ARO 06 01 was measured every 0.5 cm over the split cores wrapped in plastic film using the point sensor magnetometer *Geotek® MSCL-XYZ* at LacCore facilities (Geotek MSCL manual) of University of Minnesota (Minneapolis, EEUU). Because the Rano Aroi peat record contents very low mineral and is dominated by organic matter (diagenetic, that acts such as a diluting substance) magnetic susceptibility obtained from ARO 06 01 was rejected as an environmental proxy.

Peat or sediment density has been widely used as a non-destructive method to support and refine facies characterization indicator of lithology or porosity changes (Chambers et al., 2011). ARO 06 01 gamma density was obtained using the *Geotek® MSCL-S* at LacCore center. The measurements were carried out every 0.5 cm over split cores. Unfortunately, gamma density obtained in Rano Aroi peat sequence gave strong shifts at the sections edges evidencing alteration by water loss after core splitting. For this reason density measurements have not been used for paleoenvironmental reconstruction.

3.4 Geochemical analyses over core sections

Organic chemistry

3. 4. 1 TC, TN, TS and stable isotopes

ARO 06 01 and ARO 08 02 were sampled every 5 cm for determining total carbon, total nitrogen and total sulphur (TC, TN, TS) and stable isotopes ($\delta^{13}C$, $\delta^{15}N$, $\delta^{34}S$). The 286 samples (218 for ARO 06 01, 68 for ARO 08 02) were dried up at 60ºC during 48 hours, frozen with liquid nitrogen and grounded in a ring mill. 2.5 mg of ground sample were weight in a microbalance and packed in a tin (Sn) capsule (Figure 3.4).

Figure 3.4: Tin capsules used for T TC, TN, TS, $\delta^{13}C$, $\delta^{15}N$ and $\delta^{34}S$ (left, from http://www.microanalysis.co.uk). Microtiter plate used to contain stable isotope samples (right, http://www.isotope.nau.edu).

TC, TN and their stable isotopes ($\delta^{13}C$ and $d^{15}N$) were carried out using a Finnigan delta Plus® EA-CF-IRMS spectrometer (precision of 0.2‰ and 0.3‰ respectively) in the

Serveis CientificoTècnics (SCT) of the Universitat de Barcelona (Figure 3.5). The CF-IRMS transforms the sample in gas to be introduced to the spectrometer automatically. The procedure consists in the sample combustion, gas treatment (CO_2, N_2, CO, SO_2), and gases separation in a chromatographic column to be separately analyzed by the mass spectrometer. Combustion takes places in an oven with oxygen atmosphere where the small tin capsule is introduced.

$\delta^{13}C$ results depict two variability frequencies (a long-term trend and high frequency oscillations). For this reason, $\delta^{13}C$ short-term oscillations ($\delta^{13}C_{res}$) was obtained by subtracting a 19-sample mean running average from the raw $\delta^{13}C$ data (further details are given on Section 4.3.1)

Figure 3.5. Images of the Finnigan delta Plus® EA-CF-IRMS spectrometer from the Serveis CientificoTècnics (SCT) of the Universitat de Barcelona (photographies of J.J. Pueyo).

Tin capsules with 17-20 mg of grounded sample were prepared for measurement of TS and $\delta^{34}S$. Vanadium pentoxide (VO_5) was added to catalyze oxidation. S stable isotope measurements were performed by a Finnigan MAT CHN-IRMS Finnigan DeltaPlus XP (precision of 0.4‰), also in the Serveis CientificoTècnics (SCT) of the Universitat de Barcelona. The references substances used to calibrate the stable isotope measurements are shown in Table 3.1.

Stable Isotope	Reference	Isotopic signature (‰)	Standard desviation
$\delta^{13}C$	Antropina	-28,8	-
	IAEA CH7	-32,2	0.05
	IAEA CH6	-10,4	0.033
	USGS 40	-26,3	0.042
	UCGEMA-F	-26,3	-
	UCGEMA-S	-24,9	-
$\delta^{15}N$	IAEA N1	4,7	0.2
	IAEA N2	20,5	0.2
	IAEA NO3	4,7	-
	USGS 40	-4,3	-
	UCGEMA-F	4,9	-
$\delta^{34}S$	IAEA S1	-0.3	0.2
	IAEA S3	-32.3	0.2
	NBS-127	20.3	-
	Sulfanilamida	6,2	-
	YCEM	12.78	-

Table 3. 1. References used for the stable isotope analyses, its correspondent isotopic signature value and standard deviation

Inorganic chemistry

3. 4. 2. X-Ray Flourescence (XRF) core scanning

The XRF core scanning is a non-destructive technique to measure elemental composition of sediment or peat cores. This method provides high-resolution geochemical records, saving time for exhaustive sampling. The elemental composition obtained can be used to infer environmental, sedimentological and diagenetic changes (Croudace et al., 2006; Rothwell, 2006). The principle used by this method is that after the intense emission of an X-ray beam over the sediment, the excited atoms become unstable and emit the energy excess (measurable such as X-ray) depending on atomic configuration (different elements will present different responses). The main limitation for XRF core-scanners is that only the emited energy of the elements heavier than Al can be measured (Rothwell, 2006).

The standard procedure includes first to carefully flat the split core surface to avoid irregularities. After setting core length, excitation voltage and current to the X-ray tube (as well as X-ray tube type) a topographic scan of the score is performed. This information will be used by the sensor to not collide with the core surface. Next, the measurements can be carried out (Croudace et al., 2006).

XRF core-scanning measurement was performed over ARO 06 01 cores with a new-generation XRF ITRAX core scanner (at 30 kV and 20 mA measuring time 60 s every 2mm) at the Large Lakes Observatory (Figure 3.6) (University of Minnesota, Duluth, MN).

Figure 3.6. XRF ITRAX core scanner from Large Lakes Observatory (University of Minnesota, Duluth, EEUU)

The procedure was carried out twice, with a Molybdenum and a Chromium tube. Ca, Ti, V, Cr, Mn, Fe, Ni, Cu, Zn, Br, Zr and inc/coh ratio (what gives an idea of the organic matter content) were obtained from Mo tube. Mg, Al, Si, P, S, Cl, Ar, K, Ca and Ti and the incoherent or Compton scattering to the coherent or Raleigh scattering (inc/coh) ratio were recorded by the Cr tube. Because mineral content in Rano Aroi cores is very low and organic matter and water content can have a negative effect on this type of measurements due to the matrix effect, only few elements were considered significative. In ARO 06 01 only iron (Fe) and titanium (Ti)

from the Mo tube and calcium (Ca), from Cr tube measurements (counts per second, cps) were used as a geochemical proxy.

Not only element counts per second but also X-ray images were obtained by ITRAX core scanner. These images can give relevant information of internal structures apparently not visible. The information can be used to refine facies description. X-ray images were obtained of the eleven sections of ARO 06 01 sequence (Section 5.2).

3.4.3 Mineral grains composition by Scanning Electronic Microscope (SEM)

In order to investigate the mineralogy of the sand grains present on the levels with higher inorganic content, three representative samples were selected. Sand grains from a level rich in Ca and Fe cps (4.8 m depth), and two levels with high values of Ti and Fe cps (8.3 and 10.55 m depth) were chosen. The peat samples were dried and the grains were separated by density in purified water. Together with these, a collection of sand grains (>500 μm) obtained during macrofossil selection procedure (Section 3.6.1) were also analyzed (Section 4.4.2). The grains were carefully attached to stubs using a conductive bioadhesive tape. A morphological description using a FEI ESEM-EDS in the *low vacuum mode* (around 0.5 torr) was made on selected samples in the Serveis CientificoTècnics (SCT) of the Universitat de Barcelona (Figure 3.7). Secondary and backscattered electron images and Energy-dispersive X-ray spectroscopy (EDS) analyses were used systematically to characterise the components. To recognize very small grains, the microscope was used such as a SEM, in the *high vacuum mode* (< 10^{-4} torr). In this later case, stubs were carbon-coated before observed in high vacuum mode.

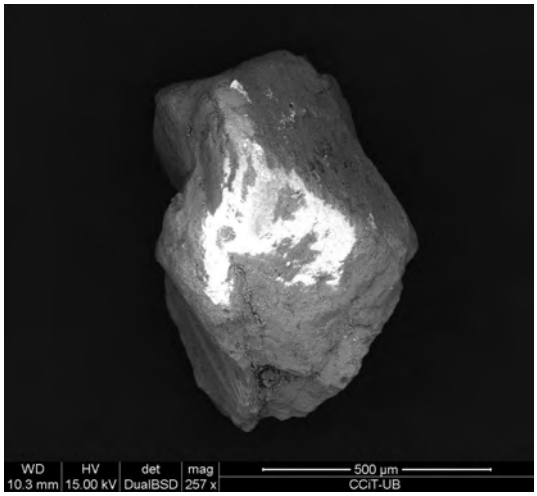

Figure 3.7 Image of a Rano Aroi sand grain obtained by ESEM in the Serveis CientificoTècnics (SCT) of the Universitat de Barcelona.

3.4.4. Major, minor and trace elements determination of peat ash by ICP-AES.

As explained in the previous section, only counts of the abundant elements (Ca, Fe, Ti) were considered significative. Because the use of just three elements cannot fully reveal the complex interactions and processes controlling biogeochemical processes at Rano Aroi such as dusts input, flood events, droughts, early diagenesis and redox changes, an alternative method was performed to measure a wider group of elements over the inorganic fraction. Total digests of bulk peat samples were analyzed by Inductively coupled plasma atomic emission

(ICP-AES) to obtain absolute concentrations of sixteen additional elements (Al, Fe, Ti, Ca, Mg, Sr, Y, Zr, Ba, Sc, Th, V, Cr, Mn, Cu, Zn, Cd).

A set of 207 samples was selected from ARO 06 01 sequence to be analyzed by ICP-AES technique (Hou and Jones, 2000). The sampling for ICP-AES was performed every 5 cm when there was enough material available while some samples were separated between 6 to 10 cm due to the lack of material due to previous samplings (e.g. dating, pollen and stable isotope analyses). The sample preparation was performed by Dr. Malin Kylander (University of Stockholm) under clean laboratory conditions using acid cleaned labware. 250 mg of sample of bulk peat was digested using a mixture of HNO_3/HBF_4 as described by Krachler et al. (2002). The microwave program included a 40 minute several-stage ramp to 200°C where samples were held for 20 minutes. The remaining solution was then transferred to Savillex vessels® and evaporated on a hotplate at 50°C. Thereafter, H_2O_2 was added and allowed to react for half a day. Samples were then sonicated and evaporated at 50°C on a hot plate. This was followed by a 2 day closed vessel digestion at 90°C with HNO_3 using a MARS-Xpress microwave system. After sonication and evaporation at 50°C an additional cycle of H_2O_2 was made. Samples were once again evaporated and then taken up in 1% HNO_3 for analysis.

The samples were analyzed for elemental concentrations using a Varian Vista AX ICP-AES at the Department of Geological Sciences, Stockholm University, Sweden by Dr. Malin Kylander. A suite of sixteen elements were analyzed including Al, Ba, Ca, Cd, Cr, Cu, Fe, Mg, Mn, Sc, Sr, Ti, Th,V, Y and Zr. Some elements were removed from the dataset because of low concentrations in the peat samples (Li and K), contamination during sampling (Zn) or because they were close to the analytical detection limits (Na). To date there is no certified reference material for peat that offers a wide range of elemental data. The analytical performance was assessed instead through related materials including NIST SRM-2711a Montana Soil, NIST SRM-2586 Trace Elements in Soil and Lake Sediment-4 (LKSD-4) issued by the Geological Survey of Canada, which all have certified/recommended values for many elements. Several procedural replicates were made of each reference material (5 for NIST SRM 2711a and NIST SRM 2586, each and 3 for LKSD-4). For NIST SRM 2711a all elements were within 14% of the reference values with the exceptions of Al (20%), Cr (18%), Cu (23%) and Ti. For NIST SRM 2586 all elements were within 15% or less of the certified values with the exception of Ti. Titanium recoveries were low for both reference materials with roughly only 30% recovered in each replicate. Note that there are no certified values for Zr in these two materials. Replicates had a percent difference of 20% or better on average for both reference materials. The analytical performance as quantified using the LKSD-4 is not as good as that based on the NIST SRM. While Cr, Cu, Fe, Mn, Sr, V and Zr all agreed within 12% or better recoveries were much lower for Ba (66%), Sc (20%), Ti (66%) and Y (22%). Despite the fact that the analytical performance for some of the elements was lower than others, all elements were included in the interpretation because even relative changes of a single element can have paleoenvironmental significance.

3.5 Geochemical analyses over rock and soil composition

Due to the remarkable isolation of Easter Island, the mineral content found in Rano Aroi record is not expected to come from long-distance transport across the Pacific Ocean. The inorganic fraction likely derives from the mire basin (transported by wind or runoff) or from other areas of the island (blown by wind). To corroborate the mineral content origin and relate changes in the peat record with soil evolution, several elemental and mineralogical measurements have been performed on rock and soil samples around Rano Aroi and other areas of the island (Figure 3.8).

Assessments of semi-quantitative bulk mineral composition of 9 rock samples of Rano Aroi basin were obtained by X-ray diffraction (XRD) while elemental composition was determined by X-ray Fluorescence (XRF).

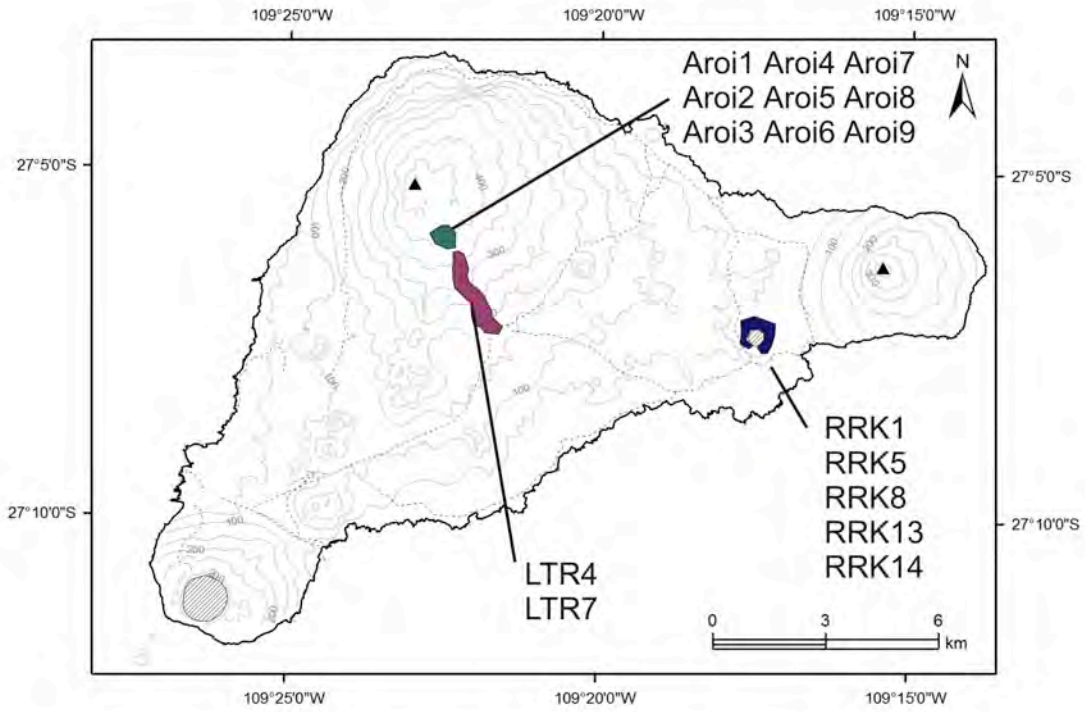

Figure 3.8. Location of the rock and soil samples analyzed with XRF, XRD and/or ICP-MS.

Nine rock samples names as Aroi (1-9) were grounded and powdered. The mineral composition of the sample powder was obtained by X-ray diffraction (XRD) with a PANalytical X'Pert PRO MPD-DY 3197 diffractometer of the the Serveis CientificoTècnics (SCT) of the Universitat de Barcelona (Środoń et al., 2001).

To determine elemental composition (mayor elements) the sample powder was dissolved by fusion in Li-metaborate and analysed the molded glass matrix by a WDXRF spectrometer Panalytical Axios PW 4400/40 at the Serveis CientificoTècnics (SCT) of the Universitat de Barcelona (Johnson et al., 1999) (Figure 3. 9).

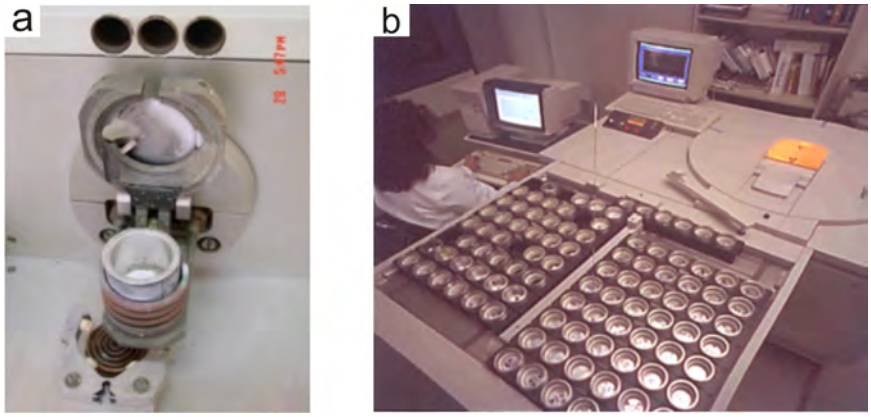

Figure 3.9 (a) Platinium crucible to fusion in Li-metaborate the analyzed sample. (b) XRF spectrometer at the Serveis CientificoTècnics (SCT) of the Universitat de Barcelona (right).

Further on, a more extensive analysis was carried out to determine soil and rock LOI (Loss on ignition) and elemental composition by Inductively Coupled Plasma mass spectrometry of 16 samples obtained on Rano Aroi, Rano Raraku basins and along the creek that communicates Rano Aroi to the sea. The samples analyzed were RRK1, RRK5, RRK8, RRK13, RRK14, LTR4, LTR7, Aroi4, Aroi5, Aroi6, Aroi7, Aroi9 (Figure 3.8). From RRK1, RRK8, RRK13 rock and soil samples are analyzed separately from the same site. The rest of the samples consist entirely of rock samples.

Rock and soil samples were ground in a ring mill and LOI values were obtained after drying samples previously dried at 90°C during 12 hours. Crucibles for each sample were weighted (weight=A). Thereafter between 0.5 and 1 g of sample were weighted in the crucibles once they had reached the room temperature in the desiccator (weight=B). After combusting them during 45 minutes in an oven at 950°C, the crucibles with the remaining sample were weighted again (weight=C). LOI was obtained following the equation: LOI= (B-C)/(B-A)*100 (Schulte and Hopkins, 1996).

For determining the elemental composition, grounded samples were treated following the protocol described in Ruggieri et al. (2012). The samples were dried at 60°C for 24h. 0.1 g of sample was then digested using a mixture of 2.5 ml HNO_3+ 5 ml HF + 2.5 ml $HClO_4$ in Teflon tubes at 135°C for 12 h. Finally, 1ml of HNO_3 and 5 ml of purified water were added until the complete dissolution of the sample. The analyses were carried out at labGEOTOP Laboratory in Institute of Earth Science Jaume Almera-CSIC (Barcelona) using a high resolution HR-ICP-MS (*Element XR Thermo Scientific*). Twenty-three elements were measured in ppm (Ti, Al, Fe, Mn, Mg, Ca, Na, K, P, Li, Be, Sc, V, Cr, Co, Ni, Cu, Zn, Ga, Ge, As, Rb, Sr).

3. 6. Biological proxies

3. 6. 1. Macrofossil analyses

Macrofossil analysis is a very useful proxy and has been traditionally used in lacustrine and mire records to reconstruct past vegetational and faunal changes (Birks and Birks, 2006).

Samples (30–45 cm^3) for plant and animal macrofossil analysis were extracted from ARO 06 01 (30 samples, 1 sample every 45 cm) and ARO 08 02 (16 samples, 1 sample every 20 cm), measured by water displacement, and sieved over 125-µm and 500-µm sieves with a gentle stream of tap water (Birks, 2001). The residues were examined systematically under a stereomicroscope at x12 magnification. The identification of macrofossils (seeds, coleoptera, oribatid mites and other remains) was carried out by comparisons with reference materials (Birks, 2001), in collaboration with the specialist in oribatid mites, Dr. Torstein Solhøy (University of Bergen), and the specialist in Coleoptera, Dr. Alex Riedel from Museum für Naturkunde (Karlsruhe, Germany). The remains were stored in the general reference collection of biological micro and macro remains at the Botanical Institute of Barcelona, following the nomenclature code IBB- for unknown remains (Cañellas-Boltà et al., 2012).

3. 6. 2. Pollen analysis

The quantitative analysis of pollen and spores is a very efficient proxy for investigating vegetation evolution and its responses to climate changes or human landscape modifications (Ortu et al., 2006, Twidley, 2012). However, in the framework of this PhD the pollen analysis has only been used as a complement of the biogeochemical dataset (25 samples counted). Nevertheless, many efforts have been dedicated to the laboratory procedure and the methodological training in identification and counting pollen grains.

Twenty-five peat samples were extracted from ARO 06 01 according to the criteria of being equally distributed (around each 50 cm) but also be representative of the four described facies. Rano Aroi peat samples were processed for pollen analysis according to a standard laboratory procedures modified from Rull et al. (2010b) and Montoya (2011) which include sieving, digestions with KOH, HCl and HF, and acetolysis. As an exotic marker, *Lycopodium* spores tablets (Batch. No. 177745, Lund University, Sweden) were added to each sample before processing in order to infer pollen total concentration. The protocol was followed such as described:

- Transfer the samples into 50 ml glass test tubes
- Spike with Lycopodium tablets
- Add 15 ml of potassium hydroxide solution (10%), stir and heat in a water bath for 20 min
- Add distilled water up to 50 ml, stir, centrifuge and decant
- Rinse minimum two times with water until the pH of distilled water is attained
- Sieve trough a 200 µm mesh
- Add 15 ml of hydrochloric acid (37%), stir and heat in a water bath for 10 min
- Add distilled water up to 50 ml, stir, centrifuge and decant
- Rinse minimum two times with water until the pH of distilled water is attained

- Rinse two times with glacial acetic acid
- Add 15 ml of acetolysis mixture (9 parts of acetic anhydride (%) and 1 part of sulfuric acid (%)), stir and heat in a water bath for 4 min
- Add glacial acetic acid up to 50 ml, stir, centrifuge and decant two times
- Rinse minimum two times with water until the pH of distilled water is attained
- Transfer the suspension to Teflon test tubes, centrifuge and decant
- Add 15 ml of hydrofluoric acid (70%), stir and heat in a water bath for 20 min, centrifuge and decant
- Add 15 ml of HF, stir and left overnight (~12 hours)
- Add distilled water up to 50 ml, stir, centrifuge and decant
- Add a mixture (1:1) of ethanol (96%) and distilled water up to 50 ml, stir centrifuge and decant
- Add pure ethanol (96%) up to 50 ml, stir centrifuge and decant
- Add a mixture (1:1) of ethanol (96%) and tertiary butyl alcohol (TBA, 99%) up to 50 ml, stir centrifuge and decant
- Add pure TBA up to 50 ml, centrifuge and decant
- Transfer the suspension to small glass vials with screw cap
- Add 4-5 drops of silicon oil (12,500 cs) and homogenize
- After the complete evaporation of the TBA, the silicone suspension is ready for mounting

The slides were mounted in silicone oil to be counted under optical microscope using x40 and x60 objectives mounted on a ZEISS® microscope with x10 ocular (ZEISS® Axioplan, ZEISS® Axiostar plus, ZEISS® Axio Scope A1 and ZEISS® Axio Lab. A1). Microscope images were taked using a Deltapix invenio II 5S® camera coupled coupled to ZEISS® Axio Scope A1. Pollen counting was carried out until at least 150 pollen grains were reached of palms, trees, herbs and shrubs excluding aquatic or semiaquatic plants (Cyperaceae, *Typha* and *Polygonum*) and fern spores. To simplify data presentation the fern spores are shown (see appendices) such as a sum of Filices (F.) Monolete-Psilate, F. Monolete-Verrucate/Areolate, F. Trilete-Psilate, F. Trilete-Verrucate/Auroleate, *Ophioglossum* and *Pteris* types. This is because despite they can have slightly different ecological requirements all of them represent fern species grow preferentially on moist areas. The counting of pollen grains and spores was carried out in the Botanical Institute of Barcelona (IBB) and Institute for Botany (University of Greifswald) in Greifswald (Germany) by comparisons with reference books and atlases for pollen and the guidance of Dr. Valentí Rull and Núria Cañellas-Boltà (Heusser, 1971; Tryon and Lugardon, 1991; Reille, 1992; Hoeve and Hendriskse, 1998; Hesse et al., 2009). Pollen percentages were calculated excluding fern spores and aquatic or semi-aquatic plants. Statistically significant pollen zones were obtained over the percentages with psimpoll 4.26 software, using the method of optimal splitting by least-squares and information content (Bennett, 2009).

3. 7 E-W SST gradient of Pacific Ocean calculation

Rano Aroi and Easter Island environmental changes can be attributed to climate oscillations that affected also marine and continental records located in the tropical and subtropical Pacific and Atlantic Oceans (Sections 1.6.1, 1.6.2). In particular, Rano Aroi sequence could be considered as an indicator of oceanic conditions in the equatorial Pacific

Ocean. This means that past changes in the Walker circulation could be recorded over the island. To corroborate the relation between changes in Pacific equatorial circulation and climatic reconstructions obtained from Rano Aroi, the record was compared with a new estimation of sea surface temperature (SST) changes from the Pacific Ocean, which was constructed using a combination of previously published geochemical records from two marine cores located at the ends of a longitudinal equatorial Pacific transect (Chapter 8).

A gradient of SST between the Western and Eastern Equatorial Pacific was estimated between 65 and 35 kyr BP ago by combining two independent equatorial SST records based on Mg/Ca ratios measured on *Globigerinoides ruber* from the ODP site 1240 in the Eastern Equatorial Pacific Ocean (0°01.31'N - 86°27.76'W, Pena et al., 2008) and core MD97-2141 in the Western Pacific Ocean (8°48'N - 121°18'E, Dannenmann et al., 2003) (Figure 3.10). This W-E gradient was estimated by determining the difference between MD97-2141 and ODP 1240-SST after resampling the ODP 1240 record at age intervals corresponding to those of the MD97-2141 record. The error of these SST estimates is considered to be ca. ±0.6°C, and the discussed gradient changes are above 1ºC and are even larger than 2°C in most cases. The chronologies of the two cores are independent of each other and they are based on a combination of ^{14}C dates and oxygen isotope stratigraphy (Pena et al., 2008). Age uncertainties for this period (35-70 kyr BP) have to be taken into account because some dates are found below the ^{14}C-dating period. Thus, chronological uncertainties within the studied period can range from 0.5 to 2 kyr. Nevertheless, MIS 4 is clearly expressed in the $\delta^{18}O$ records from both marine cores, and it is therefore possible to accurately locate the base of the studied period, providing confidence in the accuracy of the period's boundaries.

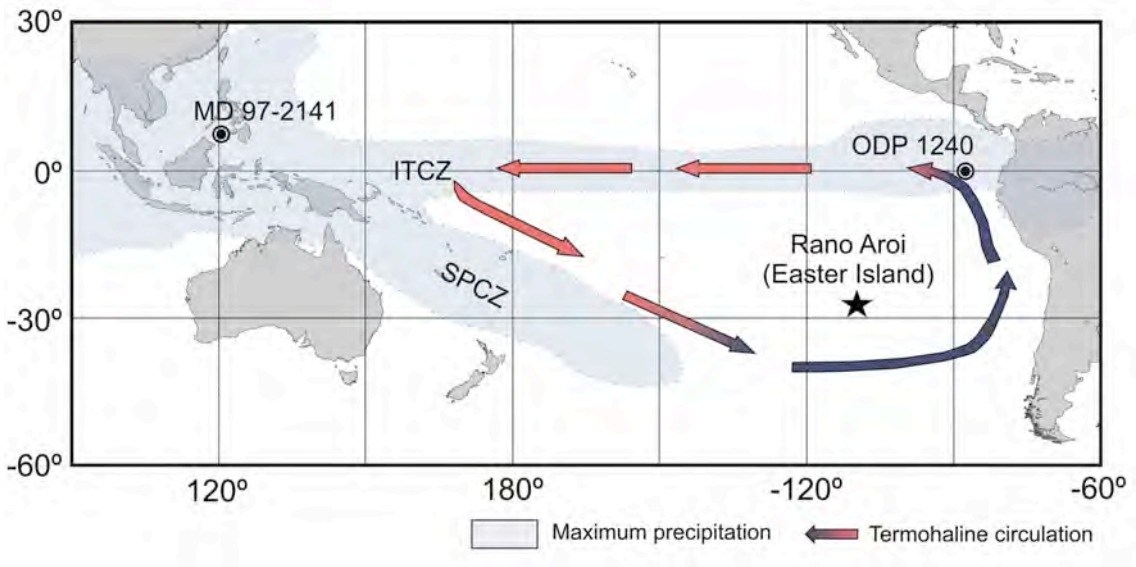

Figure 3.10. Location of MD 97-2141 (Dannenmann et al., 2003) and ODP 1240 (Pena et al., 2008), two marine records used to reconstruct Equatorial Pacific SST gradient for the period of time between 65 and 35 kyr BP. Intertropical Convergence Zone (ITCZ) and South Pacific Convergence Zone (SPCZ) determine zones of maximum precipitation. Very simplified South eastern Pacific termohaline circulation is shown.

3. 8 Statistical treatment

3.8.1 Principal Component Analysis (TC, TN, $\delta^{13}C_{res}$, Fe, Ti, Ca) from ARO 06 01

To characterize the general environmental evolution of Rano Aroi, a statistical treatment of organic matter elemental composition and stable isotope and XRF core scanner results was performed with R version 2.14.1 software (R Development Core Team, 2011) together with the 'vegan' package version 2.0-2 (Oksanen et al., 2007). Principal component analyses (PCA) over the correlation matrix was run to extract the main components of variability of the geochemical data of entire ARO 06 01 sequence using 6 variables (TC, TN, $\delta^{13}C_{res}$, Fe, Ti, Ca) and 200 samples. This statistic approach was used to corroborate facies characterization and, at the same time, elucidate the main processes occurring within the mire responsible for Rano Aroi biogeochemical characterization through time. XRF and stable istope data was measured at different frequency and for this reason, all data was standardized and resampled with a spacing of 5 cm and omitting rows with missing values. Because the elemental and stable isotope data of organic matter was obtained every 5 cm, this spacing among samples was chosen to resample the entire dataset (see Section 4.8.1 for results, Chapter 5).

3.8.2 Principal Component Analysis (TC, TN, $\delta^{13}C_{res}$, Fe, Ti, Ca) from ARO 06 01 between 65 and 38.5 kyr BP

To better understand mire state shifts that took place in Rano Aroi between 65 and 38.5 kyr BP (a period characterized by the occurrence of millennial wet events in Easter Island) a PCA with the same variables (6 variables) as the previous section was performed, but constrained specifically to this time interval from 65 o 38.5 kyr BP (142 samples). The dataset was again standardized and resampled to obtain a 5 cm spacing series (see Section 4.8.2 for results, chapter 8 for discussion).

3.8.3 Cluster of the ICP-AES database

In order to classify the elements obtained from ICP-AES, a cluster analysis was performed over the standardized data with R software (R Development Core Team, 2011) together with the 'pvclust' package version 1.2-2 (Suzuki and Shimodaira, 2013). The hierarchical clustering ('complete linkage' method) and *p-values* were calculated via multiscale bootstrap analyses (number of bootstrap=1000) and approximately unbiased (AU) and bootstraping probabilities (bp) values (>0.95) were used to define the groups (see Section 4.8.3 for results).

3.8.4 Principal Component Analysis (V, Al, Sc, Y, Cr, Cd, Ti, Zr, Cu, Th, Fe, Mn, Ba, Mg, Ca, Sr) from ARO 06 01

To reduce the large dataset obtained from ICP-AES analyses to a smaller number of variables (principal components) a PCA on the correlation matrix was applied. The principal components can be interpreted afterwards in terms of geochemical and environmental processes. SPSS statistical software was used to perform the PCA including varimax rotation to

maximize the sum of variance of the square loadings (Wood et al., 1996; Gefen and Straub, 2005; Costello, 2009) over the previously logged (ln) and standardized ICP-AES dataset (see Section 4.8.4 for results).

3.8.5 Principal Component Regression analyses of TC, TN, TS, $\delta^{13}C$, $\delta^{15}N$, $\delta^{34}S$ and ICP-AES PCA

To understand the relation between the inorganic and organic chemistry of the record, the ICP-AES dataset was compared to the organic matter signal. While the principal components obtained from the ICP-AES matrix are indicating the processes that can bring and distribute the inorganic fraction (as dust input by wind, runoff, or diagenetic remobilization), the stable isotope indicate the origin and decay of the organic matter. The different processes that affect the organic and inorganic chemistry have to be intimately related in a coupled interaction among the mire and the catchement area. To understand this connection, correlation coefficient between stable isotopes, organic matter composition, pollen data and Principal Components scores resulted from the PCA over the ICP-AES dataset (Section 3.8.4) were calculated. In addition, to complement the integrative study of all the chemical proxies, a Principal Component Regression (PCR) analyses of TC, TN, TS, $\delta^{13}C$, $\delta^{15}N$, $\delta^{34}S$ and ICP-AES PCA result was performed with SPSS software using a backwards *stepwise regression.* In PCR instead of regressing the dependent variable on the independent variables directly, the principal components of the independent variables are used (Jolliffe, 1982; Myers, 1990) (Section 4.8.5 for results).

CHAPTER 4

RESULTS

4.1. Facies description

ARO 06 01 and ARO 08 02 sequences were found to be mainly composed by radicel peats in the sense of Succow and Joosten (2001), which consist of fine roots (diameter <1 mm) with <10% larger remains, mainly from the Cyperaceae, Poaceae and Polygonaceae (see section 4.6.1 for detailed macrofossil results). Four facies were defined based on plant components, chemical composition, grain size, color and degree of humification under smear slide observations (Figure 4.1).

- **Facies A** (reddish peat) was mainly composed of Cyperaceae (cf. *Cyperus cyperiodes*) and Polygonaceae (*Polygonum acuminatum*) plant remains. This facies was only present in the uppermost 6.5 m of the ARO 06 01 sequence and in the first 1.5 m of the ARO 08 02 core (Figure 4.2). The facies was associated with very high C/N ratios (>60), low TN (<1.10%), low Fe (<3000 cps) and Ti (<4000 cps) and values of $\delta^{13}C$ values between −21‰ and −26‰.

- **Facies B** (granulated muddy peat) was a brown peat made up of coarse organic fragments, mainly roots and rootlets, with low terrigenous content. This facies was present over the entire record and is characterized by high C/N ratios, low Fe and Ti contents and $\delta^{13}C$ values ranging from −14‰ to −26‰ (Figure 4.1, 4.2). A few Cyperaceae seeds were found locally in the uppermost 5 m of the sequence.

- **Facies C** (organic mud) was composed of hemic and dark brown to black radicel peat with scarce and disperse sand fraction. Seeds of cf. *Axonopus paschalis* (Poaceae) were more abundant in the lower part of the ARO 06 01 sequence and most of them were associated with the organic mud facies. Facies C was found as thin layers displaying high Fe (>3000 cps) and Ti (>4000 cps) values, high TN and relatively low $\delta^{13}C$ values (−14‰ to −22‰) and interbedding sediments of Facies B (Figures 4.1 and 4.2).

- Facies D (sapric peat) consisted of dark brown fine-grained peat with high Fe (>4000 cps) and Ca (>4000 cps) values (Figure 4.1).

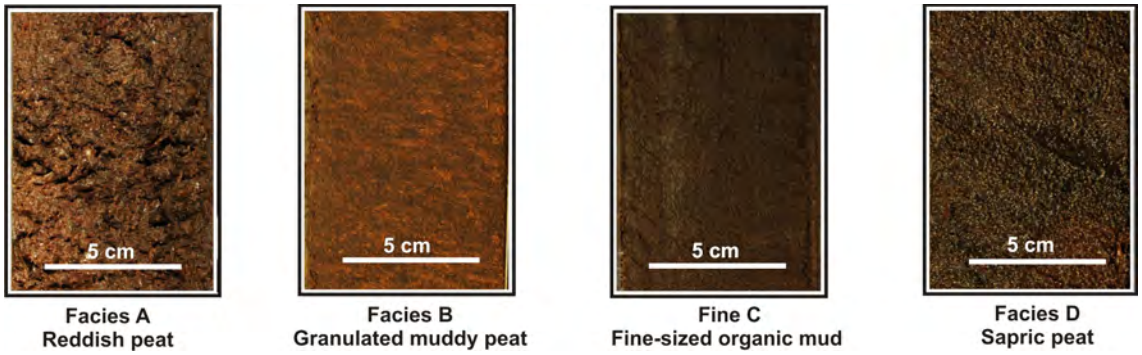

Figure 4.1. Peat facies from Rano Aroi: Facies A (reddish peat), Facies B (granulated muddy peat), Facies C (organic mud), and Facies D (sapric peat). From Margalef et al. (2013).

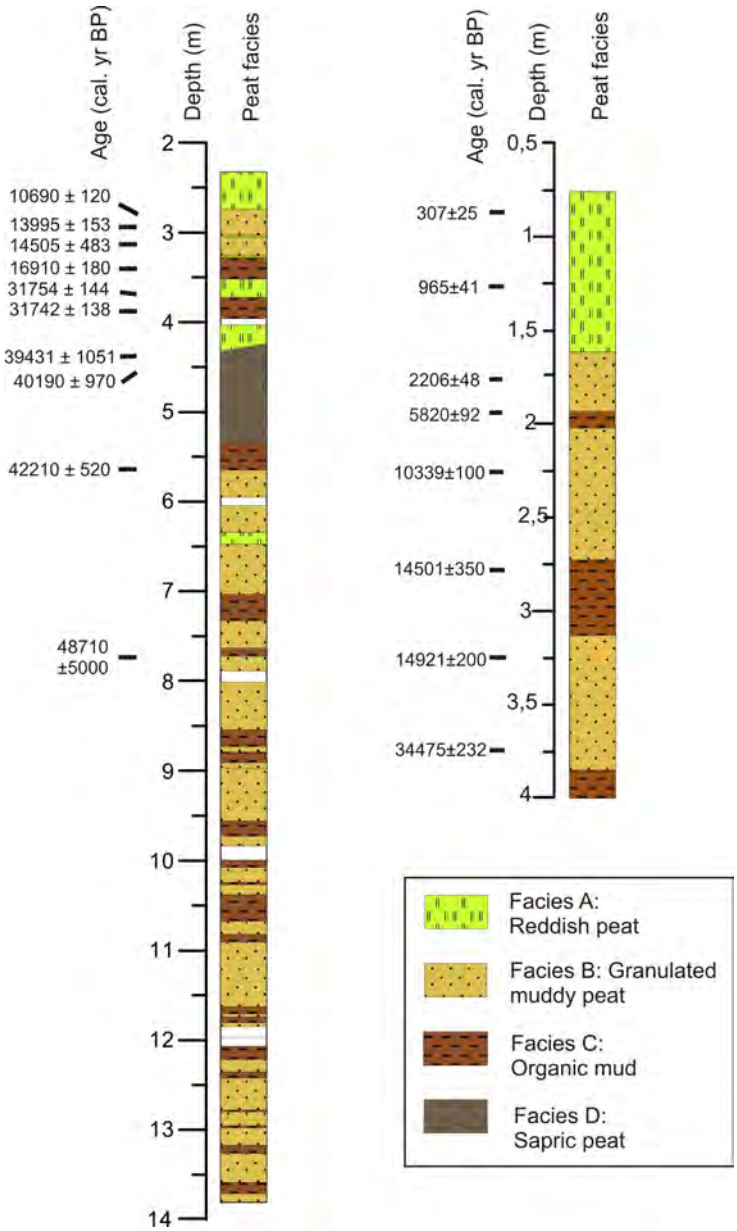

Figure 4.2. Synthetic peat facies column of ARO 06 01 (left) and ARO 08 02. Calibrated radiocarbon ages are also shown (right).

Synthetic stratigraphic columns for ARO 06 01 and ARO 08 02 have been performed based on the above described 4 peat facies distribution (Figure 4.2). On ARO 06 01, granulated muddy peat (Facies B) was the dominant facies presenting interbedded levels of organic mud (Facies C). Sapric peat (Facies D) was only located between 5.4 and 4.23 m depth. On the other hand, reddish peat facies (Facies A) was present on the uppermost part of the sequence, and presenting its lowermost level at 6.4 m depth.

ARO 08 02 sequence has been characterized by the dominance of reddish peat from the mire surface until 1.7 m depth. The rest of the core was characterized by granulated muddy peat (Facies B) with by organic mud levels at 2, 2.8 and 4 m depth.

4.2. Chronology

A total of 27 AMS 14C dates were obtained from the ARO 06 01 and ARO 02 08 core sequences, but only 19 dates were used for the Rano Aroi sequence age model (Table 4.1, Figure 5.2). The age of the intermediate samples were calculated by interpolation between the dated intervals (for detailed information on age model construction see Section 5.3).

Sample Name	Depth (cm)	Fraction dated	Dates	Calibrated ages (yr. BP)
ARO 06 01				
ARO 01-01 03	238	pollen concentrate	*2580±30**	*2730±30 **
ARO 01-01 20	255	pollen concentrate	9460±50	10690 ± 120 BP
ARO 01-01 50	285	pollen concentrate	12150±60	13995±153
ARO 01-01 70	305	pollen concentrate	12880±70	14505±483
ARO 01-01 92	327	pollen concentrate	13800±60	16910 ± 180 BP
ARO 01-01 103	338	pollen concentrate	*7440±50**	*8270±80**
ARO 01-01 143	378	pollen concentrate	26960 ±150	31742±80
ARO 01-02 23	421	pollen concentrate	*12070±60**	*13923±138**
ARO 01-02 31.5	431.5	pollen concentrate	34000±500	39431±1051
ARO 01-02 53	453	pollen concentrate	35300±600	40190±970
ARO 01-03 57	552	pollen concentrate	37600±600	42210±520
ARO 01-04 62	662	pollen concentrate	33900±500	39310±2570
ARO 01-05 67	760	pollen concentrate	45000±2000	48710±2570
ARO 01-06 72	872	pollen concentrate	49000±3000	54600±5000
ARO 01-07 83	979	pollen concentrate	52000±4000	-
ARO 01-08 83	1083	pollen concentrate	>50000	-
ARO 01-09 88	1181	pollen concentrate	53000± 4000	-
ARO 01-10 88	1288	pollen concentrate	>49000	-
ARO 01-11 88	1380	pollen concentrate	49000±3000	-
ARO 08 02				
ARO 02-02 35	85	pollen concentrate	270±30	307±25
ARO 02-03 25	125	pollen concentrate	1050±30	965±41
ARO 02-04 25	175	pollen concentrate	2265±30	2206±48
ARO 02-0 38	194	pollen concentrate	5070±40	5820±92
ARO 02-05 25	225	pollen concentrate	9180±50	10339±100
ARO 02-06 31	281	pollen concentrate	12420±60	14501±350
ARO 02-07 25	325	pollen concentrate	13880±70	14921±100
ARO 02-08 25	375	pollen concentrate	30300±300	34475±232

Table 4.1. ^{14}C AMS radiocarbon ages measured in pollen-enriched extract of Rano Aroi core samples. Rejected ages marked with an asterisk (see text in Section 5.2).

4.3. Geochemistry and mineralogy of the cores: Organic chemistry

4. 3. 1. TC, TN, TS and stable isotopes ($\delta^{13}C$, $\delta^{15}N$, $\delta^{34}S$)

The Rano Aroi deposit was mostly organic, with TC concentrations between 40% and 70% (Figure 4.3). In ARO 06 01, TC values had the higher variability from 14 m to 9 m and the lower, with a mean value of 55%, from core depths between 9 m and 5 m. TN levels varied between 0.4% and 2%, with C/N ratios ranging from 40 to 110. $\delta^{13}C$ showed a mean value around −14‰ from depths of 14 m to 9 m, whereas from 9 m to 6 m, $\delta^{13}C$ values gradually shifted from −14 to −26‰ (Figure 4.3). In the upper five meters, $\delta^{13}C$ values oscillated around −26‰. $\delta^{13}C_{res}$ curve showed high-frequency dips and significantly lower values for Facies C between 6 and 11 m in ARO 06 01. $\delta^{15}N$ values oscillated between -1 and 5‰, with some peat sections with really heavy isotopic composition, above 8‰, at 12.4 m and 10.7 m depth (Figure 4.3). Total S values were less than 1% and they showed a decreasing trend from the bottom of the core to a depth of 6 m and a slight increase from this depth to the top of the core. On the other hand, the $\delta^{34}S$ record could be divided into two main sections: below 8 m of core depth the average value is 18.04 ± 0.88 ‰ and above this depth it is 19.33 ± 1.60‰. The abrupt and irregular shift between the two sections occured between the 7.7-7.2 m interval (Figure 4.3).

ARO 08 02 showed similar values as core ARO 06 01 with respect to TC (50–60%), TN (0.8–2%, peaking to 2.5% at 140 and 80 cm) and C/N (20–80, with a marked decrease from 2 m upward) (Figure 4.4). A gentle shift of $\delta^{13}C$ from −19‰ to −23‰ occured from depths of 4 m to 3.5 m (Figure 4.4). $\delta^{15}N$ showed values between 0 and 8‰. From 4 to 2 m of core depth the $\delta^{15}N$ values stayed around 2 ‰ and it rose from that depth to the uppermost part of the sequence. The highest values were reached at 1.25 (>8‰). In ARO 08 02, TS depicted values close to 0.6% from on the bottommost part of the record until the 2.5 m depth. Between 2.5 and 2 m depth the sulfur content decreased and stayed around 0.3% until the surface of the record. Sulfur stable isotope results in ARO 08 02 showed that from 4 to 2 m depth $\delta^{34}S$ presented a decreasing trend from values near 22‰ until values close to 15‰. At 2 m depth the $\delta^{34}S$ presented a sharp increase and stayed around 22% until the 0.5 m depth (Figure 4.4).

4.4. Geochemistry and mineralogy of the cores: Inorganic chemistry

4.4.1 Ca, Fe, Ti from X-Ray Flourescence (XRF) core scanning

Only Fe and Ti and Ca from ARO 06 had enough intensity (cps) to be considered statistically significant, although these elements also have low counts (Fe = 300–700 cps, Ca = 1000–2000 cps, Ti = 100–2000 cps) all along the sequence. The general trends were similar for Fe, Ti and Ca, although some differences were apparent when comparing them (Figure 4.3). Ca and Fe reach maximum values for the 6–4 m interval, just coinciding with Facies D deposition. Fe and Ti, although they had very low background cps values, showed their higher cps in Facies C (Figure 4.3).

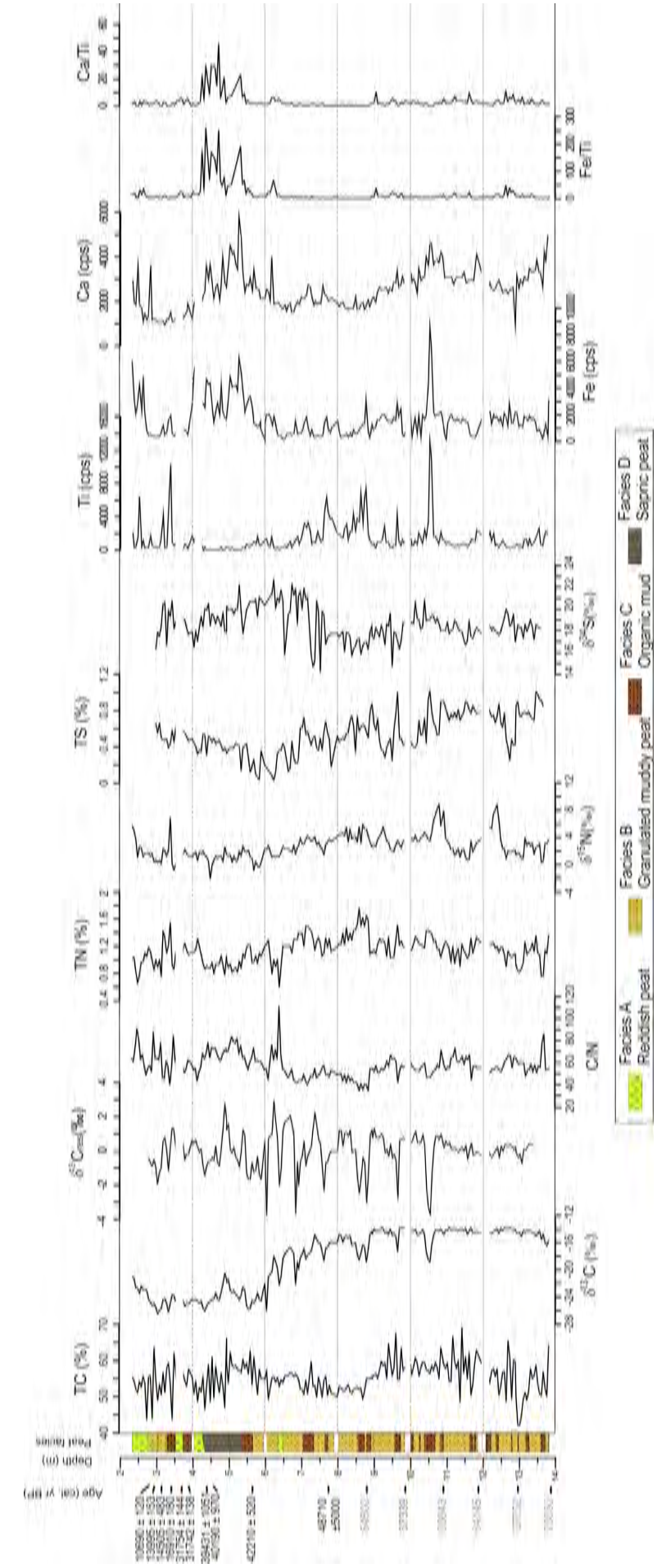

Figure 4.3. Geochemical proxies analyzed in ARO 06 01 core versus depth. Peat facies and radiocarbon ages are indicated in the first column. Geochemical proxies: TC, TN, TS (in percentages), C/N ratio, and $\delta^{13}C$, $\delta^{15}N$, $\delta^{34}S$ (‰) are indicative of the origin of organic matter. Residual values of $\delta^{13}C_{res}$ (‰) are used to enhance the presence of $\delta^{13}C$ dips. Fe, Ti and Ca FRX measurements (in cps) and Fe/Ti, Ca/Ti ratios are also shown.

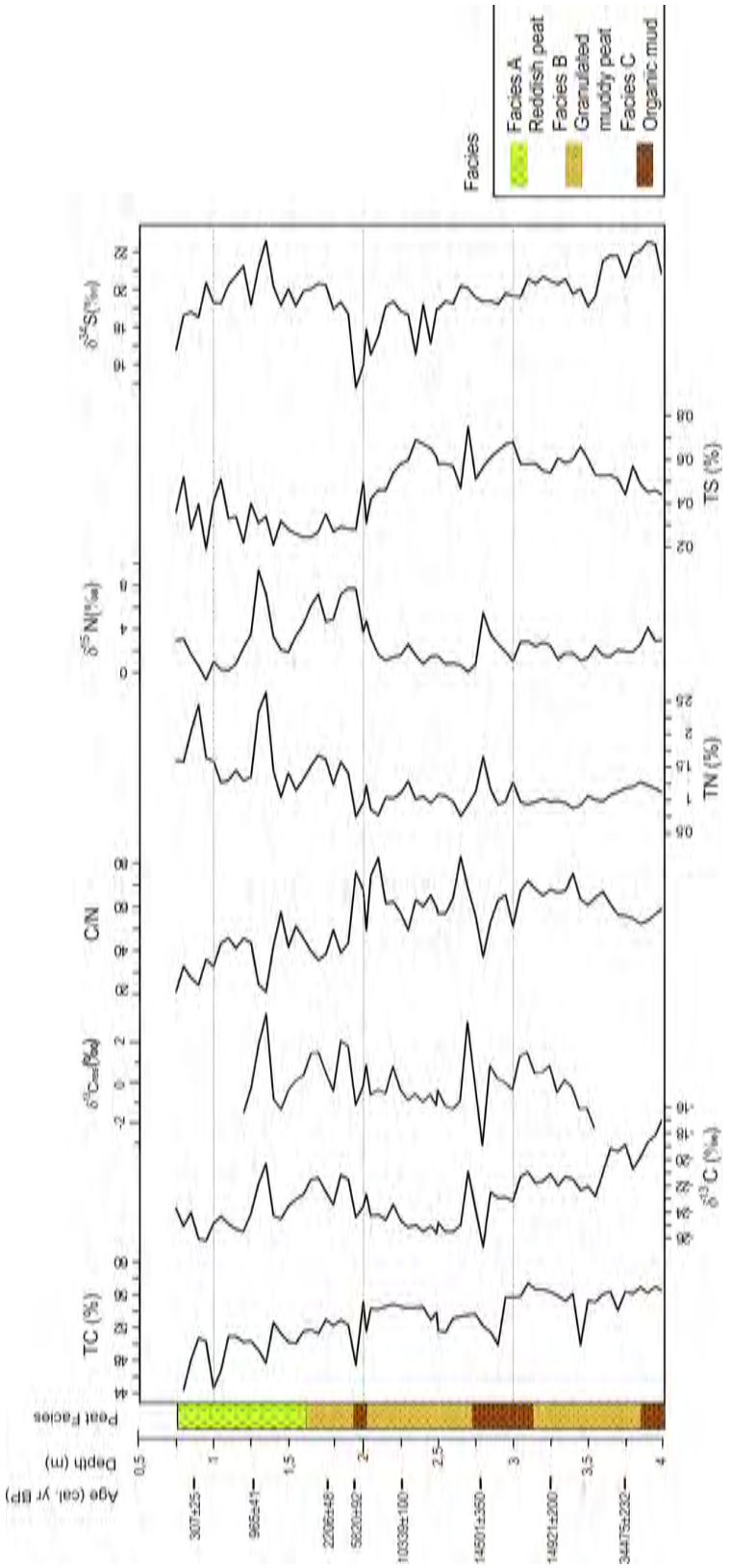

Figure 4. 4. Geochemical proxies analyzed in ARO 08 02 core versus depth. Peat facies and radiocarbon ages are indicated in the column. Geochemical proxies TC, TN, TS (in percentages), C/N ratio, and $\delta^{13}C$ (‰) are indicative of organic matter origin.

4.4.2 Mineral grains composition by Scanning Electronic Microscope (SEM)

SEM analysis of Facies C sand grains revealed the presence of plagioclase and quartz grains in the coarse fraction (>500 μm). Small silt particles (<50 μm) were present on Facies B and C, mainly compound of ilmenite, rutile and silica. SEM analysis of the terrigenous content of the Facies D (<30 μm) showed that minerals consisted of a mixture of Al, Fe, Mn oxides and organic bounded Ca as well as other organic compounds.

4.4.3 Major, minor and trace elements determination of mineral content by ICP-AES.

Cluster analyses of ICP-AES data allowed us to classify elements following significant similarities among their concentration changes in depth (Figure 4.5). Approximated unbiased (AU) and bootstraping probabilities (bp) *values* have been used to define groups on the hierarchical clustering, resulting in 5 groups: (1) Al, Y; (2), Cr, Sc, V; (3) Ti, Zr; (4) Sr, Ca, Mg; (5) Fe, Th. Cd and Cu are close to the second and third group whiles Ba and Mn show a strong similarity to Fe and Th.

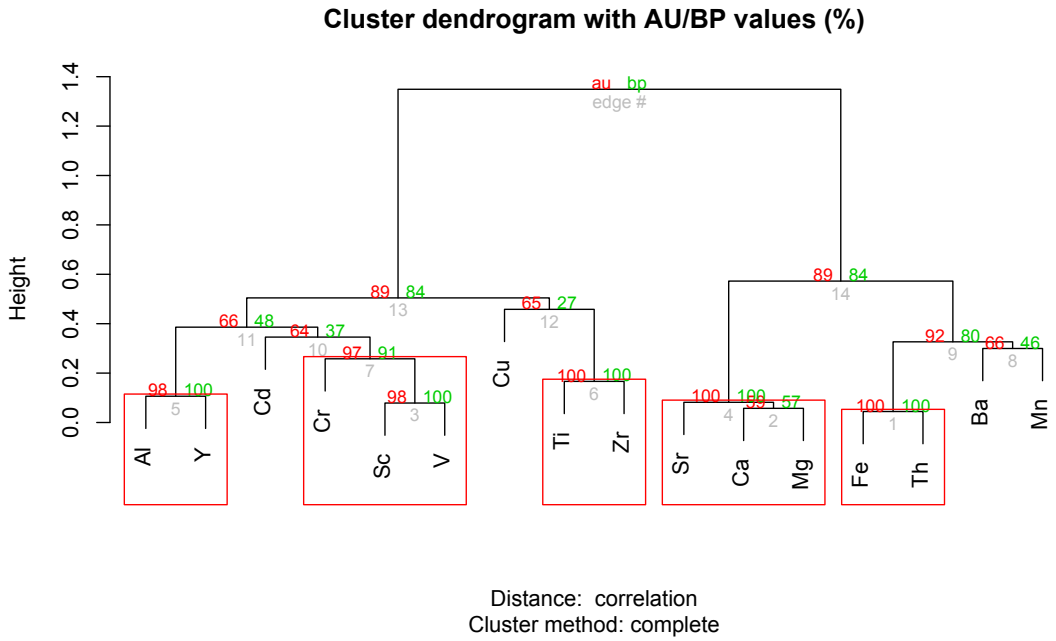

Figure 4.5. Hierarchical clustering dendrogram for ICP-AES database ('complete linkage' method). In red, the approximately unbiased (AU) and in green the bootstraping probabilities (BP) values. In gray, the number of samples that compose the cluster group.

(1) Aluminum (Al) and yttrium (Y) share the same peaky distribution and showed substantially higher basal values from 14 to 9 m depth being approximate 5300 ppm for Al and 3 ppm for Y average values (with a maximum at 8.7m depth, with concentrations of 16000 and 8.2 ppm respectively). These maxima were followed by a gradual decrease (until 5.3 m depth) and presented relatively low concentrations on the uppermost part of the record (Figures 4.5 and 4.6)

(2) Vanadium (V), scandium (Sc) and chromium (Cr) presented a similar pattern, with average values along the bottommost part of the record (from 14 to 10 m depth) being around 18.4 ppm for V, 2.6 ppm for Cr and 2.5 ppm for Sc the average values (Figure 4.6). The maximum concentration values occured between 10 and 8 m depth (74 ppm for V, 8.4 ppm for Cr and 7.8 ppm for V). On the upper part of the record the three elements became sensibly scarcer (Figure 4.6).

Copper (Cu) and cadmium (Cd) described a slightly different and very peaky signal with average values around 19.2 and 3 ppm respectively between the bottom and the 8 m depth and maximum concentrations at 12.4, 10.87, 9.6 and 8.7 m depth. From 8 m to the top, they are present in very low amounts (around 10.7 and 0.2 ppm respectively).

(3) On the other hand, titanium (Ti) and zirconium (Zr) presented a peaky distribution up to 11300 and 6.3 ppm respectively, coinciding with organic mud facies defined on Section 4.1 at 10.6, 8.7, 7.7, 4.15, 3.41, 2.5 m depth, while basal concentration is around 1200 and 1.6 ppm respectively (Figure 4.6).

(4) The concentration profiles for calcium (Ca), magnesium (Mg) and strontium (Sr) had similar trends, presenting relative constant values from the bottom of the record up to 10 m of core depth (around 2600 ppm for Ca, 1200 ppm for Mg and 23 ppm for Sr). From 10 to 6 m of core depth the results of these chemical elements evidenced diminishing concentrations interrupted by very high values between 6 and 4.5 m depth (reaching maximums of 5600, 2100 and 64 ppm respectively) (Figure 4.6). Above the maximum, and after a gradual decreasing, the uppermost 4.5 m were characterized by low values.

(5) Iron (Fe) and thorium (Th) are found in concentrations around 980 and 1 ppm respectively (Figure 4.6). Both elements present peaks at 10.6, 10 and 8.7 m depth and a prominent bump between 6 and 4.4 m depth (reaching values of 3200 and 2.9 ppm). On the upper part of the core, Fe and Th presented peaks at 4.05, 3.41 and 2.51 m depth.

Finally, manganese (Mn) and barium (Ba) presented a similar pattern than Fe and Th, with an average concentration of 9 and 2 ppm respectively and 14.6 (Mn) and 8 (Ba) ppm on the richest part of the record.

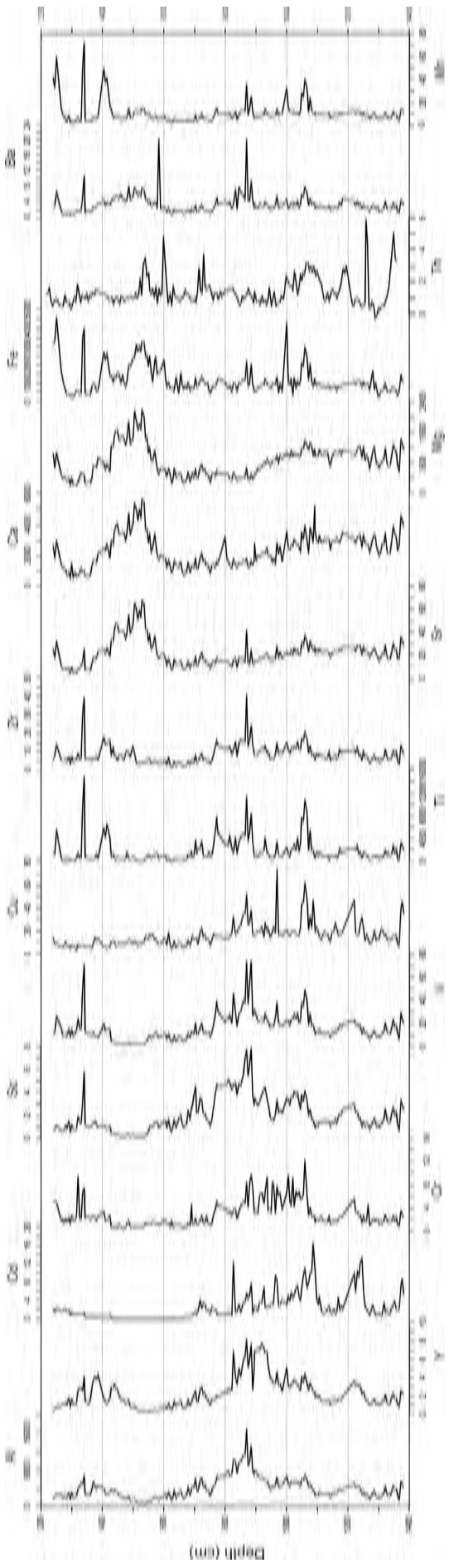

Figure 4.6 Elemental concentrations (in ppm) of the mineral fraction obtained from ARO 06 01 peat sequence. Al, Y, Cd, Cr, Sc, V, Cu Ti, Zr, Sr, Ca, Mg, Fe, Th concentrations are shown.

4.5 Geochemical analyses of the catchment rocks and soils

To investigate the inorganic fraction of the sediment material that has been delivered to the Rano Aroi mire, the mineralogical and geochemical composition of selected volcanic rock samples from the watershed were analyzed.

4.5.1 X-ray fluorescence analysis

XRF analysis of bulk samples showed that SiO_2 was the most abundant oxide of the catchement lithology, followed by Fe_2O_3, Al_2O_3 and CaO oxides (Table 4.2). Na_2O, MgO and TiO_2 oxides were present in concentrations of 3–4 wt.%, while MnO, P_2O_5 and K_2O oxide concentrations remained below 1%. Very high levels of Fe and Ti in the Rano Aroi catchment have been documented by previous petrographic studies (Baker et al., 1974).

Sample	Fe2O3	MnO	TiO2	CaO	K2O	P2O5	SiO2	Al2O3	MgO	Na2O
name	Fe5	Mn3	Ti4	Ca3	K3	P3	Si3	Al3	Mg3	Na7
	(%)	(%)	(%)	(%)	(%)	(%)	(%)	(%)	(%)	(%)
OM-1	13.09	0.18	3.18>UL	9.98	0.54	0.41	48.78	16.01	3.81	3.06
OM-2	11.75	0.16	2.73>UL	10.04	0.47	0.40	47.75	17.09	4.18	3.04
OM-3	12.88	0.16	3.20>UL	9.63	0.70	0.43	48.38	15.34	4.09	3.08
OM-4	17.92	0.25	4.13>UL	7.39	0.38	0.47	41.96	15.69	4.80	2.32
OM-5	13.20	0.17	3.17>UL	9.42	0.40	0.43	46.07	15.83	3.88	2.91
OM-6	18.54	0.18	4.95>UL	3.72	0.40	0.56	28.71	20.91	3.69	0.59<LL
OM-7	14.44	0.21	3.61>UL	5.09	0.69	0.44	38.58	18.96	4.20	1.50
OM-8	13.75	0.19	3.34>UL	7.42	0.76	0.41	45.71	17.85	3.71	2.55
OM-9	12.87	0.16	3.55>UL	8.88	0.69	0.47	48.22	14.15	4.29	3.04

UL= upper limit
LL= lower limit

Table 4.2 Bulk geochemistry from XRF expressed as major oxides (% (mass/mass))

4.5.2 X-Ray diffraction (XRD) analysis

XRD analysis showed that most rocks are mostly composed of Ca-plagioclase and pyroxenes (enstatite–diopside). Ilmenite and quartz minerals were also very abundant while Na-felspathoids, spinel, olivine and rutile constituted between the 1 and 11% (m/m) of rock sample (Table 4.3). These results indicate that rocks in the catchment range from basalts to tholeites–hawaiites.

Sample	Plgcl-Ca	Pyx (Ens-Dio)	Ilmenite	Quartz	Foid (Sod)	Spinel	Oli (For)	Rutile
	%	%	%	%	%	%	%	%
OM-1	80	17	3					
OM-2	75	21	1	3				
OM-3	82	11	2	3	1	1		
OM-4	69	18	4				9	
OM-5	67	26	2				5	
OM-6	39	47	9			5		
OM-7	49	34	5				11	1
OM-8	83	14			3			
OM-9	75	23	2					

Table 4.3 Mineral assemblage of rock samples expressed as estimated % (m/m)

4.5.3 ICP-MS analysis

The ICP-MS analyses show that basalt, hawaite and tholeiite rocks were especially rich in T-Fe_2O_3 (16-22%) and TiO (2.5-4.4%) (see appendices) as documented by previous petrographic studies (Baker et al., 1974). The other major components were found in the following range of concentrations: Al_2O_3 (16-22%), MnO (0.3-0.5 %) and CaO (3.3-9%). Minor and trace elements are present in the following amounts: Sc (24-39.3 ppm), V (170-500 ppm), Co (40-163 ppm), Cr (1-60 ppm), Ni (2.2-29.5 ppm), Cu (16-112 ppm), Zn (110-185 ppm), Sr (76-280 ppm), Y (40-85 ppm), Zr (276-497 ppm), Ba (107-202 ppm), and Th (2.4-5.2 ppm). The rock samples around Rano Aroi were particularly enriched in Ti, Al, Sc, V, Cr, Ni, Cu and depleted in Y, Zr, and Ba when compared to the samples from other parts of the island. On the other side, the Easter Island andosols sampled for this study were especially enriched in Al, Cr, Y, Zr and depleted in Mg, Ca, Sc, V, Co, Ni, Cu, Zn, and Sr.

4. 6. Biological proxies

4.6.1 Macrofossil analyses

The most common remains in the Rano Aroi peat core were Cyperaceae seeds, oribatid mite and coleopteran fragments (Figure 4.7). As explained in Section 3.6.1, the remains have been named with a code (IBB-).

In ARO 06 01 record, seeds of *Axonopus paschalis* cf. were found at 10.56, 8.32, 6.71, 3.49 and 2. 76 m depth, coinciding with the presence of Facies C. The other plant remains were present only above 4 m depth. *Apium prostratum* cf., described as a native species by Zizka (1991), was found in two samples, at 3.71 and 2.76 m depth. *Scirpus californicus* cf. seeds are present at 4.55, 4.16, 3.31, 2.76 and 2.55 m depth. This last plant largely dominates mire vegetation nowadays, together with *Polygonum acuminatum cf.* (Figures 4.7, 4.8). *Cyperus cyperoides* cf. seeds are abundant at 4.16, 2.55, and 2.4 m depth. Finally, *Polygonum acuminatum cf.* seeds are pretty abundant on the superficial levels of ARO 06 01 record. These seeds are found at 5.31, 4.82, 4,16, 3.49, 3.31, 3, 2.76 and 2.4 m depth (Figures 4.7, 4.8). There is an extremely high presence of this remains at 3 m depth, where more than one thousand seeds are counted per 50 cc. *Polygonum acuminatum* is a very efficient pioneer plant, therefore can be indicator of first step of vegetation succession after strong environmental changes or punctual perturbation. It is also worth to mention that *Scirpus californicus* rhizomes have been found at 5.65 and 6.44 m depth. ARO 06 01 record is rich in oribatid and coleoptera remains. Oribatid mites (Hydrozetidae/Ameronothoroidea) are present along the entire record, being more abundant between 8.5 and 6.5 m depth (Figures 4.7 and 4.8). These remains have been identified thanks to the specialist Dr. Torstein Solhøy from University of Bergen. Coleoptera remains have been identified as *Curculionidae Molytinae - Cossoninae* with the help of Dr. Alex Riedel from Museum für Naturkunde (Karlsruhe, Germany). Weevil (Curculionoidea) remains were present on the entire record but become much abundant from 7.24 m depth until the surface levels (Figures 4.7 and 4.8). *Ephydridae* larva, which would indicate aquatic conditions, was present at 8.51, 5.31, 4.16 and 3 m depth. On ARO 08 02 *Cyperus cyperoides* cf. seeds were found in abundance between 3.37 and 3.01 m depth, between 1.62 and 1.42m depth and in the uppermost samples, at 0.89 and 0.87m depth. 1.62, 1.17 and 9.35 m

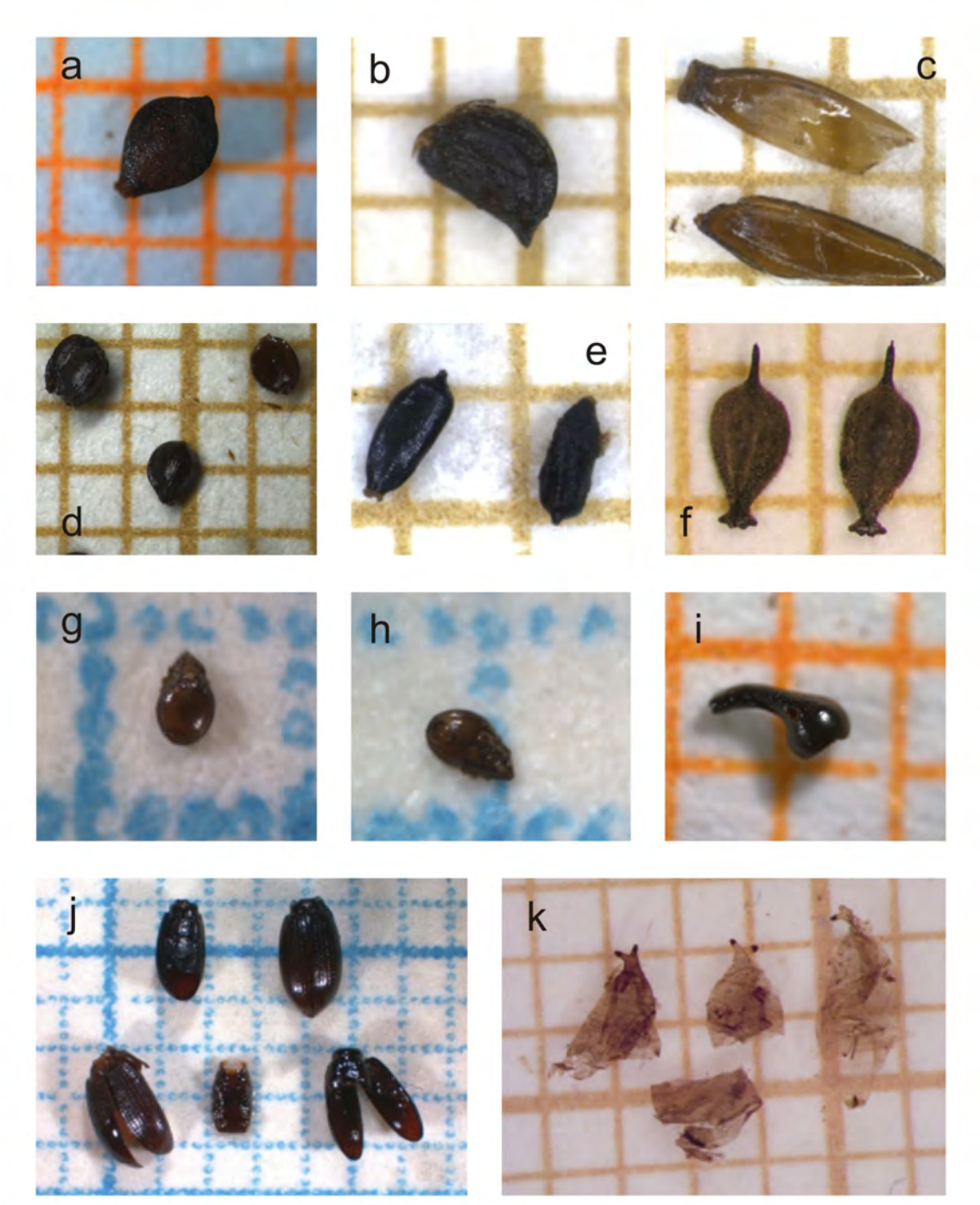

Figure 4.7. Plant and animal macrofossils frequently observed in the Rano Aroi peat record. The square scale in all macrophotographs is 1 mm. From left to right and from up to down: a) IBB-62, *Scirpus californicus* cf. Fruit, b) *Apium prostratum* cf. Seed, c) *Axonopus paschalis* cf. Seed, d) *Polygonum acuminatum* cf. Seed, IBB-60, e) *Cyperus Cyperoides* cf. Fruit, (pictures by Olga Margalef) f) *Scirpus eragrostis* cf. seed. (picture by Núria Cañellas-Boltà), g) IBB-50, Oribatid mite (*Hydrozetidae/Ameronothoroidea*) cf.); h) IBB-50, Oribatid mite (*Hydrozetidae/Ameronothoroidea*); i) IBB-*61 Curculionidae Molytinae* e *Cossoninae*; j) IBB-64 elytron and ventral part of thorax of Curculionidae Molytinae e Cossoninae cf. (Pictures by Olga Margalef); k) IBB-51, Diptera larvae *Ephydridae* (Picture by Núria Cañellas-Boltà).

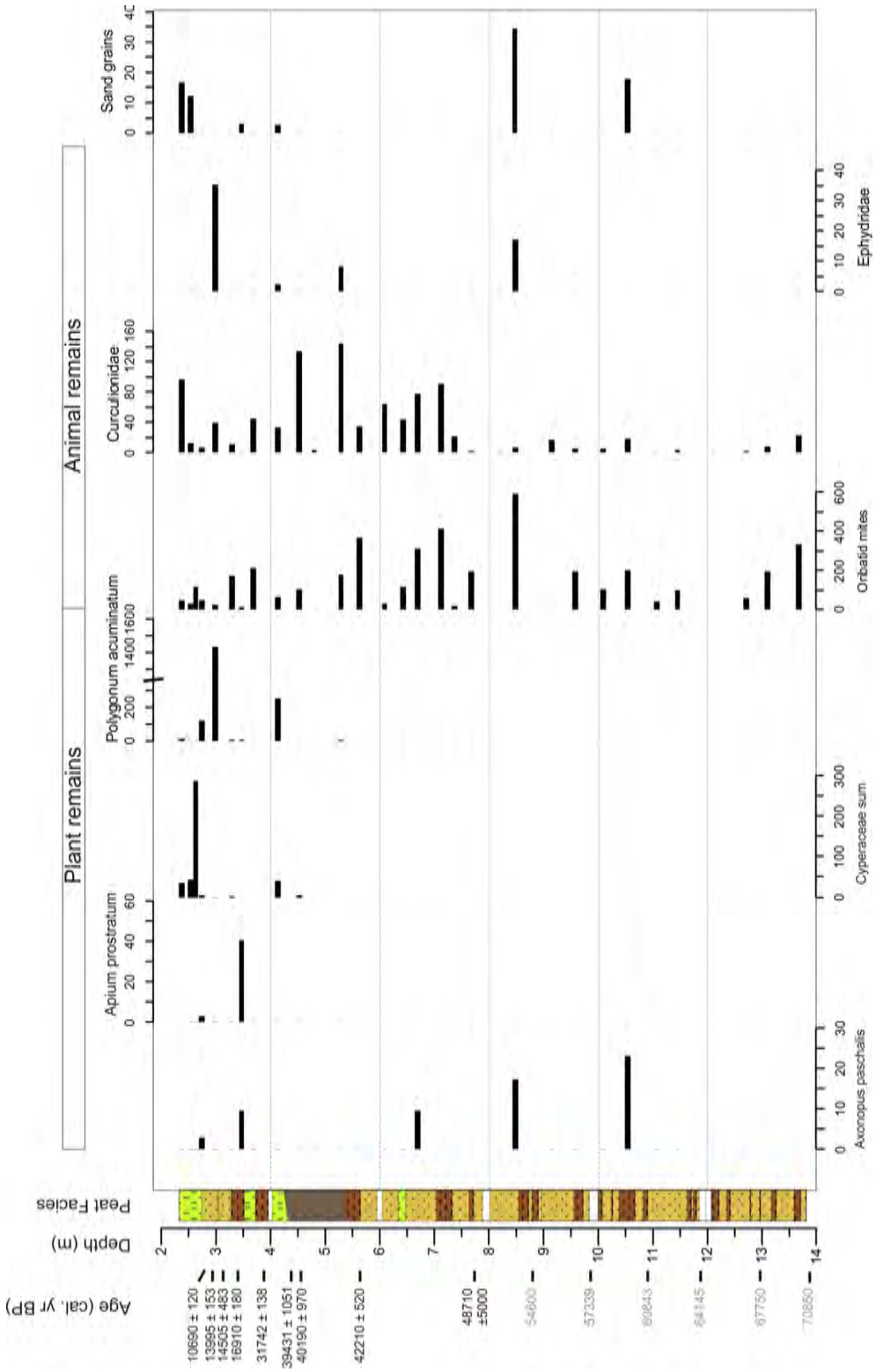

Figure 4.8. Stratigraphic diagram of the main macrofossils observed in the ARO 06 01 record. Peat facies and radiocarbon dates are shown at the left side of the diagram. Seeds of *Axonopus paschalis* cf., *Apium prostratum* cf., *Cyperaceae* sum (including *Scirpus californicus* cf. and *Cyperus cyperoides* cf.) and *Polygonum acuminatum* cf. are shown. *Curculionidae* (sum of trunk, torax and elytron remains), Oribatid mites and *Ephydridae* as well as sand grains (>500 µm) are also plotted.

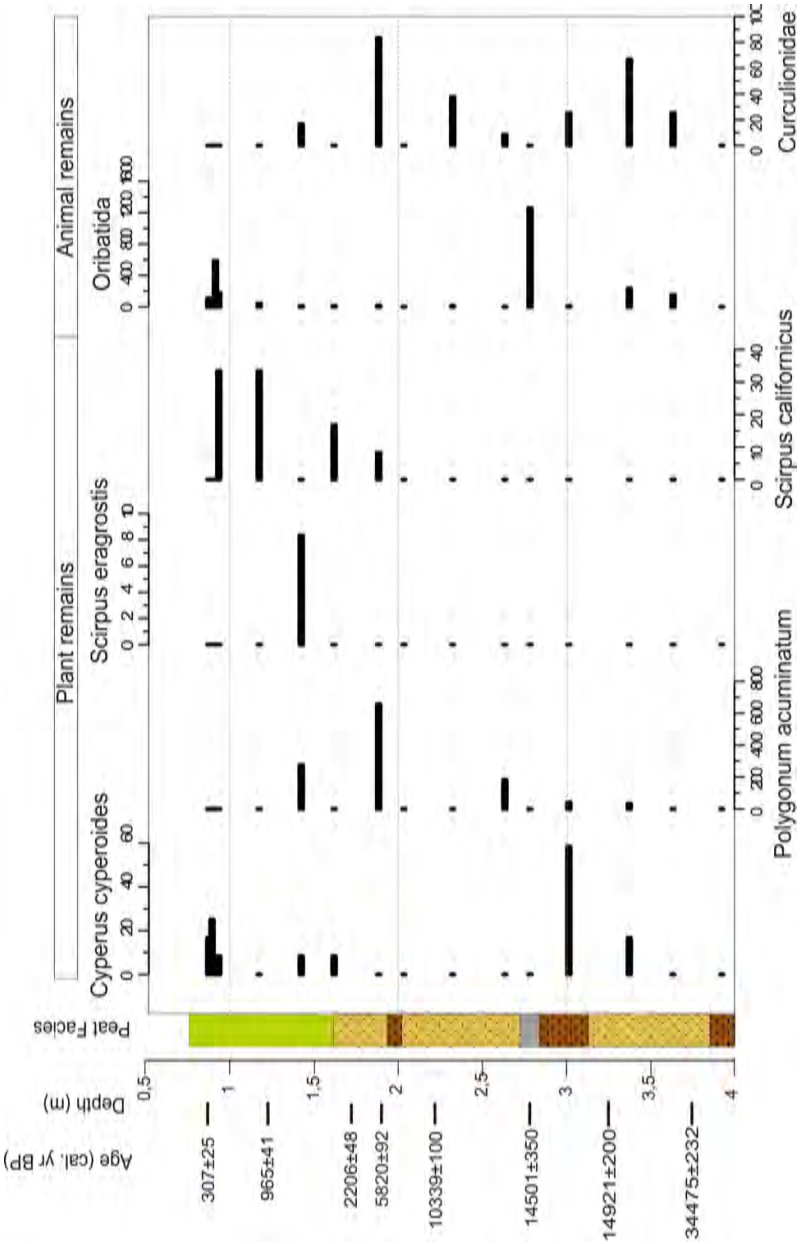

Figure 4.9. Stratigraphic diagram of the main macrofossils observed in the ARO 08 02 record. Peat facies and radiocarbon dates are shown at the left side of the diagram. Seeds of *Cyperus cyperoides, Polygonum acuminatum* cf., *Scirpus eragrostis* cf. and *Scirpus californicus* cf. are shown. *Curculionidae* coleoptera remains (sum of trunk, torak and elytron remains), Oribatid mites are also plotted

Scirpus californicus remains were found at 1.88, depth, while *Scirpus eragrostis* cf. was only present at 1.42 m depth (Figures 4.7 and 4.9). *Polygonum acuminatum* cf. seeds were present at 3.37, 3.01, 2.63 and appear at 1.88 being extremely abundant (more then 600 per 50 cc) (Figures 4.7 and 4.9). *Polygonum* remains were found again at 1.42 m depth. Oribatida remains were present along the entire record, very abundant at 2.78 m depth and on the uppermost part of ARO 08 02. *Curculionidae* remains were less concentrated than Oribatid mites ones, but also present along entire ARO 08 02, presenting peaks at 3.01 and 0.93 m depth (Figures 4.7 and4.9).

4.6.2 Pollen analysis

Pollen identification

In total, 27 different pollen and spore types have been identified (total counts can be found as annexes). The most abundant taxa on ARO 06 01 record were *Asteraceae, Poaceae, Cyperaceae* and *Arecaceae* (Figures 4.10 and 4.11). Fern spores (including Monolete psilate, Trilete psilate, Monolete verrucate, Trilete verrucate, *Pteris* and *Ophioglossum* types) were also very abundant, sometimes being the most abundant palynomorph of the sample. Besides the predominant elements, other pollen types as the ones attributed to *Triumfetta semitriloba* Jacquin, *Sophora toromiro* (Philippi) Skottsb. *Coprosma* sp. were also identified through the record. Herb types as *Plantago* cf. and wetlands plants as *Polygonum acuminatum* Kunth (*Persicaria acuminatum*) were present in moderate to relatively high percentages (Figure 4.11, 4.12). Information about possible native or extinct species corresponding to these pollen types can be found in Section 2.3.2.

There was a pollen type, named as Pollen A, that was in relatively high abundances (up to 8% of some samples) in Rano Aroi record, which has not been definitely identified. The grain is a monad with three short colpi and around 27 μm diameter (E (PV)) with scabrate exine (Figure 4.10). It could tentatively classified as a different type of Macaranga (also tricolporate, short colpis, very thick walls, markedly planaperturate) (Dr. Matthew Prebble, personal communication). However a definitive identification would require a further research. Macaranga family presents extremely variable pollen types (for example having 3, 4 or 5 colpi and very different wall width the same plant specimen) (Dr. Matthew Prebble, personal communication).

Pollen zones

For core ARO 06 01, two zones resulted statistically significant when psimpoll software was applied over the entire dataset (Section 3.6.2). The main change identified was the replacement of the herbaceous plant pollen (primarily *Poaceae*) by woody plant pollen (mainly *Asteraceae-tubiflorae*) as well as aquatic plants and fern spores. Zone II has been divided, in turn, into three more zones in a subjective manner (IIa, IIb, IIc):

- Zone I (13. 89-7.34 m depth) showed a scenario completely dominated by Poaceae (70-90%) with an important contribution of Arecaceae pollen and fern spores. Scattered evidence of *Triumfetta, Sophora, Coprosma* trees were found, especially between 12.9 and 12.3 m depth and between 10.5 and 9.7 m. depth (Figures 4.11, 4.12).
- Zone IIa (7. 34-5.4 m depth) was characterized by an increase of Asteraceae at the expense of Poaceae and Arecaceae pollen. A higher amount of Cyperaceae supports the presence of *Scirpus* in the mire. Ferns start to be abundant, indicating maybe a growth on the edges of the mire or the establishment under a landscape with more shadows due to the expansion of small trees and shrubs (especially Asteraceae but also *Coprosma*) (Figures 4.11, 4.12).

- Zone IIb (5.4-3.4 m depth) depicted similar Poaceae percentage than zone IIa, but the amount of Arecaceae pollen grains sensibly raises as well as the number of fern spores (especially monolete psilate type). Asteraceae abundance stayed around 40% and Cyperaceae pollen percentage was similar to what is described on zone IIa. On the upper part of this zone *Polygonum* cf. appear, right above the stratigraphic hiatus previously described (4. 23 m depth) (Figures 4.11, 4.12).
- Zone IIc (3.4-2.35 m depth), this zone only includes the two uppermost samples. It showed an increase of Asteraceae, Arecaceae pollen and Fern spores and a diminishing presence of Poaceae. Cyperaceae presented an extraordinary abundance, completely dominating the sample in some cases (Figures 4.11, 4.12).

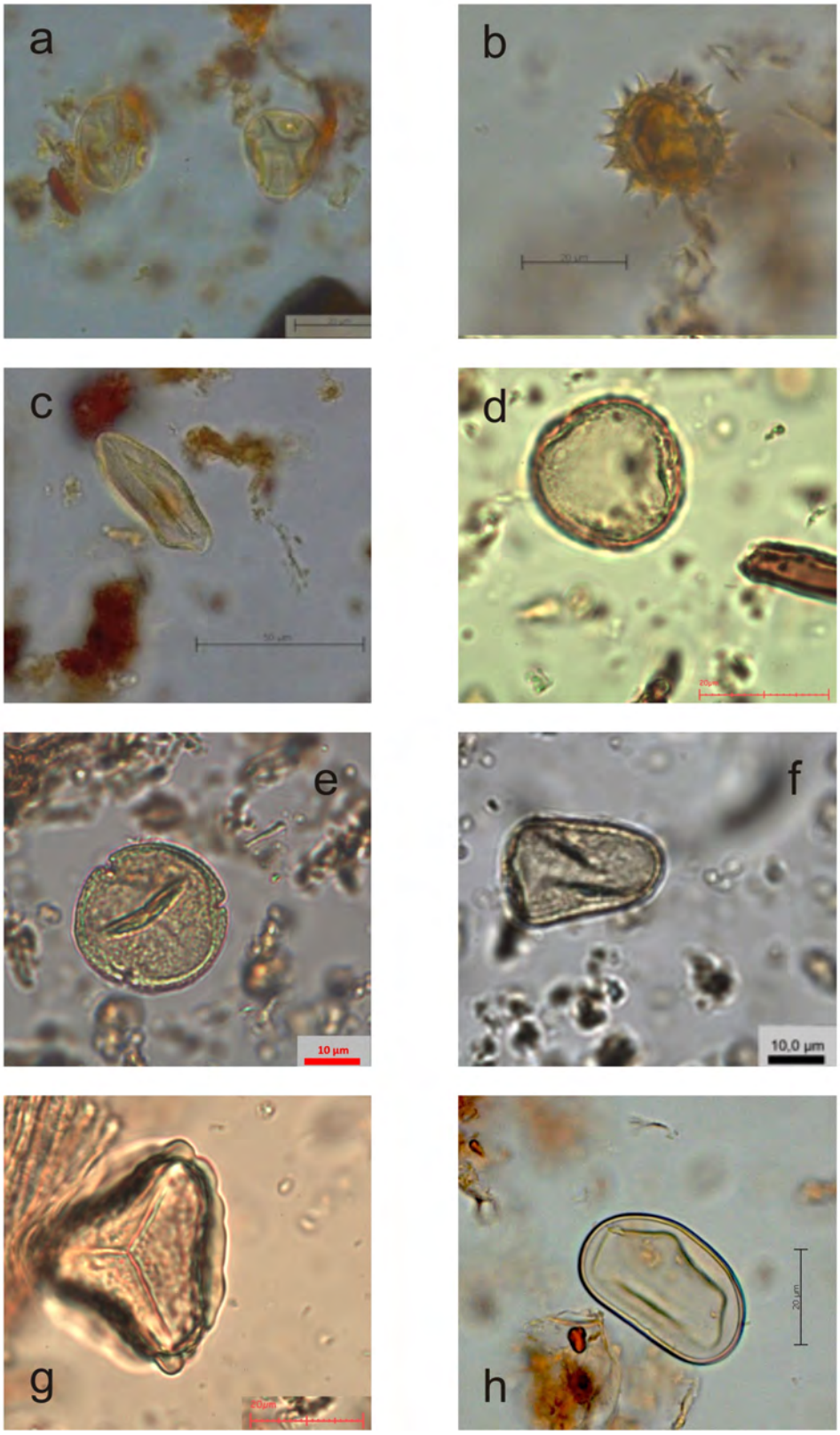

Figure 4.10. Selection of pollen types found in ARO 06 01 record. From left to right and from up to down: a) Asteraceae, b) Poaceae, c) Arecaceae, d) *Coprosma*, e) Pollen A (Pictures by O. Margalef), f) Cyperaceae (Picture by Núria Cañellas-Boltà), g) *Pteris*, h) Monolete psilate (Pictures by O. Margalef).

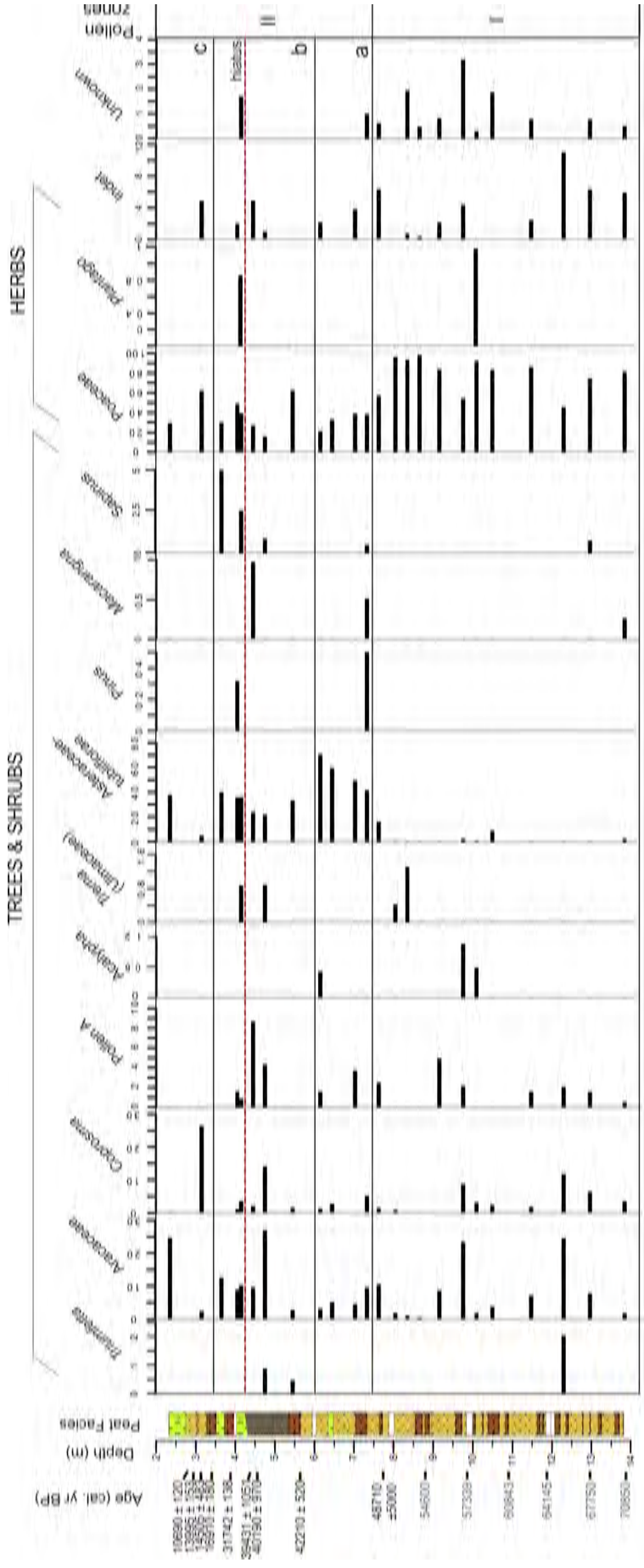

Figure 4.11. Pollen dia gram of the sequence from Rano Aroi (ARO 06 01) including trees and shrubs and herbs plant types. Calibrated radiocarbon dates are indicated on the left of the diagram and pollen zones are indicated on the right.. It also includes different unidentified taxa that appear only one or twice in the whole record. Red line indicates a stratigraphic hiatus

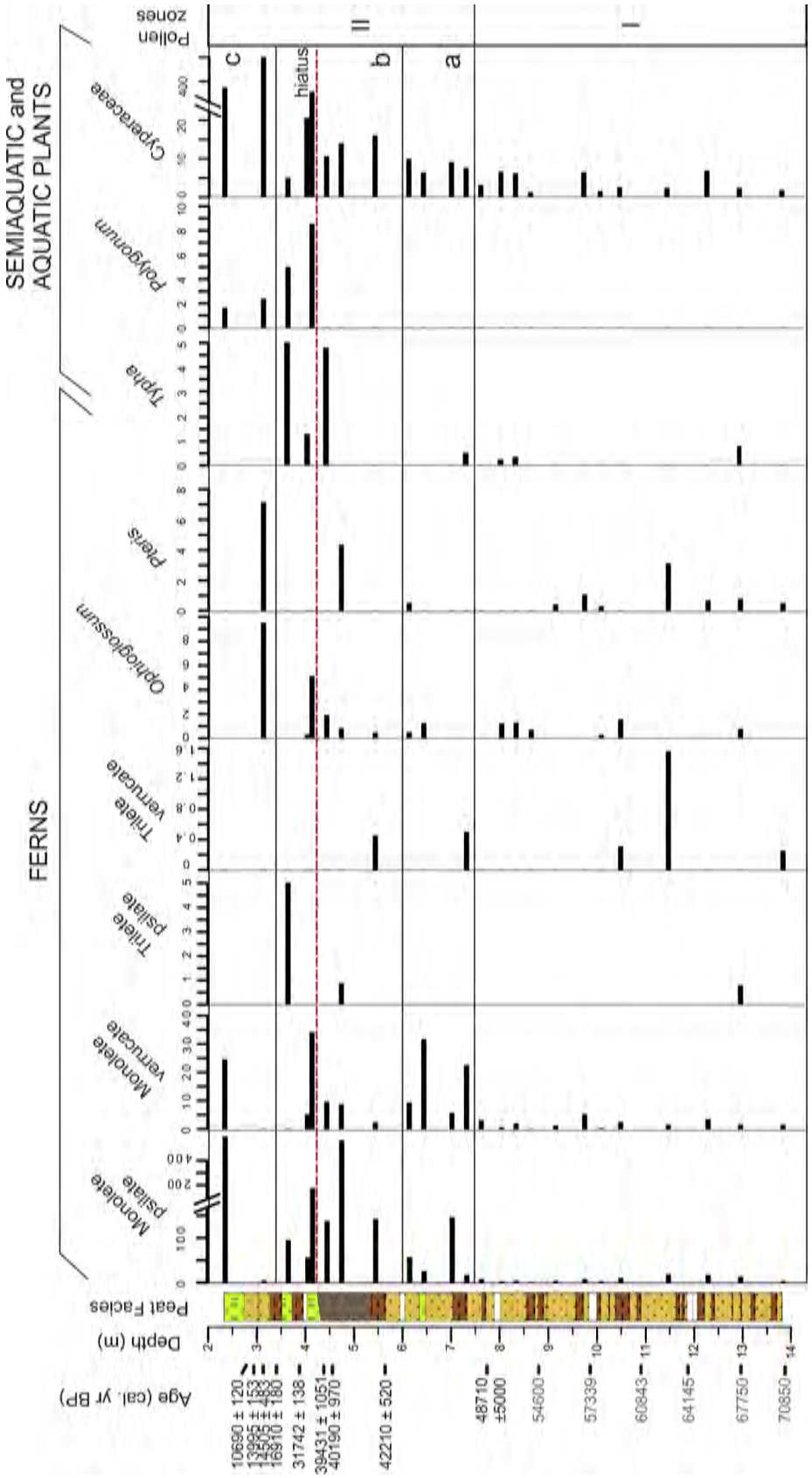

Figure. 4.12. Fern and aquatic and semiaquatic plants pollen diagram of the sequence from Rano Aroi (ARO 06 01). Data calculated as percentages over the pollinic sume, which does not include Pteridophyta and aquatic plants. Calibrated radiocarbon dates are indicated on the left of the diagram and pollen zones are indicated on the right. Red line indicates a stratigraphic hiatus.

Pollen results used on Chapter 6

Only the most abundant taxa, Asteraceae, Arecaceae, *Coprosma* Poaceae, Cyperaceae and fern spores have been used in Chapter 6 to complement to environmental changes identified by geochemical proxies (see discussion Chapter 6) (Table 4.4, Figure 4.13). These 6 taxa constitute between the 70 and the 100% of total pollen counts per samples and consequently were chosen to reflect the main environmental changes recorded in ARO 06 01.

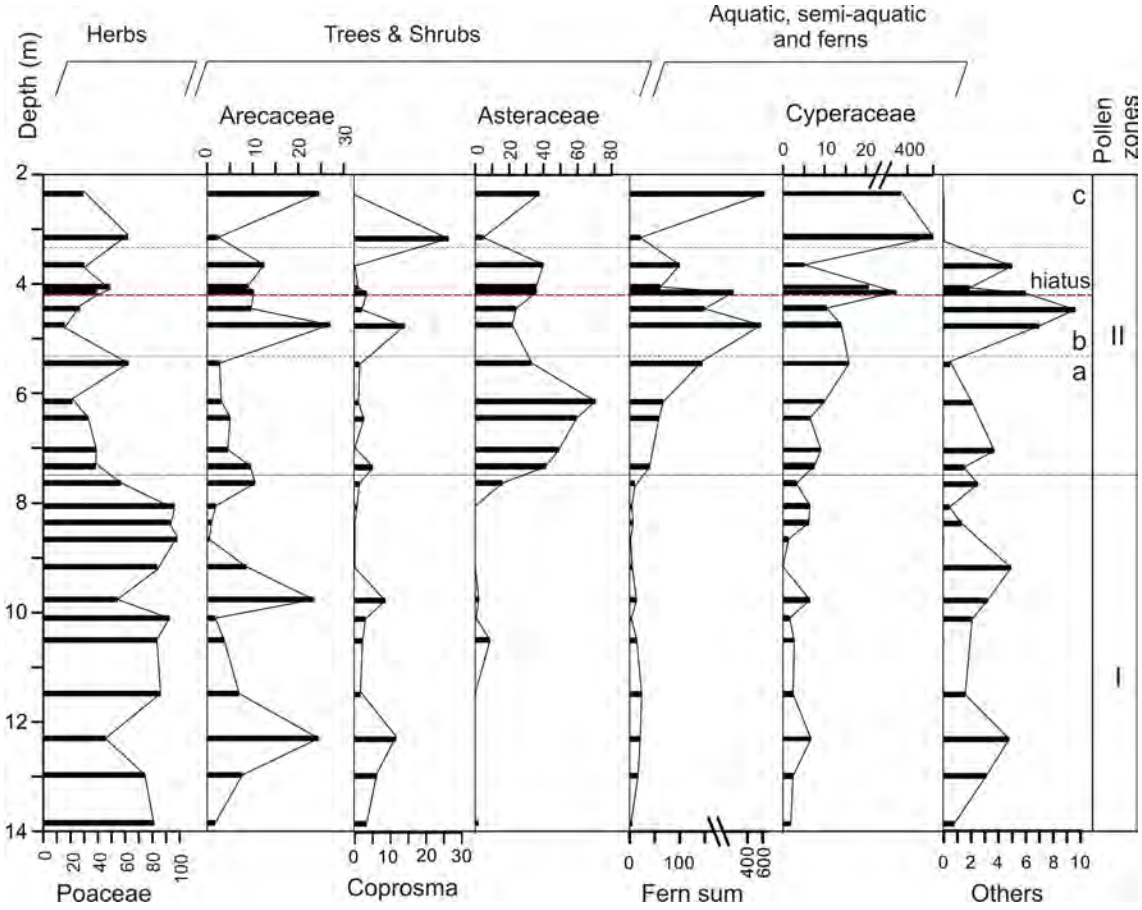

Figure 4.13. The most abundant pollen and spore types of Rano Aroi record are represented against depth: Poaceae, Arecaceae, Asteraceae, *Coprosma*, Fern sum, Cyperaceae and others. The results are presented as percentage over the pollen sum excluding aquatic and semi-aquatic plants (*Polygonum*, Typha, Cyperaceae) and spores.

Non Pollinic Palynomorphs

Although Non Pollinic Palynomorphs (NPPs) where not the object of study of the performed counting, several of them have been identified but not counted. In fact, Rano Aroi peat record is very rich in fungal spores of different kinds.

However, it is worthy to distinguish a NNP that might become very useful for environmental reconstruction. It can be described as round-shaped with short spikes, hyaline texture and around 20 μm diameter. It was found in several samples, but being especially abundant at 12.3, 11.48, 8.66, 8.05, 4.5, 3.15 m depth (Figure 4.14).

Despite we cannot guarantee a definitive identification so far, two hypothesis have been contemplated:

(1) This remain could be an hyaline algae cyst or spore as similar examples found by Van Geel et al., 1980 in European bogs.

(2) Although it is not common to find phytoliths in pollen samples due to the strong acid digestion they can be partially resistant to the treatment. The NPP pictures have been shown to several phytolith specialists. Dr. Claire Delhon (University of Nice Sophia Antipolis, France) who formerly worked on Easter Island microfossils (Delhon and Orliac, 2007), confirmed that these remains had the appearance of Palm phytoliths. Palm phytoliths have been identified in Rano Kau sediments (Dudgeon and Tromp, 2012) and in Rano Raraku (Dr. Doreen Bowdery, personal communication). The differences among the types of Palm phytoliths suggest that there was a changing mosaic of palms through time (Dr. Doreen Bowdery, personal communication). This information suggests that the phytoliths in Rano Aroi could have also been different. Further work on identification from phytoliths samples will be determining to confirm this hypothesis. If these remains were Palm phytoliths this would involve that palm trees are growing near the shore or relatively close to Rano Aroi. Contrary to pollen, that is easily blown, this type of remain is transported by runoff and is therefore indicative of a local signal.

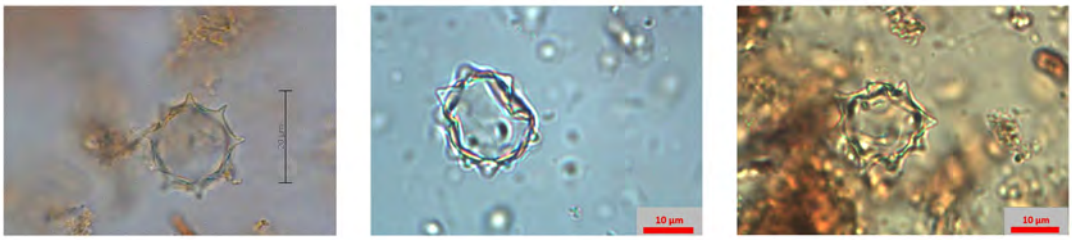

Figure 4.14 Hyaline NPP found in several ARO 06 01 pollen samples.

4. 7 E-W Sea Surface Temperature (SST) gradient of Pacific Ocean calculation

The estimated SST E-W gradient from 38 to 65 kyr BP showed average values of 3.9˚C, with maximum values reaching 5˚C and minimum values at approximately 2.5˚C (Chapter 8). Minimum SST gradients occurred during Heinrich stadials H6, H5a, H5 (yellow bars) or other stadials (grey bars) (Figure 4.15). Higher SST gradient values should be consistent with intensified upwelling in the eastern equatorial Pacific Ocean, whereas a reduced gradient indicates more homogenous hydrographic conditions along the Equator. The current annual average SST gradient between the two sites chosen (ODP 1240 and MD97-2141) is 3.3˚C, according to the World Ocean Data 2009 (Locarnini et al., 2010). However, this gradient oscillates from 1.2˚C in winter to 6˚C in summer when the eastern equatorial upwelling system is fully developed.

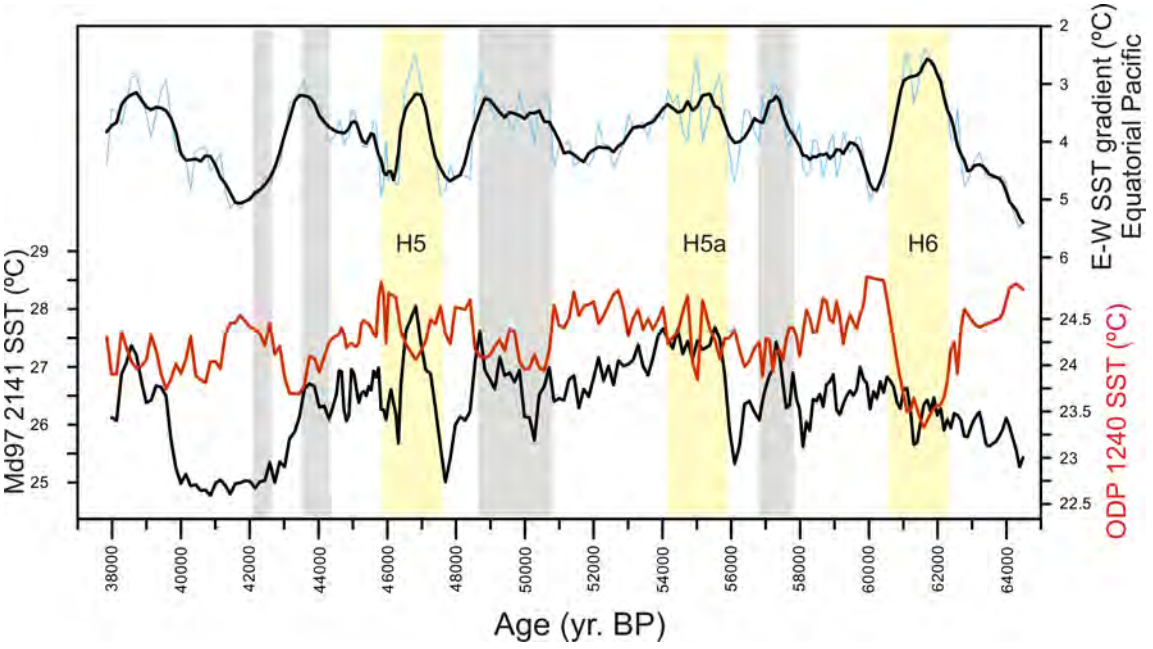

Figure. 4.15. W-E gradient over the Equatorial Pacific (thin blue line) and its corresponding 5-point running average (thin black line). The E-W SST gradient was obtained from the difference between ODP 1240-SST (thick black line, Pena et al., 2008) and MD97-2141-SST (thin red line, Dannenmann et al., 2003) after resampling the ODP 1240 record at the age intervals of those used in the MD97- 2141 record. Yellow bars indicate Heinrich stadials (H6, H5a, H5) while gray bars show other stadials.

4.8 Statistical treatment

4.8.1 Principal Component Analysis (TC, TN, $\delta^{13}C_{res}$, Fe, Ti, Ca) from ARO 06 01

Principal Component Analysis (PCA) of 6 variables (TN, TC, $\delta^{13}C_{res}$, Ti, Fe, and Ca) and 200 samples was carried out over entire ARO 06 01 dataset to study the biogeochemical variability of the peat record. PCA showed that the first component explained 30.7% of the total variance whereas the second component explains an additional 27.8%. Ti, Fe and Ca contributed negatively to the first component, while $\delta^{13}C_{res}$ values were found at the opposite end. TN and Ti tied the negative end of PC2 while Ca, Fe, TC and $\delta^{13}C_{res}$ contributed positively to PC2. The reddish peat (Facies A) and granulated muddy peat (Facies B) showed sample scores at the center of the PCA biplot (Figure 4.16). By contrast, the scores of organic mud (Facies C) were related to Ti, TN and to lesser extent to $\delta^{13}C_{res}$, while sapric peat (Facies D) follows Ca, Fe and TC.

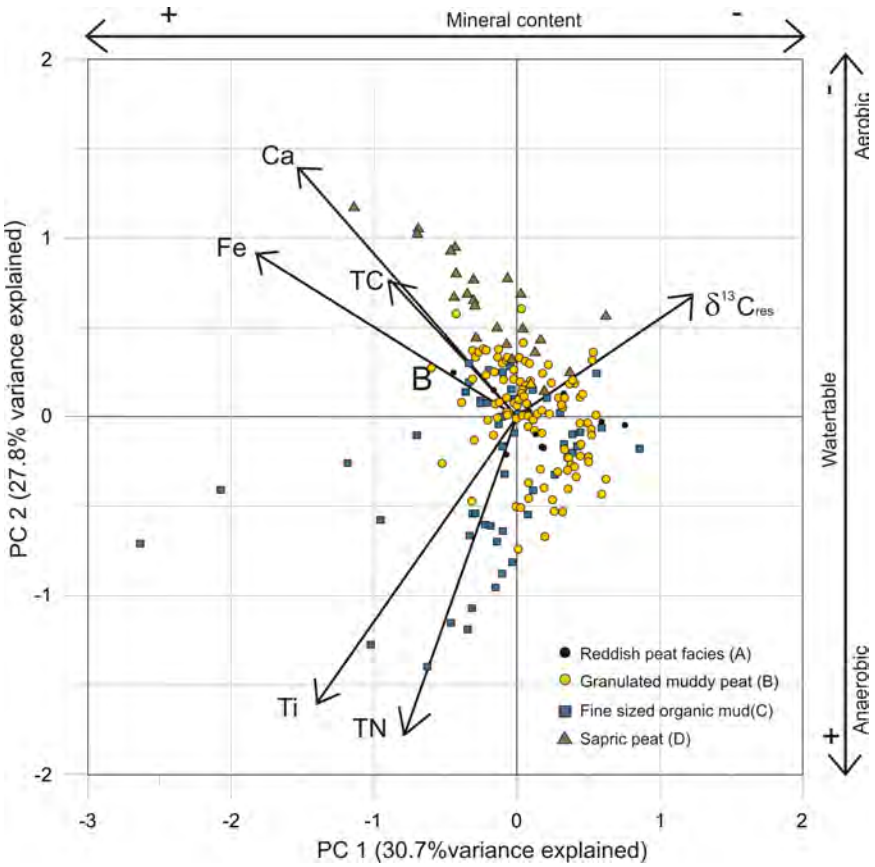

Figure. 4.16. Principal component analysis of the biogeochemical data ($\delta^{13}C_{res}$ Ti, Fe, Ca, TN and TC). Variable loadings and sample scores are presented in the plane defined by these first two principal components. To elucidate the relationship between the PCA results and the established facies, the scores are plotted following a facies color code. The diagram shows how granulated muddy peat (Facies B) and reddish peat (Facies A) lay near the center. Organic mud (Facies C) is associated with high Ti and TN and low $\delta^{13}C_{res}$. By contrast, sapric peat (Facies D) was related to Ca, Fe and TC variability and represents exposure and oxidation of the peat surface.

4.8.2 Principal Component Analysis (TC, TN, $\delta^{13}C_{res}$, Fe, Ti, Ca) from ARO 06 01 between 65 and 38.5 kyr BP

A second PCA was performed on a ARO 06 01 6 variables dataset (TN, TC, δ^{13}Cres, Ti, Fe and Ca), but only with 142 samples that represented the aforementioned 38.5 to 65 kyr BP period (Section 3.6.1). Results are very similar to what is obtained for the entire ARO 06 01 (see Section 4.8.1). The first component explained 34.7% of the total variance and the second component explains an additional 30.6%. Ti, Fe and Ca contributed positively to the first component, whereas TN and $\delta^{13}C_{res}$ values are found at the opposite end of the first component. TN and Ti are found at the positive end of PC2, whereas Ca and $\delta^{13}C_{res}$ contributed negatively to the second component (Fig. 4.17). Facies C scores were related to Ti, TN and $\delta^{13}C_{res}$ variability, indicating that they are well represented by PC2 (Fig. 4.17).

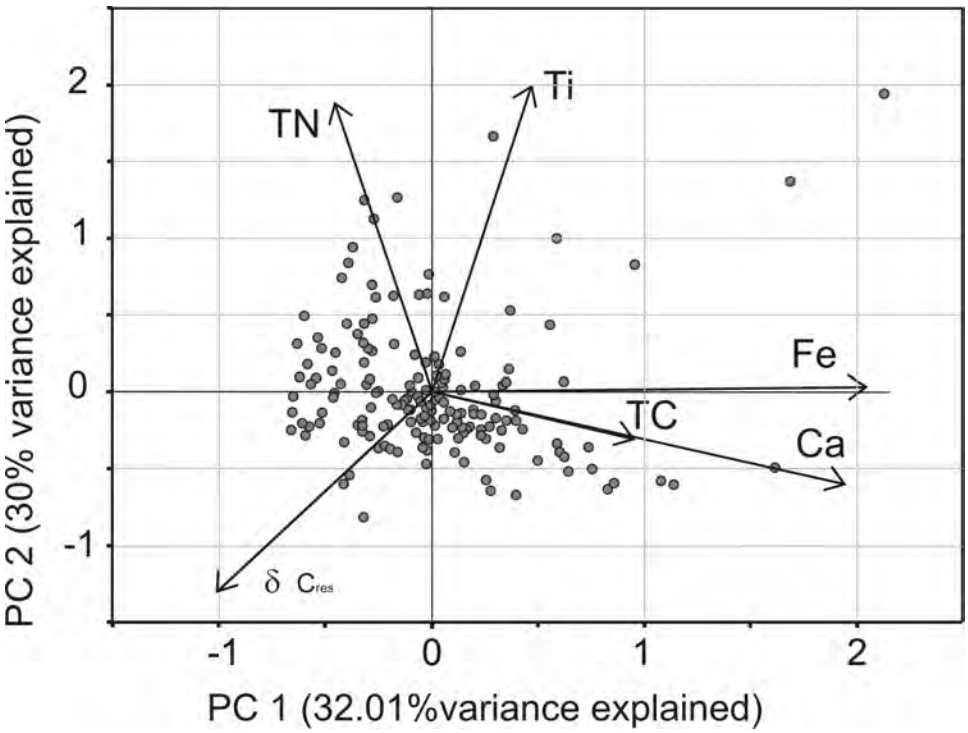

Figure. 4.17. Principal component analysis of the biogeochemical data ($\delta^{13}C_{res}$ Ti, Fe, Ca, TN and TC) comprised between 38.5 and 65 kyr BP. The first two principal components explain more than 60% of the variability (Axis 1: 34.7%, Axis 2: 30.6%).

4.8.3 Principal Component Analysis (V, Al, Sc, Y, Cr, Cd, Ti, Zr, Cu, Th, Fe, Mn, Ba, Mg, Ca, Sr) from ARO 06 01

A third PCA was performed using the suite of selected elements from the bulk ICP-AES peat analysis. The three main components explained up to 85% of the matrix variance. The results of the PCA are presented in terms of the factor loading of each element in the extracted PCs by showing the fractionation of the communalities (i.e., the proportion of the variation of each variable explained by each PC) (Figure 4.18) and by the depth records of the PCs scores (Figure 4.19). The first component (PC1, 40.8% of the variance) was tied to V, Al, Sc, Cr, Cd and to a lesser extent to Ti, Zr, Cu and Mn (communalities shown in Figure 4.18). The second component (PC2, 23.1% of the variance) was characterized by large positive loadings of Th,

Fe, Mn and Ba with significant contributions from Ti, Zr and Sr (communalities shown in Figure 4.18). And the third component (PC3, 21.3% of the variance) was characterized by large positive loadings of Mg, Ca and Sr and moderate ones of Cu and Ba (communalities shown in Fig. 4.18).

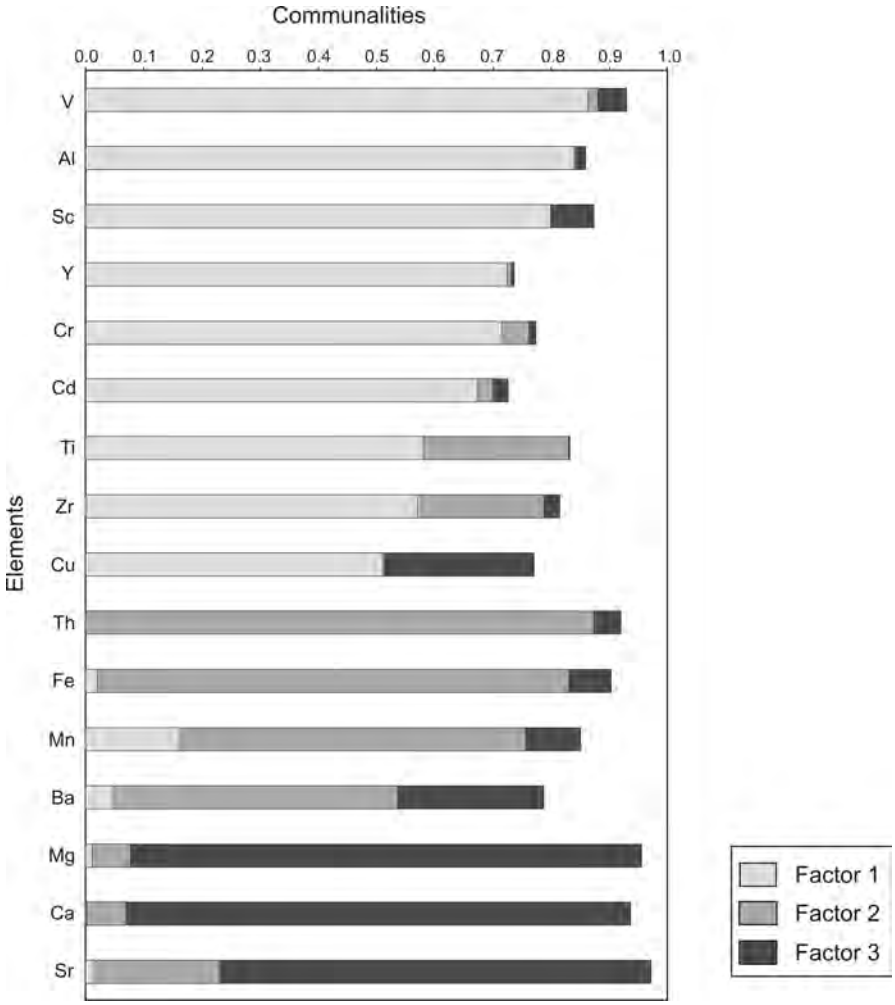

Figure 4. 18. Communalities of the analyzed elements

The score of the three components (PC1, PC2, PC3) will be used to interpret the main geochemical processes concerning elemental distribution on the inorganic fraction and to correlate their changes in depth with other already known proxies (Chapter 6). For this reason they are described in detail. The record of PC1 scores showed values around 0 from 13.82 m to 11.5 m, with a smooth peak (score up to 1.28) at 12.21 m (Figure 4.19). From 11.5 m to 8.5 m the values around 1 with two main peaks at 10.6 m and 8.7 m, where the maximum score (2.37) is reached. From 8.5 m to 5.26 m the values decline gradually until a minimum value (-2.44). From 5.26 m to 3.41 m factors scores slowly increased up to the 0 value is attained. Finally, the trend started to decline again to negative scores until the top of the core (Figure 4.19). PC2 scores show a peaky pattern. From the bottom of the core to 6.1 m values were around -0.5 presenting peaks at 10.6 m, 10.01 m, 8.7 m and 7.73 m (values of 1.8, 2.1, 2.35 and 1.04 respectively). From 6.1 m to 4.8 m values became quite stable around 1 and decline gradually until 2.96 m reaching a score factor of -1.68 (Figure 4.19). Two prominent peaks

occur in this interval: at 4.05 m (PC score value of 2.71) and at 3.45 m (PC score value of 4.15) the latest being the maximum value of the entire record. At the upper part of the sequence, from 2.96 m to 2.40 m values progressively increased from -1.68 to 3.24. The PC3 scores values are quite constant at the bottom part of the sequence. From 13.82 m to 10.49 m values varied around 1. From this depth upwards they started declining until 8.15 m to values close to -1 following a marked see-saw pattern until 5.79 m. Scores rapidly increased from 5.79 m to 5.41 m up to values greater than 1, defining a broad peak until 4.25 m. PC3 scores declined irregularly reaching the minimum value between 4.25 m and 3.16 m (PC score value of -2.59). A peak (0.58) standed out in this interval at 3.86 m. The uppermost part of the sequence presented an increasing trend, factor scores rising from -2.59 to 0 from 3.16 m to 2.40 m. (Figure 4.19).

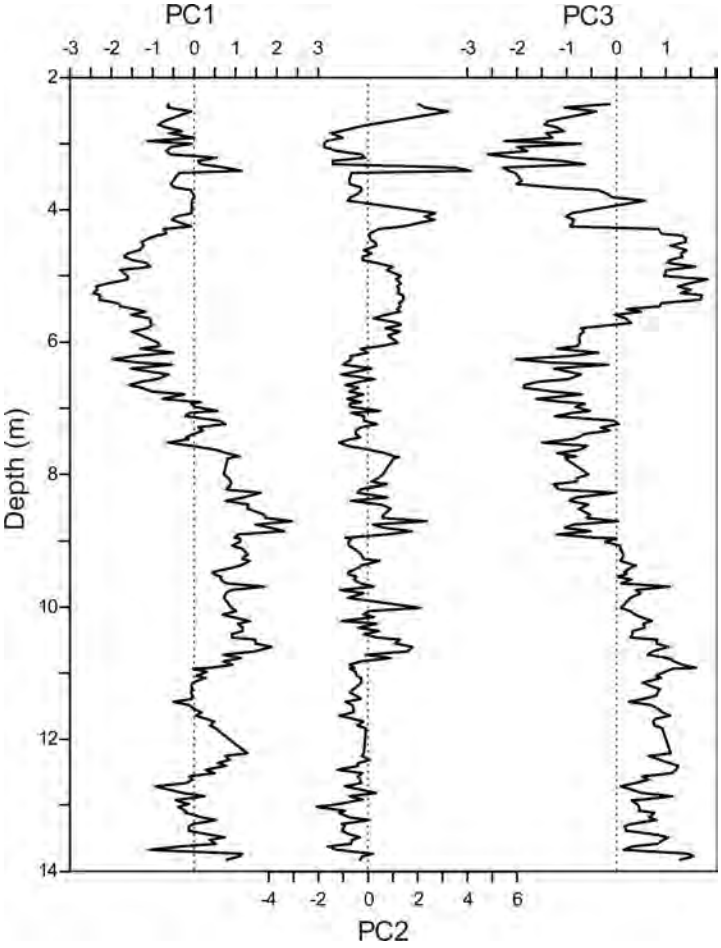

Figure 4.19. Variations of principal components scores of PC1, PC2 and PC3 against depth in Rano Aroi peat sequence.

4.8.4 Principal Component Regression analyses of TC, TN, TS, $\delta^{13}C$, $\delta^{15}N$, $\delta^{34}S$ and ICP-AES PCA

In the third PCA described in Section 4.8.3 we did not include the variables that characterize the chemical nature of the peat organic matter, since the intention of the PCA was to determine the chemical nature of the minerogenic fraction in the peat. The elements considered in the analysis are mainly hosted by inorganic phases, therefore, the three main principal components extracted are assumed to characterize the chemical signature of the inorganic matter. These components can be correlated with the main organic features (TC, TN, TS, and the isotopic composition) in order to look for covariance between the changes in peat inorganic and organic matter. The objective is to determine whether the external and internal

(i.e. postdepositional) processes are involved in controlling peat biogeochemistry. Although the largest correlations were found between PC1 scores and TN, C/N ratios, $\delta^{15}N$, $\delta^{13}C$, the correlation coefficients are moderate although significative at 0.01 level (r values oscillate between 0.5 and 0.66; Table 4.6). Significant correlations ($p<0.01$) were also found between PC1 scores and TS (r=-0.45), PC2 scores and $\delta^{13}C$ (r=-0.31), and PC3 scores and TC, C/N ratios and $\delta^{34}S$ (r=0.30-0.35; Table 4.6).

The relatively weak correlation structure may indicate that individual factors were not responsible for main observed peat organic chemistry changes. But it may also reflect that it is the combination of factors that is important to determine final peat chemistry. To check this latter possibility we performed a principal components regression (PCR) using as input variables the three extracted principal components (Desta Fekedulegn et al., 2002). The results of the PCR models can be found in the Table 4.7. And as expected, the models showed larger correlation coefficients. Nevertheless, TC and $\delta^{34}S$ showed low regression coefficients (r=0.35 and r=0.49, respectively) with the three principal components, which may be taken as evidence that C and S cycling in Rano Aroi was not totally coupled to the main processes responsible for the changes in the inorganic chemistry. On the contrary, TN, C/N ratio, $\delta^{13}C$, and $\delta^{15}N$ show significantly large correlation coefficients (r values between 0.72 and 0.75), while TS showed a moderate correlation (r=0.66). For these variables PC1 had the highest regression coefficients (positive for TN, TS, $\delta^{13}C$, and $\delta^{15}N$, and negative for the C/N ratio; Table 4.7) and it was thus the most influential, being PC2 and PC3 associated to secondary drivers. A visual representation of the adjustment of the predictive models to the original data can be found in Figure 4.20. For TN and C/N ratio the similarity of the records of observed and expected values is quite remarkable, while for $\delta^{13}C$ and $\delta^{15}N$ the model basically accounts for the long-term changes but not for the short term events.

	N	PC1	PC2	PC3
TC	207	0.02	0.02	0.30
TN	207	**0.66**	0.10	-0.15
C/N	206	**-0.62**	-0.04	0.32
TS	194	**0.50**	-0.21	0.35
d13C	207	**0.59**	-0.31	0.29
d15N	207	**0.65**	0.11	0.15
d34S	194	-0.45	0.11	-0.02

Table 4.6. Correlation coefficients between peat organic matter variables and the three Principal Components. In bold, significant correlation values at p-values > 0.01.

	PC1	PC2	PC3	R
TC			0.330	0.35
TN	0.634	0.184	-0.184	**0.72**
C/N	-0.529		0.350	**0.75**
TS	0.453	-0.241	0.326	**0.66**
d13C	0.594	-0.302	0.306	**0.74**
d15N	0.560	0.140		**0.75**
d34S	-0.468			0.49

Table 4.7. Results of the multiple regression model (stepwise regression mode) using the scores of the extracted principal components obtained for TC, TN, TS, $\delta^{13}C$, $\delta^{15}N$, $\delta^{34}S$. R values indicates the multiple correlation coefficient analyses. The CP1, CP2 and CP3 columns indicate the regression coefficients derived from the PCR analysis.

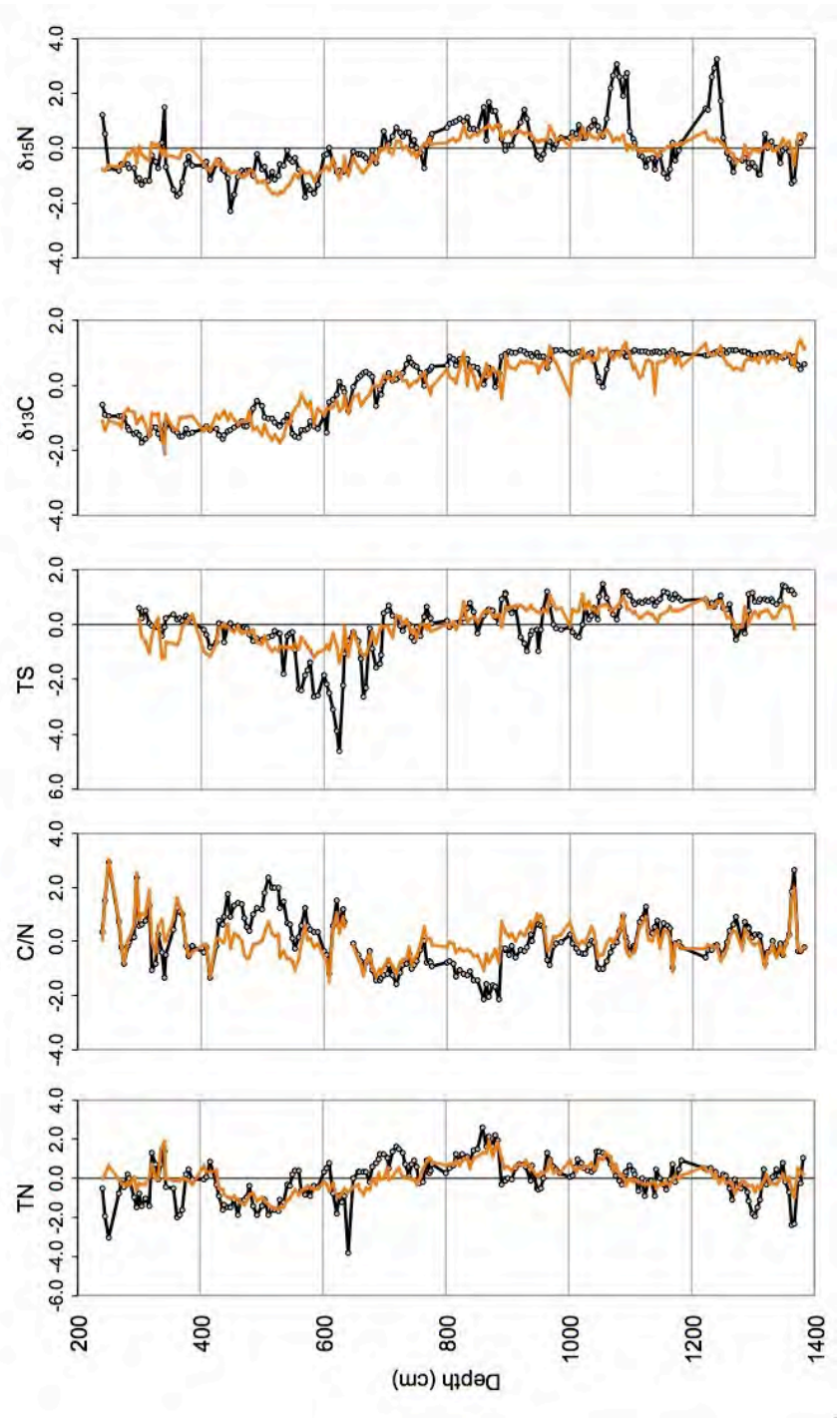

Figure 4.20. Representation of the adjustment of the predictive PCR models (orange) to the original data (black). Only TN, C/N, TS, $\delta^{13}C$, $\delta^{15}N$ are shown, by virtue of being the variables that give significative multiple regression coefficient ($r > 0.5$) values.

DISCUSSION

CHAPTER 5

MAIN ENVIRONMENTAL AND HYDROLOGIC CONDITIONS OF RANO AROI FOR THE LAST 70 KYR BP

5.1 Objectives, methods and results

The aim of this chapter is to provide insights into Rano Aroi environmental history as revealed from multiproxy analyses from the two peat cores ARO 06 01 and ARO 08 02 (Margalef et al., 2013). In this chapter we used the biogeochemical profiles (TC, TN, $\delta^{13}C$ and $\delta^{13}C_{res}$, Ti, Fe, Ca content) (Sections 4.3.1 and 4.4.1), peat facies description (Section 4.1) and macrofossil analyses (Section 4.6.1). The watershed rock mineralogy and geochemistry analyses have been also considered (Sections 4.5.1 and 4.5.2). The use of this wide dataset has allowed us to define different states of hydrological configuration. To be able to explore Rano Aroi changes through time, an age model has been constructed with 19 AMS ^{14}C radiocarbon dates (from 27 performed) (Section 4.2).

5.2 Rano Aroi age model

The obtained ages of the Facies A reddish peat in the uppermost part of ARO 06 01 were found as systematically too young (Table 4.1). On the X-ray radiographs (Figure 5.1), this facies showed less compaction and horizontal structures, suggesting that it might represent well preserved Cyperaceae (*Scirpus* sp.) peat mats that are composed of roots, rootlets and rhizomes. Plant remains and macrofossil composition of Facies A are similar to the structure of the buoyant mats that are currently present in Raraku and Kau lakes. Similarly, Rano Aroi may have had similar, partially buoyant peat patches during episodes with high water table. This type of patches allow simultaneous top down peat growth in floating mats and debris aggregation at the lake bottom. Floating vegetation dynamics can cause peat mats to invert or flip over, as documented for Rano Kau (Butler et al., 2004).

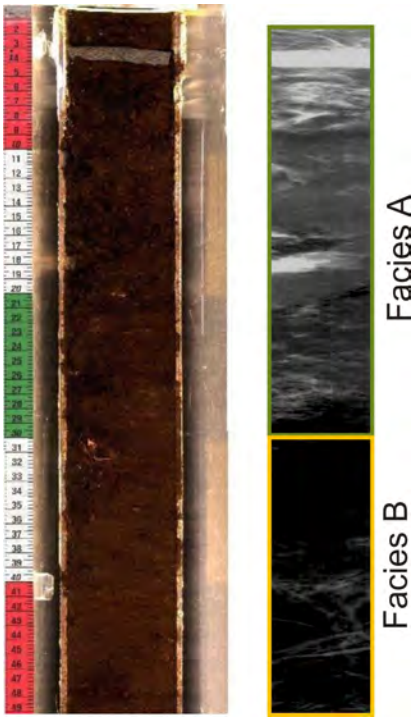

Figure 5.1 Top of ARO 06 01 composed by Facies A and correspondent X-Ray radiography showing less compaction and the presence of roots and rootlets

Moreover, if these too young ages are used to establish age–depth relationships between the ARO 06 01 and ARO 08 02 cores, the steep slope of the peat deposits would be inconsistent (too steep) with the peat accumulation pattern of a kettle hole or a percolation mire (Gaudig et al., 2006).

From 8.5 m to the bottom of ARO 06 01, we obtained ages older than 50 kyr BP (Table 4.1, Figure 5.2), beyond the radiocarbon detection limit. As the accumulation rate between 40 and 48 cal kyr BP (3.7–7.6 m), based on four dates, was constant and the peat facies were the same until the base of the sequence, it can be assumed that sedimentation rates have also been the same. Consequently, the lower part of the core was indirectly dated by linear extrapolation of the accumulation rate obtained in the well constrained dated part of the record. Therefore, the ARO 06 01 sequence probably contains de environmental history of Easter Island for the last 70 kyr BP (Table 4.1, Fig. 5.2). Accumulation rates varied from 0.02 to 1 mm/year, which are common rates for peats worldwide (Couwenberg et al., 2001; Dommain et al., 2011). The mean accumulation rate from 13.90 to 4.31 m depth was 0.3 mm/year but between 4.31 m and 3.78 m it abruptly decreases. The very low accumulation rate is just over a sharp unconformity at 4.31 cm, where highly oxidized peat (Facies D) was covered by low humified peat (Facies A). Peat facies analysis suggests that during this time interval the wetland suffered from drought and erosion. Peat accumulation must have started again soon after, as downward extrapolation of the very low accumulation rates between approx. 31 and 17.5 cal kyr BP (0.03 mm/year) indicate (Table 4.1, Figure 5.2). This extrapolation also shows that – probably at the onset of the resuming peat accumulation – accumulation rates must have been somewhat larger. After approx. 14–15 cal kyr BP accumulation rates increased again in both ARO 06 01 and ARO 08 02. The mid-to-late Holocene (5–2.5 cal kyr BP) is characterized by very low accumulation rates in ARO 08 02; the rate rose again during the last 2.5 cal kyr BP up to the present time (Figure 5.2).

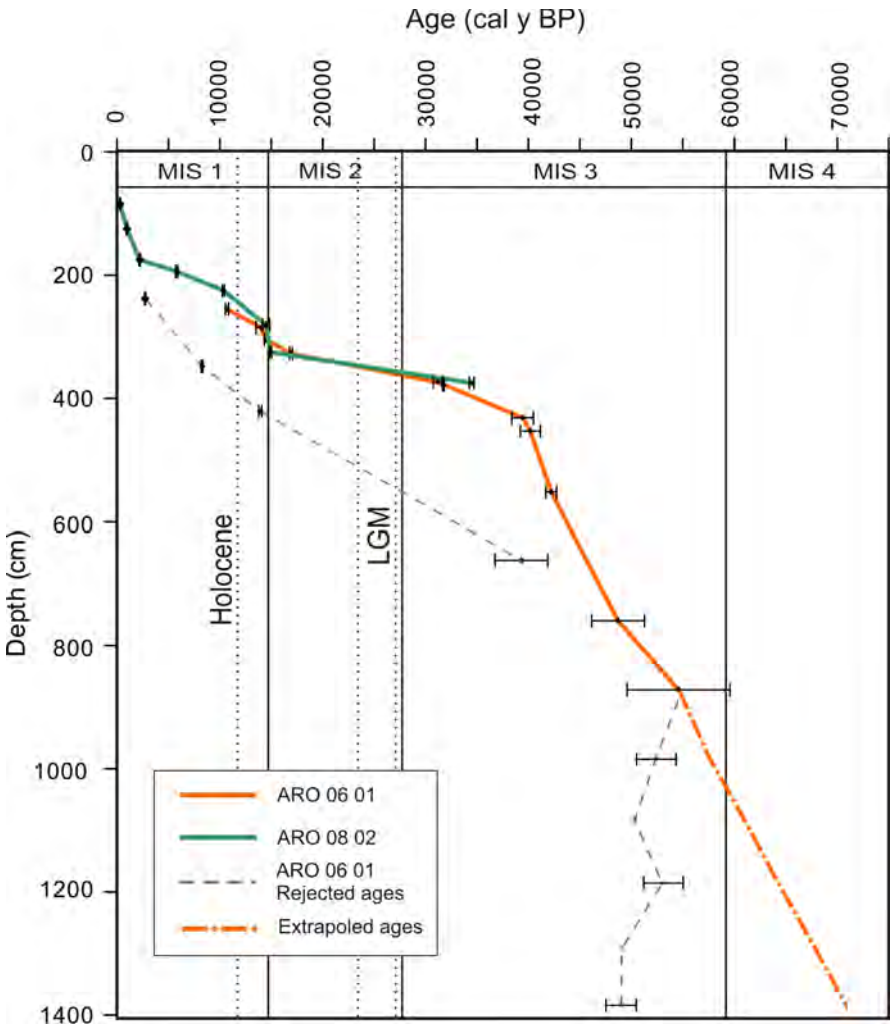

Figure 5.2. Rano Aroi sequence age models for ARO 06 01 (central) and ARO 08 02 (marginal) cores built with AMS 14C dates. Error bars for each radiocarbon date are shown as horizontal bars. Ages in dashed lines were rejected (see text for details). Dotted line indicates extrapolated ages (see text for details). The recovered sequence of Rano Aroi spans the last ca. 70 kyr BP.

5.3 Origin of the organic matter present in the cores

As diagenetic shifts in carbon isotopes values over the millennial time scale are generally much lower than source differences, $\delta^{13}C$ may be used to distinguish between remains from plants with C_3 and C_4 metabolic pathways of photosynthesis (Talbot and Johannessen, 1992; Meyers, 1994). Significant methanogenesis as the single source of significant fractionation in peat is improbable because no correlation existed between $\delta^{13}C$ and C/N changes in ARO 06 01 and AR0 08 02 records (Figures 4.3, 4.4). Moreover, $\delta^{13}C$ values were within the common limits of changes between C_3 to C_4 land plants (Section 1.2.2). The range of $\delta^{13}C$ and C/N also allowed us to reject important contribution of lacustrine (phytoplantonik) organic matter (Section 1.2.2). From 70 to 55 kyr BP, the $\delta^{13}C$ values of ARO 06 01 indicate the predominance of C_4-type plant remains (Section 4.3.1 and Figures 4.3 and 4.4). A gradual transition from C_4 to C_3 plant remains is reflected by progressively lower values of $\delta^{13}C$, reaching −26‰ at approximately 47 cal kyr BP. The uppermost part of the record showed low values of $\delta^{13}C$ (−26‰), which suggests that the mire from that time on

until the present time has been dominated by C_3 plants (Section 4.3.1 and figure 4.3). This interpretation is supported by the presence of seeds of the C_4 grass species *A. paschalis* from 70 to 47 cal kyr BP, whereas seeds of C_3 plants, including *S. californicus*, cf. *C. cyperoides* and *P. acuminatum*, were found in the uppermost part of the sequence (Section 4.6.1 and Figures 4.8 and 4.9).

High-frequency oscillations of relatively low $\delta^{13}C$ values, coinciding with Fe and Ti peaks in organic mud (Facies C) stand out from this general trend (Figures 4.3, 4.4). In addition to differences in metabolic pathways of peat-forming vegetation, $\delta^{13}C$ can provide information on changes in productivity and environmental conditions, such as insolation or humidity (Hong et al., 2001). At the same time, C_3 plant fractionation is sensitive to humidity and precipitation, as shown in isotope measurements on cellulose and macrofossils on peatland records (Aucour et al., 1999; Hong et al., 2001). Higher levels of precipitation and soil moisture and a closer canopy result in lower $\delta^{13}C$ values in C_3 plants and vice versa (Aucour et al., 1999; Hong et al., 2001; Muller, 2006).

5.4 Facies interpretation and mire development

5.4.1 Mire development

Rano Aroi mire currently receives water from a perched aquifer with low permeability that is located to the north and loses water to surface outflow and infiltration towards the south (Herrera and Custodio, 2008). This hydrological configuration indicates that Rano Aroi is a self-sealing mire (sensu Joosten and Clarke, 2002), fed by discharging deeper groundwater but at the same time easily affected by changes in precipitation. Moreover, the small catchment basin volume amplifies rainfall sensitivity. Although we did not recover the oldest peat layers deposited in Rano Aroi, it is likely that the crater evolved from a formerly dry basin into a very wet mire (Facies B) that was regularly flooded (Facies C). As the peat deposits and the identical age-depth curves of both ARO 06 01 and ARO 08 02 indicate, the water level must have steadily risen, probably as a result of formation of stagnating layers on increasingly higher levels (Gaudig et al., 2006). Earlier stages of this process, which is typical for kettle-hole mires (Joosten and Clarke, 2002) can be observed in other small craters on the island.

5.4.2 Principal Component Analysis (PCA)

The main biogeochemical processes that controlled depositional development are illustrated in the PCA plot (Section 4.8.1 and Figure 5.3) that shows that the negative end of first component (PC1) is tied by Ca, Fe and Ti, which have a lithogenic origin. These elements would have originated from the weathering of volcanic rocks in the Rano Aroi catchment (Section 4.5), which are rich in Ca-plagioclase, pyroxenes, ilmenite and rutile (Tables 4.2 and 4.3). This suggests that PC1 primarily responds to the presence of terrigenous components that have been brought to the mire by runoff and incorporated into the peat as particulate sediment. The second component (PC2) of the PCA clearly displays that the chemical behavior of Ca and Fe (positive end of PC2) differs from that of Ti (negative end of PC2), although all three elements can be incorporated into the mire as terrigenous particles (Section 4.4.2). In organic soils, Ca and Fe contents are not only related to primary input, but can suffer post-

depositional remobilization (Section 1.2.3). To check this hypothesis, Ca and Fe data were normalized to Ti, which is considered to be immobile in peat (Weiss et al., 2002; Muller et al., 2006, 2008b). The extremely high Ca/Ti and Fe/Ti ratios between 4 and 6 m depth (Figure 4.3) resemble the enrichment levels that are found in peat profiles on the fen-to-bog transition, indicating the change from geogenous (fen) to ombrotrophic (bog) conditions (Gorham and Janssens, 2005). High Fe/Ti ratios can be attributed to Fe^{2+} migrating upwards from the anaerobic peat below followed by precipitation as Fe^{3+} oxide in the upper aerated peat. Through this process Fe in ombrotrophic peat profiles accumulates in the zone of water table fluctuations (Damman et al., 1992). The distribution of Ca in ombrotrophic mires has been related to bioaccumulation in the biologically active zone (Damman et al., 1992; Shotyk, 1996; Shotyk et al., 2001).

To elucidate the relationship between the PCA results and the established facies, the scores are plotted following a facies color code in Figure 5.3 (Section 4.1).

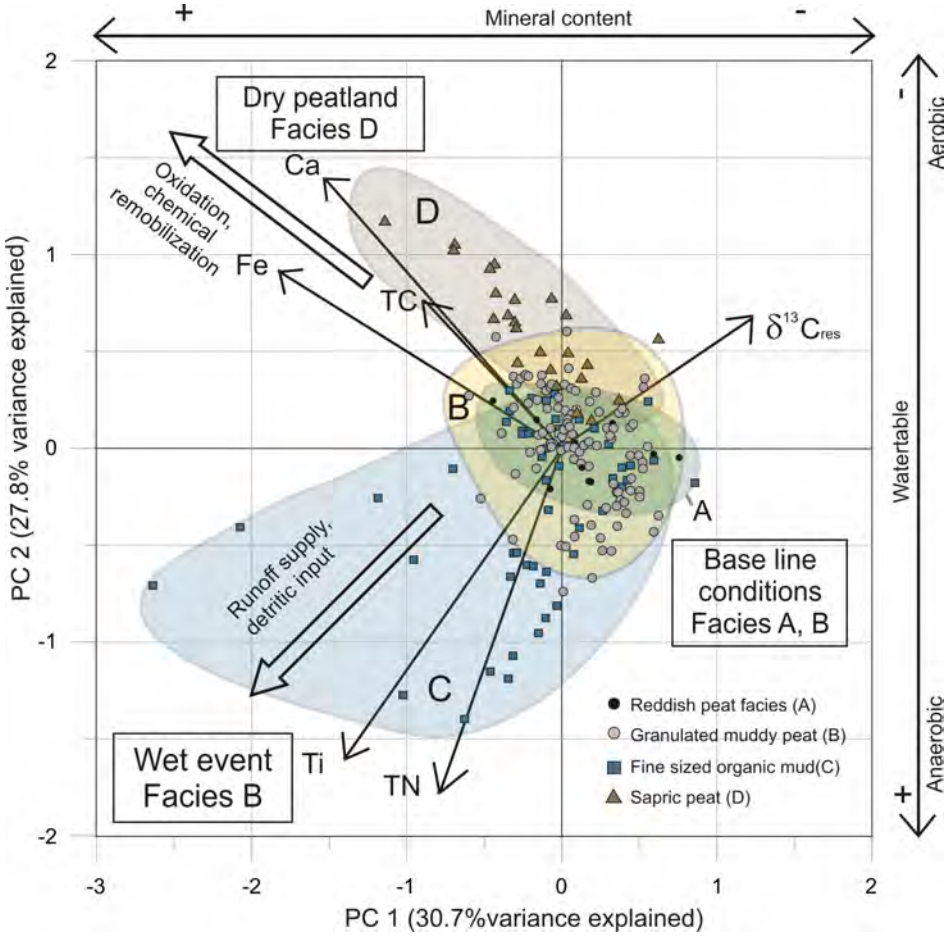

Figure 5.3. Principal component analysis of the geochemical data ($\delta^{13}C_{res}$ Ti, Fe, Ca, TN, TC). Variable loadings and sample scores are presented in the plane defined by the first two PC axes. To elucidate the relationship between the PCA results and the established facies, the scores are plotted following a facies color code. The diagram shows how granulated muddy peat (facies B) and reddish peat (facies A) lie near the axes origin and are therefore interpreted as Rano Aroi baseline conditions (termed water rise mire). Organic mud (facies C) is associated with high Ti and TN and low $\delta^{13}C_{res}$, and are representative of flood conditions. By contrast, sapric peat (facies D) is related to Ca, Fe and TC variability and represents exposure and oxidation of the peat surface (dry peatland stage).

Samples located in the area defined by negative PC1 and positive PC2 (Facies D) values can be related to Fe and Ca complexation with organic matter, i.e. when a lowering water table leads to oxic conditions in Rano Aroi basin. These processes indicated that Facies D underwent early diagenetic changes after peat exposure and oxidation.Samples present in the area that creates negative PC1 and negative PC2 (facies C) with high TN and lower $\delta^{13}C_{res}$ can be explained by a higher water table and higher detrital input processes. In consequence, we interpret PC2 as being indicative of changes in water table level and redox conditions and Facies C is therefore representative of flood conditions. The diagram shows how granulated muddy peat (Facies B) and reddish peat (Facies A) lie near the axes origin and are therefore interpreted as Rano Aroi baseline conditions (see Section 5.4.3).

5.5 Three environmental and hydrologic conditions of Rano Aroi

In the development of Rano Aroi three main environmental and hydrologic settings can be distinguished on the basis of the Principal Component Analysis and the characterization of the four facies (Figure 5.2):

5.5.1 Flooded mire (Facies C)

In the PCA, Facies C samples are directly tied to the TN and Ti loadings (negative PC1 and PC2 values), i.e. to a high content of Ti (Section 4.8.1). Facies C might represent an open water phase when terrigenous material would not have been transported through dense mire vegetation and suspended material could be transported to the center of the mire during periods of high precipitation (Figure 5.5). The lower $\delta^{13}C_{res}$ isotopic values are in accordance with organic matter that originated in conditions of higher soil moisture or precipitation (Muller, 2006; Hong et al., 2001, see section 5.2). The lower isotopic values could be also result from the increasing presence of C_3 plants, and therefore these isotopic values would point to a change in vegetation during wet events. The abundant roots and rootlets that cross-cut the Facies C layers would have penetrated the lake sediments from above in subsequent mire phases (displacement peat, Weber, 1930).

The timing of occurrence of this environmental stage (flooded mire) obtained by high PC2 score values will be used in Chapter 8 to infer the main precipitation events on the island (see Chapter 8 for further details).

5.5.2 Dry mire (Facies D)

The dark color and fine grain size demonstrate advanced humification of the facies D sapric peat. Facies D scores are located in the area defined by the negative PC1, positive PC2 plane, which can be, interpreted as oxidized peat. This facies depicts a biogeochemical signal that evidence advanced decomposition (see Section 6.2.3 for further details) and can be interpreted as a result of diagenesis over Facies B or A. Therefore, Facies D was generated by a long-term drought phases that likely entailed strong decomposition to formerly accumulated peat (Figure 5.4). Indeed this facies ends on a hiatus caused by the drough event (Section 5.2).

5.5.3 Baseline mire conditions (Facies B and A)

The brown-reddish peats of facies B and A are mainly composed of roots, rootlets and other macroremains of sedges and herbs with constant $\delta^{13}C_{res}$ and high C/N ratios. These facies are interpreted as being deposited in a kettle-hole mire (Joosten and Clarke, 2002), similar to the present Rano Aroi conditions, in which long-term stable water tables near the surface allow for the constant accumulation of low-decomposition peat with very restricted terrigenous input (Figure 5.4). Facies A is better preserved and has a lower degree of humidification than facies B, likely due to more constant water tables and faster burial. They illustrate the lower variability of baseline conditions that are interrupted by wetter phases of allochtonous sediment delivery (Facies C) or drier phases with stronger decomposition or even peat erosion (Facies D). Contrary, direct shifts from facies C to D are not found on the Rano Aroi stratigraphic record. The processes that provoke shifts from one stage to the other and therefore fully control peat biogeochemistry are detailed in Chapter 6.

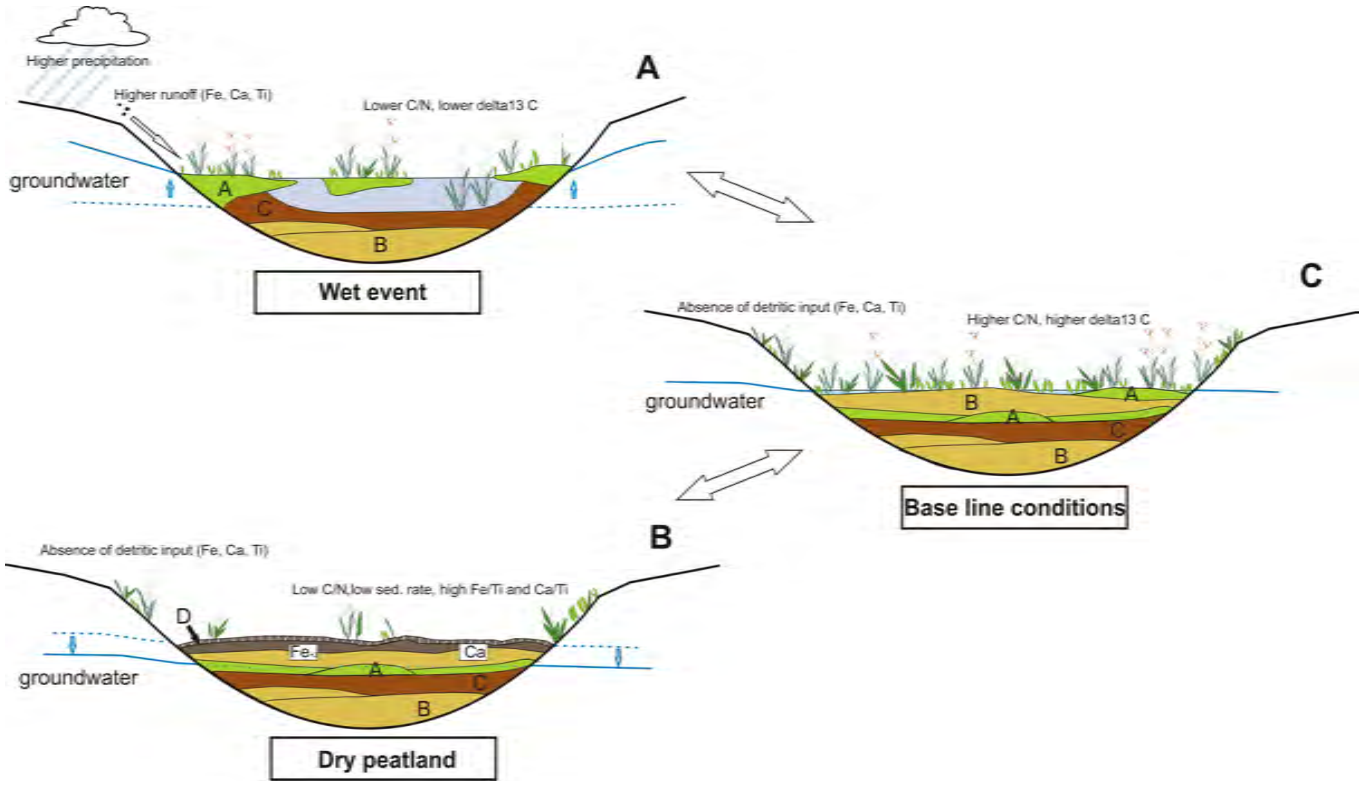

Figure 5. 4 Mire accumulation facies model by different water level stages. This model is based on the PCA analysis of the geochemical characteristics of facies (Figure 5. 3). Three stages of water level have been differentiated. A) The wet events stage entails a flooded area where fine-sized organic mud facies is deposited. High values of Ti, Fe and Ca are recorded due to increased runoff produced more intense precipitation. B) The dry peatland stage occurs when water restriction leave the mire in a negative hydric balance. Surface peat is mineralized, and Fe and Ca are concentrated at the uppermost levels. C) Water rise mire is a stage that is representative of Rano Aroi baseline conditions and was dominant for the last 70 kyr BP: granulated peat facies are formed from the continuous accumulation of organic matter that is mainly composed of sedge and grass roots.

5.7 Conclusions

The Rano Aroi sequence is the oldest and longest terrestrial record recovered on Easter Island, spanning the last 70 kyr BP and documenting water level and vegetation changes during the Late Pleistocene. Radicel peat facies indicate that Rano Aroi grew as a kettle-hole mire from a formerly dry basin, creating impervious layers on increasingly higher levels. The geochemical record and peat characterization allowed us to define three peatland types depending on the hydrological conditions: (1) baseline mire conditions (Facies A and B), (2) flooded mire (Facies C) formed during periods of enhanced precipitation and (3) dry mire (Facies D) when drier climatic conditions prevailed (provoking a diagenesis from Facies A or B to Facies D). The alternation of these phases through time will be used in Chapter 7 to reconstruct the environmental history of the mire and the island from MIS 4 to the present.

CHAPTER 6

MAIN ENVIRONMENTAL PROCESSES CONTROLING PEAT BIOGEOCHEMISTRY IN RANO AROI MIRE DURING THE LAST 70 KYR BP

6. 1 Objectives, methods and results

The objective of this Chapter is to decipher what processes determined the composition of the inorganic fraction of Rano Aroi peat record. In Chapter 5, we combined facies and macrofossils description (plant seeds), bulk peat total carbon (TC), and total nitrogen (TN) and $\delta^{13}C$ data with XRF core-scanner results (Ca, Fe and Ti elements) to reconstruct the three main environmental stages of the site. To fully reveal the complex interactions and processes controlling the peat geochemical signatures at Rano Aroi such as soil dusts, flood events, droughts and redox changes, a more comprehensive geochemical analyses is needed. In this chapter, we have used the elemental composition of peat ash obtained by ICP-AES and provided by Dr. Malin Kylander. The results include Al, Fe, Ti, Ca, Mg, Sr, Y, Zr, Ba, Sc, V, Cr, Mn, Cu, Zn, Cd and Th measurements (Sections 4.4.3, 4.8.3). This geochemical dataset was complemented with TC, TN, TS content and the isotopic composition ($\delta^{13}C$, $\delta^{15}N$, $\delta^{34}S$). The strength of associations between the inorganic and organic processes was quantified using multiple regression models (Section 4.8.4). The determination of the elemental composition of rocks and soils from Rano Aroi and Rano Raraku craters and other parts of the island was also considered (section 4.5.3). Finally, geochemical changes were compared to the results of pollen analysis (Section 4.6.2). The use of all these proxies represents a more advanced approach to Rano Aroi environmental reconstruction compared to what is shown in Chapter 5. The use of such a broad dataset allowed us to establish links between vegetation changes, mineral inputs and geochemical processes within peat as responses to autogenic (internal) and external forcings.

6.2 Factors controlling the elemental composition of peat ash

Total digests of bulk peat samples were analyzed by ICP-AES to obtain absolute concentrations of seventeen chemical elements: Al, Fe, Ti, Ca, Mg, Sr, Y, Zr, Ba, Sc, V, Cr, Mn, Cu, Zn, Cd, andTh (Section 4.4.3). A Principal component analysis (PCA) was applied to this new dataset in order to enable the identification of variables (i.e., chemical elements in this case) whose behavior is similar and, thereby, likely controlled by the same process. This PCA performed identified three PCs that were related to the different facies (Section 5.4, 5.5), stable isotope record (Section 6.3), vegetation changes (Section 6.3) and inferred climate conditions (Chapter 7) since MIS 4.

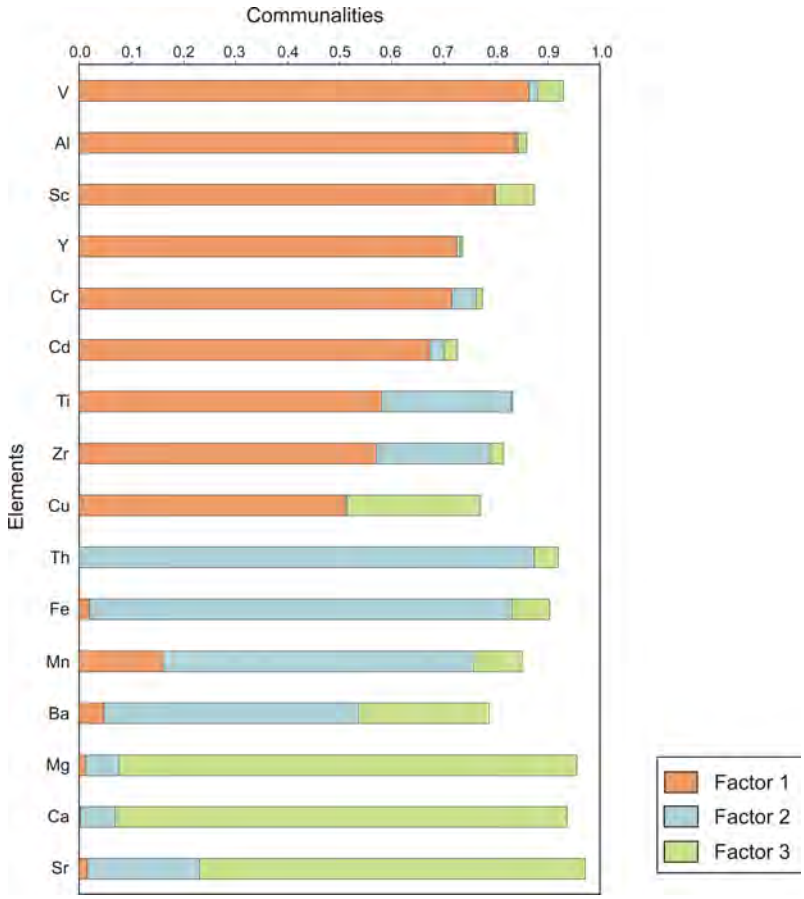

Figure 6.1 PCA Communalities of the analyzed elements.

6.2.1 Long-term mineral fluxes of very fine particles (V, Al, Sc, Y, Ti, Zr, Cr, Cd, Cu)

PC1 is characterized by large loadings (>0.7) of typical lithogenic elements (V, Al, Sc, Y, Ti, Zr) and some metals (Cr, Cd, Cu) (Figure 6.1). These elements are associated to very fine particulate material and this component can confidently be related to the deposition of soil dust (Dr. Antonio Martínez-Cortizas, personal communication). Given the isolation of Easter Island, this signal is most probably dominated by fluxes from the catchment of the mire, which is composed of volcanic rocks and soils. Many elements on this component (like Al, Ti, Zr, Cr, Cu and other metals) are enriched in volcanic soils with increasing degree of pedogenesis (Martínez Cortizas et al., 2007a). Almost the same association of chemical elements (V, Al, Ti, Sc, Cu) was found by Muller et al. (2008b) in the study of the composition of the Lynch's Crater (a mire in NE Australia with remarkable similarities with Rano Aroi, both minerotrophic and formed within a volcanic crater), and interpreted as reflecting mineral particulate input due to soil erosion in the crater basin. The weathering of volcanic materials leads to the distribution of the elements in (1) secondary minerals or organo-metallic compounds, which are poorly crystalline or in (2) primary minerals which are very resistant to weathering. Most of the mineral phases are characterized by very fine (probably ≤ 50 μm) particles, becoming easily mobilized by eolian or hydric erosion. Actually, particle size of most peat layers was dominated by fine silt and clay fractions (<50 μm) as shown in Section 4.4.2 (Table 6.1). Therefore, PC1 would track the long-term *background* fluxes of inorganic particulate material

coupled to soil pedogenesis and erosion. Fine airborne dust particles are enriched in many elements compared to coarser ones (Schuetz, 1989), and these chemical processes lead to potential physical and chemical fractionation during dust transport, which seems to be more intense at short distances from the source area and attenuates during long-range transport, as the grain size of the dust decreases and homogenizes (Schuetz, 1989). The elemental composition reflected by PC1 is consistent with these chemical enrichment processes associated to dust input variability.

6.2.2 Strong runoff events and coarser detritic input (Th, Fe, Mn, Ba, Ti, Zr)

The second component, PC2, is characterized by large positive loadings of Fe, Mn and Ba and moderate positive loadings of Ti and Zr (Figure 6.1). These elements are associated to coarser particles entering the mire. Non-systematic SEM observations of the peat layers corresponding to high PC2 scores showed an abundance of sand (50-600 μm) and coarse silt (20-50 μm) particles (Table 6.1). Iron (Fe) and Manganese (Mn) are elements which can show a strong redox behavior, tending to be depleted under anoxic conditions due to the mobility of their reduced forms and accumulated under oxidizing conditions in peatlands (Steinmann and Shotyk, 1997; Chesworth et al., 2006). The PC2 scores (and the elemental profiles, Figure 4.19) do not show a long-term trend as it has been documented for redox sensitive elements (Mn) in the Lynch's Crater record (Muller et al., 2008b). Instead, PC2 loadings curve against depth has rather a peaky pattern resembling an "event signal" (Figure 4.19). Despite its potential mobility, Fe has been found to be immobile in certain peatlands, including Lynch's Crater and previously formed Fe oxides/hydroxides were found to be stable in lake sediments even under anoxic conditions (Gälman et al., 2009, Weiss et al., 2002; Muller et al., 2008b). Additionally, in most soils developed on volcanic rocks such as those in the Rano Aroi catchment, Fe is largely hosted by primary minerals and the Fe which is released during weathering accumulates as non-crystalline Fe forms (i.e. ferrihydrite, Fe-organic matter associations) and stable secondary Fe phases (oxides and hydroxides) (García-Rodeja et al., 2007). Barium, Ti, Th and Zr have only one oxidation state and are not sensitive to redox changes, and major hosting minerals of Ba (barite, witherite), Ti (ilmenite, rutile) and Zr (zircon, baddeyelite) are highly resistant to weathering. Thus, in Rano Aroi PC2 is not likely to reflect diagenetic changes due to redox conditions. Therefore, while PC1 reflects the long-term particulate terrigenous input into Rano Aroi, PC2 most likely represents strong, highly erosive, runoff events capable of transporting solid particles by suspension or eventually traction to the center of the mire. Peaks in PC2 scores coincide with the presence of Facies C, organic mud, which has been interpreted as being representative of wet events and higher water table levels in the mire (Chapter 5, Section 5.4).

6.2.3 Post-depositional enrichments (Ca, Sr, Mg)

PC3 is characterized by large positive loadings of Ca, Sr, and Mg (Figure 6.1). These elements are transported into the mire included in very fine soil particles as primary minerals like plagioclases, but because they are also highly mobile as ions, they are transported to the mire as dissolved species too. Due to their chemical mobility, groundwater can also greatly contribute to their distribution, sometimes by diffusion from the underlying sediments as a

result of the chemical dissolution of Ca-bearing minerals (Shotyk et al., 2002). Furthermore, as essential nutrients they are also subjected to intense biocycling.

The same Ca-Sr-Mg chemical association was found by Muller et al. (2008b) in the Lynch's Crater record and was interpreted to reflect inputs of dissolved solutes. The record of factor scores (Figure 6.2) shows higher concentrations of these elements in the C_4 section of the core, and decreasing factor scores in the C_4-C_3 transition phase.

The most prominent feature of the PC3 record is the maximum values (Figure 4.18) attained between ca. 42-39 kyr BP (4.25m and 5.41 m. depth) coinciding with facies D or highly decomposed peat defined in Chapter 5 (Table 6.1, Section 5.4). Age model, geochemistry and the sharp discontinuity described at the uppermost limit of facies D suggest that there was a loss (i.e erosion) of previously accumulated peat layers. This would also mean that the unique geochemical features exhibited below the sedimentary hiatus between 5.41 m and 4.25 m depth were acquired as a result of diagenetic changes caused by peat exposure and long lasting oxidizing conditions. The lowering of the mire water table due to drought phases is known to accelerate peat decomposition (Ise et al., 2008) and produce an enrichment of certain elements in the peat (Martínez Cortizas et al., 2007b; Biester et al., 2012). At Lynch's Crater, Ca, Sr and Mg were also enriched in the more decomposed peats (Muller et al. 2008b). Another example of similar chemical enrichments comes from a Canadian mire (Zoltai and Johnson, 1985), composed of a 153 cm thick layer of ombrotrophic, moderately decomposed peat overlying highly humified, minerotrophic peat: Ca was enriched 10 fold; Mg 2-3 fold; Fe 3 fold in the highly decomposed peat. In Rano Aroi the maximum concentrations for Ca, Mg and Sr in the c. 42-31 Kyr BP (6-4 m depth) peat are around 5 fold, 3 fold and 2.5 fold higher than average concentrations in the peat deposited c. 55-42 kyr BP (8-6 m) respectively. Iron is also enriched about 3 fold, but only in the first half of the c. 55-42 kyr BP (6-5 m) section.

PC	Associated to facies	Predominant grain size	Elements	Related to organic chemistry
PC 1	A, B, C	≤ 50 μm	V, Al, Sc, Y, Ti, Zr, Cr, Cd, Cu (Mn)	$\delta^{13}C$, $\delta^{15}N$, TS, $\delta^{34}S$
PC 2	C	20-500 μm	Th, Fe, Mn, B (Ti, Zr, Sr)	$\delta^{13}C$, TN
PC 3	D	10-20μm	Ca, Sr, Mg (Ba, Cu)	C/N, TS

Table 6.1. Relation between the three Principal Components obtained from ICP-AES data and: (1) Rano Aroi peat facies (2) Predominant grain size of the mineral fraction (3) Elements with high loadings, therefore the combination representative of the component. Elements between brackets have higher loadings in other component but are still important contributors. (4) Relation between principal components and the elemental composition and stable isotope of peat. For further details see Sections 6.2 and 6.3 in the text.

6.3 Linking the organic and inorganic peat chemistry

6.3.1 PC1 and organic chemistry

PC1 shows high scores in peat older than 55.5 kyr BP (below 9 m), a shift from higher to lower values between 55.5 and 41.47 kyr BP (9-5.16 m), a moderate recovery until 31 kyr BP (3.76 m) and stabilization thereafter (Figure 6.2). This general trend is similar to the long-term evolution of the $\delta^{13}C$ record that has a declining trend from 55.5 to 43.9 kyr BP (9-6 m),

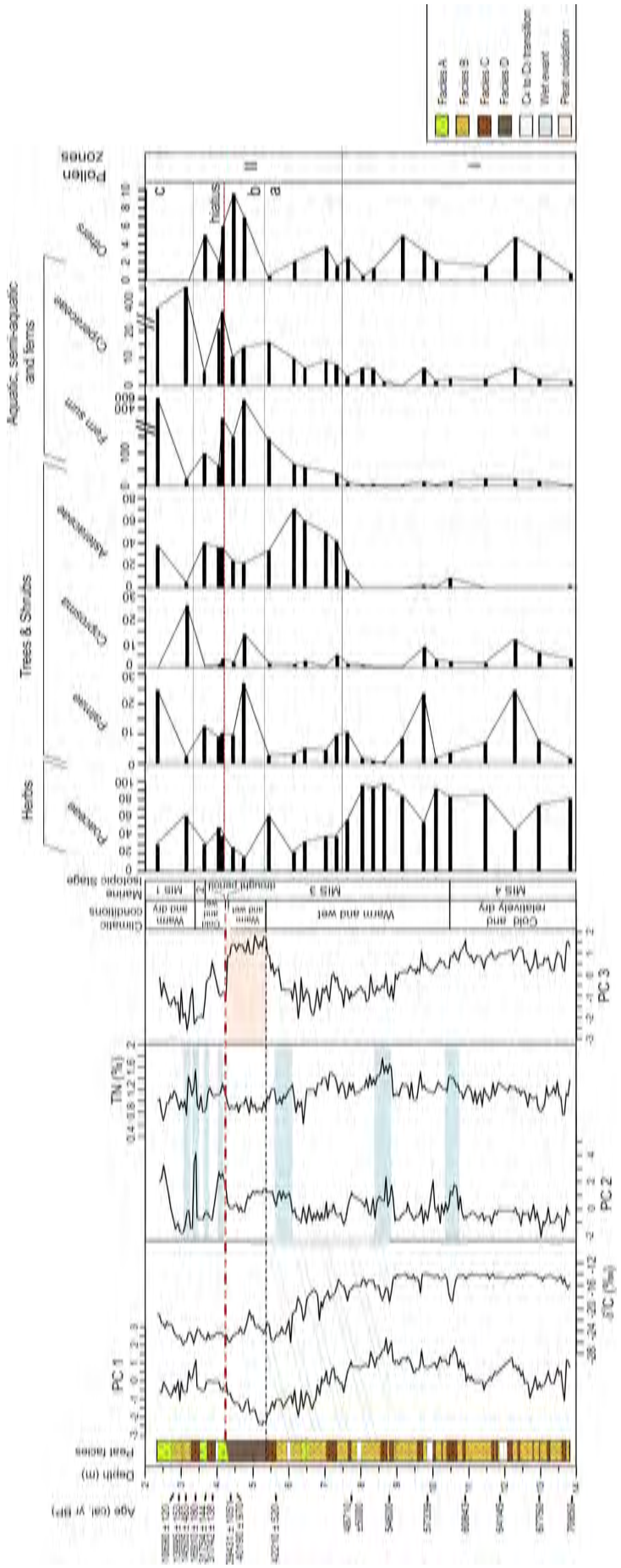

Figure 6.2. Synthesis of Rano Aroi environmental mire evolution. Stratigraphy and calibrated radiocarbon ages are shown, at the left side of the diagram. Four facies are distinguished in Rano Aroi: Facies A (Reddish peat), Facies B (granulated muddy peat), Facies C (organic mud) and Facies D (sapric peat). PC1 indicates changes in the long-term mineral matter fluxes into the mire due to soil evolution and erosion. $\delta^{13}C$ shows an important vegetation change from C_4 to C_3 plant dominance occurred from 55 to 50 kyr BP (shown as a green-line dashed area). The $\delta^{13}C$ and PC1 record are directly related, evidencing the feedbacks between vegetation shifts and basin soil evolution. The occurrence of high precipitation events is showed by PC2 reflecting the input of large amounts of detrital material (shown as blue bands). PC3 tracks peat oxidation caused by a long term drought event. Main oxidation event is shown with a pink band. Pollen results confirm the vegetation shift recorded by $\delta^{13}C$: A grass dominated landscape was gradually replaced by sedge dominated mire likely surrounded by small shrubs and ferns

in agreement with the results of the PCR analysis (Table 4.7). The $d^{13}C$ trend shows a shift from values typical from C_4 plant type to lighter ones (characteristic from C_3 type) and suggests a change in the peat forming plant community (Chapter 5). This agreement between $d^{13}C$ and PC1 reveals an intimate relation between soil evolution and vegetation cover (Figure 6.2). Pollen results presented in this study confirm the C_4/C_3 relation shift, indicating a change not only in the mire itself, but also in the surroundings. In the lower part of the record (between 71 and 48 kyr BP) both mire and catchment were completely dominated by Poaceae (Figures 4.13, 6.2, 6.3). Synchronously to the $d^{13}C$ transition, the presence of Asteraceae, (likely small trees) and ferns partially replaced the Poaceae and become more abundant. At the same time, Cyperaceae started to be more abundant on the mire (likely C_3 species). The vegetation change around the mire and the presence of scarce forest, trees and shrubs may have prevented soil erosion and reduced the fluxes of mineral matter to the mire (PC1). Finally, the expansion of Cyperaceae (e.g. *Scirpus californicus* (C_3)) probably constituted an important physical barrier during the C_3 dominance period, slowing the runoff input, except during stronger wet events (PC2).

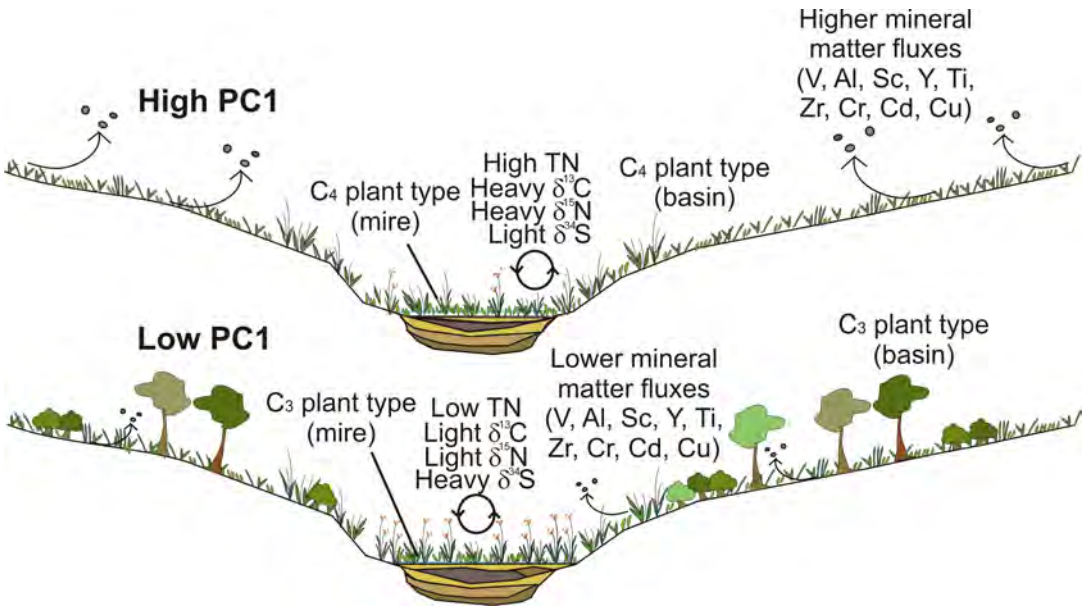

Figure 6.3. Schematic pictures showing main environmental processes related to PC1. PC1 indicates changes in the mineral matter fluxes that reach the mire. Other processes recorded by changes in the organic chemistry of Rano Aroi peat are intimately related (see text).

The TN content decreases in the upper part of the sequence suggesting a link to PC1 scores (Table 4.7) and also to $\delta^{13}C$ and vegetation changes. At Rano Aroi the average $\delta^{15}N$ is around +2.7 ‰, which is an isotopic signature typical of nitrogen fixation. The general $\delta^{15}N$ trend directly correlates to PC1 variation, as denoted by the high PCR regression coefficient (0.56) obtained with the Principal Component Regression models (Section 4.8.4). Two hypotheses can be proposed in order to explain this relationship: (1) larger inputs of fine and very fine mineral particles to the mire may have triggered conditions of enhanced productivity and consequently, higher $\delta^{15}N$ values; or (2) the vegetation change can entail a differential fractionation of the peat forming plant remains (Figures 6.2, 6.3). Because these two hypotheses are not exclusive, $\delta^{15}N$ can be explained by the combination of both. However, two

prominent peaks of $\delta^{15}N$ at 66.8 kyr BP and 62.4 kyr BP (12.36 m and 11.07 m) are not accounted for by the PCR model and therefore, they are apparently not related to the influx of mineral matter (Figure 4.20). These very high $\delta^{15}N$ values ($\delta^{15}N \geq 7$ ‰) may have been reached by the preferential loss of light nitrogen through denitrification or ammonization indicating anoxic phases (Talbot et al., 2001).

Total S decreasing and $\delta^{34}S_{CDT}$ increasing trends from 55.5 to 43.9 kyr BP (9-6 m) (Figure 4.3) also show a differential S assimilation and fractionation through time. The changes in S cycling, especially $\delta^{34}S_{CDT}$ seem partially related to PC1. The sulfur is incorporated by plants and bacteria, especially in the form of organosulfur compounds, which seem to be the dominant S fraction on peat (Wieder and Lang, 1988, Novák et al., 1994). Chemical composition of Rano Aroi basin lithology proves that inorganic S-content is null or negligible to be considered as a source of sulphate (S) to the mire (Baker et al., 1974, Section 4.5.1, 4.5.2). Because neither volcanic eruption has been recorded nor ash levels have been described in Rano Aroi and Rano Raraku in late Quaternary sediments (Flenley 1991, Sáez et al. 2009) the most likely dominant source of S is marine (Figure 6.4). Sulphate aerosols may derive from marine splash (sea-salt sulphate: SS-sulphate), which has an average isotopic signature of 20.6±1.3 ‰ (Sihna et al., 2009), and from non sea-salt sulphate (NSS-sulphate), likely the biogenic dimethylsulphide (DMS) of $\delta^{34}S_{CDT}$ =13-21‰ (Calhoun and Bates, 1989). A study over remote areas of the South Pacific (50º N-60ºS - 170ºW-105ºW) shows that NSS-sulphate submicrometer aerosol particles have an average $\delta^{34}S_{CDT}$ of+15.6±3.1‰ value, indicating that biogenic sulphate can largely be the primary source of NSS-sulphate in remote oceanic areas (Calhoun et al., 1991).

$\delta^{34}S_{CDT}$ on groundwater (+18.9‰) at Vaitea (near Rano Aroi) borehole (Herrera & Custodio, 2008) and the minimum peat $\delta^{34}S_{CDT}$ values (ca. +15 ‰) reflect a contribution of both isotopic signatures (NSS and SS-sulphate) (Figure 6.4). If we consider that S input has remained relatively constant (although sea level and marine primary productivity could have changed the amount of S blown over the island), concentration variations in sediments would only dependent on the loss after early diagenesis (bacterial sulphate reduction and fixation) that discriminates against the heavier isotope ^{34}S. Reactive S^{2-} and H_2S species are produced by bacteria in peatlands and can be fixed again by available iron or cycled into organic molecules C-S or C-O-S (Novák et al., 1994). H_2S emission to the atmosphere is limited hence by the availability of iron (Fe^{2+}) and organic compounds formation. In Rano Aroi, the arrival of C_3 plant type could have led to an increase oxygen demand on the peat from plant roots and therefore to favored sulphate reduction due to a lower redox potential. This would have produced a net loss of S to atmosphere (lower TS values) after the establishment of C_3 vegetation. The $\delta^{34}S_{CDT}$ pattern reveals that the resemblance to PC1 happens on a long-term scale, but high frequency oscillations follow a different dynamic (Table 6.1, Figure 4.3). This is due to the fact that processes that change sulphur concentration and isotope signature can act at smaller scales (local changes in redox conditions, changes in splash and DMS input and/or their proportion). This could be the reason of the lower correlation of $\delta^{34}S_{CDT}$ with PC1 (r = -0.47, see Table 4.7).

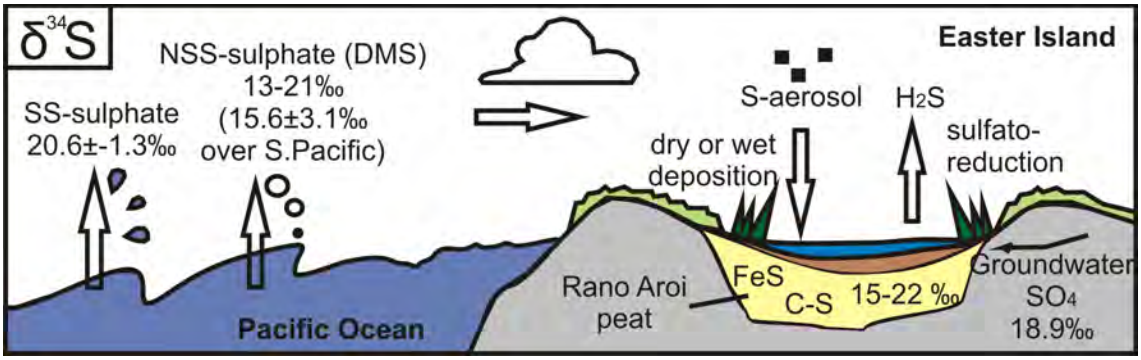

Figure 6.4. Synthetic picture of isotope signature and cycling of Rano Aroi peat sulfur.

6.3.2 PC2 and organic chemistry

Principal Component Regression (PCR) analyses show that organic matter composition does not significantly correlate with PC2. However several cause-effect relations can be stated from the stable isotope and TC, and TN records. $\delta^{13}C$ high-frequency oscillations show lower values coinciding with Facies C and PC2 peaks until 6 m depth, becoming lighter during higher precipitation periods (see Section 6.4). This relationship between organic matter and facies has been explained by differential fractionation due to moisture changes or a higher proportion of C_3 plants and algae during wet events occurring between the period of C_4 dominance and the transition C_4-C_3 (Chapters 5 and 7). TN values also match PC2 peaks. High TN values (low C/N ratios) could be attributed to a higher contribution of algal material, opposite to elevated C/N ratio values, which identify higher proportions of terrestrial or aquatic plants (*versus* algae) organic matter (Figure 6.2).

6.3.3 PC3 and organic chemistry

The composition of the organic matter of the peat does not correlate with PC3. Nevertheless, the drought event (between 5 m and 4.23 m depth) may have partially determined the $\delta^{13}C$ signature as the lighter ratios on the highly decomposed part of the record show (Figure 6.2). The same can be stated for the C/N ratios that are slightly higher between 5 m and 4.23 m depth. Total S displays a relative enrichment while the underlying level, from 6.5 m to 5.5 m depth, becomes depleted in S. This pattern could respond to bioaccumulation through the formation of organic S compounds which are more stable under oxidizing conditions at the expense of the S released from the layers that remained under reducing conditions near the watertable interphase (coherently when $\delta^{34}S_{CDT}$ reaches the maximum values).

6.4 Conclusions

The organic matter composition (TC, TN, TS, $\delta^{13}C$, $\delta^{15}N$, $\delta^{34}S$), inorganic geochemistry and pollen data from Rano Aroi mire provide a coherent reconstruction of the paleoenvironmental history of Easter Island. Principal components analysis (PCA) of peat geochemistry reveals that three main environmental processes have controlled the elemental composition of the peat accumulated over the last 70 kyr in Rano Aroi. The first process, depicted by PC1 (combined signal of V, Al, Sc, Y, Cr, Cd, Ti, Zr and Cu), reflects changes in the

Aroi catchement background erosion and transport of the mineral matter as very fine particles into the mire and it is linked to soil evolution and aeolian input. In Rano Aroi, $\delta^{13}C$ can be used to infer an important vegetation change from C_4 to C_3 plant dominance occurred from 55 to 50 kyr BP. The $\delta^{13}C$ and PC1 record correlation reveal that vegetation shifts and the evolution of the soils of the basin were intimately related to the rate of allochtonous material transported into the peatland. These environmental changes also affected $\delta^{15}N$ signal that integrates variability in mire productivity and redox conditions. $\delta^{34}S$ signatures indicate that sulphur source is primarily marine consisting of a mixture of NSS (from DMS and other biogenic particles) and SS-sulphate (from marine splash). The $\delta^{34}S$ ratio and TS concentration suggest that sulphur may have been differentially mobilized depending on vegetation assemblages by sulphate reduction bacteria. The second process is the occurrence of high precipitation events (identified by PC2 signal of Fe, Mn, Th, Ba, Zr, Ti) related to strong runoff and delivery of large amounts of terrigenous particles coarser than the mobilized by PC1 process. These events occurred at approximately 60 kyr BP, 52 kyr cal BP and 42 kyr cal BP. Finally, the third process illustrated by PC3 mainly reflects peat oxidation caused by a long term drought after 39 kyr cal BP. This period led to peat mineralization and a diagenetic relative enrichment of elements as Ca, Sr, Mg, and Fe, and a relative loss of Al, Sc, and Ti.

CHAPTER 7

ENVIRONMENTAL EVOLUTION OF RANO AROI DURING THE LAST 70 KYR BP: PEATLAND, BASIN AND CLIMATE INTERACTIONS

7.1 Objective, methods and results

The aim of this chapter is to provide a detailed environmental reconstruction from Rano Aroi site for the last 70 kyr BP. The transitions among the three main hydrologic states of Rano Aroi (Chapter 5) and the changes in intensity of the three processes constraining peat chemistry (Chapter 6) through time permited us to draw a complete environmental history of the site. The timing of shifts occurred in the mire were integrated with and tested against the results of previous studies from Raraku and Kao lacustrine records and other marine and terrestrial sequences from Pacific and Circum Pacific areas (Lamy et al., 1998; Stuut and Lamy, 2004; Valero-Garcés et al., 2005; Heusser and Heusser, 2006; Muller, 2006; Wang et al., 2007; Pena et al., 2008). In this way, Rano Aroi dataset allowed us to reconstruct paleoenvironmental changes considering the intimate interplay between climate forcing, basin evolution (soil and vegetation changes) and peat processes.

7.2 MIS 4 (70–60 kyr BP in Rano Aroi)

During the MIS 4, the homogenous sequence of Facies B (Figures 4.2 and 4.3) shows that Rano Aroi was stable in its base-line state (Section 5.5), likely accumulating peat as a kettle-hole mire. This time period shows a complete dominance of C_4 plant types (*Poaceae*) on the Rano Aroi basin and Terevaka area (Figure 6.2). The contributions of Arecaceae and *Coprosma* pollen evidence the presence of both taxa in the island during MIS 4. A prevalence of C_4 suggests not only colder but also drier conditions what would lead to a low degree of pedogenesis in the catchment soils, a scenario that is coherent with the global reduced temperatures (Kaiser et al, 2005; Grant et al., 2012). Additionally, herbaceous plant dominance may have facilitated higher soil erodibility, either eolian and/or hydrological. This is because open landscapes as meadows or grasslands confer weaker protection in front soil erosion that "closed" vegetation or forested areas. The result was a higher dust flux of typical lithogenic elements and metals into the mire as summarized by PC1 in Chapter 6 (Figures 6.3, 7.1).

The MIS 4 stadial was regionally characterized by low southern Pacific SST (Kaiser et al., 2005). Wind circulation around Antarctica was intensified, and the northward migration of the Westerlies and the Antarctic Circumpolar Current (ACC) brought sub-Antarctic cold waters up to temperate latitudes (Kaiser et al., 2005). Sea level was globally low, between 90 and 100 m below the present day (Grant et al., 2012). Rano Aroi environmental conditions indicate cold and slightly humid conditions in accordance with the regional climatic configuration.

7.3 MIS 3 (60–27.8 cal kyr BP)

Two different MIS 3 states (Early and Late) can be distinguished in Rano Aroi.

The Early MIS 3 took place from ca. 60 to 42 cal kyr BP and was defined by short and abrupt events of high sediment delivery (Figure 6.2), which implied the establishment of moister conditions on Easter Island. These episodes have been recorded as Facies C (Chapter 5, Section 5.4) and recognized by high PC2 values in Chapters 5 (Section 5.4.2) and 6 (Section 6.2.2). The millennial-scale range of these events is coherent with climatic instability and temperature and humidity suborbital cycles that were globally identified for MIS 3 what will be extensively treated in Chapter 8 (Clement and Peterson, 2008).

The transition from MIS 4 to MIS 3 was globally characterized by a warming trend. The Sea Surface Temperature (SST) of mid latitudes of Pacific Ocean increased around 5°C between 62.7 and 61.5 kyr BP (Kaiser et al., 2005). This change was coupled to a fast sea level rise, and between 62.9 and 61.2 kyr BP sea level shifted from -96 m.a.s.l to -75 m.a.s.l (Grant et al., 2012). In the South Pacific, important atmospheric reorganizations accompanied sea level and SST variations. The ODP 1002 record from the Cariaco Basin indicates that between 61.2 and 59.9 kyr BP, the ITCZ was situated in a stable southern position, leading to very dry conditions in northern hemisphere tropics and a wet conditions in the southern ones (Figure 7.1) (Peterson et al., 2000). Southern displacements of the ITCZ and the SPCZ together with intensification of the Southern Westerlies result in a regional configuration that favors the occurrence of higher moisture and storminess on Easter Island (Wang et al., 2004; Muller, 2006). Such moister conditions, which affect most of the South Pacific region (Lamy et al., 1998; Stuut and Lamy, 2004), could have been responsible for the Rano Aroi wet events. Records from the central Coast of Chile (Lamy et al., 1998; Stuut and Lamy, 2004) indicate a wet period from 50 to 40 cal kyr BP explained by a boreal position of SW caused by precession forcing.

During the Early MIS3 period Antarctica underwent millennial-scale warming events that were simultaneous to temperature drops in the north Atlantic region (Heinrich events), configuring an interhemispheric teleconnection known as the “bipolar seesaw” (Blunier and Brook, 2001). Many studies note the time coincidence of millennial-scale cycles of humidity and marine productivity in the tropical Atlantic and Pacific Oceans with cooling episodes in the Northern Hemisphere and Greenland (Baker et al., 2001; Haug et al., 2001; Oppo et al., 2003; Wang et al., 2004, 2007; Muller, 2006; Clement and Peterson, 2008). In Rano Aroi main Early MIS 3 wet events occurred at ca. 60 kyr BP, 52 kyr cal BP and 42 kyr cal BP, thus during North Atlantic Heinrich events 6, 5a and 5. Several mechanisms have been proposed to explain these teleconnections, including thermohaline circulation (THC) variability, sea ice feedbacks and changes in convection or movement of the ITCZ (Clement and Peterson, 2008). The nature of MIS 3 climate variability and the proposed global teleconnections will be largely developed in Chapter 8.

Coinciding with the onset of MIS 3, Rano Aroi deposits record a change in the prevalence of C_4 to C_3 peat forming plants starting at 55 cal kyr BP as shown by $\delta^{13}C$ gradual decline (Chapter 5). A coherent increase in Cyperaceae pollen was recorded during this period

(Chapter 6, Figure 6.2) indicating that probably the peat forming community underwent a gradual shift from Poaceae (C_4) dominance to a combination of herbs and sedges (C_3). In ARO 06 01, at 45 cal kyr BP, extremely well-preserved *Scirpus californicus* rhizomes, were found in peat with very high C/N values. These rhizomes represent the oldest S. californicus remains that have been found to date on the island. The pollen data also indicates a progressive change of the vegetation of the surrounding areas between 51 and 48 kyr BP. Concretely, the data shows how the complete dominance of Poaceae (mainly C_4 species) was substituted by the combination of Asteraceae, *Coprosma*, Poaceae and ferns. However, the percentages of Arecaceae pollen remained relatively constant (Chapter 6, Figure 6.2). The later fern expansion was probable caused by the initial establishment of small trees (Asteraceae-tubiflorae, *Coprosma* among others) that created more shade and humid (but not flooded) environments adequate for Pteridophyta. The vegetation change around the mire and the presence of scarce forest, trees and shrubs probably prevented soil erosion and reduced the fluxes of mineral matter into the mire as summarized by PC1 in Chapter 6. The diminishing of mineral flux can be also attributed to the expansion of Cyperaceae (such as *Scirpus californicus*) that likely constituted an important physical barrier during the C_3 dominance period, slowing the runoff input, except during strong precipitation events (PC2).

Changes in the ratio of C_3/C_4 plants are generally associated with climate changes (Talbot and Johannessen, 1992; Street-Perrott et al., 1997; Huang et al., 1999; Meyers and Terranes, 2001; Street-Perrott et al., 2004). Low concentrations of atmospheric CO_2, low temperatures and restricted water supply are the major selective forces for the dominance of C_4 over C_3 (Street-Perrott et al., 1997; Huang et al., 1999; Ehleringer et al., 1997). In the case of Rano Aroi, vegetation succession towards a dominance of C_3 plants could reflect the expansion of C_3 sedge species as a response to both milder temperatures and globally higher atmospheric CO_2 concentration, and the progressive increase of humidity as indicated by the occurrence of abrupt wet events. At Rano Aroi, the changing C_4-to-C_3 signal can, however, also be ascribed to the arrival of *S. californicus* on the island. The arrival of this species, which originates from the South American continent, is attributed to wind or bird transport (Heiser, 1974), with both vectors having a possible climatic and a substantial stochastic component.

The Late MIS 3 (42-27.8 cal kyr BP) was characterized by a diagenetic imprint of peat oxidation, which allowed us to identify an ancient aerated level dated at ca. 39 cal kyr BP (Facies D). A lowering of the Rano Aroi water table provoked peat exposure and aeration, what accelerates peat decomposition. Decomposed peat became enriched in elements representative stable in organic compounds under oxic conditions, as summarized by PC3 from Chapter 6. Peat can be highly effectively lost by oxidation with a rate of up to few centimeters per year (Couwenberg et al., 2001). This oxidation event must have happened between 39 and 31 cal kyr, resulting in a failure to record environmental changes during and before the event. Because old carbon could be incorporated to younger roots, the exact date of the reactivation cannot be assessed.

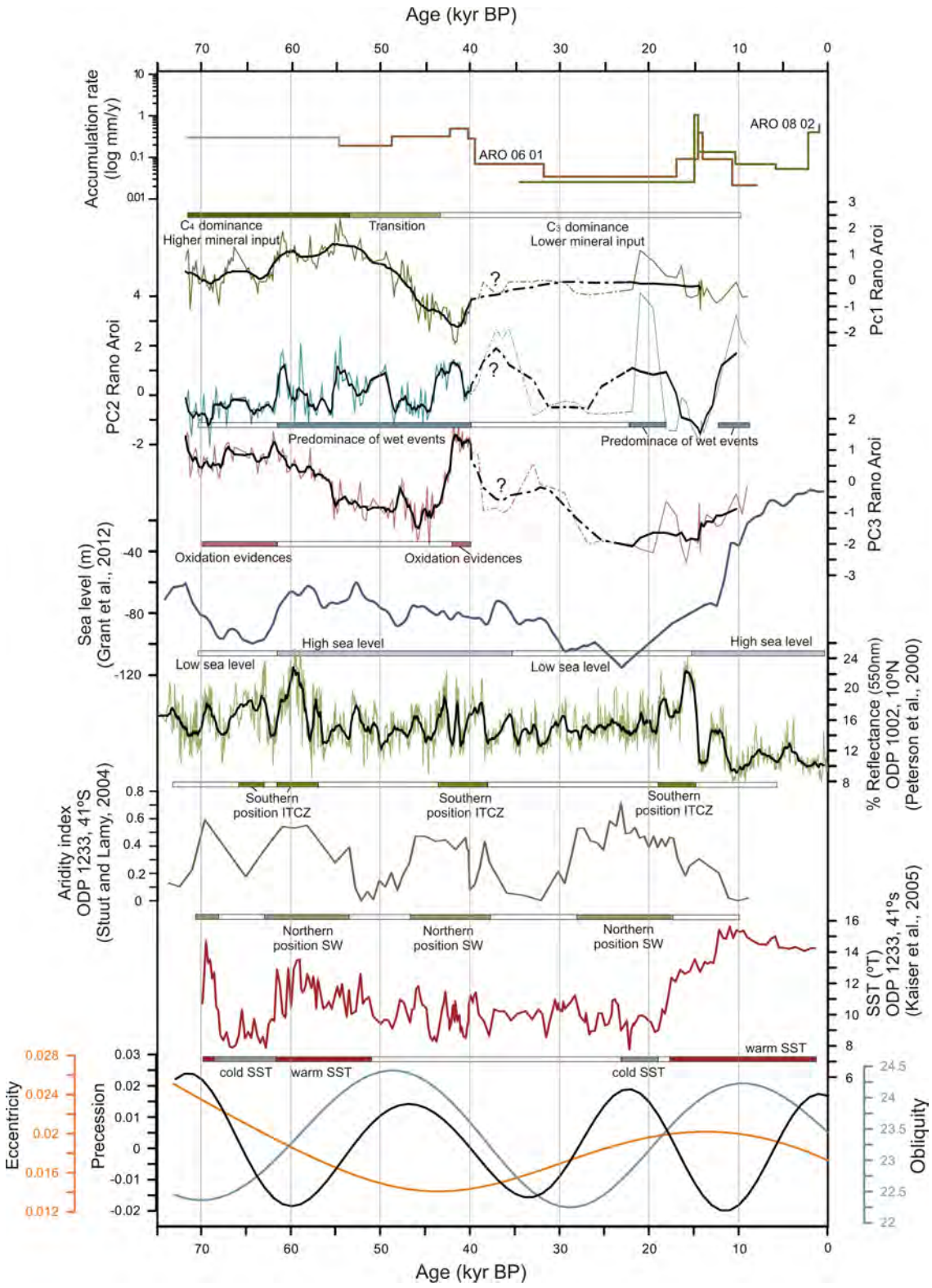

Figure 7.1 Rano Aroi accumulation rates and PC1, PC2 and PC3 from Chapter 6 plotted against age together with a selection of environmental and climatic Southern Pacific records. Dotted line on Rano Aroi scores shows the part of the record under chronological uncertainty (see text). From top to bottom: PC1 scores obtained by this study indicating the transit from a period with elevate mineral input into the mire and C_4 plant type dominance to an scenario of C_3 dominance and lower mineral fluxes into the mire. PC2 scores, high values indicate the occurrence of strong runoff events (enhanced precipitation). PC3 scores, high values indicate the mobilization of Sr, Ca, Mg due to peat exposure and oxidation. Global sea level (Grant et al., 2012) can be considered a relevant factor influencing

water table in Rano Aroi. The reflectance record (Peterson et al., 2000) from Cariaco basin reveals changes in latitudinal position of the ITCZ. The southward migration of ITCZ has been related to higher precipitation rates over Southern tropical Pacific and intensification of SPCZ, bringing humid conditions to Easter Island. Aridity index obtained by Stuut and Lamy (2004), the coastal sediments of Chilean offshore have been used to reconstruct the latitudinal position of Southern Westerlies (SW). A northern position of this storm track contributes to transport the SPCZ cyclones to Easter Island. Southern Pacific SST (Kaiser et al., 2005) shows the temperature changes at 41º latitude for the last 70 kyr BP. Finally, the orbital parameters are also plotted: Eccentricity, Precession and Obliquity (Laskar et al., 2004).

Thus, conditions between 39 and 31 cal kyr BP were probably dry and relatively cold in Easter Island as has been also observed in South American continent records where a dry period was identified between 37 and 31 cal kyr BP (Lamy et al., 1998; Stuut and Lamy, 2004, Figure 7.1). Rano Aroi record shows very low accumulation rates during the final period of Late MIS 3 (31 to 27.8 cal kyr BP). Low temperatures would have lasted until the end of MIS 2 (Sáez et al., 2009).

7.3 Early MIS 2 and Last Glacial Maximum (LGM) (27.8–19 cal kyr BP)

During MIS 2, global temperatures reached a minimum between 19 and 22 cal kyr BP (Heusser and Heusser, 2006; Lea et al., 2006; Kaiser et al., 2008), caused by the arrival of colder waters to intermediate latitudes (Lamy et al., 1998; Pena et al., 2008). The lowest peat accumulation rates at Rano Aroi were recorded between 27.8 and 17.5 cal kyr BP (0.03 mm/year) (Figure 7.1). Lower temperatures likely lead to a change in peat forming vegetation assemblage. Unfortunately the low accumulated rates and the pollen counting resolution does not permit to validate this hypothesis. This vegetational response could explain the hampering of the normal accumulation rates recorded for this period of time. In spite of the low accumulation rates, a wet event is recorded in Rano Aroi by the presence of chemical elements characteristic of coarse terrigenous input (PC2 from Chapter 6) at 20.9-19.5 cal. kyr BP likely representing enhanced precipitation during Heinrich event 2. Although sea level reached a minimum c. 23 cal. kyr BP (Lambeck and Chappell, 2001; Grant et al., 2012) and could have negatively affected the groundwater level and consequently the hydrological balance at Rano Aroi, peat formation was active during the LGM probably maintained by elevate precipitation rates. Previous studies from the Rano Raraku site attribute humid and cold conditions to the island during the Last Glacial Maximum (Azizi and Flenley, 2008; Sáez et al., 2009) and the reconstructed high water table of Raraku Lake suggests substantial rainfall coupled with low evaporation. These can be explained by permanent cold conditions preventing strong evaporation and a northernmost position of Southern Westerlies whose influence reached subtropical latitudes during glacial times (Figure 7.1, Sáez et al., 2009; Lamy et al., 1998).

7.4. Late Glacial (19–11.7 cal kyr BP)

Rano Aroi provides evidence of a warmer climate at 17.5 cal kyr BP, when peat accumulation accelerated. A high water table event was recorded at ca. 15-16 cal kyr BP, likely representing enhanced precipitation during Heinrich event 1 (Figure 7.1). From 15 to 14 cal kyr BP, this event is followed by an episode of very high peat accumulation (1 mm/year, Figure 7.1) and high concentration of *Polygonum acuminatum* seeds, a pioneer species that is commonly found in the first stages of succession.

Marine records from the central Pacific region show that deglaciation warming started approximately at 19 cal kyr BP, parallel to the retreat of the Antarctic sea ice (Kaiser et al., 2008) and appreciably earlier than the continental response (Sáez et al., 2009). This warming has been related to phases of low precession and high obliquity (Pena et al., 2008), which drove storm tracks southward and enhanced the E–W Pacific thermal gradient, favoring La Niña-like conditions (Koutavas et al., 2002; Pena et al., 2008). Studies developed at the Raraku Lake record describe the Easter Island hydrological and vegetational response to deglaciation at 17.3 cal kyr BP (Sáez et al., 2009). In Rano Aroi maximum peat accumulation rates at 14 cal kyr BP (Figure 7.1) coincide with the highest rates of sea level rise during deglaciation as a response to the Melt Water Pulse A1 (Figure 7.1) (Hanebuth et al., 2000; Dickinson, 2001; Lambeck and Chappell, 2001) what suggests that eustatic level might have played an important role regulating Easter Island climate, for example influencing the development of convection storms.

7.5 Early and Mid Holocene (11.7–2.5 cal kyr BP)

The Holocene period started with evidence of strong runoff events in Rano Aroi at 10.2 cal kyr BP, while the accumulation rates were low (0.1 mm/year)(Figure 7.1). From a regional perspective, early Holocene has been characterized by a warming trend (Pena et al., 2008). Pacific Ocean SSTs were maximal at approximately 12 cal kyr BP and generally decreased thereafter, until modern SSTs were reached (Kaiser et al., 2005; Kaiser et al., 2008). Arid conditions during the early Holocene occurred in Central Chile (Moreno and León, 2003; Paduano et al., 2003; Tapia et al., 2003; Valero-Garcés et al., 2005) and lasted until approximately 5–4 cal kyr BP. Dominant dry conditions have been also inferred for Easter Island because Raraku Lake underwent a gradual drop in water level, leading to the establishment of a shallow swamp system from 11 to 5.5 cal kyr BP (Sáez et al., 2009). The dry period was interrupted by a short-term flood episode, dated at 5.8 cal kyr BP in Rano Aroi (ARO 08 02, Figure 4.4) and between 6.2 and 5.8 cal kyr BP in Rano Raraku (Sáez et al., 2009). This mid Holocene wet interval is synchronous with the global climatic event between 6 and 5 cal kyr BP (Mayewski et al., 2004), an enhanced precipitation period from 6 to 5.8 cal kyr BP on the Galápagos Islands (Conroy et al., 2008) and stronger SW activity in Southern Chile (Heirman, 2011). However, dry conditions on Easter Island lasted until the Late Holocene. Very low water table conditions during this period of time caused a sedimentary hiatus in the center of Raraku Lake, from 4.2 to 0.8 cal kyr BP (Mann et al., 2008; Sáez et al., 2009). However, the erosion was sensibely lower in the eastern lake margin, conserving a lake sequence with a reduced sedimentary gap (Cañellas-Boltà et al., 2013). In Rano Aroi, the 5.5–2.5 cal kyr BP period is characterized by low accumulation rates (0.06 mm/year).

7.6. Late Holocene (2.5 cal kyr BP to present)

The peat growth rate at Rano Aroi recovered completely at 2.5 cal kyr BP, and relatively humid conditions were inferred up to the present time. The shift to humid conditions in Easter Island coincided with the arrival of wetter conditions in mid-latitude Chile (van Geel et al., 2000) and the Antarctica warming due to increased southern summer insolation (Ingolfsson et al., 1998). A humid Late Holocene is a consistent regional pattern, related in eastern Pacific to stronger convective summer rains due to increased summer

insolation together with a northward shift of the Southern Westerlies (Lamy et al., 2001; Jenny et al., 2002; Paduano et al., 2003; Valero-Garcés et al., 2005).
At 1.3 cal kyr BP (655 AD), a decrease in C/N suggests enhanced mineralization, while high $\delta^{13}C$ values indicate that there was a higher contribution of C_4 grass organic matter (features on ARO 08 02 record, Figure 4.4). The age of this event lies in the time interval proposed for human arrival or expansion (Rull et al., 2010a), so these features could be interpreted as peat exposure and vegetation opening caused by anthropogenic disturbance. Nevertheless, this event could also reflect climate change during the Medieval Climate Anomaly (1205–705 yr cal BP), which brought warm and dry conditions, a low degree of interannual variability and less storminess to the eastern Pacific (Nunn, 2007).

Conclusions

The environmental evolution of Rano Aroi mire, largely driven by hydric changes, is coherent with the regional climatic variability described for the last 70 kyr BP.

During MIS 4, the hydric and environmental conditions in the mire were stable and resembled mire baseline conditions. The Rano Aroi catchement area was occupied by grasslands and C_4 Poaceae dominated the mire owing to the general cold and relatively dry climate conditions

Early MIS 3 is characterized by the occurrence of abrupt wet events owing to the progressive increase of humidity. After 45 kyr BP vegetation in Rano Aroi changed from C_4 to C_3 plant dominance, which might have been triggered by the wetter and warmer conditions, allowing sedge colonization or by the arrival of *Scirpus californicus* to the island. At the same time, Asteraceae and other small trees became gradually more abundant, forming scantily wooded areas around the Terevaka volcano. The vegetation change has been intimately related to reduction in the mineral input into the mire due to changes in soil coverage and erosion (Chapter 6). Late MIS 3 was a very dry period, which led to peat oxidation and exposure shortly after 39 cal kyr BP.

During early MIS 2 (27.8–19 cal kyr BP), peat accumulation rates were low, apparently due to cold conditions, which will have hampered vegetation development. Evidence of the onset of deglaciation is concordant with Raraku Lake environmental development and was dated at 17.5 cal kyr BP at Rano Aroi, when peat accumulation rates began to increase again. The regional mid-Holocene dry period is well characterized at Rano Aroi from 5 to 2.5 cal kyr BP. Our Rano Aroi record shows a development that is in accordance with regional paleoclimate records and illustrates the terrestrial response to the main Late Pleistocene phases in the Pacific region in terms of vegetation and paleo-hydrological change. The lack of sedimentary sequences that indicate Late Pleistocene precipitation over the remote Pacific region demands further studies into the correlation among circum Pacific series to characterize the moisture distribution mechanisms from a regional perspective. The interplay of ENSO patterns, SPCZ interglacial position and high-latitude responses over atmospheric features is addressed in Chapter 8.

CHAPTER 8

MILLENNIAL-SCALE PRECIPITATION VARIABILITY OVER EASTER ISLAND DURING MIS 3: INTER-HEMISPHERIC TELECONNECTIONS WITH NORTH ATLANTIC ABRUPT COLD EVENTS

8.1 Objective, methods and results

As stated in Chapter 7, the temporal resolution of the Rano Aroi record is adequate for the detailed study of millennial-scale oscillations, providing an exceptional opportunity to understand Marine Isotope Stage (MIS) 3 climate variability in the South Pacific. In this chapter, a humidity index inferred from Rano Aroi peat biogeochemical proxies (Sections 4.3.1, 4.4.1 and 4.8.2) has been compared to marine and continental records located in the tropical and subtropical Pacific and Atlantic Oceans (Sections 3.7 and 4.7). We also compared the Rano Aroi record with low and high latitude datasets from the Northern and Southern Hemispheres to discuss the inter-latitudinal connections responsible for the propagation of rapid climate variability in the past (Figure 8.1). In summary, the occurrence of the Rano Aroi wet events and the long-term drought episode previously described in Chapter 7 have been contextualized in a broad Southern Hemisphere perspective, showing the links between the hydrological changes observed on Easter Island and the atmospheric/oceanic restructuration of Central Pacific during Dansgaard-Oeschger (DO) oscillations along MIS 3.

8.2 Introduction to MIS 3 climate variability

On suborbital timescales, the climate in the Northern Hemisphere during MIS 3 has been typically characterised by rapid millennial-scale temperature variations defined as Dansgaard-Oeschger (DO) stadial-interstadial cycles (Dansgaard et al., 1993) (Section, 1.6.1). Some of the DO stadials (named as Heinrich stadials (HS)) consisted in a large spread of icebergs associated to the weakening of the Atlantic Meridional Overturning Circulation (AMOC) (Ganopolski and Rahmstorf, 2002 Hemming, 2004).

Although most of the records documenting rapid climate variability are concentrated in the North Atlantic region, a relevant number of studies pointed towards a linkage between cooling episodes in the North Atlantic and changes in the tropics (Baker et al., 2001; Haug et al, 2001; Wang et al., 2004, 2007; Muller, 2006; Clement and Peterson, 2008).

Currently, there are few records available with an appropriate temporal resolution to characterise millennial-scale changes in tropical and subtropical areas (Figure 8.1). Most of the existing records are situated North of the Equator and consist of coastal marine sediments (i.e., Peterson et al., 2000; Rosenthal et al., 2000; Haug et al., 2001) or speleothems (Wang et al., 2004). Further south, evidence regarding changes in the ITCZ is very scarce and is derived

primarily from speleothems from South America (Cruz et al, 2005; Wang et al., 2004; 2007), lacustrine (Conroy et al., 2008, Sáez et al., 2009) and marine sediments (Arz et al., 1998) and peat records from North Australia (Muller et al., 2008a). However, none of these records allow for the tracking of changes in the South Pacific Convergence Zone (SPCZ). A targeted region that would allow for such a study of the SPCZ is centred in the South Pacific subtropical gyre, where extremely low marine primary productivity prevents the accumulation of marine palaeoclimatic archives to track changes in the SPCZ (Figure 8.1).

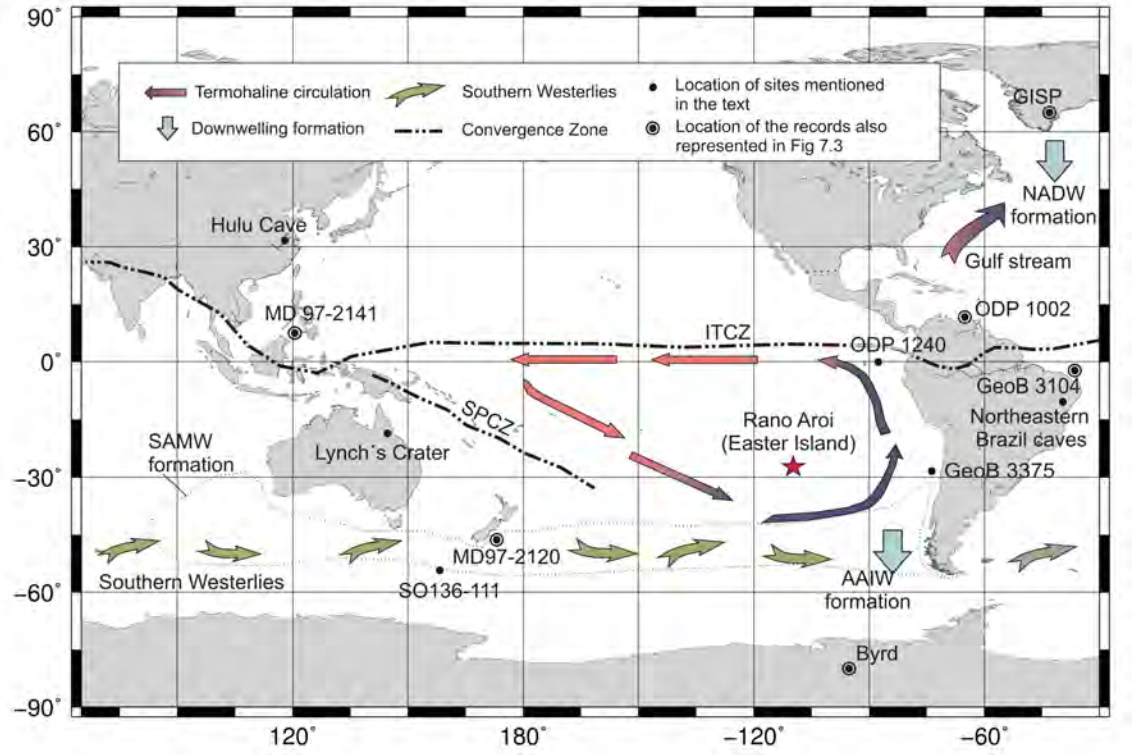

Figure 8.1. Oceanic and atmospheric spatial patterns of millennial-scale climate change events that acted as climatic teleconnection mechanisms or feedbacks during MIS 3 including termohaline circulation, atmospheric structures (Intertropical Convergence Zone, ITCZ; South Pacific Convergence Zone, SPCZ; Southern Westerlies. SW) and downwelling formation (AAIW, NADW). Black dots indicate the relevant sites mentioned in the text, double circles indicate records also represented in Figure 7. 3 and Rano Aroi (Easter Island) is designated as a red star.

8.3 Rano Aroi humidity index for MIS 3

As shown in Chapter 5, Principal Component Analysis (PCA) of Ti, Ca, Fe, $\delta^{13}C_{res}$, TN and TC allowed us to interpreted three environmental stages that defined three different hydrologic states. These are (1) base line conditions, (2) flooded mire, (3) dry peatland. For the discussion that concerns the present Chapter, the PCA was performed again including the same parameters, but only for the MIS 3 period (38.5-65 kyr BP) (Sections 3.8.2 and 4.8.2). The result is shown in Figure 4.17. High values of the second principal component (PC2) have been interpreted in Chapter 5 as indicative of the flooded mire state (Section 5.5) and therefore a good tracer of wet events (defined by high values of TN, Ti and light $\delta^{13}C_{res}$). For this reason, PC2 values can be used as a Rano Aroi humidity-index (Figure 8.2).

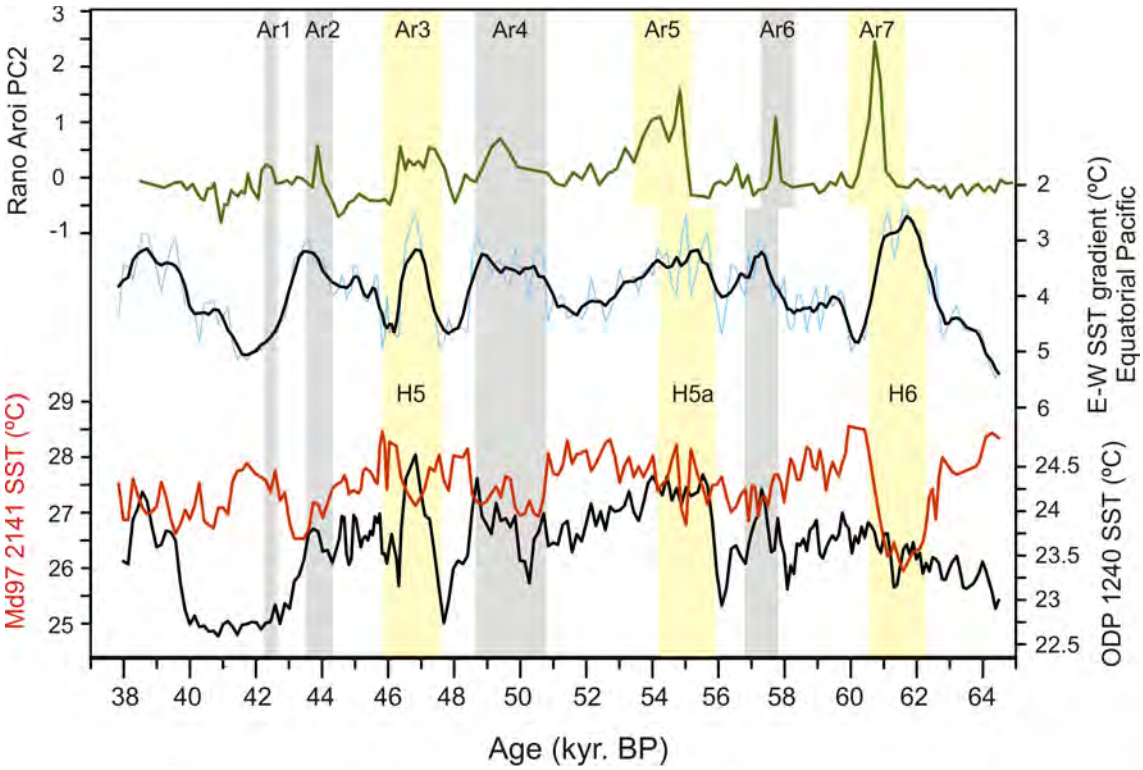

Figure 8.2. Comparison between Rano Aroi PC2 humidity index (thick green line) and E-W gradient over the Equatorial Pacific (thin blue line) and the corresponding 5-point running average (thick black line). The E-W gradient was obtained from the difference between ODP 1240-SST (thin black line, Pena et al., 2008) and MD97-2141-SST (thin red line, Dannenmann et al., 2003) temperature reconstructions after resampling the ODP 1240 record at the age intervals of those used in the MD97-2141 record (Sections 3.7 and 4.7). The E-W equatorial SST gradient is used in the Section 8.5 of this Chapter to understand changes in South Pacific Walker circulation dynamics along MIS 3. Wetter events in the Rano Aroi record are marked with vertical bands and named as Ar. Yellow bands correlate the main wet events with Heinrich stadials, while grey bands show the ones that coincide with other DO stadials. Rano Aroi wet events coincide with a lower E-W gradient, which implies the displacement of the ITCZ and the SPCZ is associated with weaker oceanic circulation over the Equatorial Pacific, resembling an El Niño-like state (Section 8.5).

8.4. Precipitation patterns over the tropical and subtropical Pacific during MIS 3

Between 65 and 38.5 kyr BP, seven main wet periods, labelled Ar1 to Ar7, are identified in the Rano Aroi record based on their high PC2 values (Figures 8.2 and 8.3). Three of these wet periods (Ar3, Ar5 and Ar7) are particularly outstanding. These three periods are characterised by an abrupt onset and, on average, they last for approximately 2,000 years. The other four wet events (Ar1, Ar2, Ar4 and Ar6) are of minor intensity and duration, lasting approximately 1,000 years or less (Figure 8.3). The comparison of the PC2 scores of the Rano Aroi record with other well-established climate records from the Northern and Southern Hemispheres indicates that the three major Rano Aroi events can be correlated with the North Atlantic Heinrich stadials 5 (ca. 45 kyr BP), 5a (ca. 54 kyr BP) and 6 (ca. 60 kyr BP), whereas the other four minor events can be correlated with other DO stadials (Figure 8.3).

Because of the chronological uncertainties of the Rano Aroi record (Section 5.2), which are particularly high in the lower-most part of the record, the correlation with other palaeoclimatic records described above could be called into question. To test the robustness of the correlation of the Rano Aroi wet events with the DO stadials, a comparison was performed

between the PC2 humidity index and the $\delta^{18}O$ record from NGRIP using the GICC05 chronology, which is the most current and most accurate chronology published from the Greenland ice cores (Svensson et al., 2008). For this exercise, the ages of the Rano Aroi wet events were first correlated to the ages of the closest Greenland DO stadials and, secondly, the same ages of the Rano Aroi wet events were compared to those of the closest Greenland DO interstadials (Figure 8.4). The correlation to the DO stadials displayed a closer agreement with the 1:1 line than the correlation to the interstadials, with the exception of the last event (Ar6), which accumulated the larger chronological error. This could be due to the fact that it lies within the period of time that has been calculated by extrapolation in Rano Aroi record (Section 5.2). Consequently, the chronology of the Ar1-Ar6 wet events supports a more solid correlation of the Rano Aroi wet events with the DO stadials rather than with the DO interstadials (Figure 8.4). It is important to remark than Ar1-Ar4 events lie in the well-constrained time period of Rano Aroi age model, while Ar5-Ar7 constitute part of the extrapolated ages. The good fitting of the first ones (Ar1-Ar4) proves the reliable correlation between stadials and Rano Aroi wet events.

Independently of the chronological framework, an additional line of evidence supports the correlation of Rano Aroi wet events and DO stadials rather than Rano Aroi wet events and interstadials. This evidence is based on the climatic mechanisms proposed to explain the tropical and subtropical MIS 3 climatic scenarios described in previous studies (see below). Some of the most solid evidence of these interhemispheric teleconnections comes from Northern Hemisphere records such as the Hulu cave speleothems in China (32º30'N; Wang et al., 2001), the reflectance record from the Cariaco basin, northern Venezuela (10º43'N, Peterson et al., 2000; Haug et al., 2001) and changes in surface salinity in the Sulu sea indicated by core MD 97-2141 (8º48' N, Oppo et al., 2003; Dannenmann et al., 2003; Rosenthal et al., 2000). All of these records consistently indicate the dominance of dry conditions during the HS and other DO stadials (Figure 8.3) in the Northern Hemisphere. Low latitude North Hemisphere dry periods have been associated with enhanced rainfall in the Southern Hemisphere. Proves of stronger precipitation have been documented in Northern Brazil travertine formations (Wang et al., 2007) or in the South American Atlantic coast (3º40'S, Arz et al., 1998) coinciding with Rano Aroi wet events. A similar climatic pattern has been described by Muller et al. (2008a) in the Lynch crater (17ºS) peat record in North Australia over the last 45 kyr cal BP. Changes in the AMOC and atmospheric coupling during DO stadials (interstadials) have been proposed to provoke the southward (northward) displacement of the ITCZ (Zhang and Delworth, 2005, Clement and Peterson, 2008, Chiang and Bitz, 2005; Timmermann et al., 2005).

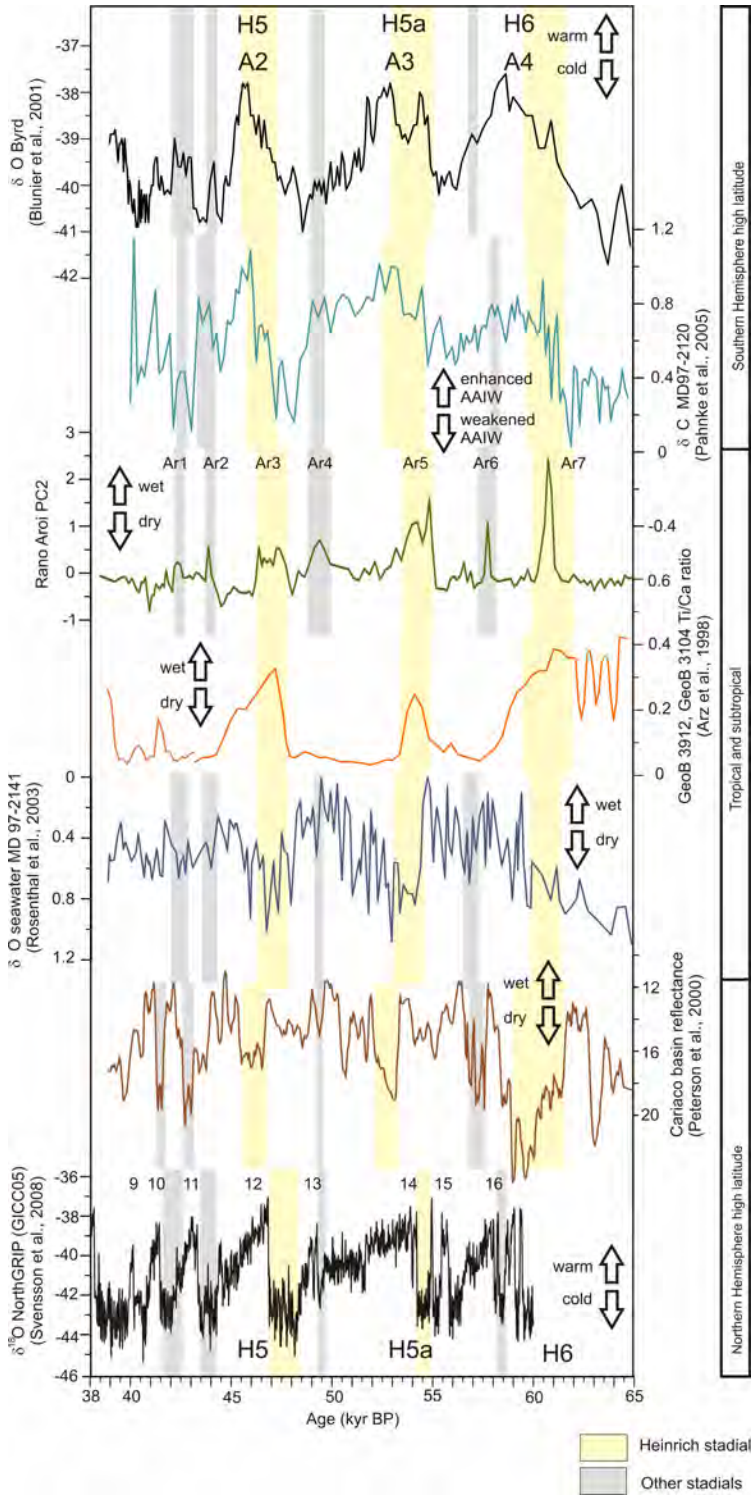

Figure 8.3 Comparison of the Rano Aroi humidity index with marine sediment records from the Cariaco Basin (ODP 1002C, Peterson et al., 2000), Sulu Sea (MD97 21-41, Dannenmann et al., 2003; Oppo et al., 2003; Rosenthal et al., 2003), South Pacific (MD97 21-20, Pahnke and Zahn, 2005) and Atlantic Caribbean (GeoB3912, GeoB3104; Arz et al., 1998) and the ice core datasets of NorthGRIP (Svensson et al., 2008) and of Byrd (Blunier and Brooks, 2001). Heinrich stadials (H5, H5a, H6), Antarctic warmings (A), Rano Aroi wet events (Ar), Dansgaard-Oeschger events (with their corresponding number 9-16) are shown in the Figure. Yellow vertical bands indicate the identification of Heinrich stadials in each record and its correlation to NorthGRIP ice sequence. Grey vertical bands show other DO stadials. The data presented and the correlations between each dataset have been reproduced from their original publications.

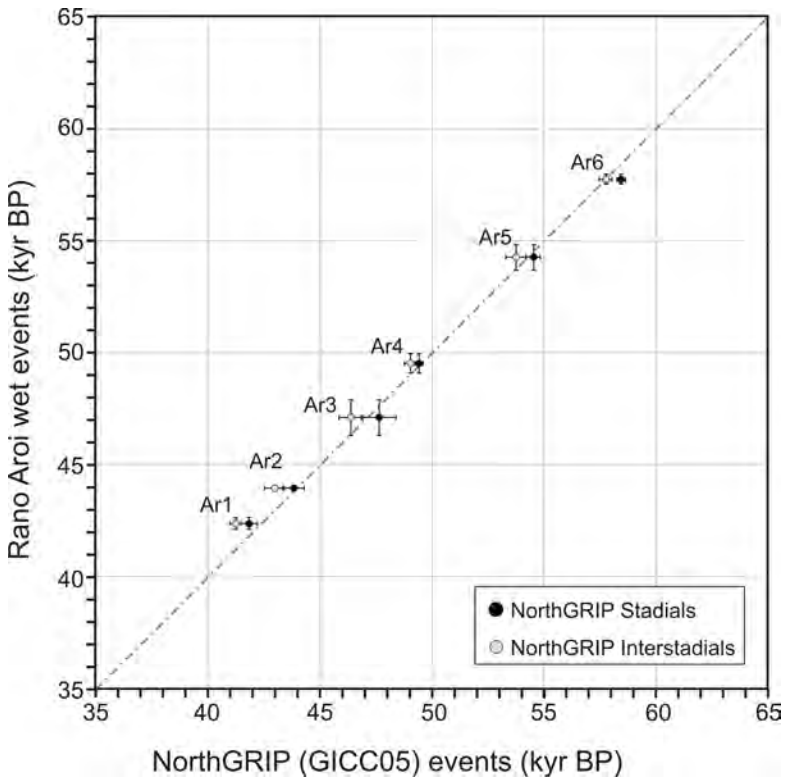

Figure 8.4 The timing of Rano Aroi wet events compared with the timing of the NGRIP closest stadial (black dots) and interstadial (grey dots) events according to the GICC05 chronology (Svensson et al., 2008). The middle point of the time interval of the event has been plotted, and the bars indicate the limits of the period. The excellent fitting between Easter Island wet events and NGRIP stadials during the well-constrained time windows (Ar 1, Ar2, Ar3 and Ar4) support the proposed age model and the correlation between the beyond the radiocarbon limit Rano Aroi events and the DO stadials.

The Rano Aroi record further supports this proposed hemispheric asynchrony during MIS 3 and further extends this phenomenon to the SPCZ region, indicating that abrupt hydrological oscillations were present not only during Heinrich stadials but also during other shorter DO stadials. The hydrologic response occurred during HS but also other DO stadials indicate that atmospheric teleconnections also operated during events associated with weaker changes in the AMOC (DO stadials) (Figure 8.3). Moreover, the timing of these hydrological oscillations suggests that the tropical atmospheric response to changes in the AMOC was very rapid as the thermal answer in the North Hemisphere. Rano Aroi abrupt hydrological changes differed from the Southern Hemisphere high latitude thermal response (as the Antarctic ice core records), which has been characterized by gradual onsets and terminations (Schmittner et al., 2003; Blunier et al., 1998; Blunier and Brooks, 2001; EPICA, 2006) (Figure 8.3).

8.5 Climate forcing of the ITCZ and SPCZ migration and Rano Aroi precipitation patterns at millennial timescales

The precipitation patterns observed in the Rano Aroi record are similar to those of other tropical records from the Southern Hemisphere (Figure 8.3). All these records agree with a number of model simulations indicating that during DO stadials, an increase in global heat transport occurred from south to north, which caused a reorganisation of the Hadley cell (Broccoli et al., 2006; Chiang and Bitz, 2005). Modelling results show a displacement of the

ITCZ to the South (North) over either Atlantic or Pacific Oceans as a result of a strengthening (weakening) of the north-easterly trade winds when additional ice volume is introduced in the Northern (Southern) Hemisphere (Figure 8.5) (Xie, 1994; Chiang and Bitz, 2005). This situation would induce an anomalous cross-equatorial transport of moisture, which would play a prominent role in amplifying the climatic impact of the ice expansion initiated over high latitudes (Chiang and Bitz, 2005). The modelled southward migration of the ITCZ during cold stadials in the North Atlantic is coherent with palaeo-data retrieved from records over the Indo-Pacific and Atlantic basins (Section 8.4). Nevertheless, although several records support the occurrence of these ITCZ migrations, changes in the position of the SPCZ low-pressure belt are less well known. Precipitation over Easter Island is primarily determined by the arrival of cyclogenic storms generated on the SPCZ, rather than directly by the ITCZ activity directly (Junk and Claussen, 2011). We suggest that a southward shift in the ITCZ during the MIS 3 was associated with an eastward expansion of the SPCZ, resembling an austral summer Pacific configuration (Figure 8.5).

It is noticeable that some climate models stress the importance of the Atlantic-Pacific atmospheric link through the Central American isthmus to explain the tropical Pacific hydrologic changes associated with DO climatic variability (Figure 8.5) (Zhang and Delworth, 2005; Dong and Sutton, 2002; Clement and Peterson, 2008). In coupled models developed by Zhang and Delworth (2005) and Vellinga and Wood (2002) there is an increase in the trade winds in the northern tropical Atlantic and an anomalous southerly flow across the equator, for this reason the answer is not confined to the Atlantic Ocean (Clement and Peterson, 2008). Dong and Sutton (2002) and Clement and Peterson (2008) propose that North Atlantic melting events signal can be propagated via atmospheric Rossby waves, altering the Pacific surface winds, what would lead to an El Niño-like oceanic and atmospheric pattern. This hypothesis states that southeastern trade winds (and therefore Walker circulation) are weakened during cold stadials; and consequently, the eastern equatorial Pacific upwelling is drastically reduced (Zhang and Delworth, 2005). This assumption can be tested by examining a reconstruction of the SST gradient across the equatorial Pacific, which reflects a relative temperature contrast between the eastern cold tongue and the western warm pool (Figure 8.2). The lower zonal SST gradient along the Equator (values close to 3°C or less) indicates weaker upwelling and hence a deepening of the thermocline in the eastern equatorial Pacific and more homogeneous surface conditions across the equatorial Pacific (Zhang and Delworth, 2005).

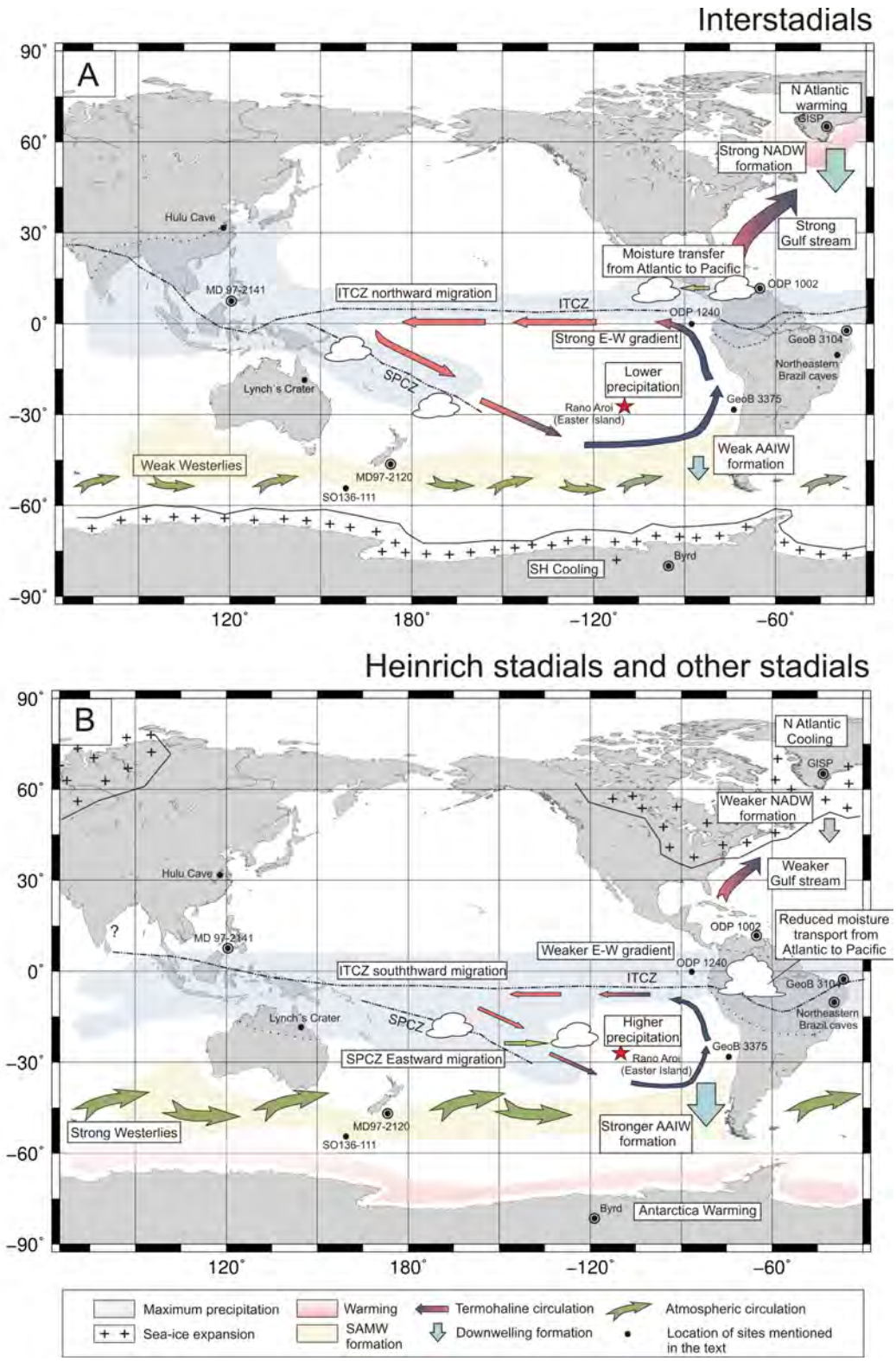

Figure 8.5 Proposed oceanic and atmospheric spatial patterns of millennial-scale climate change events that acted as climatic teleconnection mechanisms or feedbacks during MIS 3 interstadials (Map A) and stadials (Map B). Interstadial periods are characterized by vigorous Pacific equatorial circulation, weaker Southern westerlies and a northern position of the ITCZ, resembling a La Niña-like state. On the other hand stadials are characterized by a reduced Pacific equatorial gradient, stronger Southern Westerlies and a southern ITCZ, resembling a El Niño-like state. The sites mentioned in the text with black dot. Double circles indicate records also represented in Figure 4 and Rano Aroi is designated as a red star.

Several events of reduced SST gradients occurred during the studied period and can be tentatively correlated to most of our defined Rano Aroi wet events (Figure 8.2). This correlation is solid for the HS and for other DO stadials as well, with both correlations showing a comparable gradient reduction (Figures 8.2 and 8.5).

Another prominent feature is the magnitude of the H5a stadial, which is typically weaker in North Atlantic records and, in contrast, is the most intense wet event over Easter Island (Figure 8.2). The synchronicity between our wet events indicator (PC2) and the SST gradient and the resemblance of their structures, with an abrupt onset leading towards a progressive termination, support a correlation between these two records and the coupled connection between the equator and the SPCZ (Figures 8.2 and 8.3).

A reduced SST gradient across the Equator is consistent with a weakening of the Walker circulation, which is in agreement with some climatic models and studies as mentioned above (Stott et al., 2002; Huang et al., 2000; Dong and Sutton, 2002; Zhang and Delworth, 2005). The migration of the ITCZ and the occurrence of an ENSO linkage have also been suggested by studies of late Pleistocene environmental reconstructions (Haug et al., 2000; Fedorov and Philander; 2000, Koutavas et al., 2006). During the early-middle Holocene, a 20-30% higher SST gradient between the Galápagos Islands and the Sulu Sea has been attributed to a northern position of ITCZ, which in turn, has been related to a lower recurrence of ENSO warm events (Koutavas et al., 2006). An analogous situation could be described based on instrumental data: extreme El Niño events have been characterised by a mean southward migration of the Pacific ITCZ (Haug et al., 2000; Fedorov and Philander; 2000) and by an eastward and northward migration of the SPCZ (Vincent et al., 2009).

Nevertheless, other models consider these atmospheric mechanisms less relevant and highlight the role of the ocean's circulation. These models propose that the reduction in the AMOC when the North Atlantic cooled provked a global baroclinic adjustment. According to these authors, North Atlantic water density variations could lead to changes in the global thermocline within a few years to decades (Huang et al., 2000). These authors argue that climatic fluctuations can be explained without invoking a link between El Niño and stadials but the existence of such a linkage cannot be excluded (Huang et al., 2000, Timmermann et al., 2005).

8. 6. Tropical connections to Southern Hemisphere high latitudes

The southward migration of the ITCZ results in both a reinforcement of the equator-to-pole pressure gradient over the Southern Hemisphere and in an intensification of the South Westerlies (Toggweiler et al., 2006; Anderson and Carr, 2010; Heirman, 2011). Changes in the position and the intensity of the SW during MIS 3 should have contributed to an eastward movement of storms generated under the SPCZ during this time period (Figure 8.5). This storm propagation might have in turn become an important high latitude mechanism controlling precipitation over Easter Island. Another process intimately linked with the SW is the formation of intermediate water masses in the Southern Ocean. Changes in the formation rate of the Antarctic Intermediate Water (AAIW) associated with DO cycles have been described in a marine record from Chatman Rise, East New Zealand (MD97-2120, 45º32.06' S,

174º55.85' E, Pahnke and Zahn, 2005) based on the benthic foraminiferal $\delta^{13}C$ record (Figures 8.3 and 8.5). That study demonstrated that periods of increased AAIW production were in phase with a Southern Hemisphere warmings and a southward shift of the ITCZ. During the DO stadials (by the bipolar seesaw) the Antarctic continent and the Southern Ocean warmed provoking Antarctic sea ice retreat (Anderson and Carr, 2010; Skinner et al., 2010). This reduced sea ice extent would further lead to a southward shift of the ITCZ and a strengthening and northward migration of the SW, which would contribute to enhanced upwelling of circumpolar deep water and to a more efficient downwelling of the AAIW (Toggweiler et al., 2006; Anderson and Carr, 2010; Skinner et al., 2010) (Figure 8.5). A recent study using Neodymium (Nd) isotopes as a proxy for water mass provenance demonstrated that an increased export of AAIW from the Southern Ocean into tropical regions occurred during Northern Hemisphere cold periods such as the Heinrich stadials (Pena et al, 2013). This oceanic circulation scenario also induced the release of oceanic CO_2, which was stored in poorly ventilated deep-water masses to the atmosphere (Anderson and Carr, 2010; Skinner et al., 2010). CO_2 release from Southern Ocean during DO stadials contribute to global warming and therefore constitutes a negative climate feedback. In the context of the Rano Aroi wet events, these specific oceanic conditions in the Southern Ocean during the DO stadials could have also reinforced the SPCZ extension over Easter Island.

8.7 Conclusions

The Rano Aroi peat record provides a unique opportunity to understand the evolution of South Pacific climate during the late Pleistocene. This record contains information concerning climate variability during MIS 3 and is located thousands of kilometres away from other continental and marine palaeoclimatic records. Seven main humid events occurred in Rano Aroi during MIS 3 as a result of an eastward expansion of the SPCZ and thus can be correlated with the North Atlantic HS and with other DO stadials.

Anti-phase changes in precipitation and hydrology have been observed in low-latitude areas of the Northern and Southern Hemispheres. These changes have already been linked to North Atlantic cold stadials through a southward displacement of the ITCZ, as described by several studies based on both numerical climate models and environmental reconstructions from Circum-Pacific sites. The geographical position of Rano Aroi record allowed us to propose that these stadials were also associated with an eastward expansion of the SPCZ, highlighting a close coupling between the migration of the ITCZ and the SPCZ on millennial timescales. The abrupt character of the Rano Aroi humid events demonstrates the rapid atmospheric response of the tropical regions to the DO-related sudden changes in the AMOC, in contrast to the more progressive heat redistribution in the Southern Ocean led by the bipolar seesaw. The Rano Aroi wet events have been correlated with periods of a reduced SST gradient along the Equator, suggesting that more humid conditions over the Easter Island region occurred when the Walker circulation was reduced. These atmosphere-ocean connections in the tropical Pacific are analogous to modern El Niño-Southern Oscillation conditions. The reconstructed changes in the Central South Pacific rain patterns are also consistent with changes in the Southern Ocean, where the DO stadials, particularly the Heinrich stadials, occurred with enhanced AAIW production and sea ice retreat, processes that

are linked to the Antarctic warming led by the bipolar seesaw and that are reinforced by strengthened Southern Westerlies.

CHAPTER 9

DISCUSSION SYNTHESIS: AN INTEGRATIVE APPROACH TO RANO AROI ENVIRONMENTAL AND CLIMATIC EVOLUTION

From the multiproxy study of Rano Aroi peat record three hydrologic mire stages have been described (Chapter 5). The first of these stages (1) has been defined as a base line state, with a watertable close to peat surface, that allowed a constant accumulation and low decomposition in a kettle-hole mire. This situation was recorded in Rano Aroi sequence by reddish peat (Facies A) and granulated muddy peat (Facies B). While reddish peat consists in fresh mats preserving coarse vegetation remains, granulated muddy peat facies present smaller grain size and depict lower C/N ratios thus recording higher degree of humidification (but still low). Base line state illustrates the peatland baseline conditions that were interrupted by wetter or drier phases (Chapter 5). (2) The flooded mire stage represents an Rano Aroi mire open water state. During this period higher runoff and groundwater level allowed terrigenous material to reach the centre of the mire in form of relatively coarse sand grains. Higher soil moisture and the presence of aquatic organic matter imprinted particular isotope values on peat. During this weter phase, organic mud facies (Facies C) were accumulated (Chapter 5). This facies consisted in a dark fine sized peat that captured aquatic evidence. (3) Finally, a dry peatland state occurred when the lowering of the water level lead to an aerial exposure of peat surface. As a consequence of this exposure, the affected level (sapric peat facies) acquired a marked diagenetic imprint. The consequence is that this facies presents evidence of degradation (of previous deposited facies) and an important enrichment in elements that form very stable compounds under oxidated conditions (Chapter 5). Because peat can be effectively lost by oxidation with a rate of few cm per year it is likely that during this phase an uncertain part of the record was eroded away. Organic and inorganic chemistry together with the study of macrofossil remains contributed to define these three stages (Figure 9.1).

Organic mud facies (flooded mire stage) were present as centimetric layers inter-bedded in a sequence dominated by granulated muddy peat (baseline conditions). Interestingly, geochemical proxies and peat facies description showed that the base of organic mud facies (Facies C) consisted in a sharp change (entailing a fast water rise) while the transits back to baseline (Facies B) conditions were gradual (entailing slow shift to previous conditions). This can be related to the mire type: In sealf-sealing mires as Rano Aroi, the small pores of the permeable bedrock can be clogged by organic matter (Joosten and Clarke, 2001). This process prevents a free drainage of the water table and guarantizes a low and stable water level that maintains the peat formation. However, if the atmospheric water supply is very large, the water level in the basin suddenly rises. After it, the water level oscillation will depend on (1) the permeability of the substrate and (2) the efficiency of how the substrate pores can be blocked by the organic matter. In case of a rapid water rise and sufficient organic

matter, the porosity blocking can be effective even to the extent that the mire gets flooded (Prof. Hans Joosten, personal communication). The organic matter clogging does not have a reversal mechanism and therefore the water table stays until is reduced by (1) evapotranspiration or (2) accumulation of new organic matter that gradually fill up the peat surface (Prof. Hans Joosten, personal communication). Consequently, in sealf-sealing mires, a sudden rise in water level can be recorded as a rapid change in the peat record while but end with a smoother shift (as seen in Rano Aroi record). This process is based in a slow rise of the peat surface level under constant water levels, which promotes a progressive lowering of relative water table depth (Prof. Hans Joosten, personal communication).

The timing of the flooded mire stages has been controlled by the occurrence of strong precipitation events. By contrast, the presence of sapric peat (dry peatland) is found only once in the entire record evidencing that the site underwent a severe long-term drought only once during the last 70 kyr BP.

The alternation of the three different hydrologic stages and the consequent peat geochemistry features were driven not only by strong precipitation and drought events, but also by vegetation changes on Rano Aroi catchment (Chapter 6). Different stages of plant dominance lead to a differential imprint in peat geochemistry by controlling the amount and nature of the mineral fraction input into the mire. The recognition of these important processes combined with the age model of Rano Aroi record allowed us to draw a complete environmental reconstruction for the last 70 kyr BP of the island and the mire itself (Figure 9.1).

During MIS 4 the mire depicted a constant accumulation rate and was entirely dominated by C_4 Poaceae (Chapter 7). At the beginning of early MIS 3 entailed warmer temperatures and strong precipitation events. From 55 to 45 kyr BP and likely as a response to these climatic changes, the vegetation of the mire and surroundings underwent an important shift (Chapter 7). A landscape dominated by C_4 herbs and a reduced proportion of palm trees gradually turned into to a more closed landscape with scantily forested areas by small trees or bushes (as *Coprosma* or Asteraceae) around Terevaka area (Chapter 5). This change propitiated the expansion of different fern types in the new shady areas or around the mire itself. On the mire, the peat forming community also changed. A C_4-Poaceae dominance was displaced by a combination of Cyperaceae (presumably C_3) and Poaceae. Because similar Arecaceae pollen percentages are present along the entire record in Rano Aroi we are not able to describe any significative change concerning the distribution of palms. However, while some studies proposed an ancient island completely covered by palm trees (Flenley et al., 1991), other authors claim for a revision of this idea (Rull et al., 2010a). This last group of authors invokes that palynologic results so far are also compatible with the idea of mosaic vegetation and forested areas restricted to lakes and mires surroundings and along the coastal line and creeks where higher freshwater supply was available because it is the preferential area of aquifer discharge (Herrera and Custodio, 2008).

In Rano Aroi is observed how this vegetation shift couples to an important change in the inorganic fraction deposited in the mire (Chapter 5). A higher mineral input of fine to medium dust particles characterized by typical lithogenic elements is related to the C_4 period.

The elevate dust flux can be explained as the result of high erosion rates over a slightly protected soil (Chapter 6). During the C_3 dominance period this dust flux was reduced presumably because the soil became more protected by a closed landscape. However, the presence of Cyperaceae around Rano Aroi could also play an important role in buffering the entrance of these fine particles. This is likely because the most common native Cyperaceae in permanent waterbodies of the island nowadays is the *Scirpus californicus.* This species composes an important physical barrier in front terrigenous input. However, the periods with very high precipitation rates were anyway recorded in the mire when an open water situation allowed the transport of coarse terrigenous material of different composition to the center of the basin (Chapter 6).

While the Early MIS 3 period in Easter Island is defined by the onset of a series of wet events, Late MIS 3 is characterized as a dry phase. A sharp unconformity at 39 kyr cal BP above the sapric peat facies represents an ancient exposure surface (Chapter 5). The age of peat accumulation recovery above it is uncertain because new levels could have incorporated old carbon. Moreover, between 39 and 31 kyr cal BP a water table drop caused an advanced humification and probably loss of the uppermost peat layers (Chapter 7).

The MIS 2 and the LGM were globally cold and related to very low sea levels, but Rano Aroi and Rano Raraku records showed that both sites conserved a permanent and significant water table during that period (Chapter 7). Setting aside the differences, MIS 4 and MIS 2 entailed similar global climate patterns. However, contrary to what would be expected, Rano Aroi presents very differentiated stages. While during MIS 4 C_4 plants were dominating, during MIS 2 the mire and basin remained C_3 dominated. It can be suggested that the system dominated by a single plant type (Poaceae C_4) as occurred during MIS 4 could be strongly perturbed by either (1) the arrival of a new species at the island (i. e. *Scirpus californicus*) or (2) by environmental differences between MIS 2 and MIS 4 stages in water supply and temperature (i. e. MIS 3 onset). However, it seems that the vegetation distribution brought by MIS 3 conditions was more resilient or less sensitive to depict a change of the same magnitude in front of changing climate conditions (i. e. MIS 2 onset). Nevertheless, Rano Aroi peat accumulation rates during MIS 2 are very low and a proper paleoecological approach would require much higher sampling resolution to understand how Aroi ecosystems respond during both periods (MIS 2 and MIS4). For these reasons this interpretation has to be taken with care. Another important factor to take into account to explain MIS 4 and MIS 2 differences is that during the LGM (MIS 2) the combination of the northern position of the Southern Westerlies and the southern position of ITCZ indicate that the island could have received higher precipitation than during MIS 4. This fact, together with very low evaporation rates due to cold regional temperatures could account for the preservation of effective water tables in Rano Aroi and Raraku.

Evidence for deglaciation arrived as higher accumulation rates, at 17.5 kyr cal BP in Rano Aroi. Similarly, studies of the Raraku Lake record describe the Easter Island hydrological and vegetational response to deglaciation at 17.3 cal kyr BP. A high water table event was recorded at 16 cal kyr BP, followed by an episode of very elevate peat accumulation from 15 to 14 cal kyr BP. Early Holocene started in Rano Aroi with low accumulation rates (Chapter 7). A drying trend is well recorded in the island from Rano Raraku sediments, where a drop in

water level leaded to the conversion of Raraku lake system into a shallow swamp. In Easter Island, the mid-Holocene described dry conditions were interrupted by a flood episode at 5.8 cal kyr BP. The Rano Aroi record shows that Late Holocene wetter conditions began on Easter Island approx. 2.5 cal kyr BP, and relatively humid conditions were inferred up to the present time. At 1.3 cal kyr BP (655 AD), evidence of enhanced mineralization and higher contribution of organic matter from C_4 grasses appeared (Chapter 5). The age of this event lies in the time interval proposed for human arrival or expansion (Section 2.4), so these features could be interpreted as peat exposure and vegetation opening (increase in C_4 grass) caused by anthropogenic disturbance. Nevertheless, this event could also reflect climatic change during the Medieval Climate Anomaly (1205–705 yr cal BP), an important feature of Pacific climate during historical times.

The general picture of Rano Aroi environmental evolution described above and its correlation with paleoclimatic records of circum Pacific, tropical and subtropical sites and high latitude sequences not only brings new insights on the **environmental history** of Easter Island but also on the **climatic history** of Southern Central Pacific (Figure 9.1). As stated in various chapters of this PhD Thesis, Easter Island is situated in a key area for understanding South Pacific climate, where the interplay among the SPCZ, ITCZ, South Pacific Anticyclone (SPA) and SW can be observed.

An exhaustive comparison between the Rano Aroi record and several Southern Pacific climate records has been carried out as a main focus of this PhD Thesis. In this way, Rano Aroi reconstruction has been compared to marine sequences situated along the continetal offshores of South American continental, for example in Galápagos Islands and Sulu Sea. All these sequences provided (among other contributions) information on South Pacific SST oscillations and therefore also on changes in temperature gradients and surficial ocean circulation intensity. Additional marine records, as some studies performed on the coast of New Zealand revealed changes in the formation of deep or intermediate water masses on Southern Pacific. Sulu Sea records also give important information on shifts on the hydrologic cycles, tracking rainfall variability. However, hydrological changes have been preferentially recorded on tropical and subtropical continental sites as speleothems and lakes. Finally, polar ice records have been also used for correlation. These are indicative of temperature tendencies of north and south poles and they effectively prove the bipolar seesaw mechanism. The integration of all these climate information, including the environmental reconstruction of Easter Island, permited us to propose new contributions to central Pacific paleoclimatology, an area that has been poorly understood due to the lack of reliable sequences spanning a wide period of time with adequate resolution.

The main conclusion of this integrative work is the idea of the coupled migration of the ITCZ and the SPCZ as a response to North Atlantic stadials during MIS 3. Although the ITCZ migration related to the DO variability is a widely accepted process, the SPCZ behaviour for this time period was uncertain. The SPCZ is the climatic feature that provides storminess and rainfall over the south Pacidic and particularly over Easter Island. The synchrony between Rano Aroi wet events and evidence for ITCZ migration show how the southern movements of the ITCZ were accompanied by an eastern migration of the SPCZ (Chapter 8). This process involves a shrinking of the SPA and the South Pacific gyre that has been tested with the

proposed E-W Equatorial Pacific SST gradient (Chapter 8). Results show a reduced gradient when SPCZ was situated at its easternmost position (Chapter 8). This would entail an ENSO-like situation of Southern Pacific during North Atlantic cold periods, a configuration that has been predicted by some atmosphere-ocean coupled models (Chapter 8). Hence, high latitude processes could be also important in controlling the South Pacific restructuration during Heinrich Stadials. Apparently, during North Atlantic cold events enhanced Southern Westerlies accounted for the effective arrival of the SPCZ storminess over Easter Island and also for a positive influence on AAIW formation (Chapter 8). Enhanced downwelling of Antarctic deep and intermediate waters in the Southern Ocean probably changed deep ocean water ventilation and consequently, atmospheric CO_2 balance.

This variability described specifically refers to the tropical response to Heinrich stadials (H6, H5a and H5) and other stadials occurred during MIS 3. However, a similar restructuration is expected during North Atlantic cold periods on other isotopic stages. For instance, wet events described at Rano Aroi at 20 and 16 kyr BP can be tentatively attributed to H2 and H1.

Temperature and water supply are the major factors controlling peat formation and accumulation (Section 1.1). Despite in Rano Aroi record hydrological changes have been recognized as biogeochemical and facies changes (Chapter 5), it is difficult to state the role that temperature oscillations played in peat formation because it can have opposite effects. While high temperatures can enhance decomposition of organic matter, at the same time, they can promote productivity (Yu et al., 2010). Moreover, if the global temperature changes are related to CO_2 increases; enhanced productivity could be attributed to a CO_2 fertilization effect (Prentice et al., 2011).

High accumulation rates occurred in Rano Aroi between 17 and 10 kyr cal BP, depicting a maximum at 14 kyr cal BP. Enhanced peat formation interval in Rano Aroi (17-10 kyr cal BP) coincides with the period in which more peat basal ages have been documented on the Southern Hemisphere (Yu et al., 2010). The major part of Southern peatlands initiated before 10 ky cal BP, with initiation peaks around 17-14.5 kyr and 13 kyr cal BP. Northern peatlands show most initiation rates around 11-9 kyr cal BP, sensibly later than the Southern ones. This rapid expansion of peat accumulation in the Southern Hemisphere has been attributed to a warming climate during the Antarctic Thermal Maximum (Yu et al., 2010). However, althought the temperature rise was a main factor for ice retreat and peatland development at Southern high latitudes, hydrological supply and sea level changes have been pointed as the decisive influences in tropical peat formation during the Holocene period (Dommain et al., 2011; Dommain et al., submitted). Surface sea water of the Eastern margin of tropical and subtropical Pacific warmed up around 4° C between 17 and 10 kyr cal BP (30°S, Kaiser et al., 2008, 0° 0.1' N, Pena et al., 2008), but at the same time other global parameters as greenhouse gases concentration or the eustatic level underwent important changes. Between 15 and 11 kyr cal BP, CO_2 concentrations experienced an important increase (40 ppm, Monnin et al., 2001), as well as sea level (60 m, Grant et al., 2012). To test the real impact of temperature changes over Rano Aroi accumulation rates, independent temperature proxies from Easter Island would be required as well as larger integrative studies combining tropical

and subtropical accumulation rates with environmental data during Late Pleistocene and Holocene.

On millennial time scales, sea level wes also an important factor influencing Easter Island environment. It is known that glacial-interglacial eustatic displacements had important impacts in hydrology on coastal areas and small islands (Nunn, 2007). Easter Island lies on a very steep sea-mountain, almost without littoral platform, and thus, a lowering of sea level would not excessively change the surface area of the island. However, we suggest that for such a tiny piece of land with very permeable lithology a lowering up to several meters (as happened during the last glacial cycle) had to have a direct effect over groundwater balances. Although many discharging spots of freshwater are found nowadays along the coastline, the underground water distribution of the island is still an open question that would require specific hydrogeological studies. Despite these uncertainties, Rano Aroi record shows that wetter periods and higher accumulation rates happened in relation to high eustatic levels or/and rapid sea-level rise. This fact suggests that higher sea level maybe contributed to maintain higher groundwater levels on Terevaka area (Rano Aroi catchment). Furthermore, changes in eustatism and SST could have played an important role on the formation of convective storms. Although it is known that convection is nowadays a very important factor regulating rainfall in Easter Island, it is difficult to interprete what was the effect of the eustatic and thermal changes at millennial time scales. A sea level increase would result in a reduction of insularity effect, provoking in turn, less effective convections. But at the same time, high eustatic levels are globaly related to warmer global temperatures, fact that could trigger more powerful convection episodes due to higher sea-land temperature contrast. Among all, Rano Aroi geochemical and sedimentological data indicate wetter conditions and higher accumulation rates during sea level rise what would imply a predominance of the described effects over groundwater level and/or enhanced convection by temperature contrast.

As a summary, it can be stated that coupling geochemical and biological proxies improves our ability to decipher depositional processes in tropical and subtropical peatlands and to use these sequences for paleoenvironmental and paleoclimate reconstructions. The Rano Aroi record shows a development that is in accordance with regional paleoclimate records and illustrates the terrestrial response to the main Late Pleistocene phases in the Pacific region in terms of vegetation and paleo-hydrological change and provides a unique opportunity to understand the evolution of South Pacific climate during the late Pleistocene.

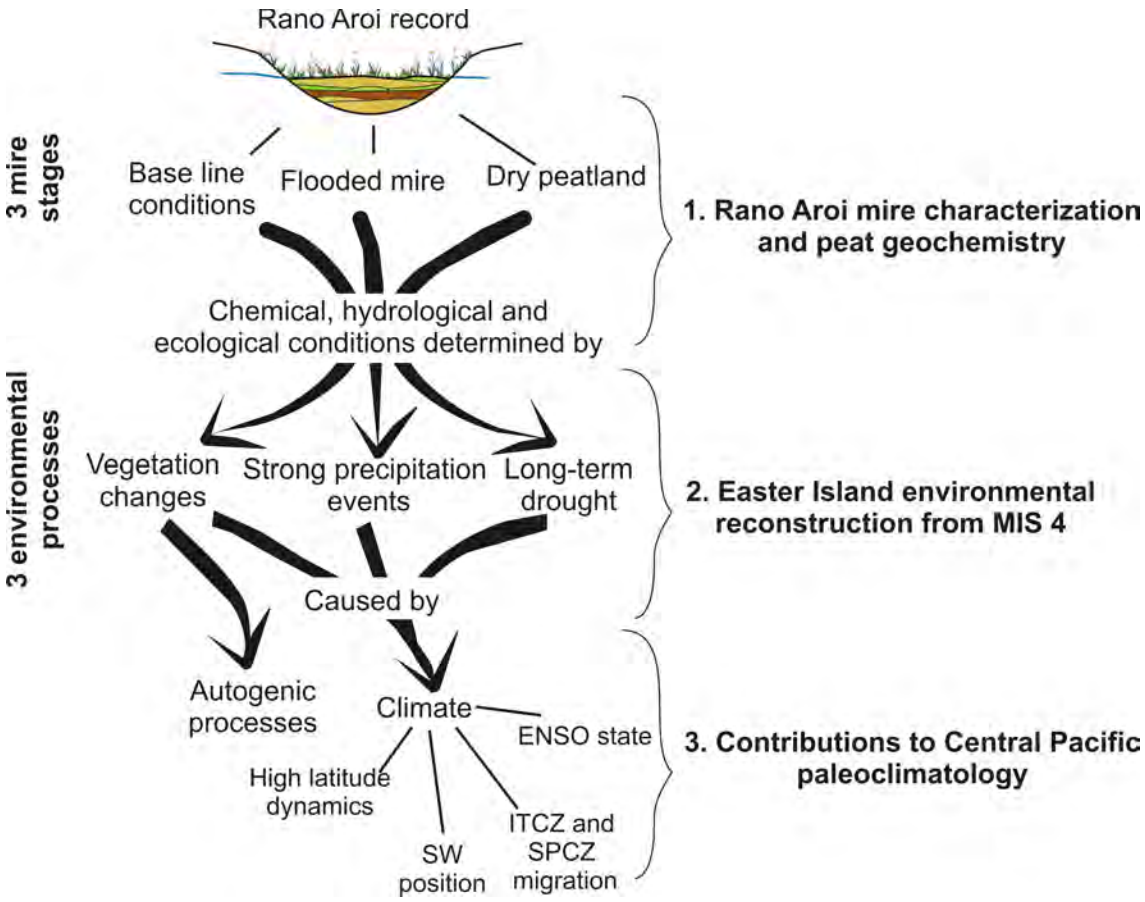

Figure 9.1 Conceptual diagram of Rano Aroi study achievements and conclusions. Three mire stages (Base line conditions, flooded mire and dry peatland) are defined from the first interpretative step (1) using peat geochemistry and facies characterization. The alternation of these stages in time allows us to infer a (2) environmental evolution and to define the processes that controlled peat composition from MIS 4 (vegetation changes, strong precipitation events, long-term droughts). The comparation of Rano Aroi environmental evolution with other circum-Pacific records permit to draw a climate history for the Central Pacific area therefore (3) contributing to Central Pacific paleoclimatology.

CHAPTER 10

CONCLUSIONS AND FUTURE WORKS

10. 1 Concluding remarks

Rano Aroi peat record constitutes the oldest and longest record recovered on Easter Island. Our multi-proxy approach allowed us to reconstruct the environmental history for the last 70 kyr BP, including the complex interactions between the mire, its catchment area, and climate.

As a result of this work the following goals have been achieved:

1. Relevant **contributions to mire characterization and peat chemistry**. The Rano Aroi study results particularly valuable for the research dealing inorganic and organic biogeochemical cycles of geogenous subtropical mires.

2. New insights in the **environmental reconstruction of Rano Aroi and Easter Island** from MIS 4, represented by changes in precipitation rates, vegetation cover or the evidence of severe drought events.

3. The study of environmental processes allowed us to attribute them to the specific climatic context. As a result a **contributions to Central Pacific paleoclimatology** from MIS 4 is performed, and the correlation of Rano Aroi record with other circum Pacific sites

Beyond this general picture, the multiproxy study of Rano Aroi peat records yield the following conclusions:

10.1.1 Mire characterization and peat geochemistry

- The Rano Aroi peat characterization together with basic hydrologic information indicate that Rano Aroi grew as a kettle-hole mire from a formerly dry basin, creating impervious layers on increasingly higher levels.

- Four facies have been described: Facies A (reddish peat) is composed of Cyperaceae (cf. *Cyperus cyperiodes*) and Polygonaceae (*P. acuminatum*) plant macrorests. This facies is associated with very high C/N ratio, low TN, low Fe and Ti values and $\delta^{13}C$ values between −21‰ and −26‰. Facies B (granulated muddy peat) is a brown peat composed of coarse organic fragments, mainly roots and rootlets, with low terrigenous content. This facies is characterized by low TN, high C/N ratios, low Fe and Ti contents and $\delta^{13}C$ values ranging from −14‰ to −26‰. Facies C (organic mud) is composed of

hemic and dark brown to black radicel peat with scarce and disperse sand fraction. Facies C was found as thin layers displaying high Fe and Ti values, high TN and relatively low $\delta^{13}C$ values (−14‰to−22‰) and interbedding sediments of Facies B. Facies D (sapric peat) consists of dark brown fine-grained layers with high Fe and Ca counts values.

- A vegetation change in the mire and surroundings has been confirmed by bulk peat $\delta^{13}C$ changes and palynological results. The progressively lighter values of $\delta^{13}C$ that occurred indicate a transition from C_4 to C_3 plant type. The main feature identified from pollen diagram is the replacement of the herbaceous plant pollen (primarily *Poaceae*) by woody plant pollen (mainly *Asteraceae*) as well as Cyperaceae and fern spores.

- Redox environmental changes and early diagenetic processes have been reconstructed from $\delta^{15}N$ and $\delta^{34}S$ measurements. Anoxic events have been recorded as very high $\delta^{15}N$ values (>8‰) due to denitrification. The presence of heavy sulphur isotope ratios when TS concentrations are lower suggest that part of the incorporated S in the mire may have been lost by bacteria sulphate reduction. At the same time, the deposited S in Rano Aroi is primarily attributed to a marine origin, consisting of a mixture of NSS (from DMS and other biogenic particles) and SS-sulphate (from marine splash) incorporated in iron or organic molecules.

- Changes in the catchment area background erosion linked to soil evolution and to eolian and hydric transport were recorded in the studied record by changes in the composition of the mineral matter entering to the mire. During the period of dominance of C_4 plant type, lower vegetation coverage lead to higher erosion and transport of a combined signal of lithogenic elements and metals (V, Al, Sc, Y, Cr, Cd, Ti, Zr and Cu). On the other hand, during the C_3 dominance period, higher pedogenesis leaded to lower background levels of mineral matter transport.

- The occurrence of high precipitation events was identified by the signal of Fe, Mn, Th, Ba, Zr, Ti, related to delivery of large amounts of these elements into the peatland as a solid terrigenous particles through runoff. These episodes were also characterized by high-frequency oscillations of relatively light $\delta^{13}C$ and high TN values.

- A paleo-surface has been defined at 4. 31 m caused by peat exposure and oxidation during a long-term drought. This period led to peat mineralization and a diagenetic relative enrichment of elements as Ca, Sr, Mg, Fe, and a relative loss of Al, Sc, Ti

- Three peatland types depending on the hydrological conditions have been defined from the biogeochemical record and peat characterization: baseline mire conditions (Facies A and B), the flooded mire (Facies C) formed during periods of enhanced precipitation and the dry peatland stages (Facies D formed by diagenetic processes), when drier conditions prevailed.

10.1.2 Rano Aroi and Easter Island (Rapa Nui) environmental reconstruction from MIS 4

The Rano Aroi record shows a development that is in accordance with regional paleoclimate records and illustrates the terrestrial response to the main Late Pleistocene phases in the Pacific region in terms of vegetation and paleo-hydrological change.

- During MIS 4 (70 to 60 kyr BP in Rano Aroi), the hydric and environmental conditions in the mire were stable and resembled mire baseline conditions. Rano Aroi basin catchment area in open grasslands and C_4 *Poaceae* dominated the mire owing to the general cold and relatively dry climate conditions.

- Early MIS 3 (60 to 40 cal kyr BP in Rano Aroi) was marked by the onset of wet events. During the first half of MIS 3 and probably driven by the wetter and warmer conditions *Asteraceae* and other small trees became gradually more abundant, forming small and scattered forests around the Terevaka volcano, while C_3 peat forming plants colonized the Aroi mire.

- Late MIS 3 was a very dry period, which led to peat oxidation and exposure shortly after 39 cal kyr BP. The long-term drought led to water table drop and enhanced peat mineralization at some time between the 39 and 31 kyr cal BP.

- During early MIS 2 (27.8–19 cal kyr BP) the water table recovered and peat accumulation resumed under C_3 plant dominance. Nevertheless, peat accumulation rates were low, apparently due to cold conditions, which will have hampered vegetation development.

- The evidence of the onset of deglaciation is concordant with Raraku Lake environmental development and was dated at 17.5 cal kyr BP in both sites, when in Rano Aroi peat accumulation rates began to increase again.

- The regional mid-Holocene dry period is well characterized at Rano Aroi from 5 to 2.5 cal kyr BP.

10.1.3 Contributions to Central Pacific paleoclimatology

- Seven main humid events occurred in Rano Aroi during MIS 3 as a result of an eastward expansion of the SPCZ and thus can be correlated with the North Atlantic Heinrich Stadials and with other DO stadials.

- The Rano Aroi record allowed us to propose that these stadials were also associated with an eastward expansion of the SPCZ, highlighting a close coupling between the migration of the ITCZ and the SPCZ on millennial timescales.

- The abrupt character of the Rano Aroi humid events demonstrates the rapid atmospheric response of the tropical regions to the DO-related sudden changes in the

AMOC, in contrast to the more progressive heat redistribution in the Southern Ocean led by the bipolar seesaw.

- Rano Aroi wet events have been correlated with periods of a reduced SST gradient along the Equator, suggesting that more humid conditions over the Easter Island region occurred when the Walker circulation was reduced. These atmosphere-ocean connections in the tropical Pacific are analogous to modern El Niño – Southern Oscillation conditions.

- The reconstructed changes in Central South Pacific rain patterns were also consistent with changes in the Southern Ocean, where DO stadials, particularly HS, occurred with enhanced production of the AAIW production and Antarctic sea ice retreat. Both processes that have been linked to the Antarctic warming led by the bipolar seesaw and that were reinforced by strengthened Southern Westerlies.

- The above block of conclusions were obtained from the detailed study of early MIS 3 period, by virtue of being the period presenting better resolution without discontinuities, it is expected that the exposed teleconnections were also active during MIS 2 and Holocene, when the occurrence of wet events during cold periods on North Atlantic have been also described.

10.2 Perspectives and future works

This work reveals the need of multi-proxy studies on peat records as a powerful tool to understand the chemical, hydrological and ecological processes from an holistic perspective. However, further work might be proposed to improve interpretation and constrain several open questions.

- Advanced dating techniques could be applied as $^{234}U/^{230}Th$ dating in peat. This method is difficult to apply in peat records owing to the large needs of sample requeriments to perform the dating, but can be extremely useful to constrain age uncertainties of the bottommost part of ARO 06 01 section.

- A detailed identification and counting of oribatid mites (previously selected and picked out after sample sieving) is still undergoing and no conclusive result were obtained. Nevertheless, this work can provide additional information on local environmental conditions such as watertable changes or vegetation type.

- In this study, pollen counting has been done over a relatively reduced number of samples what allowed to draw a long-term vegetation reconstruction. Vegetational changes associated to higher-frequency changes as the occurrence of Rano Aroi wet events remain still unknown. A detailed pollen counting (every 5 cm) could contribute to obtain a detailed understanding of vegetational response to external forcing.

- Although it has not been included in this volume, the results of Rare Earth Element (RRE) concentrations over Rano Aroi mineral matter have been obtained from ICP-

AES analyses. Further work on RRE anomalies can bring new insights about the origin of the terrigenous material and its transport (eolian or hydric) as well as being useful to elucidate if there has been dust transport from the American continent or Australia (as other sites of Oceania). If this is the case, relevant contributions about the wind pattern dominance along regional Southern Pacific are expected.

REFERENCES

Alamos, F. and Peralta, F., 1992. Recursos hídricos de Isla de Pascua: estudio del regadío de Isla de Pascua, I etapa: estudio hidrogeológico [Water resources of Easter Island: study of Easter Island irrigation, 1st stage: hydrogeological study]. Alamos y Peralta, Ingenieros Consultores. Comisión Nacional de Riego, Santiago, Chile, 130 pp.

Alexander, M. A., Bladé, I., Newman, M., Lanzante, J. R., Lau, N. C., Scott, J. D., 2002. The atmospheric bridge: The influence of ENSO teleconnections on air-sea interaction over the global oceans. Journal of Climate, 15 (16), 2205-2231.

Anderson, A., Chappell, J., Gagan, M., Grove, R., 2006. Prehistoric maritime migration in the Pacific Islands: an hypothesis of ENSO forcing. The Holocene 16 (1), 1–6.

Anderson, R. F., and Carr, M. E. 2010. Uncorking the Southern Ocean's Vintage CO2. Science, 328, 1117-1118.

Andersson, A., Bakan, S., Fennig, K., Grassl, H., Klepp, C.-P., and Schulz, J. 2007. Hamburg Ocean Atmosphere Parameters and Fluxes from Satellite Data – HOAPS-3 – monthly mean, World Data Center for Climate, 3097, 385-393.

Andreasen, D. J., A. C. Ravelo, and A. J. Broccoli, 2001. Remote forcing at the Last Glacial Maximum in the tropical Pacific Ocean, J. Geophys. Res., 106, 879 – 897.

Anshari, G., Kershaw, A.P., van der Kaars, S., 2001. A Late Pleistocene and Holocene pollen and charcoal record from peat swamp forest, Lake Sentarum Wildlife Reserve, West Kalimantan, Indonesia. Palaeogeography, Palaeoclimatology, Palaeoecology 171, 213-228.

Appleby, P.G., 2001. Chronostratigraphic techniques in recent sediments. In: Last, W.M. & Smol, J.P. (eds.) Tracking Environmental Change Using Lake Sediments, Volume 1: Basin Analysis, Coring, and Chronological Techniques. Kluwer Academic Publishers, Dordrecht, 171–203.

Appleby, P.G. and Oldfield, F., 1978. The calculation of 210Pb dates assuming a constant rate of supply of unsupported ^{210}Pb to the sediment. Catena, 5, 1–8.

Appleby, P.G., Oldfield, F., Thompson, R., Huttunen, P. & Tolonen, K., 1979. ^{210}Pb dating of annually laminated lake sediments from Finland. Nature, 280, 53–55

Appleby, P.G., Shotyk, W. & Frankhauser, A., 1997. ^{210}Pb age dating of three peat cores in the Jura Mountains, Switzerland. Water, Air & Soil Pollution, 100, 223–231.

Arnold, M., Orliac, M., Valladas, H., 1990. Donées nouvelles sur la disparition du palmier (cf. Jubaea) de l'Ile de Pâques. Courier Forschungsinstitut Senckenberg 125, 217–219.

Arz, H. W., Pätzold, J., Wefer, G. 1998. Correlated millennial-scale changes in surface hydrography and terrigenous sediment yield inferred from last-glacial marine deposits off Northeastern Brazil.Quaternary Research **50**, 157 - 166.

Aubert, D., Le Roux, G., Krachler, M., Cheburkin, A., Kober, B., Shotyk, W., Stille, P., 2006. Origin and fluxes of atmospheric REE entering an ombrotrophic peat bog in Black Forest (SW Germany): evidence from snow, lichens and mosses. Geochim. Cosmochim. Acta 70, 2815–2826.

Aucour, A. M., Bonnefille, R., Hillaire-Marcel, C., 1999. Sources and accumulation rates of organic carbon in an equatorial peat bog (Burundi, East Africa) during the Holocene: carbon isotope constraints. Palaeogeography, Palaeoclimatology, Palaeoecology 150, 179–189.

Azizi, G., Flenley, J.R. 2008. The last glacial maximum climatic conditions on Easter Island. Quaternary International 184, 166–176.

Baker, P.A., Rigsby, C.A., Seltzer, G.O., Fritz, S.C., Lowenstein, T.K., Bacher, N.P., Veliz, C., 2001. Tropical climate

changes at millennial and orbital timescales on the Bolivian Altiplano. Nature 409, 698–700. http://dx.doi.org/10.1038/35055524.

Baker, P.E., Buckley, F., Holland, J.G., 1974. Petrology and geochemistry of Easter Island. Contributions to Mineralogy and Petrology 44, 85–100.

Barber, K.E., Chambers, F.M., Maddy, D., 2003. Holocene palaeoclimates from peat stratigraphy: macrofossil proxy climate records from three oceanic raised bogs in England and Ireland. Quaternary Science Reviews 22, 521–539.

Barberi, M., Salgado-Labouriau, M. L., & Suguio, K., 2000. Paleovegetation and paleoclimate of "Vereda de Águas Emendadas", central Brazil. *Journal of South American Earth Sciences*, *13*(3), 241-254.

Bates, R.L. and Jackson, J.A. (Editors), 1980. Glossary of Geology. American Geological Institute, Falls Church, Va., 2nd ed., 751 pp.

Beaufort, L., T. de Garidel-Thoron, A. Mix, and N. G. Pisias, 2001. ENSO-like forcing on oceanic primary production during the late Pleistocene, Science, 293, 2440 – 2444, doi:10.1126/science.293.5539.2440.

Bender,M.,T.Sowers,M.-L.Dickson,J.Orchardo, P. Grootes, P. A. Mayewski, and D. A. Meese, 1994. Climate correlations between Greenland and Antarctica during the past 100,000 years, Nature, 372, 663– 666.

Bennett, K.D., 1996. Determination of the number of zones in a biostratigraphical, sequence. New Phytologist 132, 155-170

Berger, A., Loutre, M.F., 1991. Insolation values for the climate of the last 10 million years. Quat. Sci. Rev. 10, 297–317.

Biester, H., Keppler, F., Putschew, A., Martínez-Cortizas, A.; Petri, M, 2004. Halogen retention, organohalogens and the role of organic matter decomposition on halogen enrichment in two Chilean peat bogs. Environmental Science Technology, 38, 1984-1991.

Biester H, Hermanns Y-M, Martínez Cortizas A. 2012. The influence of organic matter decay on the distribution of major and trace elements in ombrotrophic mires - a case study from the Harz Mountains. Geochimica Cosmochimica Acta 84: 126-136.

Bindler R., 2006. Mired in the past-looking to the future: geochemistry of peat and the analysis of past environmental changes. Global Planet. Change 53, 209–221.

Birks, H.H., 2001. Plant macrofossils. In: Smol, J.P., Birks, H.J.B., Last, W.M. (Eds.), Tracking Environmental Change Using Lake Sediments, vol. 3. Kluwer, Dordrecht, pp. 49–74.

Birks, H.H., Birks, H.J.B., 2006. Multiproxy studies in palaeolimnology. Vegetation History and Archaeobotany 15, 235–251.

Blaauw, M., 2010. Methods and code for 'classical' age-modelling of radiocarbon sequences, Quaternary Geochronology, Volume 5, Issue 5, Pages 512–518

Blaauw, M., Christen, J. A., Mauquoy, D., 2010. Peatlands as a model system for exploring and reconciling Quaternary chronologies. Wetlands 25, 259–278.

Blaauw, M., Christen, J.A. 2011. Flexible paleoclimate age-depth models using an autoregressive gamma process. Bayesian Analysis 6, 457 – 474.

Blunier, T., and E. J. Brook, 2001. Timing of millennial-scale climate change in Antarctica and Greenland during the last glacial period, Science, 291, 109– 112.

Blunier, T., Chappellaz, J., Schwander J., Dällenbach, A., Stauffer, B., Stocker, T. F., Raynaud, D., Jouzel, J., Clausen, H. B., Hammer, C. U., Johnsen, S. J. 1998. Asynchrony of Antarctic and Greenland climate change during the last glacial period. Nature 394, 739.

Bond, G., Showers, W., Cheseby, M., Lotti, R., Almasi, P., Priore, P., Cullen, H., Hajdas, I., Bonani, G., 1997. A pervasive millennial-scale cycle in North Atlantic Holocene and glacial climates. science, 278(5341), 1257-1266.

Booth RK, Jackson ST., 2003. A high-resolution record of late- Holocene moisture variability from a Michigan raised bog, USA. The Holocene 13:863–876

Borren, W., Bleuten, W., Lapshina, E., D., 2004. Holocene peat and carbon accumulation rates in the southern taiga of western Siberia. Quaternary research, 61, 42-51.

Bostock, H. C., Opdyke, B. N., Gagan, M. K., & Fifield, L. K., 2004. Carbon isotope evidence for changes in Antarctic Intermediate Water circulation and ocean ventilation in the southwest Pacific during the last deglaciation. *Paleoceanography*, *19*(4), PA4013.

Brenner, M..T. J. Whitmore, J.H.Curtis, D. A. Hodell & C. L. Schelske, 1999. Stable isotope ($\delta^{13}C$ and $\delta^{15}N$) signatures of sedimented organic matter as indicators of historic lake trophic state. J. Paleolim. 22:205–221.

Broccoli, A. J., Dahl, K. A. and Stouffer. R. J. 2006, Response of the ITCZ to Northern Hemisphere cooling, Geophys. Res. Lett., 33, 1-4.

Broecker, W. 1994. Massive iceberg discharges as triggers for global climate change. Nature 372, 421-424.

Broecker, W. S., 1998. Paleocean circulation during the last deglaciation: A bipolar seesaw?, Paleoceanography, 13, 119– 121.

Brown, F. B. H. 1935. Flora of Southeastern Polynesia, Vol. 3. Bernice P. Bishop Museum Bulletin, 130, 1-386.

Burley, D. V., and Clark, J. T., 2003. The archaeology of Fiji/West Polynesia in the post-Lapita era, in: C. Sand (ed), Pacific Archaeology: Assessments and Prospects (Proceedings of the International Conference for the 50th Anniversary of the First Lapita Excavation, Kone-Noume´a 2002). Noume´a: Services des Musees et du Patrimoine, pp. 235–254.

Butler, K., Prior, C.A., Flenley, J.R., 2004. Anomalous radiocarbon dates from Easter Island. Radiocarbon 46, 395–405.

Calhoun, J. A., & Bates, T. S., 1989. Sulfur Isotope Ratios. Biogenic Sulfur in the Environment (Saltzman, ES and Cooper, WJ, eds.), 365-379.

Calhoun, J. A., Bates, T. S., & Charlson, R. J., 1991. Sulfur isotope measurements of submicrometer sulfate aerosol particles over the Pacific Ocean. Geophysical Research Letters, *18*(10), 1877-1880.

Cane, M. A., 2005. The evolution of El Niño, past and future. Earth and Planetary Science Letters, 230(3), 227-240.

Cañellas-Boltá, N., Rull, V., Sáez, A., Margalef, O., Giralt, S., Pueyo, J.J., Birks, H.H., Birks, H.J.B., Pla-Rabes, S., 2012. Macrofossils in Raraku Lake (Easter Island) integrated with sedimentary and geochemical records: towards a paleoecological synthesis. Quaternary Science Reviews 34, 113–126

Cañellas-Boltà N, Rull V, Sáez A, Margalef O, Bao R, Pla-Rabes S, Blaauw M, Valero-Garcés B, Giralt S. 2013. Vegetation changes and human settlement of Easter Island during the last millennia: a multiproxy study of the Lake Raraku sediments. Quaternary Science Reviews 72: 36-48.

Carroll, J. & Lerche, I.,2003. Sedimentary Processes: Quantification Using Radionuclides. Elsevier, Amsterdam, 269 pp.

Chambers F. M., Charman D. J., 2004. Holocene environmental change: contributions from the peatland archive. The Holocene 14:1–6

Chambers, F. M., Beilman, D. W., Yu, Z., 2011. Methods for determining peat humification and for quantifying peat bulk density, organic matter and carbon content for palaeostudies of climate and peatland carbon dynamics. Mires and peat, vol 7 issue 07.

Chapman, S.B., 1964. The ecology of Coom Rigg Moss, Northumberland, II. The chemistry of peat profiles and the

development of the bog system. J. Ecol., 52: 315- 21.

Charman, D.J., 2001. Biostratigraphic and palaeoenvironmental applications of testate amoebae. Quaternary Science Reviews, 20, 1753–1764

Charman, D.J., 2002. Peatlands and environmental change, John Wiley, Chichester.

Charman D. J., Chambers F.M. (eds), 2004. Peatlands and Holocene environmental change. The Holocene 14:1–143

Castañeda, I. S., and Schouten, S., 2011. A review of molecular organic proxies for examining modern and ancient lacustrine environments. Quaternary Science Reviews, 30 (21), 2851-2891.

Chesworth W, Martínez Cortizas A, García-Rodeja E. 2006. The redox-pH approach to the geochemitry of the Earth's land surface, with application to peatlands. In IP Martini, A Martínez Cortizas, W Chesworth (eds) "Peatlands: evolution and records of environmental and climate changes. Developments in Earth Surface Process 9, Chapter 8: 175-195.

Chiang, J. C. H., and Bitz, C. M. 2005. Influence of high latitude ice cover on the marine Intertropical Convergence Zone, Clim. Dyn., 25, 477–496, doi:10.1007/s00382-005-0040-5.

Chiang, J. C., and Lintner, B. R., 2005. Mechanisms of remote tropical surface warming during El Niño. Journal of climate, 18 (20), 4130-4149.

Clarke, A.C., Burtenshaw, M.K., McLenachan, P.A., Erickson, D.L., Smith, B.D., Penny, D., 2006. Reconstructing the origins and dispersal of the Polynesian bottle gourd (Lagenaria siceraria). Molecular Biology and Evolution 23, 893e900.

Clemens, S., W. Prell, D. Murray, G. Shimmield, and G. Weedon, 1991. Forcing mechanisms of the Indian Ocean monsoon, Nature, 353, 720–725

Clement, A. C., and Cane, M. A., 1999. A role for the tropical pacific coupled ocean-atmosphere system on Milankovitch and Millennial Timescales. Part I: A modelling study of tropical Pacific Variability in Mechanisms of Global Climate Change at Millennial Time Scales, edited by Clark, P. U., R. S. Webb and L. Keigwin, pp. 363-371, American Geophysical union, Washington, DC, 1999.

Clement, A. C., Seager, R., Cane, M. A. 1999. Orbital controls on the El Niño/Southern Oscillation and the tropical climate, Paleoceanography, 14, 441-456, 1999.

Clement, A.C., Peterson, L.C. 2008. Mechanisms of abrupt climate change of the last glacial period. Reviews of Geophysics 46.

Clymo, R. S., Hayward, P. M., 1982. The ecology of Sphagnum. In *Bryophyte ecology* (pp. 229-289). Springer Netherlands.

Clymo, R. S., 1983. Peat. In: Mires: Swamp, Bog, Fen and Moor. Ecosystems of the world 4A (ed. By A. J. P. Gore), pp.159-224, Elselvier, Amsterdam.

Clymo, R. S. 1984. The limits to peat bog growth. Philosophical Transactions of the Royal Society of London B, 303:605-654.

Clymo RS, Mackay D. 1987. Upwash and downwash of pollen and spores in the unsaturated surface layer of Sphagnum-dominated peat. New Phytologist 105(1): 175–83.

CONAF, 1997. Plan de Manejo Parque Nacional Rapa Nui (Santiago de Chile, 2007). Corporación Nacional Forestal

Conroy, J.L., Overpeck, J.T., Cole, J.E., Shanahan, T.M., Steinitz-Kannan, M., 2008. Holocene changes in eastern tropical Pacific climate inferred from a Galápagos lake sediment record. Quaternary Science Reviews 27 (11–12), 1166–1180.

Costello, A. B., 2009. Getting the most from your analysis. *Pan*, *12*(2), 131-146.

Couwenberg, J., De Klerk, P., Endtmann, E., Joosten, H., Michaelis, D., 2001. Hydrogenetische Moortypen in der Zeit – eine Zusammenschau (Hydrogenetic mire types in time—an overview). In: Succow, M., Joosten, H. (Eds.), Landschaftsökologische Moorkunde. (Landscape Ecology of Peatlands), Second edition. Schweizerbart, Stuttgart, pp. 399–403 (in German).

Croudace, I. W., Rindby, A., & Rothwell, R. G., 2006. ITRAX: description and evaluation of a new multi-function X-ray core scanner. Special Publication-Geological Society Of London, 267, 51.

Cruz Jr, F. W., Burns, S. J., Kamman, I., Sharp, W. D., Vuille, M., Cardoso, A. O., Ferrari, J. A., Silva Dias, P. L., Viana Jr., O, 2005. Insolation-driven changes in atmopsheric circulation over the past 116000 years in subtropical Brazil. Nature, Vol. 434, 63-66.

Dai, A., and Wigley, T. M. L., 2000. Global Patterns of ENSO-induced Precipitation. Geophysical research letters, Vol, 27, n 9, pp: 1283-1286.

Damman A. W. H., 1978. Distribution and movement of elements in ombrotrophic peat bogs. Oikos 30, 480–495.

Damman A. W. H., Tolonen, K., Salanus, T., 1992. Element retention and removal in the ombrotrophic peat of Hadekeias, a boreal Finnish peat bog, Suo 43, 137-145.

Dannenmann, S., B. K. Linsley, D.W. Oppo, Y. Rosenthal, and L. Beaufort, 2003. East Asian Monsoon Forcing of Suborbital variability in the Sulu Sea during Marine Isotope Stage 3: Link to Northern Hemisphere Climate. Geochemistry, Geophysics, Geosystems, 4, issue 1, 1-13.

Dansgaard, W., Oeschger, H., & Langway, C. C., 1983. ICE Core Indications of Abrupt Climatic Changes. In Palaeoclimatic Research and Models (pp. 72-73). Springer Netherlands.

Dansgaard, W., S. J. Johnsen, S. J., Clausen, H. B., Dahl-Jensen, D., Gundestrup, N. S., Hammer, C. U., Hvidberg, C. S., Steffensen, J. P., Sveinbjörnsdottir, A. E., Jouzel, J., Bond, G. 1993. Evidence for general instability of past climate from a 250-kyr ice core record. Nature, 364, 218–220.

Danzeglocke, U., Jöris, O., Weninger, B. 2008. CalPal-2007 online. http://www.calpal-online.de/ accessed 2009.05.03.

de Garidel-Thoron, T., Y. Rosenthal, F. Bassinot, and L. Beaufort, 2005. Stable sea surface temperatures in the western Pacific warm pool over the past 1.75 million years, Nature, 433, 294– 298.

Dearing, J., 1999, Magnetic susceptibility. In Walden, J., Oldfield, F. and Smith, J. P. (eds.), Environmental magnetism: a practical guide. Technical Guide, No. 6, p. 35-62. Quaternary Research Association, London, UK.

Delhon, C. and Orliac, C., 2007. Palm trees on Easter Island: new phytolith and radiocarbon data. In: Poster presented at the VIIth International Conference on Easter Island and the Pacific Islands: Migration, Identity and Cultural Heritage, Gotland University, Visby, Sweden, 20-25.

Desta Fekedulegn, B., JJ Colbert, RR Hicks, ME Schuckers. 2002. Coping with multicollinearity: an example on application of principal components regression in dendroecology. USDA Forest Service, Northeastern Research Station, Research Paper NE-721, 45 pp.

Diamond, J., 2005. Collapse. How Societies Choose to Fail or Survive. Allen Lane, London.

Dickinson, W.R., 2001. Paleoshoreline record of relative Holocene sea levels on Pacific islands. Earth-Science Reviews 55, 191–234.

Dierssen, K., 1982. Die wichtigsten Pflanzengesellshaften der Moore NW-Europas [The Major Plant Communities of Northwest European Mires]. Conservatoire et Jardin Botaniques, Geneva.

Ding, Q., Steig, E., Battisti, D., Wallace, J., 2012. Influence of the tropics on the Southern Annular Mode. American meteorological society. Vol 25, Issue 18.

Dommain, R., Couwenberg, J., Joosten, H., 2011. Development and carbon sequestration of tropical peat domes in

south-east Asia: links to post-glacial sea-level changes and Holocene climate variability. Quaternary Science Reviews 30 (7–8), 999–1010.

Dommain, R., Couwenberg, J., Glaser, PH., Joosten, H., Suryadiputra, (submitted) Carbon storage and release in Indonesian peatlands since the Last Deglaciation

Dong, B.-W., and Sutton, R. T. 2002. Adjustment of the coupled ocean–atmosphere system to a sudden change in the thermohaline circulation, Geophys. Res. Lett., 29(15), 1728.

Dransfield, J., Flenley, J.R., King, S.M., Harkness, D.D., Rapu, S., 1984. A recently extinct palm from Easter Island. Nature 312, 750–752.

Dubois, A., Lenne, P., Nahoe, E., Rauch, M., 2013. Plantas de Rapa Nui. Guía Ilustrada de la Flora de Interés Ecológico y Patrimonial. Umanga mo te Natura, CONAF, ONF International, Santiago, 132 páginas.

Dudgeon, J. V., and Tromp, M., 2012. Diet, geography and drinking water in Polynesia: microfossil esearch from archaeological human dental calculus, Rapa Nui (Easter Island). International Journal of Osteoarchaeology.

Duller, G. A. T., 2008. Luminiscence Dating guidelines on using luminescence dating in archaeology. Swindon: English Heritage.

Dumont, H.J., Cocquyt, C., Fontugne, M., Arnold, M., Reyss, J.-L., Bloemendal, J., Oldfield, F., Steenbergen, C.L.M., Korthals, H.J., Zeeb, B.A., 1998. The end of moai quarrying and its effect on Raraku Lake, Easter Island. Journal of Paleolimnology. 20, 409–422.

Ehleringer, J.R., Cerling, T.E., Helliker, B.R., 1997. C4 photosynthesis, atmospheric CO2 and climate. Oecologia 112, 285–299.

Emery, W. J., Meincke, J., 1986. Global water masses: summary and review. Oceanologica acta. Vol 9. nº4

EPICA Community Members, 2006. One-to-one coupling of glacial climate variability in Greenland and Antarctica. Nature 444, 195-198.

Etienne, M., Michea, G., Díaz, E., 1982. Flora, vegetación y potencial pastoral de la Isla de Pascua. Boletín Técnico n° 47, Facultad de Ciencias Agrarias, Veterinarias y Forestales.Universidad de Chile, Santiago de Chile (in Spanish).

Fedorov, A. V., Philander S. G. 2000. Is El Niño Changing? Science 288. 1997-2002.

Fedorov, A. V., Dekens, P. S., McCarthy, M., Ravelo, A. C., Barreiro, M., Pacanowski, R. C., & Philander, S. G., 2006. The Pliocene paradox (mechanisms for a permanent El Niño). *Science*, *312*(5779), 1485-1489.

Flenley, J.R., 1993. The palaeoecology of Easter Island, and its ecological disaster. In: Fischer, S.R. (Ed.), Easter Island Studies: Contribution to the History of Rapanui in Memory of William T. Mulloy. The Short Run Press, Oxbow, Oxford, pp. 27e45.

Flenley, J.R., King, S.M. 1984. Late Quaternary pollen records from Easter Island. Nature 307, 47–50.

Flenley, J.R., Bahn, P., 2003. The Enigmas of Easter Island. Island on the Edge. Oxford, University Press, New York.

Flenley, J.R., King, S.M., Jackson, J., Chew, C., Teller, J.T., Prentice, M.E., 1991. The Late Quaternary vegetational and climatic history of Easter Island. Journal of Quaternary Science 6 (2), 85-115.

Gälman V., Rydberg J., Shchukarev A., Sjöberg S., Martínez-Cortizas A., Bindler R., Renberg I., 2009. The role of iron and sulfur in the visual appearance of lake sediment varves. Journal of Pelolimnology 41: 141-153.

Ganopolski, A., Rahmstorf, S. 2002, Abrupt Glacial Climate Changes due to Stochastic Resonance. Physical review letters, Volume 88, Number 3

Garcia, M. J., De Oliveira, P. E., de Siqueira, E., & Fernandes, R. S., 2004. A Holocene vegetational and climatic record from the Atlantic rainforest belt of coastal State of São Paulo, SE Brazil. Review of Palaeobotany and Palynology, 131(3), 181-199.

García-Rodeja E, Nóvoa JC, Pontevedra X, Martínez-Cortizas A, Buurman P. 2007. Aluminium and iron fractionation of European volcanic soils by selective dissolution techniques. In O Arnalds, F Bartoli, P Buurman, H Óskarsson, G Stoops, E García-Rodeja (eds) "Soils of volcanic regions in Europe", 326-351.

Gaudig, G., Couwenberg, J., Joosten, H., 2006. Peat accumulation in kettle holes: bottom up or top down? Mires and Peat 1 (6), 1–16 (http://www.mires-and-peat.net/map01/map_1_6.htm).

Gefen, D., & Straub, D., 2005. A practical guide to factorial validity using PLS-Graph: Tutorial and annotated example. Communications of the Association for Information Systems, 16(1), 109.

Genz, J., Hunt, T.L., 2003. El Niño Southern Oscillation and Rapa Nui prehistory. Rapa Nui Journal 17 (1), 7–14.

Georgi, D. T. , 1981. On the relationship between the large-scale property variations and fine structure in the Circumpolar Deep Water. Journal of Geophysical Research: Oceans (1978–2012), 86(C7), 6556-6566.

Geotek MSCL manual (http://www.geotek.co.uk/sites/default/files/manual.pdf)

Geyh, M.A., Müller, H., 2005. Numerical ^{230}Th/U dating and palynological review of the Holsteinian/Hoxnian Interglacial. Quaternary Science Reviwes 24, 1861-1872.

Gillet, N. P., Kell, T. D., Jones, P. D. 2006. Regional climate impacts of the Southern Annular Mode. Geophysical Research Letters, Vol 33. Issue 23.

Giresse P, Mvoubou M, Maley J, Ngomanda A., 2009. Late-Holocene equatorial environments inferred from deposition processes, carbon isotopes of organic matter, and pollen in three shallow lakes of Gabon, west-central Africa. Journal of Paleolimnology, 41, 369–392.

Glaser, P. H., 1987. The ecology of patterned boreal peatlands of northern Minnesota: a community profile. US Fish and Wildfire Service Report 85 (7.14), 1-98.

Goldschmidt, V.M., 1954. Geochemistry (ed. A. Muir) Clarendon Press, Oxford, 730 pp.
González-Ferran, O., Mazzuoli, R., Lahsen, A., 2004. In: Centro de Estudios Volcanológicos (Ed.), Geoloía del Complejo Volcánico Isla de Pascua Rapa Nui Santiago-Chile.1:30.000 Geol. map, (in Spanish).

González-Ferran, O., Mazzuoli, R., Lahsen, A., 2004. In: Centro de Estudios Volcanológicos (Ed.), Geoloía del Complejo Volcánico Isla de Pascua Rapa Nui Santiago-Chile.1:30.000 Geol. map, (in Spanish).

Gorham, E., 1991. Northern peatlands: role in the carbon cycle and probable response to climatic warming. Ecological Applications 1, 182–195.

Gorham, E., Janssens, J.J., 2005. The distribution and accumulation of chemical elementsin five peat cores from the mid-continent to the eastern coast of North America. Wetlands 25, 259–278.

Gossen, C. 2007. Report: The mistery lies in the *Scirpus*. Rapa Nui Journal 21 (2), 105-110.

Grant, K. M., Rohling, E. J., Bar-Matthew, M. Ayalon, A. Medina-Elizalde, M., Bronk Ramsey, C., Satow, Roberts, A. P., 2012. Rapid coupling between ice volume and polar temperature over the past 150 kyr. Nature 491, 744–747

Grootjans, A.P., Adema, E.B., Bleuten, W., Joosten, H., Madaras, M., Janáková, M., 2006. Hydrological landscape settings of base-rich fen mires and fen meadows: an overview. Applied Vegetation Science 9, 175–184.

Haase, K. M., and Devey, C. W., 1996. Geochemistry of lavas from the Ahu and Tupa volcanic fileds, Easter Hotspot, southeast Pacific: Implications for intraplate magma genesis near a spreading axis. Earth and Planetary Science Letters 129-143.

Hagelberg, E., Quevedo, S., Turbon, D., Clegg, J.B., 1994. DNA from ancient Easter Islanders. Nature 369, 25-26.

Handley L.L., Austin A.T., Robinson D., Scrimgeour C.M., Raven J.A., Heaton T.H.E., Schmidt S. and Stewart G.R., 1999. The 15N natural abundance (δ^{15}N) of ecosystem samples reflects measures of water availability. Aust. J. Plant Physiol. 26: 185–199.

Hanebuth, T., Stattegger, K., Grootes, P.M., 2000. Rapid flooding of the Sunda Shelf: a late-glacial sea-level record. Science 288, 1033–1035.

Haug, G.H., Hughen, K. A., Sigman, D.M., Peterson, L. C., Röhl, U. 2001. Southward Migration of the intertropical convergence Zone through the Holocene. Science 293, 1304-1308.

Hecky, R. E., H. A. Bootsma, R. M. Mugidde & F. W. B. Bugenyi, 1996. Phosphorus pumps, nitrogen sinks, and silicon drains: plumbing nutrients in the African Great Lakes. In Johnson, T. C. & E. O. Odada (eds.) The Limnology, Climatology and Paleoclimatology of the East African Lakes. Gordon and Breach, Amsterdam: 205–224.

Heijnis, H., van der Plicht, J., 1992. Uranium/Thorium dating of Late Pleistocene deposits in NW Europe, uranium/thorium isotope systematics and open-system behaviour of peat layers. Chemical Geology (Isotope Geoscience Section) 94, 161–171

Heinrich, H. 1988. Origin and consequence of cyclic ice rafting in the northeast Atlantic Ocean during the past 130000 years, Quat. Res., 29, 142–152

Heirman, K. 2011. "A wind of Change". Changes in position and intesity of the Southern Hemisphere Westerlies during Oxygen Isotope Stages 3, 2 and 1. PhD Thesis. University of Gent.

Heiser, C.B., 1974. Totoras, Taxonomy, and Thor, vol. 20 no. 2. Botanical Society of America, Inc.
Hemming, S. R. 2004. Heinrich events: Massive late pleistocene detritus layers of the North Atlantic and their global climate imprint. Rev. Geoph. 42.

Hemming, S. R. 2004. Heinrich events: Massive late pleistocene detritus layers of the North Atlantic and their global climate imprint. *Rev. Geoph.* 42, RG1005,

Henn, M. R., Chapela, I. H., 2000. Differential C Isotope Discrimination by fungi during decomposition of C3 and C4 dervide sucrose. Applied and environmental microbiology. Applied and environmental microbiology. Vol, 66, No. 10, p. 4180-4186.

Herrera, C., Custodio, E., 2008. Conceptual hydrogeological model of volcanic Easter Island (Chile) after chemical and isotopic surveys. Hydrogeology Journal.

Hesse, M., Halbritter, H., Zetter, R., Weber, M., Buchner, R., Frosch-Radivo, A., Ulrich, S., 2009. Pollen Terminology. An illustrated handbook. Springer WienNewYork. 261 pp

Heusser, C. J., 1971.Pollen and spores of chile: modern types of the pteridophyta, gymnospermae and angiospermae. The university of Arizona press. 165 pp.

Heusser, C.J., Heusser, L.E., 2006. Submillennial palynology and palaeoecology of the last glaciation at Taiquemo (50 000 cal yr, MIS 2–4) in southern Chile. Quaternary Science Reviews 25, 446–454.

Heyerdahl, T., Ferdon, E.N., 1961. Reports of the Norwegian archaeological expedition to Easter Island and the East Pacific. Archaeology of Easter Island 1. Forum, Publishing House, Stokholm.

Hillaire-Marcel, C., Aucour, A. M., Bonnefille, R., Riollet, G., Vicens, A., Williamson, D., 1989. ^{13}C/Palynological evidence of differential residence times of organic carbon prior its sedimentation in East African Rift Lakes and peat bogs. Quaternary Science Reviews, Volume 8, Issue 3, pages 207-212.

Hoeve, M. L. and Hendrikse, M. (Eds.) 1998. A study of non-pollen objects in pollen slides the types as described by Dr. Bas van Geel and colleagues. Utrech.

Hong Y. T, H.B. Jiang, T.S. Liu, L.P. Zhou, J. Beer, H.D. Li, X.T. Leng, B. Hong and X.G. Qin,, 2001a. Response of climate to solar forcing recorded in a 6000-year δ18O time series of Chinese peat cellulose, The Holocene 10, pp. 1–7.

Hong, Y.T., Wang, Z.G., Jiang, H.B., Lin, Q.H., Hong, B., Zhu, Y.X., Wang, Y., Xu, L.S., Leng, X.T., Li, H.D., 2001b. A 6000-year record of changes in drought and precipitation in northeastern China based on a 13C time series frompeat cellulose. Earth and Planetary Science Letters 185, 111–119.

Horrocks, M., Wozniak, J.A., 2008. Plant microfossil analysis reveals disturbed forest and mixed-crop, dryland

production system at Te Niu, Easter Island. Journal of Archaeological Science 35, 126–142.

Horrocks, M., Baisden, W.T., Flenley, J., Feek, D., González Nualart, L., Haoa- Cardinali, S., Edmunds Gorman, T., 2012a. Fossil plant remains at Rano Raraku, Easter Island's statue quarry: evidence for past elevated lake level and ancient Polynesian agriculture. Journal of Paleolimnology 48 (4), 767-783.

Horrocks, M., Baisden, W.T., Nieuwoudt, M. K., Flenley, J., Feek, D., González Nualart, L., Haoa- Cardinali, S., Edmunds Gorman, T., 2012b. Microfossils of Polynesian cultigens in lake sediments cores from Rano Kau, Easter Island. Journal of Paleolimnology, Volume 47, Issue 2, pp 185-204.

Huang, Y., Street-Perrott, F.A., Perrott, R.A., Metzger, P., Eglinton, G., 1999. Glacial–- interglacial environmental changes inferred from molecular and compoundspecific δ13C analyses of sediment from Sacred Lake, Mt. Kenya. Geochimica et Cosmochimica Acta 63, 1383–1404.

Huang, R. X., Cane, M. A., Naik, N., Goodman, P. 2000. Global adjustment of the thermocline in response to deepwater formation, Geophys.. Res. Lett., 27, 759 – 762.

Huffman, G. J., Adler, R. F., Bolvin, D. T., Gu, G., Bowman, K. P., Hong, Y., Stocker, E. f., Wolff, D. B. 2007. The TRMM Multisatellite Precipitation Analysis (TMPA): Quasi-global, multiyear, combined-sensor precipitation estimates at fine scales. Journal of Hydrometeorology, 8(1), 38-55.

Hughes, P.D.M. and Barber, K.E., 2003. Mire development across the fen-bog transition on the Teifi floodplain at Tregaron Bog, Ceredigion, Wales, and a comparison with 13 other raised bogs. Journal of Ecology, 91, 253–264.

Hunt, T.L., 2007. Rethinking Easter Island's ecological catastrophe. Journal of Archaeological Science 34, 485-502.

Hunt, T.L., Lipo, C.P., 2009. Revisiting Rapa Nui (Easter Island) "Ecocide". Pacific Science 63 (4), 601-616

Hunter-Anderson, R., 1998. Human vs. climatic impacts: did the Rapa Nui really cut down all those trees? In: Stevenson, C.M., Lee, G., Morin, F.J. (Eds.), Easter Island in Pacific Context: South Seas Symposium Proceedings of the Fourth International Conference on Easter Island and East Polynesia. Easter Island Foundation, Los Osos, CA, pp. 85-99.

Ingolfsson, O., Hjort, C., Berkman, P.A., Bjfrck, S., Colhoun, E., Goodwin, I.D., Hall, B., Hirakawa, K., Melles,M., Mfller, P., Prentice, L., 1998. Antarctic glacial history since the last glacial maximum: an overview of the record on land. Antarctic Science 10, 326–344.

Ise T, Dunn AL, Wofsy SC, Moorcroft PR. 2008. High sensitivity of peat decomposition to climate change through water-table feedback. Nature Geoscience 1: 763-766.

Jackson, S.T., Charman, D. (Eds.), 2010. Special issue on "Peatlands: Paleoenvironments and Carbon Dynamics": PAGES News, vol. 18.

Jenny, B., Valero-Garcés, B.L., Villa-Martinez, R., Urrutia, R., Geyh, M., Veit, H., 2002. Early to mid-Holocene aridity in central Chile and the southern westerlies: the Laguna Aculeo record (34°S). Quaternary Research 58, 160–170.

Johnson, D. M., Hooper, P. R., & Conrey, R. M., 1999. XRF analysis of rocks and minerals for major and trace elements on a single low dilution Li-tetraborate fused bead. Advances in X-ray Analysis, 41, 843-867.

Jolliffe, I. T., 1982. A note on the use of principal components in regression. Applied Statistics, 300-303.

Joosten, H., Clarke, D., 2002. Wise Use of Mires and Peatlands—Background Principles Including a Framework for Decision-Making. International Mire Conservation Group and International Peat Society, Saarijärvi, Finland.

Joosten, H., de Klerk, P. 2007. In search of finiteness: the limits of fine-resolution palynology of Sphagnum peat. The Holocene 17, 7 (2007) pp. 1023-1031.

Hou, X., and Jones, B. T., 2000. Inductively Coupled Plasma-Optical Emission Spectrometry. Encyclopedia of Analytical Chemistry.

Junk, C., Claussen, M. 2011. Simulated climate variability in the región of Rapa Nui during the last millenium. Climate of the Past 7, 579-586.

Kaiser, J., Lamy, F., Hebbeln, D., 2005. A 70-kyr sea surface temperature record off southern Chile (ODP Site 1233). Paleoceanography 20, PA4009. http://dx.doi.org/ 10.1029/2005PA001146.

Kaiser, J., Lamy, F., Arz, H. W., Hebbeln, D., 2007. Dynamics of the millennial-scale sea surface temperature and Patagonian Ice Sheet fluctuations in southern Chile during the last 70 kyr (ODP site 1233). Quaternary international 161, 77-89.

Kaiser, J., Schefub, E., Lamy, F., Mohtadi, M., Hebbeln, D., 2008. Glacial to Holocene changes in sea surface temperature and coastal vegetation in north central Chile: high versus low latitude forcing. Quaternary Science Reviews 27, 2064–2075.

Kessler, W. S., 2006. The circulation of the eastern tropical Pacific: A review, Progress in Oceanography, 69, 181-217.

Kirch, P. V., 1997a. Changing landscapes and sociopolitical evolution in Mangaia, central Polynesia, in Kirch, P. V. and Hunt, T. L. (eds), Historical Ecology in the Pacific Islands, Yale University Press, New Haven, pp. 147–165.

Kirch, P.V., 1997b. Microcosmic Histories: Island Perspectives on "Global" Change. American Anthropologist, New Series, Vol. 99, No. 1 pp. 30-42 Published by: Blackwell Publishing on behalf of the American Anthropological Association Stable

Kirch, P.V., Kahn, J.G., 2007. Advances in Polynesian prehistory: a review and assessment of the past decade (1993-2004). Journal of Archaeological Research 15 (3), 191-238.

Knutti, R., Flückiger, J., Stocker, T., Timmermann, A., 2004. Strong hemispheric coupling of glacial climate through freshwater discharge and ocean circulation. Nature 430, 851–856

Kohfeld, K.E., Harrison, S.P., 2001. DIRTMAP: the geological record of dust. Earth-Science Reviews. 54, 91–114.

Koutavas, A., Lynch-Stieglitz, J., Marchitto Jr., T.M., Sachs, J.P., 2002. El Niño-like pattern in Ice Age Tropical Pacific sea surface temperature. Science 297, 226–230.

Koutavas, A., Menocal, P. B., Lynch-Stieglitz, J. 2006. Holocene trends in tropical Pacific sea surface temperatures and the El Niño-Southern Oscillation. Pages, 13 (3), 22-23.

Krachler, M., Mohl, C., Emons, H., Shotyk, W., 2002. Influence of digestion procedures on the determination of rare earth elements in peat and plant samples by USN-ICP-MS. Journal of Analytical Atomic Spectrometry 17, 844-851.

Krishnaswami, S., Lal, D., Martin, J.M. & Meybeck, M., 1971. Geochronology of lake sediments. Earth and Planetary Science Letters, 11, 407–414.

Kuhry, P., Vitt, D. H., 1996. Fossil carbon/nitrogen as a measure of peat decomposition. Ecology, 77 (1), 1996, pp. 271-275.

Kylander, M. E., Weiss, D. J., Martínez Cortizas, A., Spiro, B., Garcia-Sanchez R., Coles, B. J. 2005 Refining the pre-industrial atmospheric Pb isotope evolution curve in Europe using an 8000 year old peat core from NW Spain. Earth and Planetary Science Letters 240, 467-

Kylander, M.E., Muller, J.,Weiss, D.J.,Wuest, R.A.F., Gallagher, K., Garcia-Sanchez, R., Coles, B.J., 2007. Rare Earth Element and Pb isotope variations in a 55,000 year old peat core from Lynch's Crater (NE Queensland, Australia): applications to paleoclimate in the Southern Hemisphere. Geochimica et Cosmochimica Acta 71 (4), 942–960.

Kylander, M. E., Bindler, R., Martínez Cortizas, A., Gallagher, K., Mörth, C-M, Rauch, S., 2013. A novel geochemical approach to paleorecords of dust deposition and effective humidity: 8500 years of peat accumulation at Store Mosse (the "Great Bog"), Sweden, Quaternary Science Reviews, Volume 69,Pages 69-82.

Lambeck, K., Chappell, J., 2001. Sea level change through the last glacial cycle. Science 292, 679–686.

Lamy, F., Hebbeln, D., Wefer, G. 1998. Late Quaternary precessional cycles of terrigenous sediment input off the Norte Chico, Chile (27.5S) and palaeoclimatic implications. Palaeogeography, Palaeoclimatology, Palaeoecology 141, 233-251.

Lamy, F., Hebbeln, D., Röhl, U., Wefer, G., 2001. Holocene rainfall variability in southern Chile: a marine record of latitudinal shifts of the Southern Westerlies. Earth and Planetary Science Letters 185, 369–382.

Lappalainen, E., 1996: *Global peat resources*, International Peat Society, Finland.

Laskar, J., Robutel, P., Joutel, F., Gastineau, M., Correia, A. C. M., & Levrard, B., 2004. A long-term numerical solution for the insolation quantities of the Earth. *Astronomy & Astrophysics*, *428*(1), 261-285.

Le Roux, G. L., Marshall, W. A., 2011. Constructing recent peat accumulation chronologies using atmospheric fall-out radionuclides. Mires and Peat, Volume 7 (2010/2011). Article 08, 1-14.

Lea, D.W., Pak, D.K., Belanger, C.L., Spero, H.J., Hall, M.A., Shackleton, N.J., 2006. Paleoclimate history of Galápagos surface waters over the last 135,000 yr. Quaternary Science Reviews 25, 1152–1167.

Leduc, G., Vidal, L., Tachikawa, K., Rostek, F., Sonzogni, C., Beaufort, L., Bard, E., 2007. Moisture transport across Central America as a positive feedback on abrupt climatic changes. Nature 445, 908–911.

Leduc, G., Vidal, L., Tachikawa, K., Bard, E. 2009. ITCZ rather than ENSO signature for abrupt climate changes across the tropical Pacific? Quaternary Research 72, 123-131.

Lee, S. Y. and Poulsen, C., J., 2005. Tropical Pacific climate response to obliquity forcing in the Pleistocene. Paleoceanography, Vol. 20, PA 4010.

Leng, M. J. (ed.), 2005. Isotopes in Palaoenvironmental Research. Chapter 4. *Isotopes in lake sediments*. Springer.

Livett, E.A., Lee, J.A. and Tallis, J.H., 1979. Lead, zinc and copper analyses of British blanket peats. J. Ecol., 67: 865-891.

Locarnini, R., Mishonov, A., Antonov, J., Boyer, T., Garcia, H., Baranova, O., Zweng, M., and Johnson, D., 2010. World Ocean Atlas 2009 in Levitus, S. ed. NOAA Atlas NESDIS 68, U.S. Government Printing Office, Washington, D.C.

MacIntyre, F., 2001a. ENSO, climate variability, and the Rapanui: part I. The basics. Rapa Nui Journal 15 (1), 17–26.

MacIntyre, F., 2001b. ENSO, climate variability, and the Rapanui: part II. Oceanography and Rapa Nui. Rapa Nui Journal 15 (2), 83–94.

Mamayev O. 1., 1975. Temperature-salinity analysis of world ocean waters, Elsevier Scientific, Amsterdam-Oxford-New York.

Mandernack K. W., Lynch L., Krouse H. R., and Morgan M. D., 2000. Sulfur cycling in wetland peat of the New Jersey Pinelands and its effect on stream water chemistry. Geochimica and Cosmochimica Acta 23, 3949–3964.

Mann, D., Edwards, J., Chase, J., Beck, W., Reanier, R., Mass, M., Finney, B., Loret, J., 2008. Drought, vegetation change, and human history on Rapa Nui (Isla de Pascua, Easter Island). Quaternary Research 69, 16-28.

Margalef , O. Cañellas-Boltà, N., Pla-Rabes, S., Giralt, S., Pueyo, J. J., Joosten, H., Rull, V., Buchaca, T., Hernández, A., Valero-Garcés, B. L., Moreno, A., Sáez, A. 2013 A 70,000 year geochemical and palaeoecological record of climatic and environmental change from Rano Aroi peatland (Easter Island). Global and Planetary Change, 108: 72-84.

Marnette E. C., Hordijk C. A., Van Breemen N., and Cappenberg Th. E., 1992. Sulfate reduction and S-oxidation in a moorland pool sediment. Biogeochem. 17, 123–143.

Martínez Cortizas, A., García –Rodeja, E., Pontevedra Pombal, X., Nóvoa Muñoz, J. C., Weiss, D., Cheburkin, A. 2002. Atmospheric Pb deposition in Spain during the last 4600 years recorded by two ombrotrophic peat bogs and implications for the use of peat as archive. The Science of the Total Environtment 292, 33-34.

Martínez Cortizas A, Biester H, Mighall T, Bindler R. 2007. Climate-driven enrichment of pollutants in peatlands. Biogeosciences 4: 905-911.

Martinsson-Wallin, H., Crockford, S.J., 2002. Early settlement of Rapa Nui (Easter Island). Asian Perspectives 40 (2), 244-278.

Mauquoy, D., Hughes, P.D., van Geel, B., 2010. A protocol for plant macrofossil analysis of peat deposits. Mires and Peat, Volume 7(2010/2011), Article 6, 1-5.

Mayewski, P.A., Rohling, E.E., Stager, J.C., Karlen, W., Maasch, K.A., Meeker, L.D., Meyerson, E.A., Gasse, F., van Kreveld, S., Holmgren, K., Lee-Thorp, J., Rosqvist, G., Rack, F., Staubwasser, M., Schneider, R.R., Steig, E.J., 2004. Holocene climate variability. Quaternary Research 62, 243–255.

McCall, G., 1993. Little ice age, some speculations for Rapa Nui. Rapa Nui Journal 7 (4), 65-70

McKenzie, J.A., Hollander, D.J., 1993. Oxygen-isotope record in recent carbonate sediments from lake Greifen, Switzerland (1750–1986): application of continental isotopic indicator for evaluation of changes in climate andatmospheric circulation patterns. Climate Change in Continental Isotopic Records, Geophysical Monograph 78, 101–8111.

McLennan, S.M., 1989. Rare earth elements in sedimentary rocks: influence of provenance and sedimentary processes. In: Lipin, B.R., McKay, G.A. (Eds.), Geochemistry and Mineralogy of Rare Earth Elements, vol. 21. Mineralogical Society of America, pp. 169–200.

McPhaden, M. J., 2006. ENSO as an integrating concept in Earth Science. Science 314, 1740-1745.
Meese, D.A., Alley, R.B., Fiacco, R.J. , Germani, M.S., Gow, A.J., Grootes, P.M. , Illing, M., Mayewski, P.A., Morrison, M.C., Ram, M., Taylor, K.C., Yang, Q., and Zielinski, G.A. 1994. Preliminary depth-agescale of the GISP2 ice core. Special CRREL Report 94-1, US.

Medeanic, S., & Silva, M. B., 2010. Indicative value of non-pollen palynomorphs (NPPs) and palynofacies for palaeoreconstructions: Holocene Peat, Brazil. International Journal of Coal Geology, 84(3), 248-257.

Meier-Uhlherr, R., Schulz, C. & Luthardt, V., 2011: Steckbriefe Moorsubstrate. HNE Eberswalde (Hrsg.), Berlin

Meyers P.A. and Ishiwatari R. 1993. Lacustrine organic geochemistry - an overview of indicators of organic matter sources and diagenesis in lake sediments. Org. Geochem. 20: 867–900.

Meyers, P. A. 1994. Preservation of elemental and isotopic source identification of sedimentary organic matter. Chemical Geology 114, 289-302.

Meyers, P. A., Lallier-Vergès, E., 1999. Lacustrine sedimentary organic matter records of Late Quaternary paleoclimates. Journal of Paleolimnology 21: 345-372.

Meyers, P.A., Terranes, J.L., 2001. Sediment organic matter. In: Last, W.M., Smol, J.P. (Eds.), Tracking Environmental Change Using Lake Sediments. : Physical and Geochemical Techniques, 2. Kluwer Academic Publishers, Dordrecht, The Netherlands, pp. 239–269.

Meyers, P. A, 2003. Applications of organic geochemistry to paleolimnological reconstructions: a summary of examples from the Laurentian Great Lakes. Organic Geochemistry 34, 261-289.

Mieth, A., Bork, H.R., 2003. Diminution and degradation of environmental resources by prehistoric land use on Poike Peninsula, Easter Island (Rapa Nui). Rapa Nui Journal 17, 34–41.

Mieth, A., Bork, H.R., 2005. History, origin and extent of soil erosion on Easter Island (Rapa Nui). Catena 63, 244-260.

Mieth, A., Bork, H.R., 2010. Human, climate or introduced rats e which is to blame for the woodland destruction on prehistoric Rapa Nui (Easter Island)? Journal of Archaeological Science 37, 417-426.

Mitchell, E.A.D., Charman, D.J. & Warner, B.G., 2008. Testate amoebae analysis in ecological and paleoecological studies of wetlands: past, present and future. Biodiversity and Conservation, 17, 2115–2137.

Miyajima, T., Wada, E., Hanva, Y. T., Vijarnsorn, P., 1997. Anaerobiv mineralization of indigenous organic matters and methanogenesis in tropical wetland soils. Geochimica and Cosmochimica Acta, Vol. 61. No 17 pp. 3739-375

Molfino, B., McIntyre, A., 1990. Precessional forcing of the nutricline dynamics in the Equatorial Atlantic. Science 249, 766–769.

Monnin, E., Indermühle, A., Dällenbach, A., Flückiger, J., Stauffer, B., Stocker, T. F., Raynaud, D., Barnola, J. M., 2001. Atmospheric CO2 concentrations over the last glacial termination. Science, 291(5501), 112-114.

Montoya, E., 2011. Paleoecology of the southern Gran Sabana (SE Venezuela) since the Late Glacial to the present. PhD Thesis. Universitat Auntònoma de Barcelona.

Montoya, E., Rull, V., Stansell, N.D., Bird, B.W., Nogué, S., Vegas-Vilarrúbia, T., Abbott, M.B., Diaz, W.A. 2011. Vegetation changes in the Neotropical Gran Sabana (Venezuela) around the Younger Dryas Chron. Journal of Quaternary Science 26, 207-218. doi:10.1002/jqs.1445.

Moreno, P.I., León, A.L., 2003. Abrupt vegetation changes during the last glacial to Holocene transition in mid-latitude South America. Journal of Quaternary Science 18, 787–800.

Moy, C. M., Seltzer, G. O., Rodbell, D. T., Andersons, D. M., 2002. Variability of El Niño/Southern Oscillation activity at millennial timescales during the Holocene epoch. Nature. Vol 420, 162- 165.

Mucciarone, D.A., Dunbar, R.B., 2003. Stable isotope record of El Niño-Southern Oscillation events from eastern island. In: Loret, J., Tanacredi, J.T. (Eds.), Easter Island: Scientific Exploration into the World's Environmental Problems in Microcosm. Kluwer Academic/Plenum, New York, pp. 113–132.

Muller, J., 2006. Reconstructing climate change of the last 55 kyr: the Lynch's Crater peat mire record, NE-QLD, Australia. PhD thesis James Cook University.

Muller, J., Wüst, R.A.J., Weiss, D.J., Hu, Y. 2006. Geochemical and stratigraphic evidence of environmental change at Lynch's Crater, Queensland, Australia. Global and Planetary Change 53, 269–277.

Muller, J., Kylander, M.E., Wüst, R.A., Weiss, D.J., Martinez Cortizas, A., LeGrande, N., Jennerjahn, T., Behling, H., Anderson, W. T., Jacobson, G. 2008a. Possible evidence for wet Heinrich phases in tropical NE Australia: the Lynch's Crater desposit.

Muller, J., Kylander, M.E., Martinez Cortizas, A.,Wüst, R.A.,Weiss, D.J., Blake, K., Coles, B.J., Garcia-Sanchez, R., 2008b. The use of principle component analyses in characterizing trace and major elemental distribution in a 55 kyr peat deposit in tropical Australia: implications to paleoclimate. Geochimica et Cosmochimica Acta 72, 449–463.

Myers, R. H., 1990. Classical and modern regression with applications (Vol. 2). Belmont, CA: Duxbury Press.

Newman, M., Compo, G. P., & Alexander, M. A., 2003. ENSO-forced variability of the Pacific Decadal Oscillation. Journal of Climate, *16*(23), 3853-3857.

Norton, S.A. and Henriksen, A., 1983. The importance of CO 2 in evaluation of effects of acidic deposition, Vatten 39: 346-354.

Novák, M., Wieder, R. K., & Schell, W. R., 1994. Sulfur during early diagenesis in Sphagnum peat: Insights from $\delta^{34}S$ ratio profiles in ^{210}Pb-dated peat cores. Limnology and Oceanography, 39, 1172-1172.

Novák, M., Buzek, F., Adamová, M., 1999. Vertical trends in $\delta^{13}C$, $\delta^{15}N$, $\delta^{34}S$ ratios in bulk Sphagnum peat. Soil Biology and Biochemistry 31, 1343-1346.

Novák, M., Buzek, F., Harrison, A. f., Prˇechova, E., Jacˇková, I, Fottová, D., 2003. Similarity between C, N and S stable isotope profiles in European spruce forest soils: implications for the use of $\delta^{34}S$ as tracer.

Nowaczyk, N. R., 2001, Logging of magnetic susceptibility. In Last, W. M., and Smol, J. P. (eds.), Tracking environmental change using lake sediments, vol. 1, Basin analysis, coring, and chronological techniques, p. 155-170. Kluwer Academic Publishers, Dordrecht, Netherlands.

Nunn, P.D., 2000. Environmental catastrophe in the Pacific Islands around A.D. 1300. Geoarchaeology 15 (7), 715-

740.

Nunn, P.D., 2007. Climate, Environment and Society in the Pacific During the Last Millennium. Elsevier, Amsterdam, The Netherlands.

O'Leary, M. H. 1981. Carbon isotope fractionation in plants. Phvtochemistrv 20:553-67

Oksanen, J., Kindt, R., Legendre, P., O'Hara, R.B., 2007. The vegan package. Community Ecology Package. URL http://CRAN.R-project.org/.

Oppo, D.W., Linsley, B.K., Rosental, Y., Dannenmann, S., Beaufort, L. 2003. Orbital and suborbital climate variability in the Sulu Sea, western tropical Pacific, Geochem. Geophys. Geosyst. 4, 20. 1- 20.

Orliac, C. 2000. The woody vegetation of Easter Island between the early 14th and the mid-17th Centuries A.D. In: Stevenson, C., Ayres, W. (Eds.), Easter Island Archaeology: Research on Early Rapanui Culture. Easter Island Foundation, Los Osos.

Orliac, C., Orliac,M., 1998. The disappearance of Easter Island's forest: overexploitation or climatic catastrophe? In: Stevenson, C., Lee, G., Morin, F.J. (Eds.), Easter Island in Pacific Context: South Seas Symposium. : Proceedings of the Fourth International Conference on Easter Island and East Polynesia. Easter Island Foundation, Los Osos, pp. 129–134.

Ortu, E., Brewer, S., Peyron, O, 2006. Pollen-inferred palaeoclimate reconstructions in mountain áreas: problems and persperctives. Journal of quaternary science (2006) 21(6) 615-627.

Paduano, G.M., Bush, M.B., Baker, P.A., Fritz, S.C., Seltzer, G.O., 2003. A vegetation and fire history of Lake Titicaca since the Last Glacial Maximum. Palaeogeography, Palaeoclimatology, Palaeoecology 194, 259–279.

Page, S. E.; Siegert, F., Rieley, J. O., Boehm, H-D. V.; Jaya, A., Limin, S., 2002. The amount of carbon released from peat and forest fires in Indonesia during 1997. Nature 420, 61-65.

Page, S. E., Wüst, R. A., J., Weiss, D., Rieley, J. O., Shotyk, W., Limin S. H., 2004. A record of Late Pleistocene and Holocene carbon accumulation and climate change from an equatorial peat bog (Kalimantan, Indonesia): Implications for past, present and future carbon dynamics. Journal of Quaternary Science, Volume 19, Issue 7 pages 625-635.

Page, S.E., Rieley, J.O., Wüst, R.A.J., 2006. Lowland tropical peatlands of Southeast Asia. In: Martini, I.P., Martinez Cortizas, A., Chesworth, W. (Eds.), Peatlands: Evolution and Records of Environmental and Climate Changes: Developments in Earth Surface Processes, vol. 9.

Page, S., Wüst, R., Banks, C., 2010. Past and present carbon accumulation and loss in Southeast Asian peatlands.

Pahnke, K., Zahn, R., Elderfield, H., & Schulz, M., 2003. 340,000-year centennial-scale marine record of Southern Hemisphere climatic oscillation. *Science*, *301*(5635), 948-952.ce

Pahnke, K., Zahn, R. 2005. Southern Hemisphere water mass conversion linked with North Atlantic Climate Variability, 2005. Science 307, 1741-1746

Pena, L., 2008. Evolución oceanográfica y procesos de teleconexión interlatitudinal en el Pacífico Ecuatorial asociados a los cambios climaticos de ls últimos 275.000 años. PhD thesis. Departament d'Estratigradfia, Paleontologia I geociències Marines. Universitat de Barcelona.

Pena, L. D., Cacho, I., Ferretti, P. and Hall, M. A. 2008. El Niño–Southern Oscillation–like variability during glacial terminations and interlatitudinal teleconnections, Paleoceanography, 23, PA3101, doi:10.1029/2008PA001620

Pena, L. D., Goldstein, S. L., Hemming, S. R., Jones, K. M., Calvo, E., Pelejero, C. and Cacho, I., 2013. Rapid changes in meridional advection of Southern Ocean intermediate waters to the tropical Pacific during the last 30 kyr, Earth and Planetary Science Letters, 368, 20-32.

Peteet, D., Beck, W., Ortiz, J., O'Connell, S., Kurdyla, D., Mann, D., 2003. Rapid vegetational and sediment change from Rano Aroi crater, Easter Island. In: Loret, J., Tanacredi, J.T. (Eds.), Scientific Exploration into the World's

Environmental Problems in Microcosm. Kluwer Academic/Plenum Publ., New York, pp. 81–92.

Peterson, L. C., Haug, G. H., Hughen, K. A. , and Rohl, U. 2000. Rapid changes in the hydrologic cycle of the tropical Atlantic during the last glacial, Science 290, 1947–1951

Plunkett, G.M., Pilcher, J.R., McCormac, F.G., Hall, V.A. 2004. New dates for first millennium BC tephra isochrones in Ireland. The Holocene, 14, 780–786.

Prentice, I. C., Harrison, S. P., & Bartlein, P. J., 2011. Global vegetation and terrestrial carbon cycle changes after the last ice age. New Phytologist, 189 (4), 988-998.

R Development Core Team, 2011. R: a language and environment for statistical computing. R Foundation for Statistical Computing, Vienna, Austria. (http://www.Rproject. org/).

Raask, E., 1984. Creation, capture and coalescence of mineral species in coal flames. J. Inst. Energy 57: 231–239.

Reddy, K. R.; D'Angelo, E. M., 1994. Soil processes regulating water quality in wetlands. In: Global Wetlands: Old World and New (ed. by W. J. Mitsch), pp. 309-324. Elservier, Amsterdam.

Reille, M., 1992. Pollen et spores d'Europe et d'Afrique du Nord. Laboratoire de Botanique historique et Palynologie. Marseille, 1992. 520 pp.

Reimann, C., Filzmoser, P., Garrett, R. G., & Dutter, R., 2008. Principal Component Analysis (PCA) and Factor Analysis (FA). *Statistical Data Analysis Explained: Applied Environmental Statistics with R*, 211-232.

Reimer, P.J., Baillie, M.G.L, Bard, E., Bayliss, A., Beck, J.W., Bertrand, C.J.H, Blackwell, P.G., Buck, C.E., Burr, G.S., Cutler, K.B., Damon, P.E., Edwards, R.L., Fairbanks, R.G., Friedrich, M., Guilderson, T.P., Hogg, A.G., Hughen, K.A., Kromer, B., McCormac, G., Manning, S., Ramsey, C.B., Reimer, R.W., Remmele, S., Southon, J.R., Stuiver, M., Talamo, S., Taylor, F.W., van der Plicht, J., Weyhenmeyer, C.E., 2004. IntCal04 terrestrial radiocarbon age calibration, 0–26 cal kyr BP. Radiocarbon 46, 1029-1058.

Robbins, J.A.,1978. Geochemical and geophysical applications of radioactive lead. In: Nriagu, J.O. (ed.) Biogeochemistry of Lead in the Environment. Elsevier Scientific, Amsterdam, 285–393.

Rose, K. A., Sikes, E. L., Guilderson, T. P., Shane, P., Hill, T. M., Zahn, R., Spero, H. J., 2010. Upper-ocean-to-atmosphere radiocarbon offsets imply fast deglacial carbon dioxide release. Nature, Vol. 466, 1093-1097.

Rose, N.L., 2001. Fly-ash particles. In: Last, W.M. & Smol, J.P. (eds.) Tracking Environmental Change Using Lake Sediments, Vol 2: Physical and Geochemical Methods. Kluwer Academic Publishers, Dordrecht, 319–349.

Rose, N.L. & Appleby, P.G. 2005. Regional applications of lake sediment dating by spheroidal carbonaceous particle analysis I: United Kingdom. Journal of Paleolimnology, 34, 349–361.

Rosenthal, Y., Oppo, D. W., Dannenmann, S., and Linsley, B. K, 2000. Millennial-scale variability in western Pacific sea surface temperatures during glacial and Holocene climates, Eos Trans. AGU, 81(48), F656, Fall Meet. Suppl.

Rosenthal, Y., Oppo, D. W., & Linsley, B. K., 2003. The amplitude and phasing of climate change during the last deglaciation in the Sulu Sea, western equatorial Pacific. Geophysical Research Letters, 30(8), 1428.

Rothwell, R. G. (Ed.). 2006. New techniques in sediment core analysis No. 267. Geological Society.

Routledge, K, 1919. The Mystery of Easter Island. The story of an expedition. London.

Rowe, P.J., Richards, D.A., Atkinson, T.C., Bottrell, S.H., Cliff, R.A., 1997. Geochemistry and radiometric dating of aMiddle Pleistocene peat. Geochimica et Cosmochimica Acta 61, 4201–4211.

Ruddiman, W. F., 2003. Orbital insolation, ice volume, and greenhouse gases, Quat. Sci. Rev., 22, 1597– 1629.

Ruggieri, F., Fernandez-Turiel, J. L., Saavedra, J., Gimeno, D., Polanco, E., Amigo, A., Galindo, G., Caselli, A., 2012. Contribution of volcanic ashes to the regional geochemical balance: The 2008 eruption of Chaitén volcano, Southern Chile. Science of the Total Environment 425, 75-88.

Rull, V., 2005. A middle Wisconsin interstadial in the northern Andes. Journal of South American Earth Sciences, 19(2), 173-179.

Rull, V., Cañellas-Boltà, N., Sáez, A., Giralt, S., Pla, S., Margalef, O., 2010a. Paleoecology of Easter Island: evidence and uncertainties. Earth-Science Reviews 99, 50–60.

Rull, V., Stansell, N. D., Montoya, E., Bezada, M., and Abbott, M. B. 2010b Palynological signal of the Younger Dryas in tropical Venezuelan Andes. Quaternary Science Reviews 29, 3045–3056.

Russell, J. M., and Johnson, T. C., 2007. Little Ice Age drought in equatorial Africa: intertropical convergence zone migrations and El Niño–Southern Oscillation variability. Geology, 35(1), 21-24.

Rydin, H., Jeglum, J., and Jeglum, J. K., 2006. The biology of peatlands. Oxford University Press.

Sáez, A., Valero-Garcés, B., Giralt, S., Moreno, A., Bao, R., Pueyo, J.J., Hernández, A., Casas, D., 2009. Glacial to Holocene climate changes in the SE Pacific. the Raraku Lake sedimentary record (Easter Island, 27°S). Quaternary Science Reviews 28, 2743–2759.

Sandweiss, D. H. et al., 2001. Variation in Holocene El Nino frequencies: Climate records and cultural consequences in ancient Peru. Geology 29, 603–606.

Schirrmeister, L., Oezen, D., Geyh, M. A., 2002. ^{230} Th/U Dating of Frozen Peat, Bol'shoy Lyakhovsky Island (Northern Siberia). Quaternary Research, 57, 253-258.

Schmittner, A. Saenko, O.A. and Weaver, A.J. 2003. Coupling of the hemispheres in observations and simulations of glacial climate change. Quaternary Science Reviews 22: 659-671.

Schneider, N., & Cornuelle, B. D., 2005. The Forcing of the Pacific Decadal Oscillation*. Journal of Climate, 18(21), 4355-4373.

Schuetz L., 1989. Atmospheric mineral dust - Properties and source markers. In M. Leinen & M Sarthein (eds) Paleoclimatology and Paleometeorology: Moedern and Past Patterns of Global Atmospheric Transport. NATO ASI Series, Volume 282, 359-383.

Schulte, E.E., and B.G. Hopkins, 1996. Estimation of soil organic matter by weight-loss-on-ignition. In F.R. Magdoff et al. (eds.) Soil organic matter: analysis and interpretation. SSSA Spec. Publ. 46, Madison, WI.

Servant, M., & Servant-Vildary, S., 2003. Holocene precipitation and atmospheric changes inferred from river paleowetlands in the Bolivian Andes. Palaeogeography, Palaeoclimatology, Palaeoecology, 194(1), 187-206.

Sharp, A., 1970. The Journal of Jacob Roggeven. Oxford University Press, London England.

Shotyk, W., 1986. The Inorganic Geochemistry of Peats and the Physical Chemistry of Waters from some Sphagnum bogs. Ph.D. thesis, University of Western Ontario, London, Canada, 748 pp.

Shotyk W., 1988. Review of the inorganic geochemistry of peats and peatland waters. Earth Science Reviews. 25, 95–176.

Shotyk, W., 1995. Natural and anthropogenic enrichments of As, Cu, Pb, Sb and Zn in ombrotrophic verus minerotrophic peat bog profiles, Jura Mountains, Switzerland. Water Ari Soil Pollution, 90, 375-405.

Shotyk, W., 1996. Peat bog archives of atmospheric metal deposition: geochemical evaluation of peat profiles, natural variations in metal concentrations, and metal enrichment factors. Environmental Reviews, 4(2): 149-183.

Shotyk, W., Weiss, D., Kramers, J.D., Frei, R., Cheburkin, A.K., Gloor, M., Reese, S., 2001. Geochemistry of the peat bog at Etang de la Gruère, Jura Mountains, Switzerland, and its record of atmospheric Pb and lithogenic trace metals (Sc, Ti, Y, Zr, and REE) since 12,370 14C yr BP. Geochimica et Cosmochimica Acta 65, 2337–2360.

Shotyk W, Krachler M, Martínez-Cortizas A, Cheburkin A, Emons H. 2002. A peat bog record of natural, pre-anthropogenic enrichments of trace elements in atmospheric aerosols since 12370 14C yr Bp, and their variation with Holocene climate change. Earth and Planetary Letters 199: 21-37.

Siddall, M., Stocker, T.F., Blunier, T., Spahni, R., McManus, J.F., Bard, E., 2006. Using a maximum simplicity paleoclimate model to simulate millennial variability during the last four glacial cycles. Quat. Sci. Rev. 25, 3185–3197.

Sigman, D. M., Hain, M. P., Haug, G. H., 2010. The polar ocean and glacial cycles in atmospheric CO_2 concentration. Nature. Vol 466, 47-55.

Sjörs, H., 1991. Phyto-and necromass above and below ground in a fen. Ecography, 14 (3), 208-218.

Skinner, L. C., Fallon, S., Waelbroeck, C., Michel, E., Barker, S. 2010. Ventilation of the Deep Southern Ocean and Deglacial CO2 rise. Science 328, 1147-1151

Skrzypek, G., Engel, Z., Chuman, T., & Šefrna, L., 2011. *Distichia* peat—A new stable isotope paleoclimate proxy for the Andes. Earth and Planetary Science Letters, 307(3), 298-308.

Smith, J.T. and Beresford N.A., 2005 Chernobyl: Catastrophe and Consequences. Springer, Berlin, 310 pp

Spratt H. G. and Morgan M. D., 1990. Sulfur cycling in a cedardominated, freshwater wetland. Limnol. Oceanogr. 35, 1586 – 1593.

Środoń, J., Drits, V. A., McCarty, D. K., Hsieh, J. C., & Eberl, D. D., 2001. Quantitative X-ray diffraction analysis of clay-bearing rocks from random preparations. Clays and Clay Minerals, 49(6), 514-528.

Steig, E. J., and R. B. Alley, Phase relationships between Antarctica and Greenland climate records, 2002. Ann. Glaciol., 35, 451– 456.

Steinmann P, Shotyk W. 1997. Chemical composition, pH, redox state of sulfur and iron in complete vertical porewater profiles from two Sphagnum peat bogs, Jura Mountains, Switzerland. Geochimica Cosmochimica Acta 62: 1143-1163.

Stocker, T. F., Johnsen, S., 2003. A minimum thermodynamic model for the bipolar seesaw. Paleoceanography, Vol 18, No. 4, 1087.

Stocker, T. F., The seesaw effect, Science, 282, 61–62, 1998.

Storey, A.A., Ramírez, J.M., Quiroz, D., Burley, D.V., Addison, D.J., Walter, R., Anderson, A.J., Hunt, T.L., Athens, J.S., Huynen, L., Matisoo-Smith, E.A., 2007. Radiocarbon and DNA evidence for a pre Columbian introduction of Polynesian chickens to Chile. Proceedings of the National Academy of Sciences U. S. A. 104, 10335e10339.

Stott, L., Poulsen, C., Lund, S., Thunell, R. 2002. Super ENSO and global climate oscillations at millennial time scales. Science 297, 222-226.

Street-Perrott, F.A., Huang, Y., Perrott, R.A., Eglington, G., Barker, P., Ben Khelifa, L., Harkness, D.D., Olago, D.O., 1997. Impact of lower atmospheric CO2 on tropical mountain ecosystems. Science 278, 1422–1426.

Street-Perrott, F.A., Ficken, K., Huang, Y., Eglinton, G., 2004. Late quaternary changes in carbon cycling on Mt. Kenya, East Africa: an overview of the record in lacustrine organic matter. Quaternary Science Reviews 23, 861–879.

Stuut, J. B., Lamy, F., 2004. Climate variability at the southern boundaries of the Namib (southwestern Africa) and Atacama (northern Chile) coastal deserts during the last 120000 yr. Quaternary Research 62, 301-309.

Succow, M., Joosten, H. 2001. Landschaftsökologische Moorkunde. Stuttgart, Sweizerbart, 622 pp

Suzuki, R., Shimodaira, H., 2013. Package pvclust Version 1.2-2: Hierarchical Clustering with P-Values via Multiscale Bootstrap Resampling. URL: http://www.is.titech.ac.jp/~shimo/prog/pvclust/

Svensson, A., Andersen, K.K., Bigler, M., Clausen, H.B., Dahl-Jensen, D., Davies, S.M., Johnsen, S.J., Muscheler, R., Parrenin, F., Rasmussen, S.O., Ro¨thlisberger, R., Seierstad, I., Steffensen, J.P., Vinther, B.M., 2008. A 60 000 year Greenland stratigraphic ice core chronology. Climate of the Past 4, 47–57.

Swindles, G. T., 2010. Dating recent peat profiles using spheroidal carbonaceous particles (SCPs). Mires and Peat, Volume 7 (2010/2011), Article 03, 1-5.

Swindles, G. T., and Roe, H. M., 2006. Constraining the age of spheroidal carbonaceous particle (SPC) stratigraphies in peats using tephrochronology. Quaternary Newsletter, 110, 2-9.

Swindles, G. T., De Vleeschouwer, F., Plunkett, G., 2010. Dating peat profiles using tephra: stratigraphy, geochemistry and chronology. Mires and Peat Volume 7 (2010/2011), Article 05, 1-9.a

Talbot, M.R. 2001. Nitrogen isotopes in palaeolimnology. Tracking environmental change using lake sediments. Volume 2. Physical and geochemical methods (ed. by W.M. Last and J.P. Smol), pp. 401-439. Kluwer Academic Press, Dordrecht

Talbot, M.R., Johannessen, T., 1992. A high resolution palaeoclimatic record for the last 27,500 years in tropical West Africa from the carbon and nitrogen isotopic composition of lacustrine organic matter. Earth and Planetary Science Letters 110, 23–37.

Tapia, P.M., Fritz, S.C., Baker, P.A., Seltzer, G.O., Dunbar, R.B., 2003. A Late Quaternary diatom record of tropical climatic history from Lake Titicaca (Peru and Bolivia). Palaeogeography, Palaeoclimatology, Palaeoecology 194, 139–164.

Taylor, S.R., McLennan, S.M., 1985. The Continental Crust: Its Composition and Evolution. Blackwell, Oxford.

Thoma, M., Jenkins, A., Holland, D., & Jacobs, S., 2008. Modelling circumpolar deep water intrusions on the Amundsen Sea continental shelf, Antarctica. Geophysical Research Letters, 35(18), L18602.

Thompson, R., and Oldfield, F., 1986, Environmental Magnetism, Allen and Unwin, London, UK, 227.

Tierney, J. E, Russell, J.M, Huang, Y., Sinninghe Damsté, J. S., Hopmans, E. C, Cohen, A. S. 2008. Northern Hemisphere controls on tropical southeast African climate during the past 60.000 years. Science 322, 252-255.

Tillman, P. K., Holzkämper, S., Kuhry, P., Sannel, A. B. K., Loader, N. J., Robertson, I. 2010. Stable carbon and oxygen isotopes in Sphagnum fuscum peat from subarctic Canada: Implications for palaeoclimate studies. Chemical Geology 270, 216-226.

Timmermann, A., Krebs, U. Justino, F., Goosse, H., and Ivanochko, T. 2005. Mechanisms for millennial-scale global synchronization during the last glacial period, Paleoceanography, Volume 20, Issue 4.

Timmermann, A., Lorenz, S. J., An, S. I., Clement, A., Xie, S. P., 2007. The effect of orbital forcing on the mean climate and variability of the tropical Pacific. American Meteorological Society, Vol 20, pp: 4147-4159.

Toggweiler, J. R., Dixon, K., Broecker, W. S., 1991. The Peru upwelling ventilation of the south Pacific thermocline. Journal of Geophysical Research, 96, 20467-20497.

Toggweiler, J. R., Russell, J. L., and Carson, S. R. 2006, Midlatitude westerlies, atmospheric CO_2, and climate change during the ice ages, Paleoceanography, 21, 1-15.

Tomezak, M., Godfrey, J. S., 2001. Regional Oceanography: An introduction, 383 pp. Pergamon Press, London.

Tryon, A. F., Lugardon., 1991. Spores of the Pteridophyta. Springer-Verlag New York. 648pp

Tsuchiya, M. Lukas, R., Fine, R. A., Firing, E., Lindstrom, E. J., 1989. Source waters of the Pacific Equatorial Undercurrent Progress in Oceanography, 23, 101-147.

Tudhope, A. W., Chilcott, C. P., McCulloch, M. T., Cook, E., R., Chappell, J., Ellam, R. M., Lea, D. W., Lough, J. M., Shimmield, G. B., 2001. Variability in the El Niño-Southern Oscillation through a Glacial-Interglacial cycle. Science,

Vol. 291, 1511-1517.

Turney, C. S., Kershaw, A. P., Clements, S. C., Branch, N., Moss, P. T., Fifield, L., K., 2004. Millennial and orbital variations of El Niño/Southern Oscillation and hihg-latitude climate in the last glacial period. Nature, Vol 428, 306-310.

Twiddle, C., L., 2012. Pollen Analysis: Not just a qualitative tool. Geomorphological Techniques, Chap. 4, Sec. 1. 4. British Society for Geomorphology.

Tyson, 1995. Sedimentary organic matter: organic facies and palynofacies. Chapman and Hall, London.

Valero-Garcés, B. L., Jenny, B., Rondanelli, M., Delgado-Huertas, A., Burns, S. J., Veit, H., Moreno, A., 2005. Palaeohydrology of Laguna Tagua Tagua (34º 30' S) and moisture fluctuations in Central Chile for the last 46000 yr. 20 (7-8) 625-641.

Van der Kaars, S., Penyy, D., Tibby, J., Fluin, J., Dam, R. A. C., Suparan, P., 2001. Late quaternary palaecology, palynology and palaeolimnology of a tropical swamp: Rawa Danau, West-Java, Indonesia. Palaeogeography, Palaeoclimatology, Palaeoecology, Volume 171, Issues 3-4, pages 185-212.

Van Geel, B., Bohncke, S. J. P., Dee, H., 1980. A Palaeoecological study of an upper late glacial and Holocene sequence from "de borchert", the Netherlands. Review of Palaeobotany and Palynology, 31: 367-448.

Van Geel, B. 2001. Non-pollen palynomorphs, In: Smol J.P., Birks, H.J.B. and Last, M. (Eds.), Tracking environmental change using lake sediments. Vol. 3: Terrestrial, algal, and siliceous indicators. Kluwer, Dordrecht, pp. 99-119.

Van Geel, B., Buurman, J. and Waterbolk, H.T., 1996. Archaeological and palaeoecological indications of an abrupt climate change in the Netherlands and evidence for climatological teleconnections around 2650 BP. Journal of Quaternary Science, 11, 451–460.

Van Geel, B., Heusser, C.J., Renssen, H., Shuurmans, C.J.E., 2000. Climatic change in Chile at around 2700 BP and global evidence for solar forcing: a hypothesis. The Holocene 10, 659–664.

Van Tilburg, J.A., 1994. Easter Island: Archaeology, Ecology and Culture. British Museum Press, London.

Vargas, P., Cristino, C., Izaurieta, R., 2006. 1000 años en Rapa Nui. Arqueología de asentamiento. Ed. Universitaria, Santiago.

Vellinga, M., Wood, R. A., & Gregory, J. M., 2002. Processes governing the recovery of a perturbed thermohaline circulation in HadCM3. Journal of Climate, *15*(7), 764-780.

Vincent, E., Lengaigne, M., Menkes, C. E., Jourdain, N. C., Marchesiello, P., Madec, G., 2009. Interannual vairiability of the South Pacific Convergence Zone and implications for tropical cyclone genesis. Clim Dyn. 36, 1881-1896

Waliser, D. E., and Somerville, R. C., 1994. Preferred latitudes of the intertropical convergence zone. Journal of the atmospheric sciences, 51(12), 1619-1639.

Wang, X., Auler, A. S., Edwards, R. L., Cheng, H., Cristalli, P. S., Smart, P. L., Richards, D. A., and Shen, C.-C. 2004. Wet periods in northeastern Brazil over the past 210 kyr linked to distant climate anomalies. Nature 432, 740 – 743.

Wang, C.; Fiedler, P. C., 2006. ENSO variability and the Eastern tropical Pacific: A review. Progress in Oceanography 69. pp 239-266.

Wang, X., Auler, A. S., Edwards, R. L., Cheng, H., Ito, E., Wang, Y., Kong, X., Solheid, M. 2007. Millennial-scale precipitation changes in southern Brazil over the past 90,000 years, Geophysical Research Letters, Vol. 34, 1-5.

Weber, C.A., 1930. Grenzhorizont und älterer Sphagnumtorf. Abhandlungen Naturwissenschaftlicher Verein Bremen 28, 57–65.

Weiss, D., Shotyk, W., Rieley, J.O., Page, S.E., Gloor, M., Reese, S., Cortizas-Martínez, A., 2002. The geochemistry of major and selected trace elements in a forested peat bog, Kalimantan, SE Asia, and its implications for past

atmospheric dust deposition. Geochimica et Cosmochimica Acta 66, 2307–2323.

Weninger, B., Jöris, O., Danzeglocke, U. 2008. CalPal-2007. Cologne Radiocarbon Calibration & Palaeoclimate Research Package.

Wheeler, B. D. , 199. Water and plants in freshwater wetlands. In: Ecohydrology (ed. By A. J. Baird and R. L. Wilby), pp. 127-180. Routledge, London.

Whitlock, C. and Larsen,C. 2001. Charcoal as a fire proxy. In: Smol J.P., Birks, H.J.B. and Last, W.M. (Eds.), Tracking environmental change using lake sediments. Vol. 3: Terrestrial, algal, and siliceous indicators. Kluwer, Dordrecht, pp. 75-98.

Wieder, R. K., & Lang, G. E., 1988. Cycling of inorganic and organic sulfur in peat from Big Run Bog, West Virginia. Biogeochemistry, *5*(2), 221-242.

Wilmshurst, J. M., Hunt, T. , Lipo, C.P. , Anderson, A. J. 2011. High-precision radiocarbon dating shows recent and rapid initial human colonization of East Polynesia. PNAS 108, 1815-1820.

Wolfe, B. B., T. W. D. Edwards & R. Aravena, 1999. Changes in carbon and nitrogen cycling during tree-line retreat recorded in the isotopic content of lacustrine organic matter, western Taimyr Peninsula, Russia. The Holocene 9: 215–222.

Wood, J. M., Tataryn, D. J., & Gorsuch, R. L., 1996. Effects of under-and overextraction on principal axis factor analysis with varimax rotation. *Psychological Methods*, *1*(4), 354.

Wüst, R. A. J., Bustin, R. M., 2004. Late Pleistocene and Holocene development of the interior peat-accumulating basin of tropical Tasek Bera, Peninsular Malaysia. Palaeogeography, Palaeoclimatology, Palaeoecology. Volume 211, Issues 3-4, Pages 241-270.

Wüst, R., A. J.; Jacobsen, G. E., van der Gaast, H., Smith, A. M., 2008. Comparison of Radiocarbon ages from different organic fractions in tropical peat cores: insights from Kalimantan, Indonesia. Radiocarbon, Vol 50, nº 3, p. 359-372.

Xie, S.P. 1994. On the genesis of the equatorial annual cycle, Journal of Climate., 7, 2008 – 2013.

Yu, Z., Campbell, I.D., Campbell, C., Vitt, D.H., Bond, G.C. & Apps, M.J., 2003. Carbon sequestration in western Canadian peat highly sensitive to Holocene wet-dry climate cycles at millennial time scales. The Holocene, 13, 801.–808.

Yuan, X. 2004. ENSO-related impacts on Antarctic sea ice: A synthesis of phenomenon and mechanisms. Antarct. Sci., 16, 415–425, doi:10.1017/S0954102004002238.

Zebiak, S. E., and Cane, M. A., 1987. A model El Niño-Southern Oscillation. Monthly Weather Review, 115, 2262-2278.

Zhang, R., Delworth, L. T. 2005. Simulated Tropical Response to a Substantial Weakening of the Atlantic Thermohaline Circulation. American Meterorological Society 18. 1853-1860

Zizka, G., 1991. Flowering plants of Easer Island. Palmarum Hortus Francofurtensis Scientific Reports, 3, pp. 1–108.

Zoltai SC, Johnson JD. 1985. Development of a treed bog island in a minerotrophic fen. Canadian Journal of Botany 63: 1076-1085.

http://www.atmos.colostate.edu/ao/introduction.html

APPENDICES

Table A. 1. ^{14}C AMS radiocarbon ages measured in pollen-enriched extract of Rano Aroi core samples. Rejected ages marked with an asterisk

Sample Name	Depth (cm)	Fraction dated	Dates	Calibrated ages (yr. BP)
ARO 06 01				
ARO 01-01 03	238	pollen concentrate	*2580±30**	*2730±30 **
ARO 01-01 20	255	pollen concentrate	9460±50	10690 ± 120 BP
ARO 01-01 50	285	pollen concentrate	12150±60	13995±153
ARO 01-01 70	305	pollen concentrate	12880±70	14505±483
ARO 01-01 92	327	pollen concentrate	13800±60	16910 ± 180 BP
ARO 01-01 103	338	pollen concentrate	*7440±50**	*8270±80**
ARO 01-01 143	378	pollen concentrate	26960 ±150	31742±80
ARO 01-02 23	421	pollen concentrate	*12070±60**	*13923±138**
ARO 01-02 31.5	431.5	pollen concentrate	34000±500	39431±1051
ARO 01-02 53	453	pollen concentrate	35300±600	40190±970
ARO 01-03 57	552	pollen concentrate	37600±600	42210±520
ARO 01-04 62	662	pollen concentrate	33900±500	39310±2570
ARO 01-05 67	760	pollen concentrate	45000±2000	48710±2570
ARO 01-06 72	872	pollen concentrate	49000±3000	54600±5000
ARO 01-07 83	979	pollen concentrate	52000±4000	57339.09
ARO 01-08 83	1083	pollen concentrate	>50000	60843.14
ARO 01-09 88	1181	pollen concentrate	53000± 4000	64145.02
ARO 01-10 88	1288	pollen concentrate	>49000	67750.15
ARO 01-11 88	1380	pollen concentrate	49000±3000	70849.88
ARO 08 02				
ARO 02-02 35	85	pollen concentrate	270±30	307±25
ARO 02-03 25	125	pollen concentrate	1050±30	965±41
ARO 02-04 25	175	pollen concentrate	2265±30	2206±48
ARO 02-0 38	194	pollen concentrate	5070±40	5820±92
ARO 02-05 25	225	pollen concentrate	9180±50	10339±100
ARO 02-06 31	281	pollen concentrate	12420±60	14501±350
ARO 02-07 25	325	pollen concentrate	13880±70	14921±100
ARO 02-08 25	375	pollen concentrate	30300±300	34475±232

Table A.2. Geochemical proxies analyzed over bulk peat in **ARO 06 01** core: TC, TN, TS (in percentages), C/N ratio, and $\delta^{13}C$, $\delta^{15}N$, $\delta^{34}S$ (‰).

Depth (cm)	Age (years BP)	TC (%)	δ13C (‰)	δ13Cres (‰)	C/N	TN (%)	δ15N (‰)	TS(%)	δ34S (‰)
235	8487	55.29	-21.00	-	63.66	1.01	5.71	-	-
240	9038	54.47	-21.26	-	61.11	1.04	5.02	-	-
245	9588	52.16	-22.63	-	73.80	0.82	3.68	-	-
250	10139	51.09	-22.69	-	90.57	0.66	1.06	-	-
255	10690	54.26	-23.44	-	80.93	0.78	2.62	-	-
260	11241	52.69	-22.38	-	63.40	0.97	2.51	-	-
265	11792	55.65	-22.90	-	67.26	0.97	1.15	-	-
270	12343	53.64	-22.84	-	56.83	1.10	1.60	-	-
275	12893	43.71	-23.05	-	48.58	1.05	1.66	-	-
280	13444	55.57	-24.30	-0.42	55.15	1.18	1.70	-	-
285	13995	55.73	-24.76	-0.68	57.52	1.13	1.29	-	-
290	14122	43.98	-25.24	-0.89	51.82	0.99	1.60	-	-
295	14250	63.52	-24.97	-0.51	87.65	0.85	0.45	-	-
300	14377	54.60	-25.44	-0.92	63.77	1.00	0.71	0.66	16.35
305	14505	49.02	-26.46	-1.92	64.24	0.89	0.30	0.55	17.85
310	15168	53.43	-25.93	-1.27	62.47	1.00	0.65	0.66	17.50
315	15719	50.62	-25.74	-0.98	77.83	0.76	0.13	0.50	18.46
320	16270	56.62	-24.35	0.55	46.34	1.43	2.30	0.48	20.43
325	16821	51.26	-24.25	0.79	45.41	1.32	2.01	0.47	20.62
330	17782	57.79	-24.97	0.07	61.29	1.10	1.25	0.48	16.63
335	19237	59.33	-26.24	-1.16	56.71	1.22	2.17	0.39	19.89
340	20691	53.20	-24.87	0.19	40.16	1.55	6.93	0.44	19.31
345	22145	43.84	-23.71	1.36	54.95	0.93	0.15	0.58	20.74
350	23599	62.14	-23.80	1.21	84.20	0.86	-0.79	0.45	18.20
355	25053	56.27	-24.66	0.25	59.88	1.10	0.07	0.61	18.89
360	26507	49.07	-24.93	-0.11	70.90	0.81	-0.45	0.54	15.44
365	27961	48.94	-25.50	-0.74	69.77	0.82	-0.52	0.55	17.68
370	29415	50.84	-25.63	-0.84	67.97	0.87	0.42	0.52	20.24
375	30870	56.51	-24.39	0.42	57.02	1.16	1.52	0.58	19.12
380	32029	54.34	-25.36	-0.52	50.94	1.24	2.27	-	19.00
385	32748	52.99	-25.00	-0.17	54.25	1.14	1.64	0.52	18.26
390	33467	57.59	-25.05	-0.19	62.26	1.08	1.34	0.47	17.70
400	34904	55.53	-24.30	0.61	58.61	1.11	1.20	0.49	17.95
405	35622	51.04	-24.52	0.44	53.20	1.12	1.53	0.45	16.48
410	36341	54.31	-24.30	0.64	55.01	1.15	1.85	0.41	17.98
415	37060	48.73	-24.65	0.26	43.31	1.31	0.61	0.32	17.08
420	37778	52.62	-24.88	-0.08	51.47	1.19	1.86	0.36	18.32
425	38497	51.32	-24.60	0.13	55.56	1.08	1.65	0.35	19.32
430	39215	55.71	-25.59	-0.86	68.43	0.95	1.96	0.54	18.35
435	39555	46.64	-26.04	-1.42	63.40	0.86	1.37	0.53	20.05
440	39731	53.03	-25.35	-0.89	68.34	0.91	1.17	0.31	19.93
445	39908	58.91	-24.82	-0.60	77.95	0.88	0.54	0.52	20.52
450	40084	48.74	-24.68	-0.61	64.36	0.88	-2.04	0.50	18.48
455	40231	60.93	-24.29	-0.36	73.67	0.96	-0.06	0.46	19.58
460	40333	49.67	-24.30	-0.52	72.63	0.80	0.66	0.49	19.28
465	40435	58.50	-23.41	0.28	73.11	0.93	1.25	0.43	18.62
470	40537	54.31	-24.27	-0.66	67.62	0.94	0.98	0.46	19.37
475	40639	51.13	-24.40	-0.87	63.59	0.94	1.20	0.47	18.92
480	40741	56.40	-23.30	0.12	61.81	1.06	1.25	0.41	18.41
485	40843	52.87	-22.07	1.24	67.28	0.92	0.46	0.36	19.67
490	40945	47.10	-20.49	2.77	70.77	0.78	2.60	0.39	17.93
495	41047	66.16	-21.38	1.82	72.72	1.06	1.45	0.35	17.89

Depth (cm)	Age (years BP)	TC (%)	δ13C (‰)	δ13Cres (‰)	C/N	TN (%)	δ15N (‰)	TS(%)	δ34S (‰)
495	41047	59.33	-21.84	1.25	70.02	0.99	1.48	0.33	20.23
500	41149	53.93	-21.46	1.56	70.32	0.89	1.32	0.37	19.97
505	41251	62.20	-22.97	0.10	76.94	0.94	1.47	0.38	20.03
510	41353	58.72	-23.30	-0.10	83.55	0.82	0.40	0.39	20.01
515	41455	58.18	-23.06	0.21	78.98	0.86	1.23	0.39	19.54
520	41557	58.60	-23.62	-0.34	77.97	0.88	0.62	0.44	19.99
525	41659	57.48	-23.87	-0.51	81.63	0.82	0.60	0.42	20.01
530	41761	57.35	-24.41	-0.93	68.12	0.98	1.92	0.41	22.21
535	41863	56.68	-23.71	-0.07	75.16	0.88	1.30	0.15	19.81
540	41965	60.33	-22.54	1.25	64.55	1.09	2.73	0.39	17.75
545	42067	57.87	-23.01	0.92	65.44	1.03	2.00	-	-
550	42169	59.22	-25.27	-1.30	58.69	1.18	1.85	0.43	19.91
555	42304	56.21	-25.77	-1.64	53.76	1.22	2.15	-	-
560	42460	62.79	-25.66	-1.65	60.66	1.21	1.15	0.12	20.73
565	42616	53.24	-24.55	-0.69	64.35	0.97	1.00	-	-
570	42773	60.99	-24.82	-1.25	73.21	0.97	-0.82	0.25	20.65
575	42929	55.71	-24.44	-1.14	61.61	1.06	0.47	0.10	20.89
580	43085	50.64	-23.39	-0.34	62.44	0.95	-0.16	-	19.31
585	43241	57.53	-24.35	-1.38	60.89	1.10	-0.37	0.04	21.10
590	43398	55.12	-24.55	-1.66	60.97	1.05	0.29	0.35	20.85
600	43710	54.80	-22.10	0.55	53.35	1.20	2.30	0.20	20.35
605	43866	57.22	-26.02	-3.77	54.12	1.23	2.23	-	-
610	44023	49.43	-21.02	0.77	44.79	1.29	2.78	-	-
620	44335	55.30	-20.30	1.02	76.33	0.80	1.10	0.08	21.44
625	44491	55.50	-18.00	2.92	62.48	1.00	1.30	0.03	22.70
630	44648	54.00	-18.80	1.74	71.84	0.90	1.10	0.12	20.04
635	44804	55.30	-19.70	0.72	63.76	1.00	1.30	0.33	21.04
640	44960	52.90	-22.20	-2.02	111.15	0.60	1.20	0.36	20.67
645	45116	54.70	-21.00	-1.06	67.53	0.90	1.80	0.36	21.74
650	45273	53.90	-18.40	1.21	53.96	1.20	2.70	0.44	20.82
655	45429	55.60	-17.70	1.68	52.98	1.20	2.40	0.39	15.83
665	45741	55.90	-16.99	1.91	46.25	1.20	2.25	0.13	19.51
670	45898	56.60	-16.68	2.08	49.97	1.20	2.06	0.16	19.78
675	46054	56.50	-17.08	1.55	53.83	1.10	1.81	0.46	22.29
680	46210	55.50	-17.63	0.96	44.43	1.30	2.82	0.28	21.26
685	46366	56.30	-22.08	-3.63	42.41	1.30	1.53	0.22	21.87
690	46523	55.50	-18.84	-0.65	41.51	1.30	2.62	0.22	18.56
693	46616	54.90	-19.84	-2.00	43.29	1.40	2.72	0.28	21.23
698	46773	52.12	-18.20	-0.62	43.91	1.39	3.92	0.61	21.60
703	46929	51.95	-17.73	-0.28	43.74	1.39	3.10	0.61	20.02
708	47085	50.72	-16.88	0.55	49.42	1.20	2.98	0.72	21.93
713	47241	54.55	-18.39	-0.87	42.85	1.49	3.66	0.54	20.94
718	47398	50.85	-17.83	-0.30	39.93	1.49	4.26	0.57	21.08
728	47710	59.67	-17.24	0.27	48.54	1.43	3.48	0.42	15.79
733	47866	52.89	-16.08	1.35	47.28	1.31	3.71	0.49	14.71
738	48023	53.10	-14.87	2.23	54.41	1.14	4.09	0.52	15.28
743	48179	49.98	-15.49	1.46	46.01	1.27	2.90	0.39	20.75
748	48335	55.46	-15.98	0.71	48.79	1.33	3.35	0.36	19.81
753	48491	53.16	-16.11	0.40	50.16	1.24	2.62	0.49	14.23
758	48648	49.85	-17.29	-0.87	55.24	1.05	2.39	0.37	19.79
763	48868	54.44	-18.65	-2.32	57.57	1.10	1.43	0.56	19.49
768	49131	55.65	-16.85	-0.69	49.24	1.32	2.94	0.68	16.76
773	49394	50.37	-16.64	-0.62	49.54	1.19	3.33	0.56	17.37
778	49657	53.20	-16.09	-0.19	47.38	1.31	3.79	0.49	17.60

Depth (cm)	Age (years BP)	TC (%)	δ13C (‰)	δ13Cres (‰)	C/N	TN (%)	δ15N (‰)	TS(%)	δ34S (‰)
783	49920	51.09	-15.91	0.01	53.15	1.12	3.41	0.18	17.73
800	50814	50.05	-16.00	-0.01	49.06	1.19	4.14	0.52	17.76
805	51077	52.76	-14.82	1.20	49.54	1.24	4.43	0.46	17.43
810	51339	52.53	-14.92	1.19	49.88	1.23	4.44	0.48	17.68
815	51602	51.79	-15.96	0.28	43.39	1.39	4.61	0.50	17.95
820	51865	51.67	-15.19	1.06	48.94	1.23	4.28	0.48	16.09
825	52128	52.39	-15.05	1.08	41.71	1.47	5.48	0.55	17.86
830	52391	53.37	-15.24	0.88	48.71	1.28	3.29	0.55	17.74
835	52654	51.39	-15.02	1.21	43.26	1.39	5.21	0.69	17.44
840	52917	51.02	-16.35	-0.07	46.24	1.29	3.77	0.74	15.68
845	53180	52.02	-16.21	0.01	42.00	1.44	4.10	0.62	16.36
850	53443	52.29	-16.06	0.07	42.24	1.44	4.13	0.34	16.60
855	53706	52.72	-17.69	-1.56	40.51	1.52	3.29	0.74	17.23
860	53969	51.90	-18.55	-2.47	34.50	1.76	5.55	0.58	17.28
865	54232	52.25	-17.56	-1.57	40.76	1.50	3.27	0.62	15.85
870	54495	49.38	-16.32	-0.38	35.66	1.62	5.88	0.64	16.59
875	54663	51.57	-16.64	-0.75	40.28	1.49	5.29	0.63	16.94
880	54832	54.90	-18.83	-3.01	39.74	1.65	5.26	0.56	16.97
885	55000	54.90	-17.04	-1.28	34.55	1.57	4.27	0.50	16.32
890	55169	54.90	-14.73	0.93	54.76	1.08	3.35	0.78	17.85
895	55337	55.50	-14.33	1.24	54.13	1.13	2.63	0.88	18.49
896	55371	55.10	-14.72	0.78	54.67	1.11	2.91	0.86	17.50
901	55539	56.10	-13.98	1.32	52.14	1.14	2.92	0.65	17.32
906	55708	56.30	-14.31	0.80	57.08	1.09	2.70	0.58	18.28
911	55876	55.10	-14.20	0.76	51.02	1.23	3.74	0.71	17.88
916	56045	57.23	-14.07	0.82	50.92	1.31	4.14	0.48	17.44
921	56213	59.78	-13.91	1.01	55.06	1.27	4.62	0.37	18.51
926	56382	58.66	-13.87	0.79	53.12	1.29	5.55	0.36	17.87
931	56550	59.29	-14.59	-0.09	55.40	1.25	4.54	0.29	16.75
936	56719	55.07	-14.35	0.10	61.30	1.05	3.50	0.39	18.68
941	56887	64.63	-14.76	-0.32	56.88	1.33	3.34	0.45	18.44
946	57055	60.03	-14.03	0.40	67.08	1.04	2.27	0.49	19.64
951	57224	55.85	-14.85	-0.41	63.33	1.03	2.10	0.25	14.70
956	57392	58.03	-14.63	-0.20	64.27	1.05	1.97	0.58	17.92
961	57561	67.46	-15.03	-0.57	61.40	1.28	2.87	0.76	17.72
966	57729	54.82	-17.29	-2.79	42.39	1.51	3.56	1.00	17.08
971	57898	54.73	-13.91	0.62	52.39	1.22	2.99	0.49	16.33
976	58066	63.42	-13.87	0.67	57.89	1.28	2.47	0.49	17.20
981	58235	57.27	-13.78	0.77	55.46	1.20	3.44	0.43	18.71
1000	58875	60.29	-14.30	0.41	61.02	1.15	3.40	0.47	18.52
1005	59043	56.08	-14.35	0.56	57.06	1.15	3.84	0.43	18.79
1010	59212	58.35	-14.28	0.88	55.14	1.23	3.60	0.40	18.65
1015	59380	60.75	-14.09	1.15	52.93	1.34	4.29	0.39	20.65
1020	59549	59.20	-14.78	0.48	52.94	1.30	3.50	0.44	19.12
1025	59717	55.74	-14.76	0.45	52.45	1.24	3.43	0.69	18.98
1030	59886	58.11	-14.50	0.55	55.77	1.22	4.01	0.53	18.13
1035	60054	59.57	-14.11	0.96	57.37	1.21	4.15	0.55	18.35
1040	60223	59.46	-14.84	0.23	59.40	1.17	4.75	0.71	20.87
1045	60391	57.53	-17.38	-2.25	47.04	1.43	4.35	0.44	18.91
1050	60560	57.13	-18.44	-3.32	46.58	1.43	3.73	0.91	19.04
1055	60728	56.43	-18.84	-3.73	46.63	1.41	3.57	1.02	19.06
1060	60896	58.65	-16.41	-1.32	49.66	1.38	4.72	0.79	19.38
1065	61065	57.24	-14.91	0.18	52.71	1.27	6.50	0.67	19.38

Depth (cm)	Age (years BP)	TC (%)	δ13C (‰)	δ13Cres (‰)	C/N	TN (%)	δ15N (‰)	TS(%)	δ34S (‰)
1075	61402	58.03	-14.14	0.87	58.41	1.16	8.18	0.53	19.20
1080	61570	55.04	-14.29	0.70	55.30	1.16	8.88	0.54	18.69
1085	61739	63.52	-14.01	0.99	71.43	1.04	5.75	0.90	18.04
1093	62008	58.81	-14.77	0.19	57.41	1.20	7.86	0.90	18.04
1098	62177	57.88	-14.21	0.57	53.35	1.27	3.88	0.83	18.07
1103	62345	59.34	-14.20	0.36	56.07	1.23	3.49	0.76	18.81
1108	62514	54.38	-13.80	0.50	54.79	1.16	3.03	0.69	17.75
1113	62682	54.37	-14.08	0.13	65.09	0.97	2.20	0.76	18.05
1118	62851	66.69	-14.03	0.15	65.32	1.19	2.33	0.72	18.12
1123	63019	59.77	-13.98	0.18	73.23	0.95	1.34	0.78	18.96
1128	63188	57.87	-14.15	0.03	61.98	1.09	1.89	0.72	18.70
1133	63356	60.00	-14.26	-0.07	60.24	1.16	2.32	0.81	18.19
1138	63524	48.61	-14.08	0.13	62.53	0.91	1.14	0.69	17.96
1143	63693	69.06	-14.01	0.20	65.47	1.23	2.12	0.74	17.94
1148	63861	56.69	-14.23	-0.02	58.20	1.14	2.26	0.78	17.22
1153	64030	61.03	-13.90	0.33	65.34	1.09	1.15	0.90	16.69
1158	64198	54.99	-14.77	-0.50	62.85	1.02	0.71	0.88	17.08
1163	64367	62.07	-14.25	0.04	67.07	1.08	0.77	0.81	18.93
1168	64535	50.50	-13.84	0.46	44.62	1.32	3.45	0.77	17.48
1173	64704	53.44	-14.52	-0.22	56.49	1.10	1.90	0.85	17.29
1178	64872	59.03	-14.49	-0.17	57.51	1.20	2.47	0.81	17.83
1183	65041	62.88	-14.36	-0.06	55.19	1.33	3.14	0.77	18.29
1210	65950	55.85	-14.74	-0.43	55.82	1.17	4.50	0.81	17.33
1215	66119	56.82	-14.27	0.03	51.73	1.28	5.35	0.86	18.61
1220	66287	53.79	-14.53	-0.24	50.53	1.24	5.42	0.79	18.43
1225	66456	57.11	-14.65	-0.36	54.04	1.23	5.37	0.73	18.06
1230	66624	57.80	-14.38	-0.14	53.91	1.25	7.46	0.75	18.30
1235	66793	55.67	-14.20	0.03	55.68	1.17	8.09	0.67	18.00
1240	66961	57.75	-14.02	0.22	55.95	1.20	8.79	0.74	17.86
1245	67130	50.47	-14.60	-0.38	52.93	1.11	6.50	0.87	17.62
1250	67298	52.76	-13.91	0.30	52.05	1.18	3.73	0.67	17.92
1255	67467	56.70	-14.25	-0.02	56.13	1.18	2.47	0.61	18.53
1260	67635	56.97	-13.86	0.35	61.31	1.08	2.31	0.77	19.20
1265	67803	48.84	-13.95	0.31	63.56	0.90	0.91	0.49	19.99
1270	67972	65.34	-13.97	0.27	67.24	1.13	1.99	0.40	19.57
1275	68140	60.71	-13.85	0.38	66.43	1.07	1.76	0.25	18.43
1280	68309	49.47	-13.96	0.26	55.42	1.04	1.89	0.48	18.69
1285	68477	60.13	-14.12	0.10	65.34	1.07	2.11	0.42	19.53
1290	68646	59.65	-14.01	0.23	64.13	1.09	2.13	0.42	17.03
1292	68713	50.06	-14.39	-0.16	62.52	0.93	1.39	0.85	17.34
1297	68882	42.22	-14.64	-0.37	58.90	0.84	1.77	0.90	18.54
1302	69050	42.21	-14.50	-0.19	60.29	0.82	1.52	0.74	18.32
1307	69219	44.69	-15.08	-0.72	60.12	0.87	1.01	0.74	18.26
1312	69387	49.31	-14.28	0.09	59.75	0.96	0.94	0.78	17.31
1317	69556	51.19	-14.41	0.04	47.56	1.26	3.91	0.78	18.60
1322	69724	49.19	-14.27	0.23	53.14	1.08	2.78	0.76	17.94
1327	69892	51.60	-14.18	0.42	53.87	1.12	3.27	0.79	18.42
1332	70061	57.73	-14.32	0.41	58.45	1.15	2.78	0.74	19.03
1337	70229	55.05	-14.48	0.34	51.37	1.25	3.13	0.71	18.39
1342	70398	55.81	-14.66	-	57.96	1.12	1.56	0.69	17.18
1347	70566	58.70	-14.96	-	50.73	1.35	2.56	1.01	18.52
1352	70735	53.66	-14.73	-	56.82	1.10	2.74	0.98	18.36
1357	70903	50.83	-14.24	-	55.66	1.07	3.08	0.92	18.27
1362	71072	50.31	-15.55	-	77.22	0.76	0.37	0.91	18.19

Depth (cm)	Age (years BP)	TC (%)	δ13C (‰)	δ13Cres (‰)	C/N	TN (%)	δ15N (‰)	TS(%)	δ34S (‰)
1367	71240	56.82	-14.71	-	85.83	0.77	0.53	0.85	-
1372	71409	52.33	-15.94	-	53.52	1.14	3.08	-	-
1377	71577	50.20	-16.45	-	53.91	1.09	3.11	-	-
1382	71746	64.28	-15.74	-	55.23	1.36	3.66	-	-

Table A.3. Geochemical proxies analyzed over bulk peat in **ARO 08 02** core: TC, TN, TS (in percentages), C/N ratio, and $\delta^{13}C$, $\delta^{15}N$, $\delta^{34}S$ (‰).

Depth (cm)	Age (years BP)	TC (%)	δ13C (‰)	δ13Cres	C/N	TN (%)	δ15N (‰)	TS(%)	δ34S (‰)
75.00	11.84	29.12	-23.72	-	21.23	1.60	2.98	0.36	16.78
80.00	119.43	44.37	-25.08	-	32.70	1.58	3.07	0.52	18.61
85.00	227.03	48.08	-24.05	-	27.44	2.04	1.71	0.28	18.80
90.00	334.62	50.73	-26.04	-	24.21	2.44	0.62	0.40	18.52
95.00	442.22	50.29	-26.19	-	35.92	1.64	-0.67	0.19	20.37
100.00	549.82	44.58	-24.87	-	32.73	1.59	1.00	0.41	19.28
105.00	657.41	46.76	-24.33	-	43.21	1.26	0.29	0.51	19.27
110.00	765.01	50.93	-24.91	-	45.75	1.30	0.21	0.33	20.25
115.00	872.61	50.91	-25.30	-	40.94	1.45	0.80	0.34	20.74
120.00	980.20	50.22	-25.48	-23.99	45.55	1.29	2.27	0.22	21.25
125.00	1087.80	50.34	-24.12	-23.87	43.56	1.35	3.51	0.40	19.17
130.00	1195.39	49.26	-21.84	-23.73	24.52	2.34	9.36	0.31	21.19
135.00	1302.99	47.69	-20.31	-23.70	21.10	2.64	7.25	0.34	22.59
140.00	1410.59	52.61	-24.27	-23.44	41.92	1.45	3.32	0.21	20.17
145.00	1518.18	51.29	-24.54	-23.19	57.49	1.04	2.08	0.32	19.15
150.00	1625.78	50.21	-23.55	-23.17	41.55	1.41	1.88	0.28	20.03
155.00	1733.38	50.09	-23.03	-23.13	51.06	1.14	3.38	0.26	19.12
160.00	1840.97	51.53	-22.66	-23.01	45.66	1.32	4.43	0.25	19.90
165.00	1948.57	51.74	-21.53	-22.96	39.81	1.52	6.12	0.25	20.03
170.00	2056.17	51.25	-21.40	-22.89	35.57	1.68	7.17	0.27	20.31
175.00	2163.76	52.97	-22.44	-22.92	38.24	1.62	4.68	0.35	20.24
180.00	2271.36	52.24	-23.43	-23.00	49.39	1.23	4.91	0.27	18.96
185.00	2378.95	52.92	-21.17	-23.23	38.86	1.58	7.18	0.29	19.32
190.00	2486.55	52.31	-21.50	-23.28	43.31	1.41	7.74	0.28	18.69
195.00	2594.15	47.44	-24.41	-23.30	75.82	0.74	7.68	0.28	14.76
200.00	2701.74	55.14	-23.59	-23.40	67.71	0.96	3.73	0.50	15.94
200.00	2702.00	51.52	-22.64	-23.51	49.22	1.22	4.75	0.31	17.87
205.00	3188.36	54.33	-24.28	-23.66	74.18	0.85	3.18	0.42	16.52
210.00	4054.76	54.23	-24.20	-23.84	82.38	0.77	1.65	0.46	17.52
215.00	4921.16	54.58	-24.60	-24.05	61.53	1.03	1.13	-	-
220.00	5787.56	54.83	-23.44	-24.21	62.39	1.02	1.41	0.54	19.36
225.00	6653.96	54.58	-24.66	-24.30	57.15	1.10	1.60	0.58	18.84
230.00	7520.36	54.34	-25.17	-24.28	49.34	1.28	2.60	0.60	18.65
235.00	8386.76	54.45	-24.98	-24.40	63.10	1.01	1.58	0.69	16.55
240.00	9253.16	54.53	-25.50	-24.52	60.09	1.05	0.80	0.67	19.19
245.00	10119.56	52.93	-25.07	-24.46	65.30	0.95	1.46	0.65	17.11
249.00	10985.00	53.85	-25.61	-24.48	59.65	1.05	1.56	0.61	18.98
250.00	10985.96	51.61	-24.80	-24.40	56.89	1.08	1.49	0.58	18.96
255.00	11852.37	51.44	-25.50	-24.35	56.83	1.06	0.80	0.58	19.37
260.00	12718.77	53.14	-25.50	-24.26	64.07	0.98	0.89	0.57	19.23
265.00	13585.17	53.36	-24.99	-24.14	82.94	0.75	0.67	0.47	20.19
270.00	14451.57	53.53	-20.90	-23.95	68.06	0.92	0.09	0.75	20.07
275.00	15317.97	53.59	-23.81	-23.77	55.81	1.12	0.78	0.51	19.57

Depth (cm)	Age (years BP)	TC (%)	δ13C (‰)	δ13Cres	C/N	TN (%)	δ15N (‰)	TS(%)	δ34S (‰)
280.00	16184.37	52.18	-26.64	-23.60	37.09	1.65	5.49	0.57	19.35
285.00	17050.77	51.46	-22.48	-23.37	53.18	1.16	3.49	0.61	19.39
290.00	17917.17	49.89	-22.93	-23.20	62.96	0.92	2.63	0.64	19.20
295.00	18783.57	55.68	-22.90	-22.98	65.40	0.98	1.93	0.67	19.79
300.00	18783.57	55.70	-23.15	-22.80	51.16	1.27	1.04	0.68	19.65
300.00	19649.97	54.16	-22.86	-22.64	53.48	1.18	3.84	-	19.26
305.00	20516.37	55.82	-21.31	-22.46	67.28	0.97	2.81	0.58	19.61
310.00	21382.78	57.42	-20.96	-22.35	71.83	0.93	2.86	0.58	20.59
315.00	22249.18	56.64	-21.80	-22.45	68.02	0.97	2.42	0.58	20.30
320.00	23115.58	56.65	-21.64	-22.30	65.14	1.01	2.77	0.55	20.68
325.00	23981.98	56.35	-21.10	-21.91	67.86	0.97	2.46	0.54	20.46
330.00	24848.38	55.87	-22.00	-21.74	66.48	0.98	1.20	0.61	20.28
335.00	25714.78	55.26	-21.30	-21.53	67.35	0.96	1.78	0.59	20.56
340.00	26581.18	56.12	-21.49	-21.42	75.22	0.87	1.79	0.60	19.76
345.00	27447.58	49.88	-22.34	-21.24	63.52	0.92	1.11	0.66	20.03
350.00	28313.98	55.29	-22.05	-21.02	60.87	1.06	1.38	0.60	19.10
350.00	28313.98	53.67	-23.00	-20.85	60.36	1.04	3.18	0.51	19.47
355.00	29180.38	55.12	-22.79	-20.65	64.31	1.00	2.40	0.53	19.65
360.00	30046.79	56.06	-20.99	-	66.85	0.98	1.57	0.53	21.52
365.00	30913.19	56.38	-19.16	-	61.29	1.07	1.49	0.53	21.81
370.00	31779.59	54.11	-19.38	-	56.45	1.12	2.07	0.51	21.80
375.00	32645.99	56.40	-18.85	-	55.86	1.18	1.93	0.44	20.65
380.00	33512.39	56.10	-20.73	-	54.65	1.20	1.91	0.57	21.85
385.00	34378.79	56.92	-19.82	-	52.27	1.27	2.58	0.49	22.07
390.00	35245.19	56.22	-18.67	-	53.65	1.22	4.13	0.45	22.57
395.00	36111.59	57.00	-18.16	-	56.57	1.18	2.89	0.46	22.40
399.00	36977.99	56.51	-17.07	-	58.89	1.12	2.95	0.44	20.87

Table A. 4. Calcium (Ca), Titanium (Ti) and Iron (Fe) FRX core-scanner measurements (in cps) obtained from the Mo tube.

Depth (cm)	Ca	Ti	Fe
235	438	429	6071
240	306	194	3062
245	354	100	2074
250	307	583	2680
255	282	1374	4237
260	274	73	2320
265	255	323	4872
270	210	57	2103
275	206	70	772
280	196	71	521
285	148	152	573
290	235	132	459
295	175	90	411
300	193	70	359
305	204	50	452
310	182	66	407
315	199	254	621
320	149	636	1244
325	170	53	521
330	189	74	789
335	130	815	1588
340	247	1038	1964
345	141	116	593
350	166	74	439
355	138	139	632
360	152	43	293
365	195	50	681
370	283	50	1230
375	209	38	911
380	220	152	908
385	244	61	686
390	213	40	525
400	259	418	2749
405	395	205	5051
410	365	356	5989
415	237	210	3970
420	290	151	2128
425	358	111	3020
430	358	16	2835
435	368	88	2557
440	531	18	4665
445	452	0	4248
450	562	64	4388
455	455	15	2535
460	385	0	1460
465	452	16	2302
470	464	31	2866
475	368	8	2004
480	405	66	4265
485	623	50	2280
490	466	22	1755
495	364	147	1666
500	480	73	3431
505	553	0	4801
510	587	78	4068
515	500	0	4114
520	496	0	4212

Depth (cm)	Ca	Ti	Fe
525	400	0	3795
530	787	0	6293
535	623	27	5137
540	492	74	3957
545	312	33	2202
550	340	152	2664
555	354	85	3225
560	341	130	3362
565	320	126	2554
570	393	195	1354
575	334	154	1258
580	335	246	1084
585	366	140	1238
590	185	82	982
600	7	0	89
605	286	223	2010
610	177	92	2048
615	212	92	1899
620	183	30	1222
625	184	28	1884
630	156	38	1400
635	236	55	520
640	182	33	463
645	183	54	402
650	167	64	189
655	199	80	224
660	171	133	541
665	196	118	581
670	197	117	596
675	152	60	511
680	142	172	621
685	178	218	1537
690	209	291	551
695	227	127	601
700	283	198	647
705	262	346	951
710	254	413	1424
715	266	370	1807
720	346	456	1074
725	335	297	423
730	218	119	897
735	235	169	357
740	181	140	382
745	218	343	525
750	238	203	390
755	210	160	339
760	245	144	477
765	290	619	1359
770	309	763	1845
775	256	606	920
780	236	472	670
785	233	542	1060
800	253	287	1536
805	285	543	702
810	251	265	347
815	229	267	412
820	210	323	448

Depth (cm)	Ca	Ti	Fe
825	196	445	589
830	197	183	316
835	277	404	620
855	224	351	600
860	229	510	933
865	258	712	1073
870	294	564	1306
875	241	627	1348
880	270	1916	3121
885	286	499	703
890	240	157	335
895	308	132	1267
900	340	118	899
905	304	29	1103
910	303	153	1624
915	370	147	1632
920	297	163	1809
925	359	223	1971
930	304	445	2022
935	347	200	1717
940	314	186	1477
945	315	99	1537
950	337	58	1424
955	383	104	1780
960	345	96	1632
965	440	702	2871
970	275	191	1867
975	359	117	2447
980	461	246	558
985	284	71	371
1000	584	290	1877
1005	504	136	322
1010	557	163	1081
1015	470	213	1788
1020	512	145	627
1025	578	381	1917
1030	520	291	337
1035	495	586	2016
1040	553	249	1682
1045	697	367	1993
1050	549	2096	4324
1055	756	2753	8578
1060	750	2262	7054
1065	625	375	2224
1070	717	282	1888
1075	607	309	2067
1080	622	189	2036
1085	691	322	2200
1090	672	118	1734
1095	622	230	495
1100	698	238	148
1105	672	260	1375
1110	731	242	1898
1115	635	170	1987
1120	539	74	1609

Depth (cm)	Ca	Ti	Fe
1125	676	151	1526
1130	587	141	1727
1135	618	135	1538
1140	619	173	1459
1145	639	199	1722
1150	633	187	1582
1155	377	153	1481
1160	579	58	1420
1165	648	134	541
1170	570	274	390
1175	582	185	327
1180	700	195	337
1185	566	195	542
1210	543	289	1953
1215	537	447	2203
1220	381	293	1332
1225	441	629	1999
1230	441	150	1788
1235	471	124	1867
1240	444	97	1518
1245	519	242	1747
1250	418	200	1188
1255	449	164	2086
1260	424	37	1799
1265	444	137	1184
1270	473	71	2884
1275	334	62	1396
1280	396	46	1374
1285	482	161	2219
1290	658	211	2175
1295	512	104	1095
1300	609	219	1210
1305	520	77	1125
1310	518	294	1871
1315	532	242	1746
1320	594	152	1541
1325	544	291	1940
1330	606	110	1678
1335	606	193	1802
1340	647	326	1483
1345	617	417	800
1350	589	537	936
1355	586	206	649
1360	513	117	216
1365	663	308	776
1370	699	445	1281
1375	636	348	318
1380	1054	774	3178

Figure A.5 Elemental concentrations (ppm) of the mineral fraction from **ARO 06 01** record measured by ICP-AES: concentrations of Al, Ba, Ca, Cd, Cr, Cu, Fe, Mg, Mn, Ni, Sc, Sr, Th, Ti, V, Y, Zr are shown.

Depth (cm)	Age (years BP)	Al	Ba	Ca	Cd	Cr	Cu	Fe	Mg	Mn	Ni	Sc	Sr	Th	Ti	V	Y	Zr
240	9038	1901.6	3.1	2600.3	2.1	5.1	13.4	3186.0	1031.7	41.1	3.0	0.8	25.1	3.3	1490.0	10.8	0.5	5.8
245	9588	2222.8	2.9	1794.5	1.4	5.0	8.9	3251.5	665.1	32.8	2.8	0.8	17.8	3.4	1220.0	12.0	0.6	7.7
251	10249	2708.7	6.6	2953.7	2.3	4.9	9.3	4576.6	1063.3	59.3	3.4	1.1	32.1	5.0	5623.0	26.0	0.8	13.9
266	11902	2577.5	1.6	1406.7	1.7	1.8	5.5	1633.3	498.9	15.0	1.5	0.7	10.9	1.7	668.0	16.5	0.9	5.4
271	12453	2077.7	1.0	1196.3	1.8	2.1	5.7	1251.3	400.3	8.8	1.4	0.7	8.3	1.2	215.8	9.8	1.1	5.3
275	12893	2265.5	0.9	1134.8	2.3	1.4	7.4	919.8	442.0	8.3	1.2	0.8	8.4	0.9	334.9	10.2	1.1	5.1
281	13554	2369.7	1.1	1008.7	2.0	2.1	10.0	576.4	398.1	4.5	2.2	1.1	8.7	0.6	488.7	10.6	1.3	5.6
284	13885	2041.0	0.8	746.9	1.6	1.5	7.8	408.6	345.8	3.2	1.7	0.8	6.8	0.5	368.7	9.2	1.1	4.6
291	14148	2934.7	1.2	882.7	1.9	2.2	7.0	406.6	390.3	8.5	2.3	1.5	8.4	0.4	578.1	14.6	1.8	7.0
296	14275	1599.4	0.6	501.8	0.9	1.2	4.5	291.7	227.3	2.2	1.4	0.5	4.7	0.2	221.6	8.4	0.8	3.3
300	14377	3064.1	1.2	1466.3	1.5	2.6	7.1	341.8	400.4	3.5	2.4	1.2	9.2	0.3	358.0	14.5	1.6	7.3
305	14505	2157.4	0.9	526.3	1.0	1.9	6.8	242.9	234.9	1.9	1.6	0.9	5.3	-0.1	296.3	9.6	1.2	4.6
311	15279	2310.7	1.1	878.9	1.0	1.8	5.2	422.6	239.0	3.2	1.7	0.8	5.9	-0.3	217.5	11.3	1.2	5.6
316	15829	2393.4	1.4	615.0	0.8	2.7	3.4	625.2	224.4	5.0	1.3	0.9	5.2	0.5	654.4	14.1	1.3	6.0
321	16380	3917.2	1.8	653.6	1.2	9.4	8.2	546.5	299.3	6.6	3.7	1.9	7.6	0.7	1560.0	24.0	2.7	9.0
326	16931	4413.9	1.4	892.7	1.1	2.1	7.3	426.2	440.8	3.2	1.7	1.4	8.8	0.4	617.8	15.6	2.9	6.0
331	18073	5105.8	1.9	1147.2	1.1	2.1	7.8	459.8	537.0	3.8	1.5	1.3	11.1	0.4	717.3	15.5	2.9	6.2
336	19527	4938.2	5.3	932.9	0.9	6.6	7.7	3458.6	510.4	50.4	2.1	3.2	14.3	4.4	9616.0	50.1	2.6	30.6
341	20982	6768.2	10.8	953.5	1.3	7.4	7.1	3990.3	484.1	71.8	1.8	5.8	25.1	5.9	14830.0	71.0	4.1	39.1
344	21854	2779.3	1.2	722.0	0.5	2.2	6.0	437.9	265.2	4.4	1.6	1.2	7.0	0.6	799.3	12.7	1.5	6.2
356	25344	2500.9	1.7	623.1	0.3	2.3	6.6	395.5	290.8	4.9	2.0	1.0	7.0	0.5	607.4	11.1	1.2	5.5
361	26798	2603.9	1.4	683.9	0.4	2.0	5.6	375.4	275.8	4.3	1.5	1.1	6.5	0.7	444.0	10.5	1.6	5.7
366	28252	3731.8	1.7	1280.1	0.3	2.3	4.8	797.1	408.9	4.5	1.9	1.2	12.3	0.9	550.0	9.8	2.9	5.1

Depth (cm)	Age (years BP)	Al	Ba	Ca	Cd	Cr	Cu	Fe	Mg	Mn	Ni	Sc	Sr	Th	Ti	V	Y	Zr
376	31160	4493.9	2.5	1557.3	0.3	2.3	14.1	892.5	701.2	6.3	1.9	1.5	16.5	0.9	635.2	9.4	4.1	6.3
381	32173	3967.0	3.0	1530.2	0.3	1.9	11.4	607.2	693.1	6.8	2.7	1.3	17.5	0.5	1329.0	9.2	3.8	7.2
386	32892	4564.2	3.4	2096.7	0.3	2.4	13.0	631.1	939.4	8.1	2.1	1.0	23.2	0.6	602.1	7.5	4.3	5.5
405	35622	3916.4	4.3	2399.4	0.4	3.4	6.3	2670.6	785.6	48.9	0.8	1.2	24.5	3.0	5853.0	19.0	1.7	17.6
410	36341	2936.4	3.0	2294.4	0.3	1.8	5.9	2283.7	632.2	37.4	0.5	1.0	21.5	2.5	4241.0	13.7	1.4	14.1
381	32173	3967.0	3.0	1530.2	0.3	1.9	11.4	607.2	693.1	6.8	2.7	1.3	17.5	0.5	1329.0	9.2	3.8	7.2
386	32892	4564.2	3.4	2096.7	0.3	2.4	13.0	631.1	939.4	8.1	2.1	1.0	23.2	0.6	602.1	7.5	4.3	5.5
405	35622	3916.4	4.3	2399.4	0.4	3.4	6.3	2670.6	785.6	48.9	0.8	1.2	24.5	3.0	5853.0	19.0	1.7	17.6
410	36341	2936.4	3.0	2294.4	0.3	1.8	5.9	2283.7	632.2	37.4	0.5	1.0	21.5	2.5	4241.0	13.7	1.4	14.1
415	37060	2795.4	3.9	2737.8	0.3	1.8	4.7	2624.1	771.5	41.2	0.4	0.9	26.2	2.8	6617.0	14.3	1.2	14.8
425	38497	3164.5	3.2	1818.9	0.8	2.6	6.5	1414.8	581.9	16.8	1.4	1.1	19.0	1.6	4075.0	14.4	1.7	16.0
429	39072	3653.8	4.0	2906.1	0.3	0.7	10.1	1394.9	1263.5	13.6	1.1	0.5	33.2	1.4	961.5	4.6	2.9	8.0
436	39843	3090.8	5.1	2734.6	0.2	0.7	11.0	1056.0	1226.1	6.4	1.1	0.5	32.1	1.0	1385.0	4.0	2.9	12.4
439	39904	3542.0	4.8	3557.8	0.1	0.6	10.5	1344.5	1495.2	7.1	1.0	0.4	42.0	1.3	685.7	3.7	3.3	7.8
444	40006	3245.8	5.3	3850.0	0.1	0.8	7.4	1280.3	1635.6	7.3	1.3	0.3	47.3	1.2	474.4	3.1	2.9	7.4
449	40108	3135.3	5.3	4067.9	0.1	0.6	7.7	1517.4	1651.4	7.2	1.0	0.3	46.6	1.5	768.0	2.7	2.8	5.3
454	40210	2497.6	4.8	3393.0	0.1	1.1	9.0	1514.9	1399.7	6.7	1.1	0.3	40.2	1.4	653.3	2.8	2.1	7.7
461	40353	2297.5	6.0	3475.8	0.1	0.7	9.0	1019.5	1455.3	6.7	1.0	0.2	40.7	0.8	533.0	2.4	1.7	8.0
466	40455	2110.6	4.7	3525.1	0.1	0.5	9.0	1411.8	1489.2	6.7	0.8	0.2	40.6	1.3	446.0	2.2	1.6	6.7
471	40557	1829.3	4.6	3439.5	0.1	0.5	8.0	1008.7	1419.6	6.8	0.8	0.2	39.5	0.9	458.7	2.0	1.5	5.6
476	40659	1658.2	4.0	2952.0	0.1	0.6	9.4	823.2	1266.8	6.1	0.9	0.2	34.1	0.8	609.2	2.2	1.2	9.2
480	40741	1764.9	4.3	3368.4	0.1	1.2	9.8	1055.0	1417.8	6.9	1.6	0.3	38.1	1.1	1640.0	3.0	1.3	10.3
486	40863	2215.7	8.0	4719.6	0.2	1.7	11.9	1972.5	1866.5	14.1	1.3	0.3	54.7	1.9	649.3	3.4	1.5	9.3
491	40965	1352.9	4.7	3343.1	0.1	0.8	11.2	1897.6	1304.5	7.0	0.8	0.2	39.1	2.0	525.3	2.0	0.9	7.3

Depth (cm)	Age (years BP)	Al	Ba	Ca	Cd	Cr	Cu	Fe	Mg	Mn	Ni	Sc	Sr	Th	Ti	V	Y	Zr
491	40965	1352.9	4.7	3343.1	0.1	0.8	11.2	1897.6	1304.5	7.0	0.8	0.2	39.1	2.0	525.3	2.0	0.9	7.3
500	41149	1533.9	5.4	4023.5	0.1	0.6	9.0	2341.2	1414.9	7.9	1.1	0.3	45.8	2.7	842.6	3.0	0.8	12.9
505	41251	1638.57	7.70	5376.85	0.17	0.60	11.34	2401.92	2140.9	11.6	45.9	0.2	65.2	2.4	609.6	2.97	0.93	8.91
511	41373	1217.7	6.7	4986.2	0.2	0.8	9.0	3071.3	1889.4	12.1	1.1	0.2	60.1	2.9	349.0	2.8	0.6	4.0
516	41475	990.0	5.8	4265.0	0.1	0.7	7.5	2747.9	1670.7	11.3	1.6	0.2	50.8	2.6	209.5	2.3	0.5	3.6
521	41577	1006.3	6.3	5003.9	0.2	0.7	8.8	2989.0	1800.1	12.0	1.2	0.2	59.0	2.9	222.3	2.2	0.5	3.7
526	41679	934.9	5.6	4412.0	0.1	0.7	8.1	2747.9	1674.2	11.5	3.2	0.1	52.9	2.7	200.0	2.1	0.4	3.6
529	41741	1051.5	7.6	5609.5	0.2	0.8	9.3	3237.9	2181.5	14.6	1.1	0.2	67.2	3.1	215.7	2.4	0.4	4.1
536	41884	938.1	6.9	5476.2	0.2	0.8	10.7	3222.2	2011.0	13.8	1.5	0.1	64.2	3.2	307.4	2.3	0.4	4.0
541	41986	879.6	4.7	3667.2	0.1	1.4	15.3	2444.1	1412.2	10.0	2.0	0.3	42.3	2.4	738.9	3.6	0.3	4.6
546	42088	1044.1	4.6	3704.4	0.1	1.2	14.4	2524.5	1467.8	10.4	1.8	0.3	42.3	2.6	677.7	4.8	0.3	4.9
550	42169	1140.3	3.8	2830.2	0.1	1.3	13.2	1950.0	1066.8	8.2	1.2	0.6	31.8	2.0	1261.0	8.0	0.3	5.3
554	42273	1432.8	4.2	3396.7	0.1	1.4	16.3	2477.4	1199.9	9.4	1.3	1.0	37.9	2.5	1066.0	9.4	0.5	5.7
559	42429	1176.8	3.1	2185.4	0.1	1.2	15.0	1686.4	866.1	6.8	1.1	0.9	25.4	1.6	565.9	6.8	0.3	3.7
564	42585	1598.8	3.0	2455.9	0.1	1.6	16.8	1065.5	854.8	6.8	1.3	1.1	26.8	1.2	913.6	8.4	0.4	4.1
571	42804	2020.8	4.0	3375.1	0.1	1.4	12.1	2244.2	1110.3	8.6	1.3	1.3	36.5	2.3	1215.0	10.8	0.5	5.1
574	42898	2005.1	3.8	2757.7	0.2	1.3	13.0	2422.6	905.7	8.0	1.5	1.4	28.9	2.6	1338.0	11.6	0.5	4.8
579	43054	1757.9	2.4	1977.6	0.1	1.4	10.0	1484.5	622.7	5.6	1.4	1.4	20.1	1.4	1383.0	10.7	0.5	4.0
584	43210	1446.7	20.3	1706.4	0.2	0.9	7.7	1600.3	515.1	6.2	0.9	0.9	17.2	1.7	565.9	7.3	0.5	3.0
590	43398	1892.6	2.3	1985.5	0.1	1.2	8.3	1696.6	646.8	6.0	1.2	1.2	19.8	1.8	932.1	9.0	0.6	3.6
601	43741	2320.6	2.6	1812.6	0.1	1.8	13.0	2246.2	649.0	8.2	1.5	1.5	20.2	2.3	1117.0	10.8	0.9	4.6
606	43898	2530.4	2.2	1800.3	0.1	1.7	11.7	1343.4	582.3	5.9	1.3	1.5	17.1	1.5	979.5	10.3	0.9	4.7
610	44023	1865.3	1.4	1217.2	0.1	1.4	7.9	794.4	445.7	4.7	1.0	1.0	11.4	0.9	387.9	6.5	0.7	2.9
616	44210	3228.1	2.3	1682.1	0.1	1.3	18.5	1029.8	649.7	5.5	1.4	1.6	16.8	1.1	713.7	10.7	1.2	6.9

Depth (cm)	Age (years BP)	Al	Ba	Ca	Cd	Cr	Cu	Fe	Mg	Mn	Ni	Sc	Sr	Th	Ti	V	Y	Zr
621	44366	2320.6	1.3	1286.9	0.1	0.7	7.5	726.6	510.4	3.6	0.9	0.8	12.1	0.7	291.6	6.3	0.7	2.7
626	44523	1323.4	0.9	860.2	0.1	1.7	4.4	730.3	271.5	2.4	1.2	0.6	7.6	0.7	171.8	3.7	0.5	1.7
631	44679	2216.8	1.2	1087.4	0.1	0.7	7.1	671.1	374.2	3.2	1.1	1.2	9.4	0.6	306.9	5.5	0.8	2.6
634	44773	3575.0	2.0	1631.7	0.2	0.9	10.9	591.3	655.8	5.6	1.8	1.6	16.5	0.5	528.3	9.1	1.4	4.4
640	44960	1927.1	1.5	1379.3	0.2	0.9	5.4	1331.2	444.5	4.5	1.1	1.0	12.7	1.4	410.9	4.8	0.9	2.6
649	45241	2953.7	1.8	1246.6	0.2	1.0	9.0	441.4	487.8	4.5	1.8	1.7	13.0	0.5	655.7	8.1	1.2	4.1
656	45460	3396.7	1.8	1559.6	0.2	0.9	8.5	1547.8	503.7	4.5	1.5	2.0	14.7	1.6	563.8	7.4	1.4	3.7
660	45585	2363.8	1.5	940.0	0.3	0.7	6.0	916.9	345.4	3.6	1.1	1.3	10.1	0.9	479.9	5.7	0.9	2.7
665	45741	1859.5	1.0	739.7	0.2	0.5	5.1	688.4	276.2	2.7	0.9	1.0	8.0	0.6	353.8	4.5	0.7	2.1
669	45866	2134.4	1.2	789.3	0.3	0.9	6.4	902.4	286.6	3.0	1.0	1.2	8.7	0.8	578.9	5.7	0.8	2.5
675	46054	2528.4	1.5	966.1	0.5	0.7	7.9	723.0	376.7	3.4	1.4	1.3	10.0	0.7	515.8	6.6	0.9	2.9
679	46179	4231.6	2.0	1533.1	0.6	1.3	11.8	1015.5	557.8	5.1	1.8	2.4	14.5	1.1	1296.0	11.3	1.5	4.6
686	46398	2491.2	1.2	873.4	0.6	0.9	7.1	621.9	314.4	3.1	1.5	1.7	8.7	0.6	1058.0	8.0	0.9	3.2
691	46554	3890.6	2.2	1239.5	0.8	4.6	12.4	788.5	446.7	4.9	3.2	2.8	12.5	0.8	1807.0	12.8	1.5	5.3
693	46616	4206.2	1.7	1301.2	0.7	1.4	15.4	741.5	521.0	4.6	2.1	2.7	12.6	0.8	906.3	11.5	1.5	4.7
698	46773	4251.2	1.8	1234.0	1.1	1.2	12.9	749.1	433.2	4.4	2.1	3.7	12.4	0.8	1037.0	11.1	2.1	4.3
704	46960	6099.5	3.1	1806.9	1.6	2.2	13.1	1281.8	639.7	9.0	2.2	4.6	18.7	1.4	3828.0	20.1	2.6	8.1
707	47054	3865.1	1.6	1154.8	1.1	1.2	13.6	838.9	445.3	4.7	1.6	2.3	11.7	0.7	1494.0	10.7	1.5	4.4
712	47210	3428.0	1.7	1129.4	1.7	1.2	8.3	866.9	415.7	5.1	1.4	2.2	11.9	1.0	2207.0	11.1	1.4	4.8
719	47429	5711.4	2.5	1856.9	4.1	1.8	19.5	1154.4	687.0	7.2	2.2	3.5	18.7	1.2	2432.0	16.2	2.7	7.2
724	47585	6274.0	3.2	2136.4	2.3	2.6	22.4	1341.2	762.4	9.8	2.2	3.3	22.1	1.6	3574.0	20.1	3.0	8.7
729	47741	4417.8	2.0	1598.6	3.4	1.4	14.5	1140.7	590.9	5.8	1.5	2.2	16.2	1.2	1097.0	12.2	2.2	5.5
734	47898	4813.8	2.0	1662.7	3.2	1.4	16.5	1055.7	633.5	6.1	1.8	2.2	16.1	1.1	976.4	13.2	2.3	6.2
739	48054	3729.9	1.8	1333.2	2.0	2.5	12.5	899.6	497.6	5.1	2.1	1.7	13.5	0.9	934.8	11.3	1.8	5.2

Depth (cm)	Age (years BP)	Al	Ba	Ca	Cd	Cr	Cu	Fe	Mg	Mn	Ni	Sc	Sr	Th	Ti	V	Y	Zr
744	48210	3433.9	1.7	1351.6	1.9	1.4	12.3	993.3	487.6	5.3	1.8	1.5	12.6	1.1	1131.0	11.8	1.6	4.9
747	48304	3218.3	1.5	1154.2	1.6	1.3	11.5	643.3	426.1	4.7	1.7	1.5	11.5	0.7	1663.0	12.2	1.4	5.0
752	48460	2352.0	1.1	825.6	1.2	1.0	7.5	451.2	300.9	3.2	1.3	1.1	8.4	0.5	1018.0	8.6	1.1	3.5
757	48616	3518.2	1.5	1316.7	2.5	1.3	12.2	707.8	493.1	4.6	1.7	1.7	12.9	0.8	1210.0	12.3	1.6	5.1
763	48868	4519.8	2.5	1369.8	2.2	3.0	17.4	875.9	507.8	7.0	2.0	2.9	14.4	1.1	3118.0	19.7	1.6	8.9
768	49131	4802.0	3.1	1205.0	1.8	3.6	15.6	845.3	455.1	11.7	2.6	3.9	12.5	1.3	5361.0	27.8	1.7	12.6
773	49394	6323.0	5.0	1596.6	1.6	5.1	16.1	993.9	592.1	14.7	3.1	4.7	17.3	1.4	7844.0	39.1	2.0	16.2
774	49446	6558.2	5.0	1431.0	0.9	4.8	15.6	1094.3	546.3	13.9	3.0	4.6	17.2	1.6	6487.0	35.1	1.8	15.1
777	49604	6246.5	3.5	1503.5	0.9	4.5	15.6	1259.5	557.2	10.6	3.1	4.5	15.8	1.6	5122.0	30.6	1.9	13.4
800	50814	6834.5	4.1	3161.5	0.8	3.9	13.5	1054.7	479.8	9.7	2.8	4.7	13.6	1.5	3001.0	21.4	2.4	11.3
806	51129	7424.5	3.7	1693.8	1.1	3.5	14.5	845.5	506.3	9.1	2.8	4.7	14.3	1.2	3149.0	24.3	2.4	11.7
811	51392	7630.3	3.4	1654.4	1.3	3.2	13.6	743.4	491.2	8.2	2.8	5.1	13.5	1.1	2965.0	23.7	2.7	11.5
815	51602	6756.1	4.0	1341.2	1.1	3.4	14.8	894.2	383.6	10.5	2.7	4.9	12.6	1.4	4565.0	27.6	2.5	12.8
822	51971	7095.2	2.4	1189.3	0.8	2.7	18.4	566.0	365.0	6.7	2.8	4.3	9.9	0.9	2334.0	20.2	2.7	8.7
827	52233	10197.9	3.3	1745.6	12.2	3.6	32.1	987.8	536.8	7.2	3.0	4.7	15.6	1.3	1591.0	45.6	6.9	10.9
834	52602	9835.3	7.2	1395.5	1.4	3.6	17.1	923.2	438.3	12.2	3.2	4.9	17.2	1.3	4175.0	29.3	4.0	15.4
839	52865	7357.8	2.2	1233.6	1.7	2.2	18.8	591.7	354.6	5.3	3.0	3.8	9.4	0.8	1487.0	17.9	3.3	7.8
845	53180	9592.2	7.8	1478.2	3.1	3.3	23.0	1023.5	403.6	9.7	3.7	4.8	17.5	1.4	3369.0	28.6	5.0	14.2
851	53496	9766.7	6.6	1451.6	1.4	4.3	24.9	1022.3	414.9	11.9	3.8	4.6	17.4	1.7	4233.0	30.3	4.1	16.3
860	53969	11246.5	5.6	1618.2	3.6	5.0	34.5	1202.7	427.3	12.1	5.7	5.6	16.0	1.5	4934.0	40.0	6.0	15.3
865	54232	11262.2	4.6	1555.7	3.8	4.8	35.1	1168.9	436.3	12.3	4.7	7.0	14.6	1.6	4526.0	37.9	6.3	15.3
870	54495	16801.1	20.3	1742.6	5.5	8.4	51.5	2203.0	667.8	35.7	6.3	7.7	41.0	3.7	11340.0	74.1	8.2	40.8
875	54663	9031.7	4.3	1244.6	4.4	4.0	25.5	849.9	376.3	9.0	3.8	5.5	12.7	1.3	3654.0	37.2	5.1	12.7
880	54832	9594.0	4.2	1277.3	5.1	8.2	27.4	983.3	366.3	14.8	5.2	6.4	12.5	1.4	5156.0	53.6	6.0	16.4

Depth (cm)	Age (years BP)	Al	Ba	Ca	Cd	Cr	Cu	Fe	Mg	Mn	Ni	Sc	Sr	Th	Ti	V	Y	Zr
885	55000	13137.9	9.3	1619.4	7.7	9.7	37.5	2009.0	498.4	25.0	4.9	7.8	24.3	2.8	8266.0	74.0	7.6	24.1
890	55169	7800.8	4.3	1353.0	1.2	7.6	17.1	926.9	377.9	11.6	3.0	3.7	12.8	1.3	3518.0	26.7	2.7	13.9
895	55337	6991.3	2.5	1665.6	2.6	3.2	16.1	562.1	447.3	6.3	2.1	2.9	12.4	0.7	1042.0	31.1	5.1	8.3
896	55371	7806.7	3.5	2763.6	2.3	3.6	16.6	666.2	519.6	6.5	2.4	3.6	14.3	1.0	1170.0	31.0	6.8	9.1
901	55539	7489.2	2.7	1686.4	2.4	3.4	17.7	587.8	534.7	6.9	2.2	3.2	13.9	0.8	1290.0	27.6	7.0	9.0
907	55741	6895.3	2.4	1952.0	1.7	3.1	19.6	741.9	666.0	7.2	2.2	2.8	15.3	0.9	875.1	22.5	7.1	8.5
912	55910	6311.2	3.4	1908.8	3.5	6.1	19.4	791.4	632.5	7.7	2.3	3.2	17.3	0.9	1464.0	22.6	7.0	10.2
920	56179	6458.2	3.0	2091.3	3.5	6.6	23.0	894.0	709.1	8.7	2.7	3.8	17.9	1.2	1733.0	24.1	7.7	11.6
927	56415	5815.3	2.9	2158.0	6.8	4.7	14.9	931.2	798.7	9.8	2.7	4.3	18.4	1.3	2025.0	22.2	7.1	11.1
930	56516	5625.2	4.0	2159.9	2.6	6.5	26.6	1232.4	771.1	13.7	3.0	4.5	20.0	1.5	4191.0	28.5	6.7	13.2
937	56752	5576.2	3.1	2450.0	2.3	9.4	19.7	984.9	889.3	10.2	2.3	3.5	21.0	1.0	1396.0	22.8	6.8	9.1
940	56853	5062.5	3.1	1994.6	2.7	3.4	22.5	899.1	840.2	9.7	2.8	3.1	18.5	1.0	1514.0	22.5	5.4	9.8
947	57089	3906.3	2.2	1960.0	2.9	3.6	14.8	792.8	740.5	7.7	2.4	1.9	16.4	0.8	666.3	16.7	4.0	6.3
950	57190	3945.5	2.3	1876.5	3.2	3.2	16.1	756.8	764.4	7.9	2.2	1.7	16.6	0.9	687.7	17.5	3.9	6.5
954	57325	4382.6	2.4	1540.0	3.1	8.4	19.3	942.8	831.8	8.3	2.1	1.7	16.0	1.0	703.6	18.3	3.7	6.6
958	57460	4282.6	2.4	1789.5	3.5	8.1	23.1	992.3	872.8	8.4	2.3	1.5	17.3	1.0	627.5	17.7	3.4	6.2
964	57662	4815.7	3.1	1448.4	9.3	3.1	18.6	953.5	867.1	8.9	2.7	2.1	17.5	1.1	1235.0	24.7	3.4	8.3
969	57830	6344.5	5.5	2800.8	8.4	7.8	73.9	1334.0	995.9	14.0	3.8	3.3	27.8	1.7	3519.0	38.3	4.6	14.6
974	57999	4429.6	2.6	2107.0	2.9	6.1	16.7	469.0	790.9	8.3	1.9	2.3	18.0	0.5	1212.0	20.5	3.2	8.8
979	58167	4756.9	3.0	2581.3	3.0	6.5	18.0	967.1	993.5	10.1	2.1	2.5	22.6	1.2	1180.0	19.1	3.3	9.5
986	58403	4684.4	2.9	1607.4	4.1	3.8	16.4	560.6	916.1	10.3	2.3	2.2	17.7	0.6	1094.0	17.6	2.5	9.1
1001	58909	6568.0	4.5	3522.1	3.0	6.6	20.2	4265.0	1068.2	32.4	2.7	3.5	22.9	4.8	2444.0	22.7	5.1	14.8
1006	59077	5139.1	2.3	2489.2	5.0	9.6	17.5	1039.0	994.1	15.3	2.4	3.4	20.6	1.3	1491.0	22.1	3.2	11.2
1011	59246	4468.5	2.8	2400.8	3.9	5.0	16.1	947.0	942.8	12.1	2.0	3.0	21.0	1.2	974.1	18.4	2.9	9.1

Depth (cm)	Age (years BP)	Al	Ba	Ca	Cd	Cr	Cu	Fe	Mg	Mn	Ni	Sc	Sr	Th	Ti	V	Y	Zr
1015	59380	5329.2	3.5	2634.2	5.7	4.4	18.0	1243.6	1114.3	11.9	2.5	3.5	24.1	1.6	2088.0	23.3	3.3	11.4
1021	59582	5235.2	2.8	2600.9	4.5	9.2	20.1	358.1	976.3	11.0	2.3	3.6	21.0	0.6	2294.0	24.1	3.4	11.3
1025	59717	5462.5	3.6	3055.6	5.2	4.2	19.2	1275.8	1063.9	12.1	2.6	4.1	26.0	1.7	2971.0	27.8	3.8	12.7
1031	59919	5362.6	3.0	2757.7	6.6	6.9	17.8	736.4	994.1	10.2	2.5	3.8	22.5	1.0	2077.0	24.3	3.5	12.0
1036	60088	5409.6	4.2	2679.3	7.2	6.0	16.1	1149.9	1022.5	11.5	2.6	4.0	24.4	1.6	4163.0	28.9	3.2	15.4
1041	60256	4878.4	2.6	2530.4	4.8	6.8	16.4	908.7	967.8	9.0	2.2	3.1	20.6	1.3	1841.0	20.9	2.9	11.5
1046	60425	4568.8	3.4	2205.0	4.0	5.5	23.4	1169.5	980.8	13.0	1.9	2.6	21.6	1.5	3282.0	22.6	2.7	11.2
1049	60526	5936.8	6.0	3482.9	6.4	5.6	42.8	2114.8	1171.1	28.3	2.8	3.8	30.5	2.5	7670.0	37.7	4.0	16.9
1055	60728	5799.6	5.5	3051.7	9.7	6.3	44.9	1963.9	1185.6	24.7	2.9	3.3	28.7	2.3	7019.0	35.4	3.6	16.1
1060	60896	6732.6	7.9	3920.0	10.9	12.3	61.6	2955.7	1374.9	40.0	5.5	4.1	36.8	3.5	10750.0	49.0	4.4	20.4
1067	61132	5840.8	6.3	2985.1	6.7	6.2	48.1	2428.4	1252.4	32.8	3.3	3.3	31.5	3.0	8723.0	40.2	3.4	17.1
1072	61301	4488.4	3.2	2152.1	7.9	2.7	21.0	1179.3	1154.2	12.0	1.9	2.1	23.3	1.2	2012.0	18.9	2.7	9.3
1077	61469	4917.6	4.7	3775.0	10.0	4.0	32.3	2050.2	1318.9	23.6	2.5	2.5	31.9	2.1	5491.0	28.2	3.4	13.0
1082	61638	4143.4	3.3	3430.0	10.1	2.6	22.6	1079.8	1235.6	13.1	2.0	1.7	27.2	1.2	1955.0	18.4	3.0	8.1
1087	61806	3610.3	3.8	2838.1	16.4	2.7	46.6	817.3	991.4	10.9	2.4	1.6	24.9	1.0	1964.0	18.5	2.5	8.5
1092	61975	3034.1	3.2	5178.3	11.5	2.4	26.9	1236.8	1161.1	11.4	1.9	1.1	27.0	1.3	852.3	13.1	2.4	6.6
1093	62008	2410.8	2.5	3667.2	10.8	1.4	19.3	1093.5	976.5	8.8	1.5	0.9	22.0	1.1	705.8	10.5	1.9	5.7
1098	62177	2548.0	2.9	2992.9	4.5	2.0	23.0	864.0	977.1	9.0	1.6	1.3	24.9	1.0	1639.0	12.8	2.1	8.9
1104	62379	2632.3	2.6	2808.7	3.1	1.8	18.9	956.3	1010.0	9.4	1.8	1.1	22.6	1.0	1143.0	12.4	1.8	7.4
1107	62480	3202.6	3.0	3275.2	4.9	2.0	15.3	963.3	1149.5	10.3	2.0	1.4	25.4	1.1	1590.0	14.3	2.0	8.8
1114	62716	2736.2	2.7	2822.4	1.7	2.4	12.7	825.0	1015.7	9.2	1.8	1.4	23.1	1.0	1315.0	11.6	1.5	7.9
1119	62884	2783.2	2.6	2869.4	1.3	1.8	16.8	823.4	1021.2	9.1	1.5	1.4	22.6	1.0	1051.0	11.2	1.5	7.2
1124	63053	2900.8	2.6	3069.4	1.4	1.6	19.2	834.2	1081.1	9.0	1.5	1.5	23.5	0.9	880.3	11.7	1.4	6.9
1129	63221	2842.0	2.4	2965.5	1.5	1.6	16.7	765.6	1040.6	9.1	1.4	1.5	23.0	0.8	824.4	11.3	1.5	6.4

Depth (cm)	Age (years BP)	Al	Ba	Ca	Cd	Cr	Cu	Fe	Mg	Mn	Ni	Sc	Sr	Th	Ti	V	Y	Zr
1134	63390	2951.8	2.5	3045.8	2.3	1.6	16.5	855.3	1083.9	8.9	1.5	1.4	23.1	1.0	1025.0	11.8	1.4	7.0
1139	63558	2718.1	3.0	3023.9	2.7	2.6	12.5	838.7	797.2	10.5	1.7	1.4	21.7	1.1	425.0	10.2	1.5	10.2
1143	63693	2071.7	1.9	2377.5	1.5	1.2	10.5	691.3	719.7	6.3	1.1	1.1	18.2	0.6	874.9	8.3	1.1	5.0
1148	63861	2757.7	2.4	2824.4	1.2	1.5	18.5	768.1	940.8	8.2	1.4	1.4	21.7	0.9	1000.0	11.0	1.4	6.3
1154	64064	2920.4	2.4	2971.4	2.0	1.7	20.4	842.2	1049.8	8.7	1.6	1.4	22.8	1.0	914.0	11.7	1.4	6.9
1159	64232	3181.1	2.7	2934.1	1.2	1.8	26.8	800.5	1084.5	9.1	1.7	1.7	23.2	0.9	1128.0	13.6	1.5	7.8
1164	64401	3020.4	2.3	3100.7	1.4	1.6	21.6	603.1	1060.2	8.7	1.5	1.4	22.8	0.6	645.8	13.0	1.4	6.3
1169	64569	3575.0	2.5	2973.3	4.7	1.9	16.7	827.1	1043.1	8.8	1.9	1.9	23.1	1.0	1076.0	15.6	1.7	7.5
1173	64704	3773.0	3.9	2818.5	2.1	2.4	18.3	785.8	1118.6	10.6	1.8	2.1	25.4	0.9	2276.0	18.4	1.7	11.4
1179	64906	3545.6	3.0	3167.4	2.8	2.4	17.3	867.9	1015.1	9.1	2.7	2.1	24.3	0.9	1568.0	16.7	1.7	9.2
1183	65041	3853.4	5.0	3498.6	2.0	2.7	19.7	889.8	1136.0	10.8	2.2	2.5	26.6	1.1	1796.0	18.7	1.9	9.9
1221	66321	4962.7	3.9	3002.7	9.9	5.6	46.6	1078.8	1036.6	12.1	3.6	3.0	26.6	1.5	2436.0	23.3	3.6	11.2
1225	66456	4343.4	2.9	2777.3	5.9	3.3	18.3	942.0	1011.8	10.4	2.7	2.3	23.3	1.2	2103.0	19.1	3.2	9.1
1231	66658	4437.4	4.1	3145.8	10.3	3.3	16.8	1085.8	1166.4	12.3	1.9	2.2	28.3	1.3	2847.0	19.4	3.3	12.3
1236	66826	4151.3	3.0	3239.9	9.2	2.7	17.4	1111.3	1226.0	11.4	1.8	1.8	27.4	1.1	1283.0	17.2	3.1	7.8
1240	66961	4053.3	3.5	3322.2	12.1	2.8	25.6	1088.6	1218.7	11.6	2.7	1.8	28.3	1.2	1681.0	18.4	3.1	8.5
1246	67163	2765.6	2.4	2506.8	13.2	1.4	31.7	815.0	943.3	8.3	1.4	1.0	20.7	0.8	683.7	11.4	2.3	5.4
1251	67332	3257.5	3.2	3343.8	6.1	2.5	22.0	1082.1	1217.2	11.2	2.0	1.4	27.3	1.2	1615.0	15.7	2.5	10.2
1256	67500	2430.4	2.6	2789.1	2.7	1.7	11.6	861.4	884.0	8.2	1.5	1.1	23.0	0.9	1327.0	11.4	1.8	7.0
1261	67669	2565.6	2.6	2724.4	2.2	1.8	16.4	914.1	1002.0	8.7	1.6	1.3	22.8	1.1	1254.0	11.2	1.5	7.5
1266	67837	2357.9	2.2	2679.3	1.5	4.5	13.4	919.6	908.1	8.7	4.1	1.2	22.1	1.1	793.0	9.5	1.4	5.9
1271	68006	1639.7	1.6	2167.8	0.8	0.9	8.8	639.9	637.2	5.4	0.9	0.8	18.4	0.7	490.6	6.4	1.0	3.8
1281	68343	2912.6	3.2	3083.1	3.0	1.9	12.3	1661.9	1093.9	9.4	1.6	1.4	24.0	1.8	791.1	11.3	1.4	6.3
1286	68511	3463.3	2.8	3332.0	1.7	2.1	20.3	672.9	1214.2	10.3	1.9	1.8	26.3	0.8	1019.0	13.7	1.7	7.9

Depth (cm)	Age (years BP)	Al	Ba	Ca	Cd	Cr	Cu	Fe	Mg	Mn	Ni	Sc	Sr	Th	Ti	V	Y	Zr
1291	68679	2516.6	2.6	3134.0	0.8	1.6	13.8	1004.5	941.2	8.4	1.4	1.3	23.2	1.0	1065.0	10.4	1.2	6.1
1292	68713	2245.3	2.2	2709.8	1.0	1.9	12.0	865.1	821.8	7.1	1.2	1.1	20.9	1.0	832.2	9.4	1.2	5.3
1298	68915	2324.1	2.5	2241.4	1.1	1.9	13.8	353.8	757.8	6.7	1.5	1.2	17.7	0.6	988.9	10.1	1.2	6.1
1302	69050	1905.3	1.5	1959.2	1.3	1.2	13.3	263.7	663.2	5.6	1.1	1.0	15.4	0.3	558.9	7.7	1.0	4.4
1308	69252	2262.6	2.0	2280.2	0.7	1.6	21.1	576.3	793.8	6.8	1.4	1.3	18.4	0.7	858.6	10.2	1.2	5.9
1311	69353	2406.9	1.9	2714.6	0.8	1.3	21.7	592.5	829.9	6.9	1.3	1.3	20.7	0.6	620.3	10.5	1.4	5.3
1318	69589	3083.7	2.5	2729.4	3.4	1.8	16.4	736.0	916.4	8.1	1.7	1.7	21.3	0.8	1201.0	14.1	1.6	7.3
1322	69724	4317.9	4.1	3437.8	1.4	2.7	17.5	980.0	1183.1	10.8	2.2	2.6	28.4	1.2	2017.0	20.5	2.2	11.2
1328	69926	2628.4	2.2	2208.9	1.7	1.7	12.4	564.3	765.0	6.8	1.3	1.5	17.9	0.5	1167.0	12.4	1.3	6.7
1331	70027	2461.8	2.2	2159.9	1.3	1.6	11.8	561.7	733.0	7.2	1.2	1.5	17.4	0.5	1450.0	12.3	1.2	5.8
1338	70263	2426.6	2.0	2165.0	1.3	1.8	11.8	536.5	745.9	6.6	1.3	1.5	16.9	0.5	1175.0	11.5	1.2	6.0
1343	70432	3384.9	2.4	2977.2	2.6	1.7	13.3	714.6	997.6	8.1	1.6	2.2	23.0	0.7	1403.0	16.2	1.9	7.3
1348	70600	4568.8	3.7	3898.4	3.0	2.6	15.4	726.8	1274.2	12.0	2.1	2.7	30.4	0.9	2896.0	23.8	2.3	10.4
1352	70735	3878.8	2.6	3457.4	3.9	1.8	14.8	712.1	1170.5	8.9	1.6	2.1	25.6	0.9	1583.0	16.9	1.8	8.2
1358	70937	3869.2	3.1	3178.2	2.2	2.3	15.4	546.0	1072.9	9.2	1.9	2.3	25.0	0.7	2242.0	18.4	1.7	10.0
1362	71072	2540.2	1.5	2310.8	2.2	1.1	8.2	331.6	741.9	5.7	1.2	1.2	16.9	0.5	524.4	11.4	1.1	4.8
1367	71240	1387.5	1.2	2631.0	2.1	0.8	7.4	588.4	570.9	4.4	0.7	0.7	17.4	0.8	363.1	6.3	0.8	3.2
1373	71442	5495.8	4.4	4566.8	7.2	3.5	39.2	1451.8	1415.7	13.3	2.9	3.3	35.4	1.6	3367.0	29.0	2.6	13.3
1377	71577	4935.3	3.9	4263.0	8.7	2.8	45.3	1103.9	1314.2	13.0	2.6	3.0	33.0	1.4	2875.0	24.0	2.4	10.9
1382	71746	4433.5	3.3	3933.7	5.4	2.5	35.3	1072.7	1148.8	11.3	2.2	2.5	29.0	1.2	2134.0	20.4	2.2	8.8

Table A. 6 Macrofossil counts of **ARO 06 01** normalized to 50 cc.

Depth (cm)	*Axonpus paschalis cf.*	*Apium prostratum cf.*	*Polygonum acuminatum*	Cyparaceae sum	Curculionidae	*Ephydridae*	Oribatid mites	Sand grains
240	0	0	12.5	33.33	95.83	0	45.83	16.67
255	0	0	0	42.42	12.12	0	27.27	12.12
276	2.86	2.86	120	2.86	5.71	0	48.57	0
300	0	0	1432.26	0	38.71	35.48	22.58	0
331	0	0	2.5	2.5	10	0	172.5	0
349	9.38	40.63	3.13	0	0	0	12.5	3.13
371	0	0	0	0	44.74	0	210.53	0
416	0	0	252.5	40	32.5	2.5	62.5	2.5
455	0	0	0	3.03	133.33	0	103.03	0
482	0	0	0.05	0	2.88	0	0.05	0
531	0	0	2.08	0	143.75	8.33	175	0
565	0	0	0	0	34.69	0	365.31	0
611	0	0	0	0	64.29	0	26.19	0
644	0	0	0	0	43.24	0	113.51	0
671	9.43	0	0	0	77.35	0	307.55	0
714	0	0	0	0	90.7	0	411.63	0
739	0	0	0	0	21.05	0	18.42	0
769	0	0	0	0	2.38	0	195.24	0
832	17.14	0	0	0	5.71	17.14	588.57	34.29
916	0	0	0	0	16.67	0	0	0
959	0	0	0	0	4.76	0	195.24	0
1011	0	0	0	0	5.26	0	105.26	0
1056	23.07	0	0	0	17.95	0	200	17.95
1109	0	0	0	0	0.13	0.02	42.22	0
1147	0	0	0	0	2.63	0	97.37	0
1216	0	0	0	0	0	0	0	0
1273	0	0	0	0	2.44	0	56.1	0
1312	0	0	0	0	7.5	0	195	0
1369	0	0	0	0	21.88	0	331.25	0

.

Table A. 6 Macrofossil counts of **ARO 06 01** normalized to 50 cc.

Detph (cm)	*Cyperus cyperoides*	*Polygonum acuminatum*	*Scirpus eragrostis*	*Scirpus californicus*	Oribatida	Curculionidae
87.5	16.7	0.0	0.0	0.0	13	0.0
89.5	25.0	0.0	0.0	0.0	12	0.0
91.5	0.0	0.0	0.0	0.0	70	0.0
93.5	8.3	0.0	0.0	33.3	21	0.0
117.5	0.0	0.0	0.0	33.3	5	0.0
142.5	8.3	275.0	8.3	0.0	1	16.7
162.0	8.3	0.0	0.0	16.7	1	0.0
187.5	0.0	658.3	0.0	8.3	2	83.3
203.5	0.0	0.0	0.0	0.0	0	0.0
232.5	0.0	0.0	0.0	0.0	1	37.5
263.5	0.0	183.3	0.0	0.0	0	8.3
278.5	0.0	0.0	0.0	0.0	151	0.0
301.5	58.3	41.7	0.0	0.0	1	25.0
337.5	16.7	33.3	0.0	0.0	28	66.7
363.5	0.0	0.0	0.0	0.0	18	25.0
392.5	0.0	0.0	0.0	0.0	0	0.0

Figure A.7. Pollen percentages from **ARO 06 01** record. Pollen counting was carried out until at least 150 pollen grains were reached of palms, trees, herbs and shrubs excluding aquatic or semiaquatic plants (Cyperaceae, *Typha* and *Polygonum*) and fern spores.

Trees and shrubs												Herbs		Pteridophyta						Semiaquatic, aquatic							
Depth (Cm)	*Acalypha* comp	Asteraceae	*Coprosma*	Palmae	*Macaranga*	*Pinus*	Pg A	*Sapinus*	*Sophora*	*Triumfetta*	Ulmaceae	Plantago	Poaceae	Filices-monolete-psilate	Filices-monolete-verrucate/areolate	Filices-trilete psilate	Filices-trilete verrucate	Pteris	Ophioglossum	Cyperaceae	*Polygonum*	*Typha*	Unknown pollen	Indeterminate pollen	exotic Lycopodium	Sum (including aquatic pollen and fern spores)	Sum (excluding aquatic pollen and fern spores)
235	0.00	45.90	0.00	24.59	0.00	0.00	0.00	0.00	0.00	0.00	0.00	0.00	29.51	596.72	24.59	0.00	0.00	0.00	0.00	98.36	1.64	0.00	0.00	0.00	42.00	440.00	61.00
315	0.00	4.76	26.19	2.38	0.00	0.00	0.00	0.00	0.00	0.00	0.00	0.00	61.90	4.76	0.00	0.00	0.00	7.14	9.52	595.24	2.38	0.00	0.00	4.76	63.00	51.00	42.00
365	0.00	52.50	0.00	12.50	0.00	0.00	0.00	5.00	0.00	0.00	0.00	0.00	30.00	95.00	0.00	5.00	0.00	0.00	0.00	5.00	5.00	5.00	0.00	0.00	40.00	80.00	40.00
405	0.00	35.76	0.95	8.86	0.00	0.32	1.58	0.00	0.00	0.00	0.00	0.00	48.73	56.01	5.06	0.00	0.00	0.00	0.32	20.25	0.00	1.27	1.90	1.90	73.00	510.00	316.00
415	0.00	39.32	3.42	10.26	0.00	0.00	0.85	2.56	0.85	0.00	0.85	0.85	39.32	174.36	34.19	0.00	0.00	0.00	5.13	22.22	8.55	0.00	1.71	0.00	42.00	367.00	117.00
445	0.00	47.12	1.92	9.62	0.96	0.00	8.65	0.00	0.00	0.00	0.00	0.00	26.92	137.50	9.62	0.00	0.00	0.00	1.92	10.58	0.00	4.81	0.00	4.81	40.00	259.00	104.00
475	0.00	35.65	13.91	26.96	0.00	0.00	4.35	0.87	0.00	0.87	0.87	0.00	15.65	565.22	8.70	0.87	0.00	4.35	0.87	13.91	0.00	0.00	0.00	0.87	40.00	782.00	115.00
545	0.00	33.18	1.36	2.73	0.00	0.00	0.00	0.00	0.00	0.45	0.00	0.00	62.27	142.27	2.27	0.00	0.45	0.00	0.45	15.91	0.00	0.00	0.00	0.00	21.00	540.00	220.00
615	0.52	70.47	1.04	3.11	0.00	0.00	1.55	0.00	0.00	0.00	0.00	0.00	21.24	56.99	9.33	0.00	0.00	0.52	0.52	9.84	0.00	0.00	0.00	2.07	26.00	323.00	193.00
645	0.00	59.49	2.53	5.06	0.00	0.00	0.00	0.00	0.00	0.00	0.00	0.00	32.91	25.32	31.65	0.00	0.00	0.00	1.27	6.33	0.00	0.00	0.00	0.00	40.00	125.00	79.00
703	0.00	49.18	0.00	4.51	0.00	0.00	3.69	0.00	0.00	0.00	0.00	0.00	38.93	145.90	5.74	0.00	0.00	0.00	0.00	9.02	0.00	0.00	0.00	3.69	29.00	614.00	244.00
733	0.00	41.50	5.00	9.50	0.50	0.50	0.00	0.50	0.00	0.00	0.00	0.00	38.50	17.00	22.50	0.00	0.50	0.00	0.00	7.50	0.00	0.50	4.00	0.00	47.00	280.00	200.00
763	0.00	21.12	1.24	10.56	0.00	0.00	2.48	0.00	0.00	0.00	0.00	0.00	57.14	7.45	3.11	0.00	0.00	0.00	0.00	3.11	0.00	0.00	1.24	6.21	40.00	178.00	161.00
805	0.00	0.82	0.61	1.84	0.00	0.00	0.00	0.00	0.00	0.00	0.41	0.00	96.32	2.66	0.61	0.00	0.00	0.00	1.23	6.54	0.00	0.20	0.00	0.00	37.00	511.00	489.00
835	0.00	0.00	0.00	0.97	0.00	0.00	0.00	0.00	0.00	0.00	1.29	0.00	95.15	3.88	1.94	0.00	0.00	0.00	1.29	6.15	0.00	0.32	1.94	0.65	42.00	331.00	309.00
866	0.00	0.00	0.00	0.48	0.00	0.00	0.00	0.00	0.00	0.00	0.00	0.00	98.81	1.43	0.00	0.00	0.00	0.00	0.71	1.19	0.00	0.00	0.48	0.24	34.00	429.00	420.00
916	0.00	0.00	0.00	8.61	0.00	0.00	4.92	0.00	0.00	0.00	0.00	0.00	83.61	3.69	1.23	0.00	0.00	0.41	0.00	0.00	0.00	0.00	0.82	2.05	156.00	257.00	244.00
976	1.06	3.19	8.51	23.40	0.00	0.00	2.13	0.00	0.00	0.00	0.00	0.00	54.26	7.45	5.32	0.00	0.00	1.06	0.00	6.38	0.00	0.00	3.19	4.26	43.00	107.00	94.00

Trees and shrubs												Herbs		Pteridophyta						Semiaquatic, aquatic							
Depth (Cm)	*Acalypha* comp	Asteraceae	*Coprosma*	Palmae	*Macaranga*	*Pinus*	Pg A	*Sapinus*	*Sophora*	*Triumfetta*	Ulmaceae	Plantago	Poaceae	Filices-monolete-psilate	Filices-monolete-verrucate/areolate	Filices-trilete psilate	Filices-trilete verrucate	Pteris	Ophioglossum	Cyperaceae	*Polygonum*	*Typha*	Unknown pollen	Indeterminate pollen	exotic Lycopodium	Sum (including aquatic pollen and fern spores)	Sum (excluding aquatic pollen and fern spores)
1010	0.59	0.59	2.96	1.78	0.00	0.00	0.00	0.00	0.30	0.00	0.00	1.18	92.31	2.96	0.30	0.00	0.00	0.30	0.30	1.48	0.00	0.00	0.30	0.00	27.00	351.00	338.00
1050	0.00	8.70	2.17	3.73	0.00	0.00	0.00	0.00	0.00	0.00	0.00	0.00	83.54	10.25	2.48	0.00	0.31	0.00	1.55	2.48	0.00	0.00	1.86	0.00	26.00	369.00	322.00
1148	0.00	0.78	1.56	7.03	0.00	0.00	1.56	0.00	0.00	0.00	0.00	0.00	85.94	17.97	1.56	0.00	1.56	3.13	0.00	2.34	0.00	0.00	0.78	2.34	42.00	159.00	128.00
1230	0.00	2.72	11.56	24.49	0.00	0.00	2.04	0.00	0.68	2.04	0.00	0.00	45.58	17.01	3.40	0.00	0.00	0.68	0.00	6.80	0.00	0.00	0.00	10.88	41.00	178.00	147.00
1297	0.00	1.55	6.20	7.75	0.00	0.00	1.55	0.78	0.78	0.00	0.00	0.00	74.42	13.18	1.55	0.78	0.00	0.78	0.78	2.33	0.00	0.78	0.78	6.20	77.00	151.00	129.00
1385	0.00	5.05	3.28	1.77	0.25	0.00	0.51	0.00	0.00	0.00	0.00	0.00	82.83	3.03	1.52	0.00	0.25	0.51	0.00	1.77	0.00	0.00	0.51	5.81	39.00	417.00	396.00

Table A. 8 Chemical composition of rock and soils from Easter Island measured by ICP-MS

Sample Name	Sample type	LOI	TiO2	Al2O3	T-Fe2O3	MnO	MgO	CaO	Na2O	K2O	P2O5	Li	Be	Sc	V	Cr	Co
UNITS		%	% m/m	% m/m	% m/m	% m/m	% m/m	% m/m	% m/m	% m/m	% m/m	ppm	ppm	ppm	ppm	ppm	ppm
Detection limit			0.001	0.040	0.032	0.001	0.014	0.03	0.016	0.007	0.0078	0.319	0.034	0.040	0.412	0.321	0.181
RRK1A	Rock	9.02	3.57	19.37	22.10	0.36	3.15	3.86	2.03	0.58	1.79	14.86	3.02	33.43	228.24	0.86	100.32
RRK1B	Soil	14.50	4.07	25.55	28.70	0.06	0.22	0.06	0.07	0.04	0.64	6.03	2.29	54.31	142.03	2.81	26.75
RRK1C	Soil	15.51	3.58	21.73	22.14	0.29	0.74	0.24	0.07	0.12	0.41	7.09	2.75	41.30	120.97	2.49	25.99
RRK5B	Soil	14.50	3.64	22.83	26.52	0.50	0.50	0.12	0.05	0.05	0.14	4.62	1.76	34.89	125.67	4.27	42.57
RRK8A	Rock	-0.49	2.68	14.37	18.07	0.37	3.23	7.32	4.57	1.16	1.36	8.17	2.32	24.64	176.65	1.40	72.03
RRK8B	Soil	10.90	2.59	15.78	17.77	0.32	2.31	4.23	2.26	0.89	0.96	8.73	2.59	26.74	144.46	1.68	58.81
RRK13A	Rock	1.29	2.79	15.23	17.26	0.40	2.97	7.32	4.55	1.34	0.88	7.18	2.63	25.40	258.96	1.40	143.34
RRK13B	Soil	6.88	2.47	13.63	17.20	0.34	2.70	5.49	2.43	1.00	1.21	8.28	2.23	23.93	130.02	1.41	28.62
RRK14A	Rock	7.48	2.54	14.72	16.56	0.35	2.35	5.47	1.99	0.94	1.33	7.83	2.43	24.45	110.30	1.86	38.62
LTR4	Rock	28.37	3.17	19.40	11.94	0.14	0.55	0.04	0.05	0.04	0.25	16.93	0.58	29.86	405.10	79.31	45.74
LTR7	Rock	10.50	3.67	18.18	17.71	0.20	3.21	4.69	1.08	0.33	0.50	6.31	1.76	36.89	450.44	76.81	49.56
Aroi 4	Rock	2.59	0.79	22.20	6.83	0.09	5.06	12.99	2.00	0.10	0.10	1.74	0.30	27.42	205.12	675.43	88.43
Aroi 5	Rock	1.20	3.33	16.81	17.33	0.25	3.74	9.06	3.22	0.37	0.42	6.16	0.93	30.32	425.19	76.99	150.08
Aroi 6	Rock	10.13	4.42	21.36	16.95	0.23	2.19	3.30	1.54	0.63	0.41	4.93	1.82	39.29	503.51	44.63	82.42
Aroi 7	Rock	7.30	3.69	21.00	18.18	0.27	4.03	5.67	1.92	0.66	0.47	8.34	1.78	37.38	490.21	60.54	163.05
Aroi 9	Rock	-0.05	3.43	14.53	16.45	0.18	4.09	8.45	3.58	0.69	0.42	4.31	1.76	34.10	479.86	43.03	87.23

Sample Name	Sample type	Ni	Cu	Zn	Ga	Ge	As	Rb	Sr	Y	Zr	Sn	Sb	Cs	Ba	La	Ce
UNITS		ppm	ppm	ppm	ppm	ppm	ppm	ppm	ppm	ppm	ppm	ppm	ppm	ppm	ppm	ppm	ppm
Detection limit		0.314	0.28	9.672	0.028	0.065	0.023	0.444	1.282	0.061	0.246	0.030	0.005	0.016	1.89	0.037	0.051
RRK1A	Rock	21.98	20.18	182.04	29.87	6.04	1.34	3.24	108.43	51.25	640.48	2.25	0.06	0.04	161.88	49.13	121.13
RRK1B	Soil	3.59	6.34	143.82	41.93	7.79	0.91	1.43	7.74	124.13	830.66	3.01	0.07	0.07	151.47	54.55	123.69
RRK1C	Soil	2.34	10.00	145.36	35.80	8.14	0.77	3.83	23.41	184.15	716.11	2.86	0.08	0.14	158.18	88.78	196.87
RRK5B	Soil	3.37	21.68	181.46	37.51	8.08	0.43	0.57	10.51	177.11	747.94	2.93	0.05	0.03	266.71	107.97	302.77
RRK8A	Rock	2.24	16.12	148.02	22.92	5.85	1.16	19.87	251.63	84.99	483.98	1.98	0.08	0.21	183.70	43.69	110.87
RRK8B	Soil	1.99	11.88	126.43	25.03	5.20	1.16	18.27	208.24	87.73	534.88	1.77	0.07	0.23	170.11	40.44	103.04
RRK13A	Rock	12.64	22.46	150.52	25.34	5.27	0.96	18.49	259.41	69.30	496.74	1.69	0.07	0.19	202.78	40.04	96.73
RRK13B	Soil	1.83	12.73	133.62	22.32	5.18	0.93	19.44	235.95	75.50	476.64	1.58	0.07	0.20	181.44	40.40	99.79
RRK14A	Rock	3.82	37.81	167.17	24.62	5.03	0.49	15.97	279.47	80.89	489.27	1.62	0.07	0.17	185.25	40.13	99.03
LTR4	Rock	34.78	60.62	76.49	20.76	3.74	2.09	<LD	18.85	14.63	317.11	1.42	0.03	0.04	66.44	14.37	65.01
LTR7	Rock	29.40	77.56	126.08	23.80	4.31	0.38	3.02	72.53	48.45	359.66	1.18	0.03	0.04	119.64	24.43	48.94
Aroi 4	Rock	62.38	18.51	32.86	14.58	2.52	0.30	0.59	280.02	9.55	53.19	0.52	0.02	0.01	28.33	4.87	11.99
Aroi 5	Rock	29.52	86.29	112.68	20.87	4.23	0.57	3.05	258.53	39.56	293.94	1.16	0.04	0.08	107.99	20.41	49.99
Aroi 6	Rock	27.04	112.99	215.25	25.43	4.55	0.47	12.10	76.57	60.30	276.51	1.25	0.04	0.11	193.33	40.53	97.45
Aroi 7	Rock	31.30	106.04	125.27	22.82	4.63	0.77	12.66	112.66	40.20	307.41	1.21	0.07	0.14	127.08	19.46	52.98
Aroi 9	Rock	23.63	93.12	110.91	20.71	4.31	0.25	5.71	248.68	49.32	314.91	1.31	0.05	0.04	124.36	25.47	59.56

Sample Name	Sample type	Pr	Nd	Sm	Eu	Gd	Tb	Dy	Ho	Er	Tm	Yb	Lu	Hf	Pb	Th	U
UNITS		ppm	ppm	ppm	ppm	ppm	ppm	ppm	ppm	ppm	ppm	ppm	ppm	ppm	ppm	ppm	ppm
Detection limit		0.007	0.034	0.010	0.007	0.013	0.002	0.009	0.002	0.005	0.001	0.004	0.001	0.005	0.683	0.005	0.012
RRK1A	Rock	15.31	62.97	14.77	4.24	14.14	2.37	14.14	2.25	6.96	0.92	6.09	0.90	13.97	1.70	5.17	1.38
RRK1B	Soil	19.40	93.86	23.02	6.69	22.31	4.23	23.98	4.31	12.99	1.63	10.66	1.56	18.55	2.06	6.32	1.80
RRK1C	Soil	30.83	150.03	35.14	10.55	35.52	6.71	37.79	6.69	19.22	2.42	15.68	2.37	15.85	2.26	5.99	1.61
RRK5B	Soil	39.17	184.14	44.03	11.62	43.89	6.80	40.94	6.79	20.76	2.58	16.37	2.46	16.27	2.31	6.19	1.40
RRK8A	Rock	14.45	70.45	16.76	4.98	18.08	3.24	17.82	3.10	8.64	1.06	6.68	1.00	10.45	1.49	3.96	1.19
RRK8B	Soil	12.83	64.69	15.07	4.55	15.40	2.88	17.06	2.89	9.09	1.08	7.37	1.06	11.17	1.57	4.06	1.12
RRK13A	Rock	12.22	59.07	14.15	3.78	13.84	2.39	14.79	2.45	7.36	0.94	6.11	0.91	10.59	1.56	4.19	1.26
RRK13B	Soil	12.85	65.40	14.90	4.58	15.72	2.79	16.11	2.66	8.05	0.95	6.30	0.88	9.75	1.50	3.79	1.04
RRK14A	Rock	12.84	63.74	14.40	4.46	14.63	2.86	15.82	2.83	8.17	1.01	6.40	0.94	9.77	1.47	3.80	1.02
LTR4	Rock	4.88	24.07	6.14	2.15	6.09	1.00	5.76	0.85	2.21	0.36	2.15	0.30	10.02	2.36	3.91	0.90
LTR7	Rock	7.87	36.98	8.82	2.61	8.41	1.75	9.79	1.77	5.24	0.69	4.54	0.68	7.23	1.18	2.96	0.64
Aroi 4	Rock	1.40	6.44	1.58	0.68	1.65	0.33	1.87	0.33	0.98	0.12	0.82	0.11	1.38	<LD	0.40	0.10
Aroi 5	Rock	6.74	32.30	7.67	2.51	8.26	1.44	8.76	1.36	4.32	0.50	3.36	0.48	6.41	1.31	2.37	0.57
Aroi 6	Rock	14.26	67.08	15.56	4.00	13.60	2.59	13.92	2.32	6.44	0.86	5.54	0.80	6.60	1.18	2.98	0.82
Aroi 7	Rock	6.41	31.52	7.43	2.51	7.38	1.43	8.73	1.50	4.66	0.58	4.02	0.57	6.68	0.94	2.67	0.77
Aroi 9	Rock	7.83	35.06	8.74	2.59	9.33	1.63	10.06	1.72	5.28	0.65	4.29	0.65	6.58	1.06	2.64	0.71

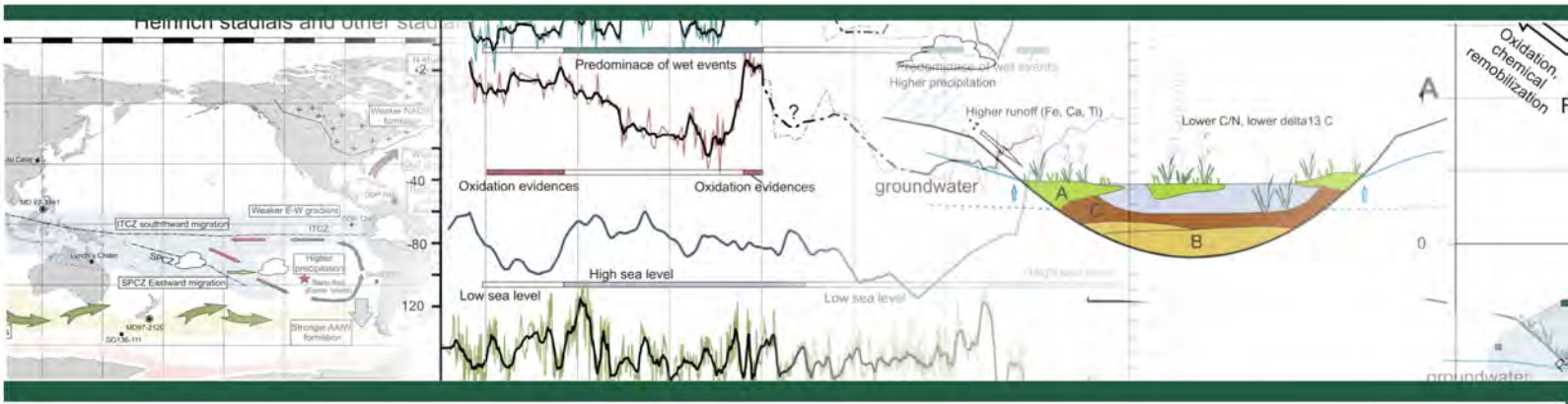

ICTJA

CSIC
Consejo Superior de Investigaciones Científicas

Universitat de Barcelona